Delft University of Technology

Master Thesis

Numerical Analysis of Stability of Steel Columns With Thermal Gradients

by:
Oscar Ivan Delgado Ojeda

Evaluation commitee:

Prof. Ir. F.S.K. Bijlaard
Ir. R. Abspoel
Dr. Ir. M.A.N. Hendriks
Ir. L.J.M. Houben
Prof. Dr. Ir. J. Maljaars

A thesis submitted in fulfillment of the requirements for the degree of Master of Science in Civil Engineering from the

Faculty of Civil Engineering and Geosciences
Department of Civil Engineering

Publicly defended on:

January 8th 2015

TU Delft Delft University of Technology

DELFT UNIVERSITY OF TECHNOLOGY

Abstract

Faculty of Civil Engineering and Geosciences
Department of Civil Engineering

Master of Science in Civil Engineering

Numerical Analysis of Stability of Steel Columns With Thermal Gradients

by Oscar I. Delgado O.

This thesis studies the buckling behavior of I-shaped steel columns under the effect of thermal gradients. The mechanical properties of steel decay significantly with increasing temperature. Therefore, in case of a fire, the buckling resistance of steel columns is considerably reduced due to the decrease in the modulus of elasticity and yield strength. Furthermore, in a realistic fire scenario, temperature gradients develop throughout the cross-section and throughout the column's length. However, the design guidelines in Eurocode 1993-1-2, as well as in other leading construction codes, specify that in the case of a non-uniform temperature distribution the column's buckling resistance must be determined by considering a uniform temperature distribution considering the maximum temperature in the cross-section. The objective of this thesis is to assess the reliability of the provisions given by the Eurocode for elevated temperature design in the presence of temperature gradients. A series of finite element models were created for five different cross-sections and analyzed at room temperature, uniform elevated temperature and non-uniform temperature along the cross-section. From the uniform elevated temperature analysis, a buckling curve for elevated temperature was derived. The finite element analysis results for the models under the effect of temperature gradients showed better agreement with this FEM-derived buckling curve than with the Eurocode provisions, which were shown to be over-conservative for the case of a temperature gradient along the column's weak axis. The FEM results were also compared to the results obtained with the American and Australian building codes...

Contents

List of Figures

Chapter 1

Introduction

1.1 Fire Safety Engineering

Building codes around the world specify requirements for the resistance, stability and serviceability of the structural elements and systems of any construction erected. Within these requirements lie the considerations for hardly predictable hazards, such as earthquakes, high wind loads, explosions, collisions and fire. This last accidental action that may present itself within a structure is of interest due to the severe consequences it may have on the occupants and the structure itself. While a skyscraper may be adequately designed to resist high wind loads and seismic actions, if proper measurements are not taken, the ignition of a fire in any compartment may result in loss of lives, heavy structural damage or even progressive collapse. To tackle this design concern, building codes include specifications for structural design, emergency exit layout, smoke control, fire suppression and other measurements that may be encompassed in what is known as fire safety engineering.

Fire safety engineering can be considered as the field of engineering dedicated towards the adequate design in case of a fire such that the elements surrounding the compartment containing the fire are able to fulfill its function, whether it is structural, insulating or separating. Its aim is to prevent or reduce the loss of lives and significant damage to the structure through the implementation of adequate preventive, protective and/or suppression systems [1].

The increasing temperature in a compartment leads to, among other things, the decrease in the material properties of the surrounding structural elements, which in turn

lead to reduced resistance and stability. Materials like concrete and timber have a relatively low thermal conductivity and, as such, their temperature does not increase as rapidly during a fire compared to unprotected steel. The relatively high thermal conductivity of unprotected steel leads to a faster increase in temperature, which in turn leads to a decay in its mechanical properties. This results in overall lower fire resistance for unprotected steel elements. As such, building codes specify safety factors and modified material properties that allow steel structures to comply with fire resistance requirements and optimize the amount of time during which these structural elements may perform their required function under fire conditions.

1.2 Resistance to fire for steel structures

As previously discussed, the mechanical properties of steel (Modulus of elasticity, yielding strength and ultimate strength) decrease with the increase of temperature. The bi-linear stress-strain relationship typically used for room temperature design begins to curve as temperature increases. Figure 1.1 illustrates the stress-strain relationships for mild steel hot-rolled cross-sections at elevated temperatures.

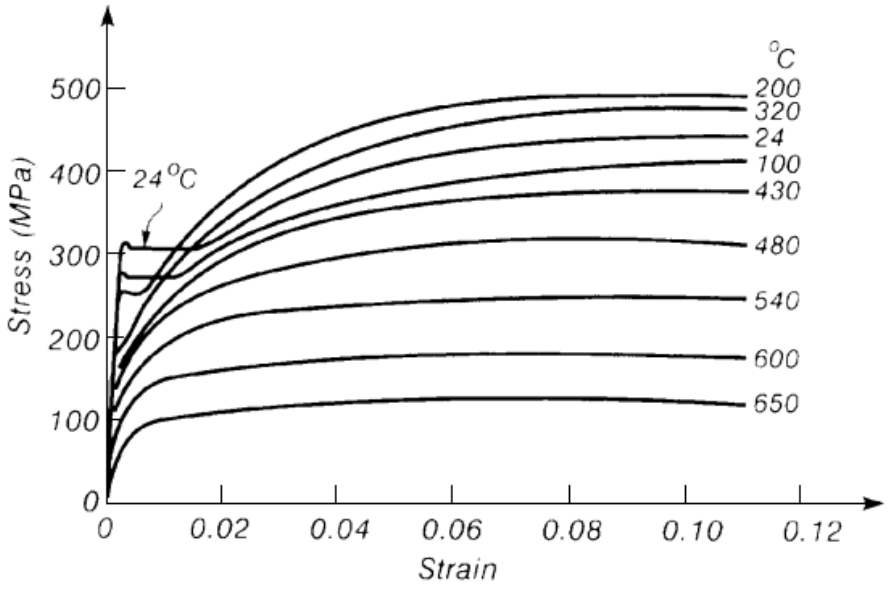

FIGURE 1.1: Stress-Strain relationships for mild steel at elevated temperatures[2].

Figure 1.1 was obtained through experimental data on hot-rolled structural steel A36 through steady-state testing by Harmathy and Stanzak in 1970 [3]. It can be seen from the figure above that the yield strength and modulus of elasticity consistently decrease with increasing temperature while the ultimate stress increases for temperatures

in the range of 180 °C-370 °C. The increase in ultimate strength is the result of strain-hardening, caused by "the immobilization of dislocations in the ferrite phase by the precipitation of carbon and nitrogen atoms" [4].Strain hardening is also considered in the Eurocode, but only for steel temperatures below 400 °C [5].Above this temperature, all mechanical properties decrease rapidly. In the end, the increase in ultimate strength of steel at moderate temperatures is of little significance, given the fact that temperatures in typical fires can exceed 1000 °C.

The modified stress-strain relationship at elevated temperatures no longer shows a clearly defined yield stress. Because of this, the concept of proof stress is necessary. A straight line parallel to the linear portion of the stress-strain relationship is traced with its origin at a specific "x" strain. Its intersection with the stress-strain curve determines the value of the x% proof stress. Kirby and Preston [6] suggest the use of a 1% proof stress for design at elevated temperatures. Eurocode 1993-1-2 uses a 2% proof stress [5], while other leading standards like AISC and AS 4100 give no specification on the strain level considered for the proof stress. British standard BS 5950 gives proof stresses at three strain levels: 0.5% , 1.5% and 2%[1]. Similarly, the EN 1993-1-2, AISC and AS 4100 codes recommend reduced values for the modulus of elasticity at elevated temperatures.

This considerable decrease in mechanical properties constitutes a serious concern regarding the resistance of the exposed structure or elements, but in particular, as it has been studied in this thesis, it represents a complicated issue regarding the stability of the steel elements since their critical buckling load will be changing in a non-linear way with increasing temperature. Added to the decay of the mechanical properties, thermal gradients through the cross-section and throughout the length of the elements, initial out-of-straightness, initial imperfections and thermal expansion restraints are all present factors that make the stability of steel elements under fire a complicated phenomenon that is not yet fully understood.

1.3 Current design considerations

The way in which leading construction codes deal with the mechanical behavior of steel at elevated temperatures is through reduction factors for the proportional limit, yield strength and modulus of elasticity. These factors are expressed as a ratio of the elevated temperature value and the room temperature value of each mechanical property and are the results of experimental testing.

[1]The standard BS 5950 has been superseded by EN 1993 since 2005, which will be commented further.

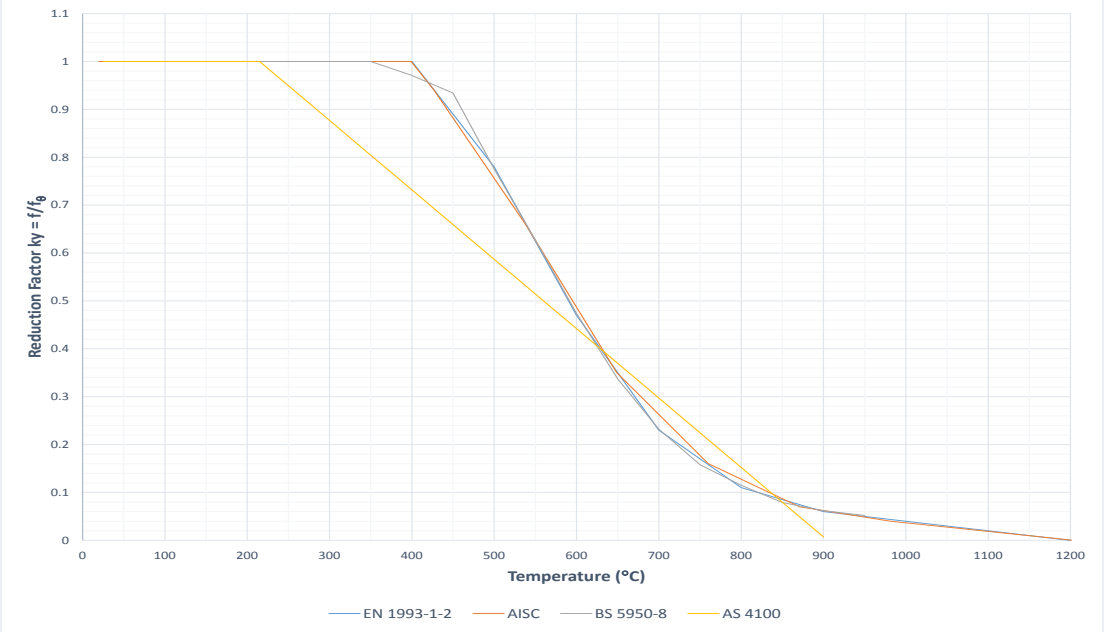

FIGURE 1.2: Reduction factors for yield strength at elevated temperatures in leading construction codes.[2]

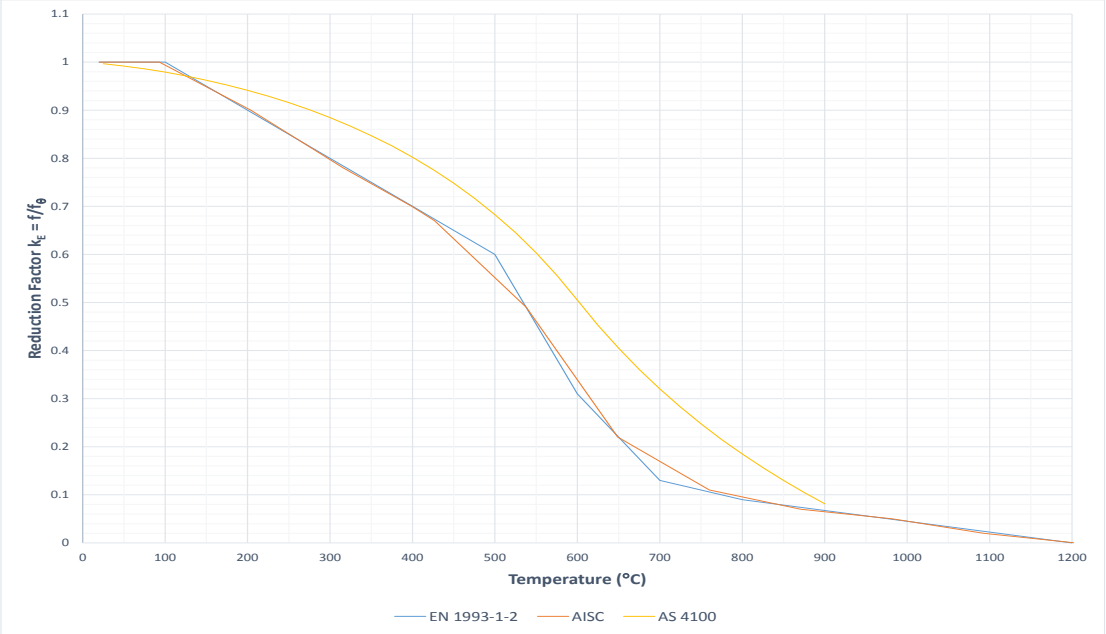

FIGURE 1.3: Reduction factors for Young's modulus at elevated temperatures in leading construction codes.

[2]The BS 5950-8 reduction factors come from the British standard published in 1990, which by now has been superseded by the Eurocode. They are only shown here for further background information.

Figure 1.2 shows the reduction factors for yielding strength as indicated in EN 1993-1-2, BS 5950-8, AISC and AS 4100. Similarly, figure 1.3 shows the reduction factors for the modulus of elasticity (in this case, BS 5950-8 does not specify reduction factors).

As it can be seen from figures 1.2 and 1.3, the reduction factors in the Eurocode and AISC codes are practically the same. This is due to the fact that the AISC material properties at elevated temperatures were adopted from the European Convention for Constructional Steelwork (ECCS) model code on fire engineering published in 2001. Annex 4 of the AISC code even mentions that "the adapted material properties are consistent with those in Eurocode 3 and 4" [7]. We can see that the only notable discrepancy comes from the Australian standard AS 4100, which is relatively over-conservative for low temperatures and slightly under-conservative for high temperatures when compared to the other standards. There is no information provided regarding the background of the strength reduction factors in the Australian standard, but this discrepancy may come from the fact that it is the most outdated standard (dating back to 1998, as compared to 2005 in the case of EN 1993-1-2) or, quite possibly, due to a different definition of the proof stress at elevated temperatures. Furthermore, since 2005 the Eurocode has superseded the British standard BS 5950, with the only particularities being found in the corresponding national annex. For this reason, this thesis will consider only the international construction codes AISC, EN 1993 and AS 4100 for comparison purposes.

1.4 Problem description

Steel column design at room temperature in Eurocode 1993-1-1 is based on the so called "buckling curves": graphical representations of a semi-empirically formulated equation for the buckling resistance reduction factor χ which are differentiated (from "a_0" to "d") according to defined imperfection factors [8]. For elevated temperature design, Eurocode 1993-1-2 follows a somewhat similar approach; slightly modifying the equation for the buckling resistance factor with temperature-dependent reduction factors for yield strength and modulus of elasticity, as shown in figures 1.2 and 1.3, resulting in the buckling resistance reduction factor for fire condition χ_{fi}; and, if applicable, modifying the buckling length depending on the exposure and location of the column [5].

The problems with this strength reduction factor approach by the Eurocode, which has been adapted by the AISC code as well, are its limited applicability and questionable reliability. In any realistic fire scenario, a thermal gradient will develop throughout the cross-section of the column and throughout its length. The Eurocode considers a

uniform distribution using the highest temperature in the section as the design temperature. This neglects the presence of the thermal gradients and assigns weaker mechanical properties to those regions of the column that are below the design temperature. This approach is possibly over-conservative, since, depending on the location of the fire and orientation of the column, the temperature gradient between the coldest and the hottest parts of the section may be significant.

Furthermore, despite the fact that initial out-of-straightness, residual stresses and surface imperfections are taken into account for room temperature design [9], their influence is not described for elevated temperature design. In addition, the development in curvature of the stress-strain relationship of steel as temperature increases and its influence in buckling resistance is not mentioned in design standards.

1.5 Aim of this research

The aim of this research is to determine the buckling resistance of steel columns under fire conditions considering realistic temperature distributions and mechanical properties and to assess the reliability of the provisions given by Eurocode 1993-1-2 for elevated temperature design.

To achieve this, a finite element model that is able to accurately predict the flexural buckling capacity of a mild steel column at room temperature was created. The results of this model were compared to the buckling curves in EN 1993-1-1 for validation. The finite element model was then modified for elevated temperatures using information found in available literature to describe the behavior of mild steel at elevated temperatures. The results obtained through this model were used to create an elevated temperature buckling curve similar to that of the Eurocode. Finally, the finite element model was used to determine the flexural buckling capacity of steel columns with a realistic temperature distribution for the case of a column under the effect of a thermal gradient. The obtained results from this last finite element model were then compared to those given by the FEM-derived buckling curve as well as to the Eurocode, AISC 2005 and AS 4100 provisions.

The results of this research could be used for prediction and comparison in future tests. Another goal in this thesis is to determine if the existing data is sufficient to predict this phenomenon and if so, to encourage further research on the subject in hopes to lead to the modification of the applicable specifications in the leading construction codes to provide more efficient and safe designs in steel structures.

1.6 Thesis layout

The main parts of the working programme for this thesis are defined as follows:

- Literature Study
- Finite Element Model: Mild steel at room temperature
  - Creation of the finite element model
  - Validation against EN 1993-1-1 buckling curves
- Finite Element Model: Mild steel at elevated temperatures
  - Modification of the finite element model
  - Comparison results to EN 1993-1-2 buckling curves
  - Analysis of the influence of residual stresses
  - Analysis of the influence of the stress-strain relationship non-linearity
- Application of the finite element model to columns with realistic temperature distributions
  - Description of thermal gradients on the strong and weak axis of a column.
  - Definition of temperature-dependent stress-strain relationship.
  - Construction of the finite element model.
  - Results
  - Comparison of FEM buckling resistance with obtained buckling curves
  - Comparison with provisions of Eurocode 1993-1-2 and other international codes
- Conclusions and recommendations

Chapter 2

Literature Study

2.1 Flexural Buckling at Room Temperature

A steel element under compression can exhibit different failure mechanisms depending on its mechanical and geometrical properties as well as its support and bracing conditions. These failure mechanisms are flexural (or lateral) buckling, flexural-torsional buckling, local buckling or complete yielding of the cross-section. The failure mechanism that is most likely to govern the design of a long, unbraced steel column with a doubly symmetric cross-section is flexural buckling. Its resistance is based on the Euler theory on long struts [9]. Modern codes use a modified version of this theory to account for several factors, and though they may seem different to one another, all of them are analogous and follow the same theoretical background.

Eurocode 1993-1-1, section 6.3.1 shows the calculation procedures for the buckling resistance of uniform members in compression. The design buckling resistance is calculated through equation 6.47 for class 1,2 and 3 cross-sections:

$$N_{b,Rd} = \frac{\chi A f_y}{\gamma_{M1}} \tag{2.1}$$

Where χ is the buckling reduction factor. This reduction factor is applied for columns with a non-dimensional slenderness greater than 0.2, called "the limiting slenderness". Stocky elements with a slenderness below this value are considered to be non-critical for buckling and so only cross-sectional checks need to be performed [10].

The buckling resistance is thus strongly determined by this buckling reduction factor χ:

$$\chi = \frac{1}{\Phi + \sqrt{\Phi^2 - \bar{\lambda}^2}} \tag{2.2}$$

With:

$$\Phi = 0.5[1 + \alpha(\bar{\lambda} - 0.2) + \bar{\lambda}^2] \tag{2.3}$$

Where α is an imperfection factor depending on the geometrical properties of the cross-section of the element. Values for α are given in table 6.1 (recreated here as table 2.1). The different values of α result in the different buckling curves shown in Figure 6.4 of EN 1993-1-1. The lower the imperfection factor, the higher the buckling resistance will be. The selection of the buckling curve depends on the yielding strength (an S460 steel uses a lower imperfection factor than a S235 steel), the thickness of the flanges, the thickness of the welds (in the case of welded sections) and the buckling axis to be considered (in the case of sections without double symmetry).

TABLE 2.1: Imperfection factor α in EN 1993-1-1

Buckling curve	a_0	a	b	c	d
Imperfection factor α	0.13	0.21	0.34	0.49	0.76

The Eurocode also allows to calculate the buckling reduction factor from a series of curves called "buckling curves", which are a graphical representation of equation 2.2 for different values of the imperfection factor α, through which, by using the non-dimensional slenderness of the element $\bar{\lambda}$, the buckling reduction factor χ is obtained. The Eurocode buckling curves are shown in figure 2.1.

Originally, the buckling resistance of a column was calculated according to the studies of Ayrton & Perry in 1886. Later on, in 1925, Robertson determined empirical values for the imperfection factor based on various column tests, where he established the initial out-of-straightness of a column to be $\frac{L}{1000}$, and recommended the use of a buckling curve that provided a safe estimation of the column resistance according to experimental data. This was referred to as the Perry-Robertson approach and it set the basis for column design in the UK in the early 20th century. However, this approach was found to be over-conservative for low slenderness (stocky columns), where columns could resist loads that exceeded its yielding capacity due to strain hardening. To account for this, a lower-bound slenderness λ_0 was introduced based on experimental data, which led to the plateau in the low-slenderness region of the buckling curves used today (the limiting slenderness of 0.2 mentioned earlier)[9].

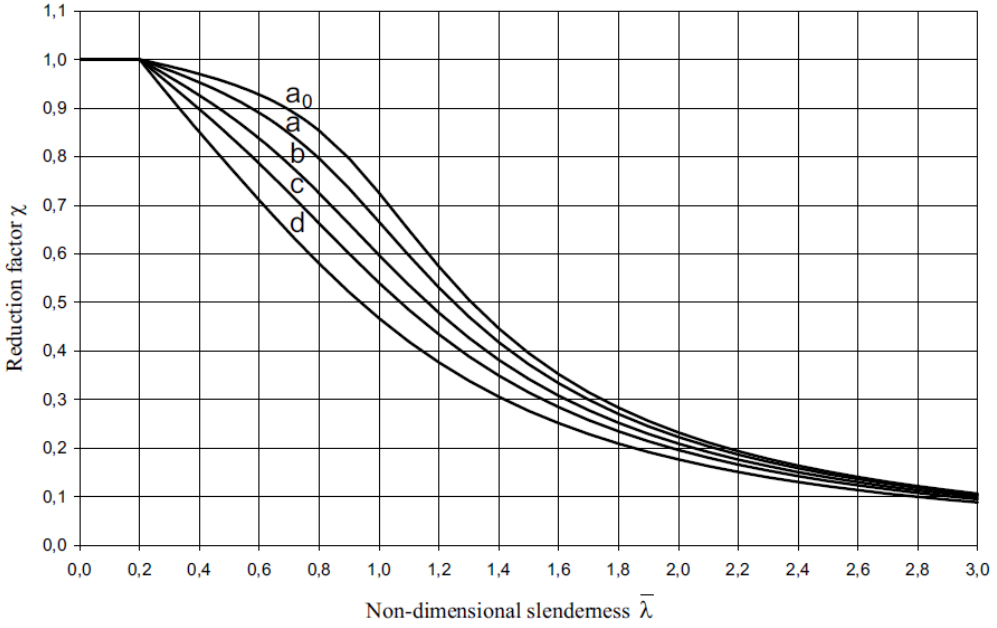

FIGURE 2.1: Buckling curves from NEN-EN1993-1-1

Subsequent research resulted in the adaptation of the current family of buckling curves ("a_0" to "d" in order of severity) in order to account for residual stresses in the most commonly used cross-sections[9].

The current state of the European design standard of steel columns therefore already accounts for initial imperfections, residual stresses and out-of-straightness based on experimental data. This design procedure has proven to be so efficient and reliable for room temperature design that similar provisions have been established for design of steel members at elevated temperatures.

2.2 Flexural Buckling at Elevated Temperatures

As mentioned in chapter 1, Eurocode 1993-1-2 provides reduction factors for the proportional limit, modulus of elasticity and effective yield strength (the 2% proof stress) for elevated temperatures. These factors represent the percentage of the remaining room-temperature strength at a specific temperature θ.They are indicated in figure 2.2.

The procedures for calculating the buckling load on steel columns at elevated temperatures are quite straight-forward and they differ very slightly from one standard to another. Once the adequate reduction factors for the material properties have been determined for a specific temperature, the same calculation procedures are to be carried

out. The equations used for these calculations are the same as the ones used for room temperature design, albeit with slight changes in safety factors and the inclusion of the reduction factors for the mechanical properties.

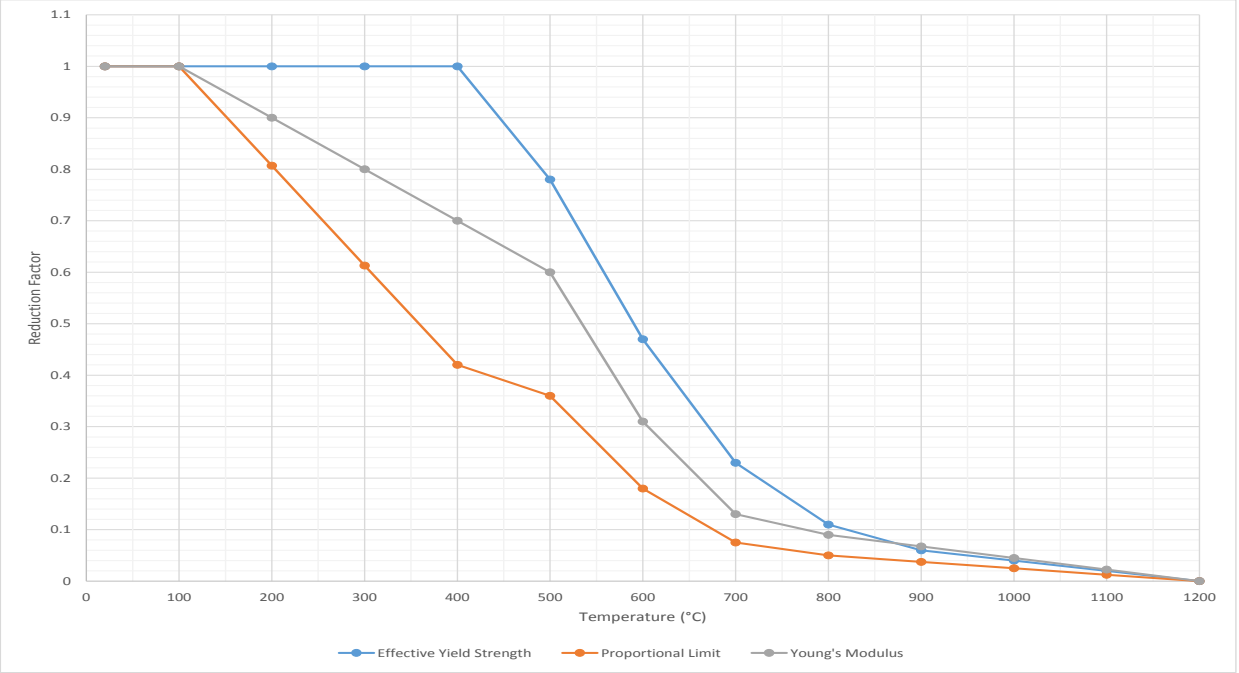

FIGURE 2.2: EC1993-1-2 Strength Reduction Factors

2.2.1 Eurocode 1993-1-2

In the case of Eurocode 1993-1-2, the calculation for the design buckling resistance is given by equation 4.5 (reproduced here as equation 2.4), which is similar to the equation for room temperature design on class sections 1, 2 and 3, with the differences being the reduction factor for buckling resistance in fire, χ_{fi}, the partial factor for fire situation, $\gamma_{M,fi}$ and the inclusion of the reduction factor for yield strength.

$$N_{b,fi,Rd} = \frac{\chi_{fi} \cdot A \cdot k_{y,\theta} \cdot f_y}{\gamma_{M,fi}} \tag{2.4}$$

Where:

$$\chi_{fi} = \frac{1}{\phi_\theta + \sqrt{\phi_\theta^2 - \bar{\lambda}_\theta^2}} \tag{2.5}$$

with:

$$\phi_\theta = \frac{1}{2}[1 + \alpha \cdot \bar{\lambda_\theta} + \bar{\lambda_\theta^2}] \tag{2.6}$$

and

$$\alpha = 0,65\sqrt{\frac{235}{f_y}} \tag{2.7}$$

With the non-dimensional slenderness $\bar{\lambda_\theta}$ for the temperature θ_a, given by:

$$\bar{\lambda_\theta} = \bar{\lambda}[\frac{k_{y,\theta}}{k_{E,\theta}}]^{0.5} \tag{2.8}$$

Where $k_{y,\theta}$ and $k_{E,\theta}$ are the reduction factors for the effective yield strength (2% proof stress) and modulus of elasticity respectively, as shown in figure 2.2 and defined as:

$$k_{y,\theta} = \frac{f_{y,\theta}}{f_y}$$
$$k_{E,\theta} = \frac{E_\theta}{E}$$

The partial factor for fire situation, $\gamma_{M,fi}$, in EN1993-1-2 is equal to 1. Buchanan recommends a value of $\gamma_{M,fi} = 1.2$ [2].

It is noteworthy that for elevated temperature design, the imperfection factor α, shown in equation 2.7, is no longer determined by the properties of the cross-section, but is rather a function of the yielding stress at room temperature. This is one of the details in EN 1993-1-2 that make the applicability of this approach questionable, since it eliminates the distinction between different cross-sections that is considered for room temperature design.

2.2.2 American Code: AISC 2005

Similarly as in the Eurocode, the AISC code allows for the design of compression members using the specified material properties for steel at elevated temperatures as shown in table A-4.2.1 of Appendix 4 and applying the provisions in chapter E of the AISC code [7]. For the case of flexural buckling:

$$\phi P_n = \phi F_{cr} \cdot A_g \tag{2.9}$$

The flexural stress, F_{cr}, is determined as follows:

When $\frac{KL}{r} \leq 4.71\sqrt{\frac{E}{F_y}}$:

$$F_{cr} = [0.568^{\frac{F_y}{F_e}}] \cdot F_y \tag{2.10}$$

When $\frac{KL}{r} \geq 4.71\sqrt{\frac{E}{F_y}}$:

$$F_{cr} = 0.877F_e \tag{2.11}$$

Where F_e is the elastic critical buckling stress as calculated from equation E3-4 (replicated here as 2.12)

$$F_e = \frac{\pi^2 E}{(\frac{KL}{r})^2} \tag{2.12}$$

In contrast to the EN-1993 specification, the slenderness parameter here is considered in the factor $\frac{KL}{r}$.

It should be noted that the resistance reduction factor ϕ, in the AISC is equal to 0.9 due to the uncertainties in material properties at elevated temperatures. Buchanan recommends a value of $\phi = \frac{1}{1.2} = 0.84$ for design in fire conditions [2].

2.2.3 Australian Code: AS 4100

Finally, the Australian standard AS 4100 determines the buckling capacity of a steel element with the following equations [11]:

Nominal member capacity (Clause 6.3.3):

$$N_c = \alpha_c \cdot N_s \tag{2.13}$$

With N_s being the nominal section capacity:

$$N_s = k_f \cdot A_n \cdot f_y$$

Where k_f is the form factor specified in clause 6.2.2 and the effective area A_e is determined according to clause 6.2.4 of AS 4100. The net area A_n may be substituted by the gross area A_g for sections without penetrations or unfilled holes.

$$k_f = \frac{A_e}{A_g}$$

The slenderness reduction factor α_c, which is analogous to Eurocode's χ factor is determined as:

$$\alpha_c = \xi \ [1 - \sqrt{[1 - (\frac{90}{\xi \cdot \lambda})^2]}] \tag{2.14}$$

With:

$$\xi = \frac{(\frac{\lambda}{90}90)^2 + 1 + \eta}{2(\frac{\lambda}{90})^2}$$

$$\lambda = \lambda_n + \alpha_a \cdot \alpha_b$$

$$\eta = 0.00326(\lambda - 13.5) \geq 0$$

$$\lambda_n = (\frac{l_e}{r})\sqrt{k_f} \cdot \sqrt{\frac{f_y}{250}}$$

$$\alpha_a = \frac{2100(\lambda_n - 13.5)}{\lambda_n^2 - 15.3\lambda_n + 2050}$$

Values for member section constant α_b are found in tables 6.33(1) and 6.33(2) of AS 4100. This member section constant is analogous to the classification of cross sections to a particular buckling curve in EC3. As in the AISC code, the safety factor for design resistance to be used here is 0.9.

2.2.4 Comparison between building codes

Some similarities and differences between the mentioned construction codes have already been pointed out in this chapter. However, to provide a clearer view of how these approaches are analogous to one another a brief additional explanation is provided in this

section.

Considering equation 2.8 from EN 1993-1-2:

$$\bar{\lambda_\theta} = \bar{\lambda}[\frac{k_{y,\theta}}{k_{E,\theta}}]^{0.5}$$

This can also be expressed as:

$$\bar{\lambda_\theta} = \frac{L_{cr}}{\pi \cdot r}\sqrt{\frac{f_y \cdot k_{y,\theta}}{E \cdot k_{E,\theta}}}$$

$$\bar{\lambda_\theta} = \frac{L_{cr}}{\pi \cdot r}\sqrt{\frac{f_{y,\theta}}{E_\theta}}$$

$$\bar{\lambda_\theta} = \sqrt{\frac{(\frac{L_{cr}}{r})^2 \cdot f_{y,\theta}}{\pi^2 \cdot E_\theta}}$$

Now, considering equation 2.10 from the AISC code for the case of $\frac{KL}{r} = \frac{L_{cr}}{r} \leq 4.71\sqrt{\frac{E}{f_y}}$:

$$F_{cr} = [0.568^{\frac{F_y}{F_e}}] \cdot F_y$$

Where $F_e = \frac{\pi^2 E}{(\frac{L_{cr}}{r})^2}$. Therefore, we can express F_{cr} as:

$$F_{cr} = [0.568^{\frac{(\frac{L_{cr}}{r})^2 \cdot f_y}{\pi^2 \cdot E}}] \cdot F_y$$

From this we can see that the AISC code equation can be expressed as:

$$F_{cr} = [0.568^{\bar{\lambda_\theta}^2}] \cdot F_y$$

The flexural buckling resistance in EN-1993-1-2 is calculated through equation 2.4:

$$N_{b,fi,Rd} = \frac{\chi_{fi} \cdot A \cdot k_{y,\theta} \cdot f_y}{\gamma_{M,fi}}$$

Which, through simple manipulation, can be written as:

$$N_{b,fi,Rd} = \frac{\chi_{fi} \cdot A \cdot f_{y,\theta}}{\gamma_{M,fi}}$$

Where $\gamma_{M,fi}$ is equal to 1.

Flexural buckling resistance, according to the AISC code, is calculated with equation 2.9:

$$\phi P_n = \phi F_{cr} \cdot A_g$$

Which, for the case of $\frac{KL}{r} = \frac{L_{cr}}{r} \leq 4.71\sqrt{\frac{E}{f_y}}$, can be expanded as:

$$\phi P_n = \phi \cdot [0.568^{\bar{\lambda_\theta}^2}] \cdot F_y \cdot A_g$$

Where ϕ is taken as 0.9 due to uncertainties in the material properties.

It must be noted that, when considering design at elevated temperatures in the AISC code, the values for E and f_y to be used are those corresponding for the design temperature in accordance with table A-4.2.1 of appendix A of the AISC code.

With the manipulation of the equations shown it can be seen how similar both codes are with regard to calculating the buckling resistance of a column. While EN 1993-1-2 uses the non-dimensional slenderness for the calculation of the buckling resistance factor χ_{fi}, the AISC code introduces it as an exponent to the empirically obtained value of 0.568. For the case in the AISC code where $\frac{KL}{r} = \frac{L_{cr}}{r} \geq 4.71\sqrt{\frac{E}{f_y}}$ the buckling resistance can be expressed in a similar way as:

$$\phi P_n = \phi 0.877 \cdot \frac{f_y}{\bar{\lambda_\theta}} \cdot A \cdot f_y$$

The coefficients 0.568 and 0.877 shown for both cases, as well as the slightly different formulation for buckling resistance in the latter case are the AISC code's way to account for element imperfections, residual stresses and initial out-of-straightness, much in the way EN-1993-1-1 does through the imperfection factor α [7, 10].

A direct comparison with the Australian standard AS 4100 is a lot more complicated given the numerous equations and tables involved in the design. However, parallels with the Eurocode and the AISC code can be found throughout the calculation procedure. The first parallel comes through the form factor k_f, shown in equation 2.2.3:

$$k_f = \frac{A_e}{A_g}$$

Where A_e is the effective area of the member and is calculated as the summation of the effective areas of the individual elements that compose the member, as specified in clause 6.2.4 of AS 4100. The effective width of an element is a function of the yielding stress (again, considering its degradation with increasing temperature) but also of the applicable value of the "plate element yield slenderness limit". The values for this slenderness limit are shown in table 6.2.4 of AS 4100 (reproduced here as figure 2.3). The form factor k_f will later on determine the value of the member section constant α_b, which differentiates various types of cross sections [11].

VALUES OF PLATE ELEMENT YIELD SLENDERNESS LIMIT

Plate element type	Longitudinal edges supported	Residual stresses (see Notes)	Yield slenderness limit, λ_{ey}
Flat	One (Outstand)	SR	16
		HR	16
		LW, CF	15
		HW	14
	Both	SR	45
		HR	45
		LW, CF	40
		HW	35
Circular hollow sections		SR	82
		HR, CF	82
		LW	82
		HW	82

NOTES:

1 SR—stress relieved
HR—hot-rolled or hot-finished
CF—cold-formed
LW—lightly welded longitudinally
HW—heavily welded longitudinally

2 Welded members whose compressive residual stresses are less than 40 MPa may be considered to be lightly welded.

FIGURE 2.3: Table 624 of AS 4100

As it can be seen from figure 2.3 and the relation between the from factor k_f and the member section constant α_b, this is how the AS 4100 code introduces the effect of residual stresses into the design.

In addition to this considerations, AS 4100 also uses the member slenderness reduction factor α_c, shown in equation 2.14 which, as it has already been mentioned, is equivalent of the buckling reduction factor in EN-1993-1-1.

2.2.5 Buckling curves at elevated temperatures

It can now be more clearly seen that the specifications in leading construction codes regarding the buckling resistance of a steel column at elevated temperatures are analogous to one another, albeit with small differences in material, slenderness, buckling, or resistance factors. Due to these similarities, this thesis will focus primarily on the Eurocode approach of the use of buckling curves and mechanical properties at elevated temperatures given that it is the most recent leading construction code and whose provisions have been adapted by the UK and the AISC (to some extent).

The design approach specified by the Eurocode for compression members at elevated temperatures is described in section 4.2.3.2 of EN-1993-1-2. The equations used in the calculations have already been described in the previous section. As mentioned, this approach is practically identical to the one for ambient temperature (20 °C) but with the use of the modified mechanical properties specified in table 3.1 of EN-1993-1-2.

In the same manner, buckling curves for elevated temperatures can be obtained by plotting χ_{fi} from equation 2.5 for different temperature levels. One of the differences that must be noted while doing this is that the imperfection factor α from equation 2.7 to be used in elevated temperature buckling curves is a function of the yielding stress at room temperature and not a function of the geometrical characteristics of the element to be evaluated. Lastly, the non-dimensional slenderness from EN 1993-1-1 section 6.3.1 is "normalized" by a factor $\sqrt{\frac{k_{y,\theta}}{k_{E,\theta}}}$ and uses the effective length corresponding to the fire scenario that is being modeled. Information on these effective lengths is found in section 4.2.3.2 of EC 1993-1-2.

Figure 2.4 shows the buckling curves for steel grade S235 at elevated temperatures. It can be seen that the behavior of the buckling reduction factor in fire χ_{fi} is very unintuitive, since an increase in temperature doesn't lead to a lower reduction factor for temperatures above 700 °C. This is due to the fact that these buckling curves are a function of the ratio $\frac{k_{y,\theta}}{k_{E,\theta}}$. The value of this ratio behaves erratically since the rate at which the factor $k_{y,\theta}$ and the factor $k_{E,\theta}$ decay are different. The reason for this is that the specific heat of steel increases with temperature, showing a large spike at around 750 °C, caused by a phase change in which the atoms in the steel structure move farther apart from each other, achieving a high energy state. During this phase change, the atoms shift from a face-centered cubic to a body-centered cubic structure. The large amounts of energy (heat) absorbed during this process is what causes the large spike in the specific heat of structural steels at 750 °C. This leads to a higher decrease in the modulus of elasticity and a slightly lower decrease in the yielding strength, thus increasing the

$\frac{k_{y,\theta}}{k_{E,\theta}}$ ratio, giving as a result higher buckling reduction factors as shown in figure 2.4 [12].

In a similar fashion, we can consider a specific temperature and determine the buckling curves for different steel grades. Figure 2.5 shows the buckling curves for a temperature of 700 °C for different steel grades.

By using either of these buckling curves, which are by themselves a graphical representation of the equation 2.5, the factor χ_{fi} is obtained and the lateral buckling capacity of a steel element can be calculated.

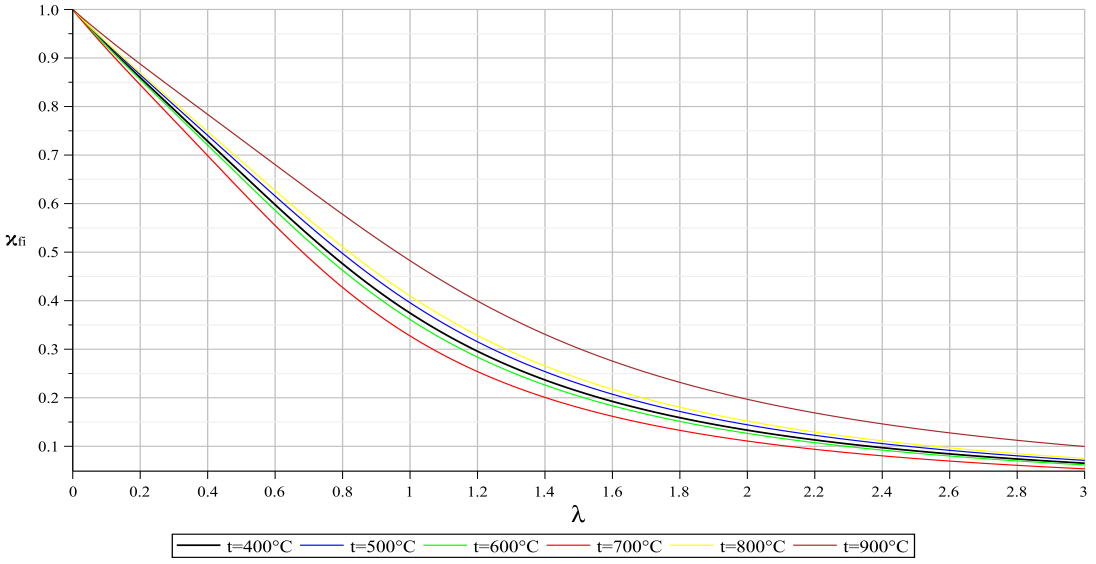

FIGURE 2.4: Buckling Curves for S235 at elevated temperatures

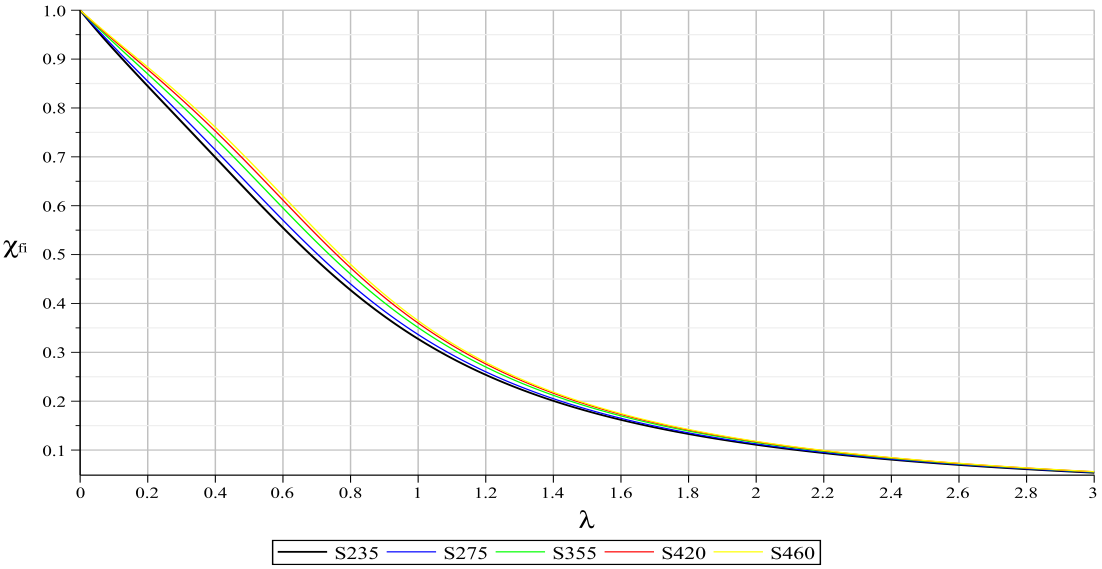

FIGURE 2.5: Buckling curves for mild steels at 700 °C

Similar curves as those depicted in figures 2.4 and 2.5 can be derived for different steel grades and temperatures. Further ahead, this will provide a basis for comparison with the results from the finite element model for mild steels at elevated temperatures.

2.2.5.1 Example of buckling resistance of a column at elevated temperatures

To illustrate how the flexural buckling resistance of a steel element decays with the increase of temperature let us consider an example with the following data:

- Section: CHS 244.5 x 10
- Steel grade: S275 ($f_y = 275N/mm^2$, $E = 210,000N/mm^2$)
- Buckling length: $L_{cr} = 4000mm$
- Section properties:
  - $d = 255.5mm$
  - $t = 10mm$
  - $A = 7370mm^2$
  - $I = 50,730,000mm^4$

Non-dimensional slenderness

$$N_{cr} = \frac{\pi^2 \cdot EI}{L_{cr}^2} = \frac{(\pi)^2(210000)(50730000)}{(4000)^2} = 6,571,491N$$

$$\bar{\lambda} = \sqrt{\frac{A \cdot f_y}{N_{cr}}} = \sqrt{\frac{(7370)(275)}{6571491}} = 0.56$$

Imperfection factor

$$\alpha = 0.65\sqrt{\frac{235}{f_y}} = 0.65\sqrt{\frac{235}{275}} = 0.6$$

With these values determined we can create a plot of buckling resistance and temperature through equations 2.8, 2.6, 2.5 and 2.4:

$$\bar{\lambda_\theta} = \bar{\lambda}[\frac{k_{y,\theta}}{k_{E,\theta}}]^{0.5}$$

$$\phi_\theta = \frac{1}{2}[1 + \alpha \cdot \bar{\lambda_\theta} + \bar{\lambda_\theta^2}]$$

$$\chi_{fi} = \frac{1}{\phi_\theta + \sqrt{\phi_\theta^2 - \bar{\lambda_\theta^2}}}$$

$$N_{b,fi,Rd} = \frac{\chi_{fi} \cdot A \cdot k_{y,\theta} \cdot f_y}{\gamma_{M,fi}}$$

The resulting graph for this example is shown in figure 2.6.

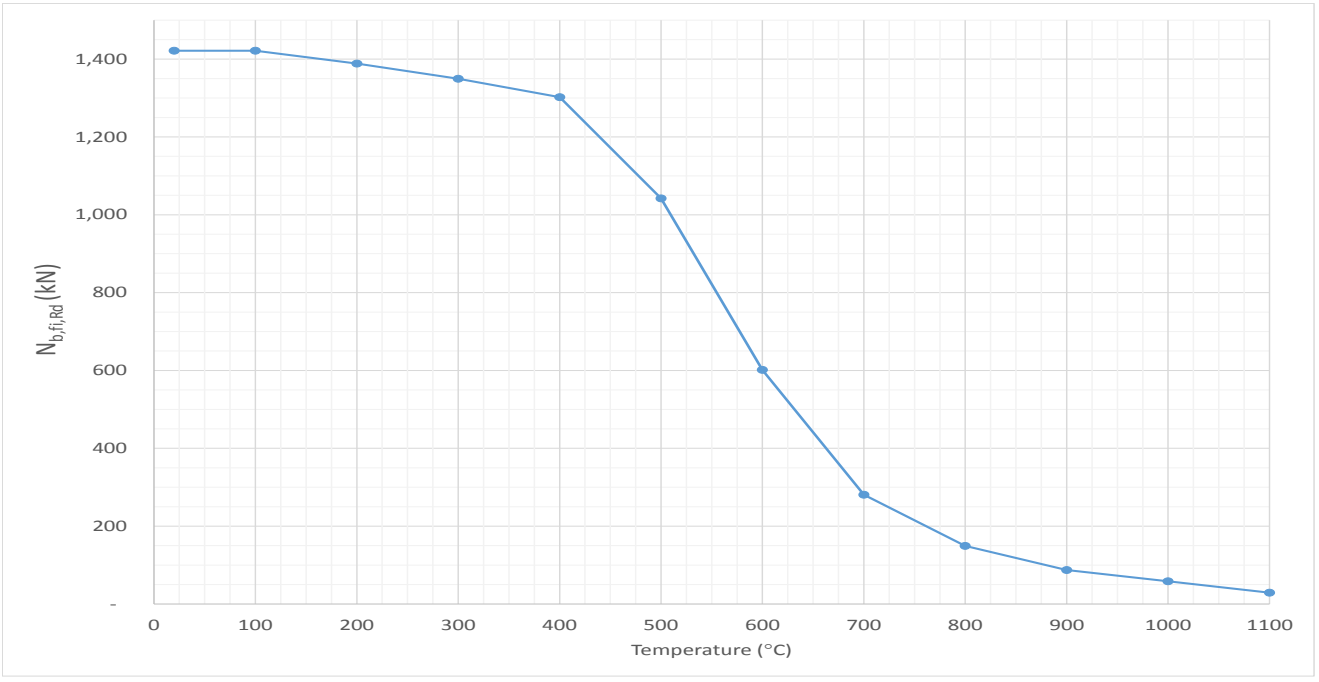

FIGURE 2.6: Flexural buckling resistance for CHS 244.5 x 10

To fully appreciate the over-conservative design approach from EN 1993-1-2 at low temperatures it is useful to calculate the room temperature resistance of this same cross-section:

Cross-section classification

$$\varepsilon = \sqrt{235/f_y} = \sqrt{\frac{235}{275}} = 0.9244$$

$$\frac{d}{t} = \frac{244.5}{10} = 24.45$$

$$50\varepsilon^2 = (50)(0.9244)^2 = 42.73 > 24.45$$

Therefore, the cross-section is class 1.

For hollow sections in S275 steel, table 6.2 of EN 1993-1-1 assigns the buckling curve a, which corresponds, according to table 6.1, to an imperfection factor α equal to 0.21. Therefore:

$$\Phi = \frac{1}{2}[1 + \alpha(\bar{\lambda} - 0.2) + \bar{\lambda}^2] = \frac{1}{2}[1 + 0.21(0.56 - 0.2) + (0.56)^2)] = 0.6915$$

$$\chi = \frac{1}{\Phi + \sqrt{\Phi^2 - \bar{\lambda}^2}} = \frac{1}{0.69 + \sqrt{(0.69)^2 - (0.56)^2}} = 0.9114$$

And the resulting flexural buckling resistance is:

$$N_{b,Rd} = \frac{\chi \cdot A \cdot f_y}{\gamma_{M1}} = \frac{(0.9114)(7370)(275)}{1.0} = 1,847,154.25N = 1,847.15kN$$

Using the equations for elevated temperature design, even while considering a temperature of 20 °C, for which the reduction factors for yielding strength and modulus of elasticity are equal to one, the flexural buckling resistance is equal to:

$$N_{b,fi,Rd} = 1,421kN$$

...which is already 22% lower than the design value given by the provisions for room temperature design. Figure 2.7 shows the development of the ratio between the flexural resistance at room temperature and the resistance for elevated temperatures for the column in this example.

The strength reduction factors provided by EN 1993-1-2 do not consider any decay in mechanical properties below 200 °C, yet the estimated flexural buckling resistance is already 25% lower than it would be at room temperature by this point. It is therefore quite evident that this might lead to over-conservative estimations, at least at relatively low temperatures.

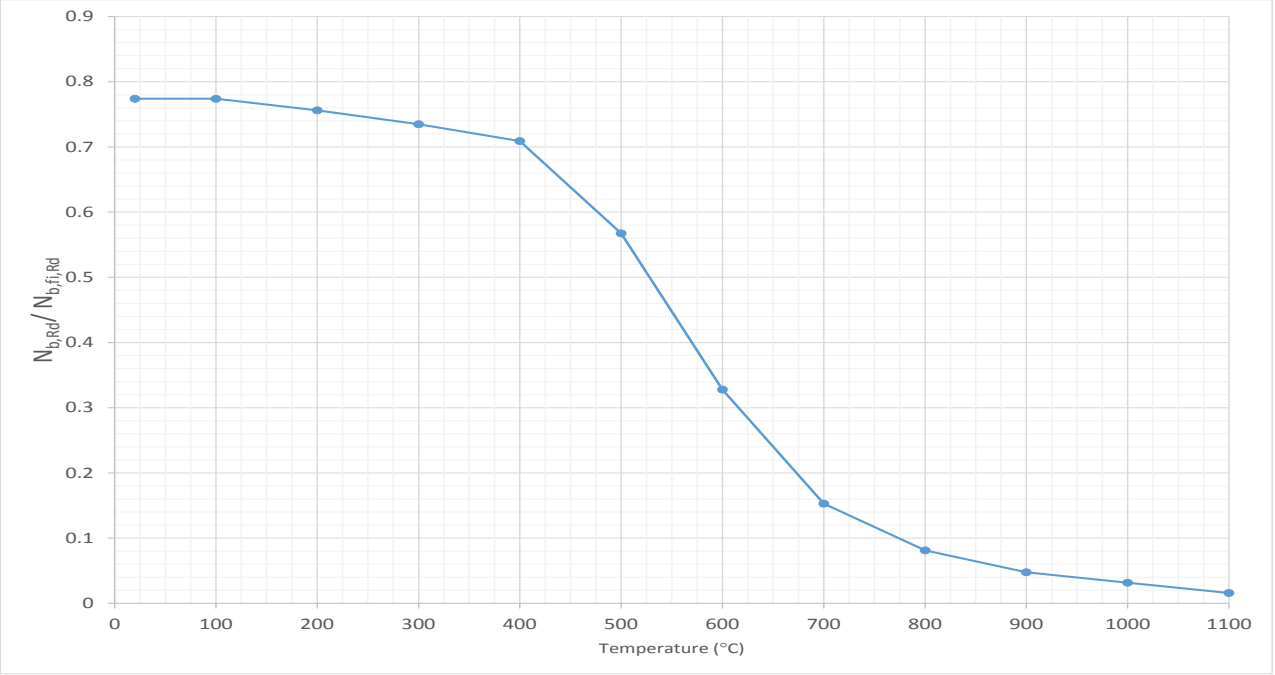

FIGURE 2.7: Ratio of flexural resistance at room temperature and elevated temperature resistance

2.3 Thermal gradients in a column

The scenarios in which a fire situation is present are infinitely varied, which makes it impossible to predict the conditions surrounding a steel column in a building fire. The inability to predict a realistic fire scenario has led to certain assumptions that stray from real life and neglect certain phenomena that may be present during a real fire. One such assumption is the uniform temperature distribution in a steel column under a fire. In a real fire, it is likely that there are columns being heated from only one or three sides (such as perimeter columns). The temperature difference between the gas in the upper and lower sections of the compartment will also create a thermal gradient throughout the length of the column. Both of these considerations are neglected in EN 1993-1-2. This might lead to over-conservative estimations of column resistance or over-spending in fire protection measures.

The reason for simplifying or neglecting temperature gradients in a steel member during a fire are mostly for simplicity purposes. Agarwal, Choe and Varma [13] mention some reasons for the neglecting of the thermal gradient throughout the length of a column during fire:

- The turbulence caused in post-flashover fires is too great and leads to the mixing of all the gas in the compartment, allowing for the designer to consider a uniform

temperature along the height of the column (single-zone model).

- The geometric properties of both fire protection and steel members are uniform throughout the length, allowing for an even temperature distribution.

When it comes to the consideration of thermal gradients through the cross-section, the main factors that determine the temperature distribution are the cross-sectional properties of the member (the section factor), the fire protection of the element and the direction of the fire [2]. For design purposes, typically a fully engulfed column is considered, and the temperature of the hottest cross-section is assigned to the entire element. The calculation of the steel temperature is mostly carried out by two 'lumped-mass' methods: the best-fit method and the step-by-step-method. This makes for a worst-case-scenario design. The problem with the uniform temperature consideration is that it may be detrimental for the design of an edge column. Olawale [14] and Garlock and Quiel [15] have shown that designing a column considering a uniform temperature distribution when that column is not being heated uniformly may lead to over-conservative estimations of its strength. This, of course, translates in higher material and fire protection costs.

When a column is non-uniformly heated, parameters such as slenderness, load level and direction of the thermal gradient come into play to determine the failure mechanism of the column. The failure of a column under the effect of a temperature gradient occurs because of two phenomena:

- Differential expansion of the cross section; the hotter side of the column expands more than the cooler side, leading to what is known as 'bowing'.
- Increase in temperature from one side only makes the section structurally asymmetric; The decrease in mechanical properties on the hotter side shift the center of stiffness towards the colder side.

Both of these occurrences will lead to second order moments within the column, making it behave like a beam-column. The specifics of the failure mechanism will be dependent on the magnitude of each of the mentioned parameters, making the column buckle towards the hot or the cold region surrounding it or, in some cases, fail through inelastic flexural-torsional buckling [13].

2.3.1 Thermal bowing

Whether it is in columns or beams, whenever there is a temperature gradient present in the steel element, the support restraints, coupled with the differential expansion of an unevenly heated member under fire will lead to what is referred to as "thermal bowing": an increasing out-of-plane deformation caused by restriction at the supports that results in second order bending moments acting in the section.

An axial restraint on a column will not lead to thermal bowing as long as it is heated uniformly (so that no temperature gradients are present in the cross-section). In this case, the column will fail by plastic yielding or flexural buckling at a certain critical temperature. Increasing the axial restraint may lead to premature failing and lower critical temperatures but, regardless, no thermal bowing will be observed [15]. The same goes for a braced perimeter column, which, even if a temperature gradient is present in the cross-section, will not exhibit thermal bowing due to the brace restraint and instead will fail by plastic yielding.

With this in mind we can say that the phenomenon of thermal bowing will be present in fixed, un-braced columns that present a temperature gradient in its cross-section.

2.3.2 Non-uniform temperature distribution in leading construction codes

In section 2.2 the provisions for the calculation of flexural buckling resistance in different leading construction codes was presented. These provisions were all for the scenario of a uniform temperature distribution. The considerations in each of the previously mentioned construction codes (EN 1993, AISC 2005 and AS 4100) for the case of a non-uniform temperature distribution will now be presented.

2.3.2.1 Eurocode 1993-1-2

As previously mentioned, Eurocode 1993-1-2 considers a uniform temperature distribution for design under fire conditions. This is specified in section 4.2.3.2 clause (6): "When designing nominal fire exposure the design resistance $N_{b,fi,Rd}$ at time 't' of a compression member with a non-uniform temperature distribution may be taken as equal to the resistance $N_{b,fi,\theta,Rd}$ of a compression member with a uniform steel temperature θ_a equal to the maximum steel temperature $\theta_{a,max}$ reached at time 't' " [10].

Overall, Eurocode 1993-1-2 provides no guidance for non-uniform temperature design in it's simplified methods and leaves the designer to determine the realistic temperature distribution and mechanical behavior of a structural element through advanced calculation models (i.e. computational tools).

2.3.2.2 American Code: AISC 2005

There are two mentions of non-uniform temperature distribution in AISC Specification for Structural Steel Buildings 2005:

- 4.2.2: The heat transfer analysis may range from one-dimensional analyses, where the steel is assumed to be at uniform temperature, to three-dimensional analyses. The uniform temperature assumption is appropriate in a "lumped heat capacity analysis" where a steel column, beam or truss element is uniformly heated along the entire length and around the entire perimeter of the exposed section...In cases with nonuniform heating or where different protection methods are used on different sides of the column, a one-dimensional analysis should be conducted for steel column assemblies.
- 4.2.4.3b: Simple methods (of analysis) may suffice when a structural member or component can be assumed to be subjected to uniform heat flux on all sides and the assumption of a uniform temperature is reasonable as, for example, in a free-standing column.

Within the commentary section of the AISC code it is mentioned that the thermal analysis provisions stipulated in this code lead to an over-estimation in member temperature [7]. It can be seen that the information provided for the designer is very limited for the case of non-uniform heating of elements and given the over-estimation of element temperature resulting from the thermal analysis provisions it is concluded that the overall approach from the AISC code is similarly conservative to the Eurocode 1993-1-2.

2.3.2.3 Australian Code: AS 4100

The Australian building code AS 4100 provides no specific information regarding non-uniform temperature distributions in members, but it does provide a distinction between four-sided and three-sided fire exposure in section 12.2 (a) [11]. AS 4100 provides separate equations to determine the time at which the limiting temperature is reached in unprotected steel members in section 12.7:

For three-sided fire exposure:

$$t = -5.2 + 0.0221T + \frac{0.433T}{k_{sm}} \tag{2.15}$$

For four-sided fire exposure:

$$t = -4.7 + 0.0263T + \frac{0.213T}{k_{sm}} \tag{2.16}$$

where:

t = time from the start of the test, in minutes
T = steel temperature, in degrees Celcius, $500\,^{\circ}\text{C} \leq T \leq 700\,^{\circ}\text{C}$
k_{sm} = exposed surface area to mass ratio, $2m^2/tonne \leq k_{sm} \leq 35m^2/tonne$.

Figure 2.8 shows a plot of the time for limiting temperature for three-sided and four-sided heating considering an exposed surface area to mass ratio of 10 m^2/tonne.

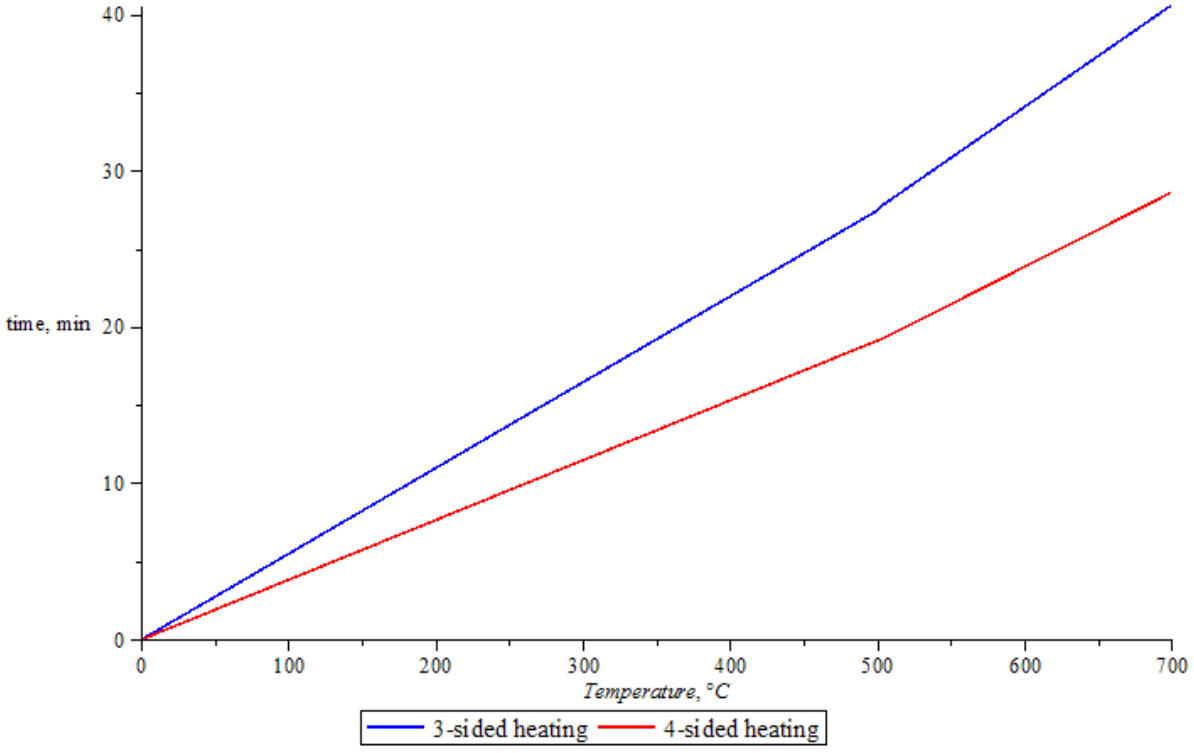

FIGURE 2.8: Time for limiting temperature for 3-sided and 4-sided heating according to AS 4100 [11].

As it can be appreciated in figure 2.8, the distinction between the two heating scenarios already provides a significant improvement in the fire resistance of columns heated on three sides. This serves as a good starting point of comparison with Eurocode 3 and the AISC code, which at this point seem relatively conservative by considering a uniform temperature distribution regardless of the fire scenario that is being considered. The Australian code provisions, however, come with a limited applicability, since equations 2.15 and 2.16 can only be used for the temperature range of $500\,^{\circ}\text{C} \leq T \leq 700\,^{\circ}\text{C}$. The AS 4100 code allows for linear interpolation for temperatures below 500 °C, which is what was done to generate the plot in figure 2.8, but it does not specify if linear interpolation is also allowed for determining the time to reach a limiting temperature above 750 °C.

As it was shown in this section, only the Australian building code makes any kind of distinction between uniform and non-uniform temperature distribution for the applicability of a simplified calculation method. The American and European standards both either consider a uniform temperature distribution, using the maximum temperature in the section, or advise the designer to use more advanced calculation models. The extensive work and time that need to be invested in performing a thermal analysis of an entire structure is so large that the question of whether these provisions are adequate for overall design becomes a more pressing matter.

2.4 Temperature distributions in literature

The significance of a non-uniform temperature distribution in a steel column has been discussed in section 2.3. It was mentioned how the shift in the stiffness center of the cross-section and the effect of differential thermal expansion have a role in determining the failure mode and the buckling capacity of the column. Given that these considerations are mostly neglected in the construction codes discussed in this chapter it is important to determine its effects on the buckling capacity of a column and to asses whether the simplifications in these construction codes are conservative or un-conservative for design of steel columns at elevated temperature. To this end, temperature distributions of unevenly heated I-shaped cross-sections obtained from literature will be presented and applied to the finite element model for a comparison with the mentioned construction codes. Three main sources were taken into account: Agarwal, Dwaikat and Boon [13, 15, 16].

The tests conducted by Agarwal et al. consisted of a series of specimens in three different fire configurations: uniform heating, a thermal gradient along the web and a thermal

gradient along the flanges. No thermal gradient along the length of the beam was considered in the tests due to the consideration of a post-flashover fire situation in which the air turbulence is high enough to allow for the consideration of a single-zone fire model. The configuration of the tests as well as the results are recreated here as figure 2.9.

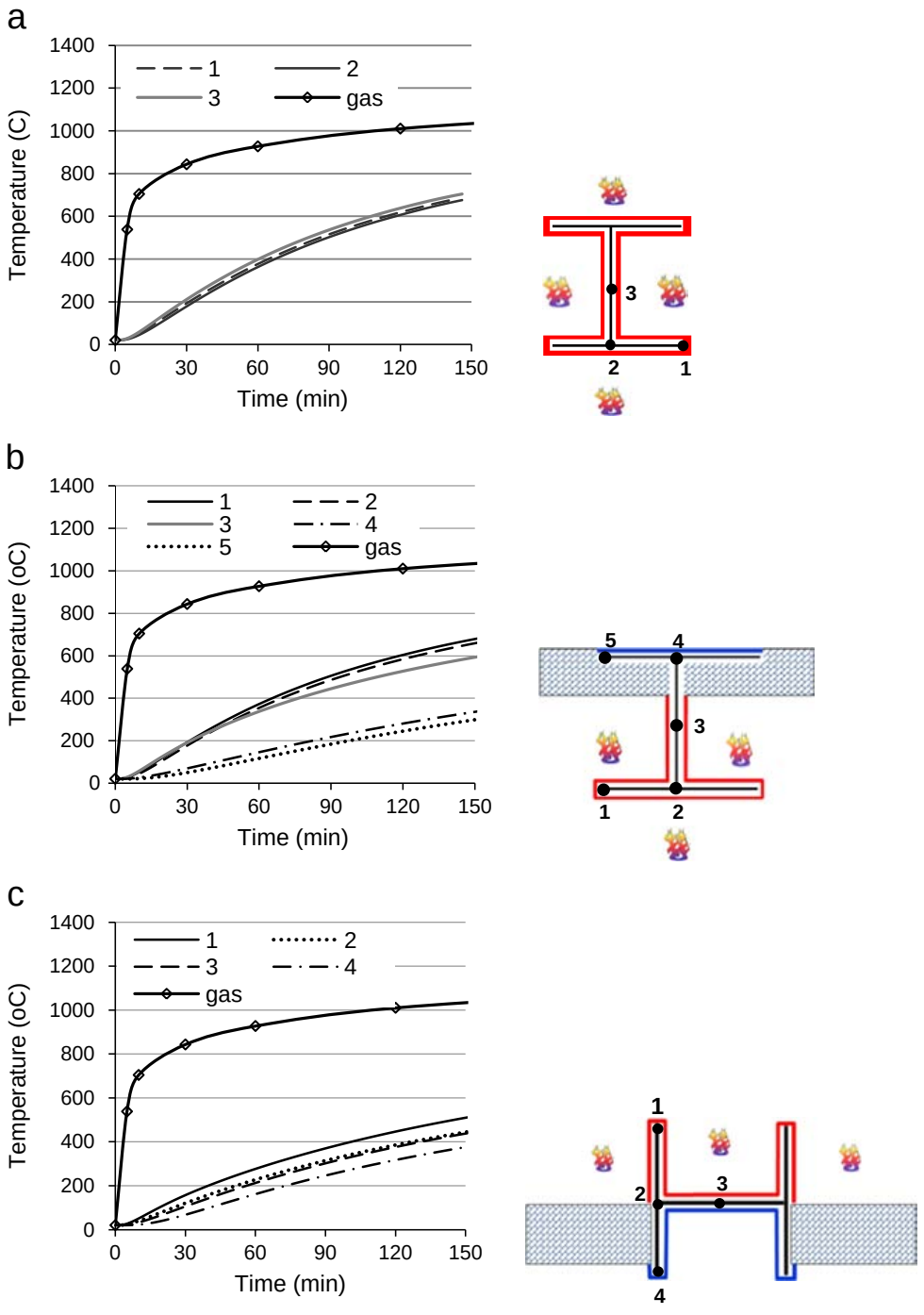

FIGURE 2.9: Testing configurations and temperature results of Agarwal et al. [13]

Figure 2.9 shows no significant temperature difference for the section with uniform heating, as would be expected. However, the sections with uneven heating show significant

temperature differences between certain points of the cross-section, particularly in the case of a thermal gradient along the web, where the maximum temperature difference is close to 400 °C. It was found that a significant moment component due to the asymmetry in the cross-sectional properties was always present. This effect, as well as the thermal bowing effect were considered simultaneously in the posterior analysis but it was unclear whether the net influence of these effects would reduce or increase the load carrying capacity of the column. In the end, Agarwal et al. concluded that there could be combination of loads, slenderness values and thermal loading patterns for which the assumption of uniform thermal loading would lead to unsafe column design [13]. This conclusion makes the necessity of an assessment of current design considerations even more imperative.

In the tests performed by Dwaikat et al., column specimens were placed in a furnace where they would be fully exposed to fire. The specimens were covered with spray-on fire resistive material which was removed in specific locations to allow for a thermal gradient to develop. Thermal gradients along the weak and strong axis were considered for exposure to two fire curves. The test configuration is shown in figure 2.10 and the tests results are shown in figure 2.11.

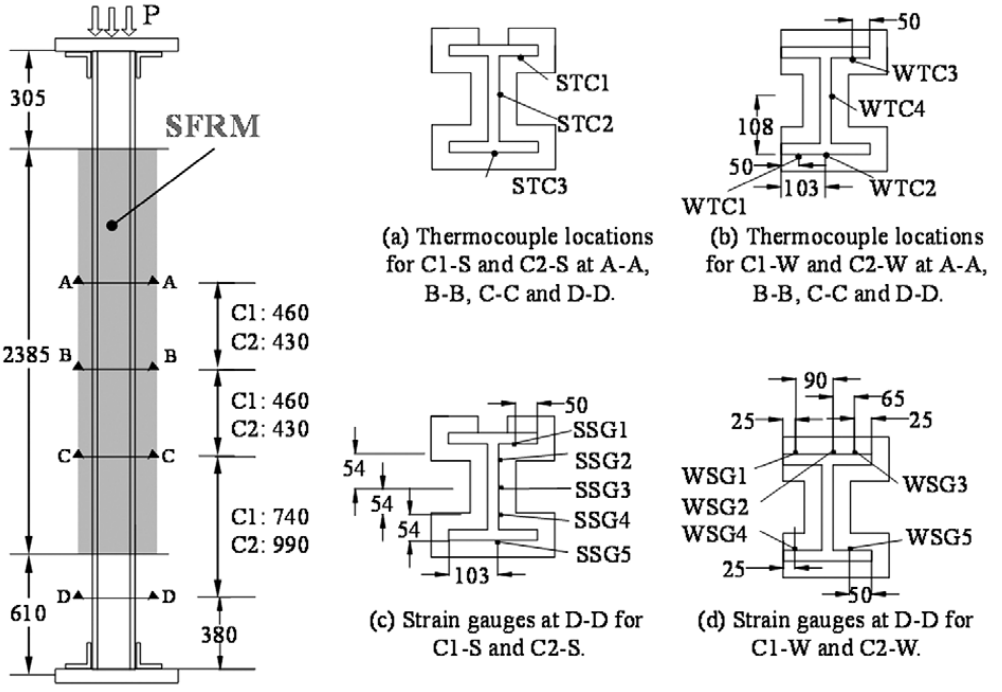

FIGURE 2.10: Test schematization ans specimen preparation in Dwaikat study [15].

The test results by Dwaikat et al. show a significant temperature difference in the specified point of the cross-section, particularly in the case of a thermal gradient along the strong axis under the effect of a design fire. It was found that failure occurred in the

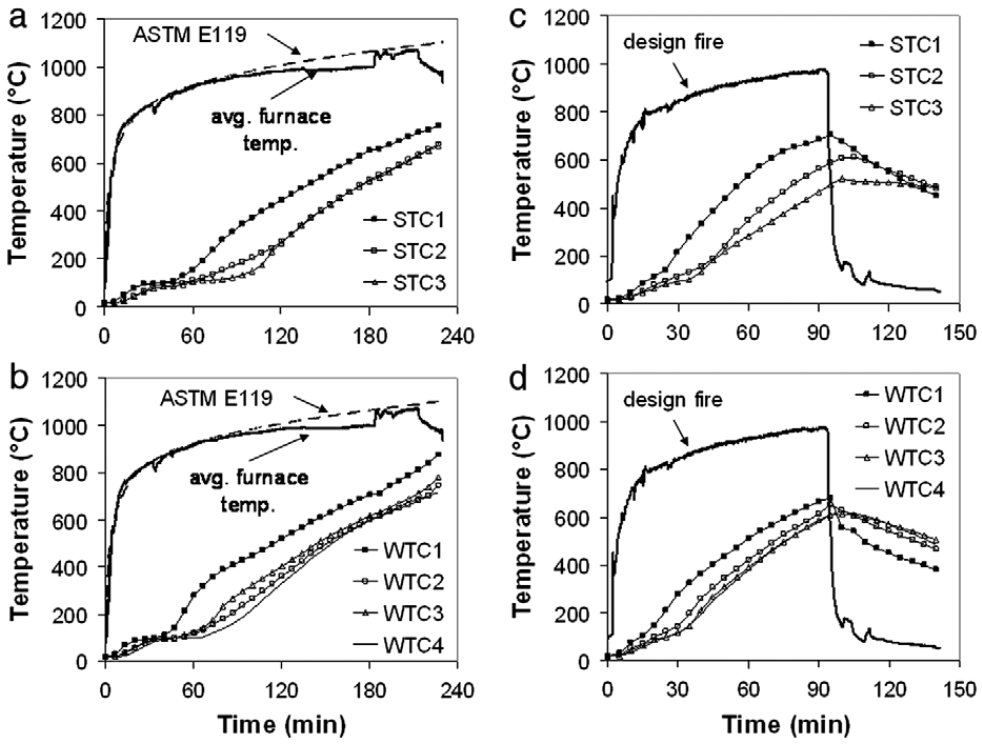

FIGURE 2.11: Temperature results of Dwaikat et al. [15].

location with the highest temperature. It was concluded that the load level, fire scenario and direction of the thermal gradient all have a significant influence on the fire response of the element [15].

The study of W. Boon consisted in analyzing the effect of thermal gradients on I-shaped steel columns under the effect of a "pool fire". To achieve this, a computational model where two columns were exposed to a design fire corresponding to a hydrocarbon combustion was created. The geometry of the compartment, the characteristics of the fire and its location relative to the steel column were modeled for a case where the element was exposed to a thermal gradient along its strong and its weak axis. Boon obtained a detailed thermal analysis for both fire scenarios, in which a thermal gradient along the length of the element was also observed. The temperature at specific points in the cross-section were monitored throughout the analysis and detailed results were provided for the cases of maximum temperature and maximum thermal gradient for each fire scenario [16].

The temperature distributions obtained from the studies by Agarwal, Dwaikat and Boon offer a reliable input alternative for the last phase of this thesis, which in turn improves the reliability on the final assessment regarding the Eurocode's accuracy for the determination of buckling resistance under fire conditions.

Chapter 3

Mild Steel at Room Temperature

3.1 Finite Element Model

The first stage of this study consisted on building a finite element model (FEM) for a simplified problem that allows for validation so that the final results can be considered reliable. For such a purpose, this first phase consisted on modeling a FEM of a mild steel column at room temperature under a compression load. The results from the analysis of this model were compared with the current Eurocode 1993-1-1 buckling curves shown in Figure 6.4 of EN 1993-1-1. Given that the buckling curves have proven efficient in calculating the buckling resistance of columns for half a century, a comparison with the results of the FEM analysis will provide a good starting point for the numerical study on column buckling under fire conditions.

The approach for this stage of the study was to select five different commercially available steel cross-sections with geometrical and mechanical properties that comply with the classification for each buckling curve (from 'a_0' to 'd'). Due to discrepancies shown in the obtained buckling curves for the 'a_0' and 'a' cross-sections, two additional steel shapes were tested, yielding a total of 7 cross-sections. Several FEMs were created for each cross-section, each with a different value for non-dimensional slenderness $\bar{\lambda}$ ranging from 0.1 to 3.0 at intervals of 0.1, giving a total of 30 FEMs for each cross section. In the analysis for each model, the maximum vertical reaction in the column was registered as the buckling load $N_{b,Rd}$, from which the buckling reduction factor χ was calculated using equation (2.1):

$$N_{b,Rd} = \frac{\chi A f_y}{\gamma_{M1}}$$

The resulting values for the buckling reduction factor were plotted against the corresponding non-dimensional slenderness value and superposed with the respective buckling curve from EN 1993-1-1.

In order to obtain results as reliable as possible, the conditions of the original tests conducted for the determination of the buckling curves were reproduced as closely as possible. These conditions refer to the support conditions of the columns, the type of loading, the initial out-of-straightness and the estimated residual stresses in the cross section.

3.1.1 Selection of steel cross-sections

The selection of the cross-sections to be used for the study was made through the "Tata steel sections interactive 'blue book'", a digital tool with the catalog of Tata steel's commercially available steel profiles and their geometrical properties. Using this tool, the available profiles were cross-referenced with the geometrical and mechanical requirements specified in table 6.2 of EN1993-1-1. The specifications for rolled sections for buckling about the z-z axis corresponding to each buckling curve are summarized in table 3.1. When a steel grade lower than S 460 is to be used Eurocode EN1993-1-1 assigns the same buckling curves for steel grades S 235, S 275, S 355 and S 420. In table 3.1 only steel grade S 275 is mentioned as it is the steel grade used in the FEMs. The geometrical properties of the shapes selected for the model are summarized in table 3.2.

TABLE 3.1: Buckling curve classification for rolled sections buckling around the z-z axis according to EN1993-1-1 table 6.2

Buckling curve	Steel grade	h/b ratio	Flange thickness, t_f
a_0	S 460	$h/b \geq 1.2$	$t_f \leq 40mm$
a	S 460	$h/b \geq 1.2$	$t_f \leq 100mm$
b	S 275	$h/b \geq 1.2$	$t_f \leq 40mm$
c	S 275	$h/b \leq 1.2$	$40 \leq t_f \leq 100mm$
d	S 275	$h/b \leq 1.2$	$t_f \leq 100mm$

3.1.2 Construction of the Finite Element Model

The finite element analysis was performed with the software Diana 9.4.4 created by TNO. The input and post-processing for the FEM were performed through the user interface FX+, also by TNO.

[1]The profile selected for curve 'd' is the same as the one selected for curve 'c', although with a thicker flange of 110 mm. This was due to lack of availability of a section suitable for curve 'd'.

TABLE 3.2: Geometrical Properties of Selected Cross-sections

Buckling Curve	Cross Section	Steel grade	h [mm]	b [mm]	t_w [mm]	t_f [mm]	I_{zz} $[mm^4]$	r [mm]	A $[mm^2]$
a_0	UKB 457 x 191 x 161	S 460	492	199.4	18	32	$42.5x10^6$	45.5	20,600
a_0	UKB 152 x 89 x 16	S 460	152.4	88.7	4.5	7.7	$89.8x10^4$	21	2,030
a	UKB 1016 x 305 x 487	S 460	1036.3	308.5	30	54.1	$267x10^6$	65.7	62,000
a	UKC 203 x 203 x 127	S 460	241.4	213.9	18.1	30.1	$49.2x10^6$	55	16,200
b	UKB 457 x 191 x 161	S 275	492	199.4	18	32	$42.5x10^6$	45.5	20,600
c	UKC 356 x 406 x 634	S 275	474.6	424	47.6	77	$981x10^6$	110	80,800
d	UKC 356 x 406 x 634[1]	S 275	474.6	424	47.6	110	$1400x10^6$	115.15	105,597

The model was built using quadratic, 8-noded, shell elements (CQ40S) in three parts; the web, the flanges and the support plates. It was decided to use shell elements to allow for an accurate modeling of the sections (which can be thought of three plates fused together) without the increased processing power that would have been required with 3D elements. The web and flange portions were fused together and the mesh was created so that in any direction at least four elements could be created. This was chosen in order to keep the computation time as low as possible while still maintaining reasonably accurate results. In cases where it was decided that more precision was required, the mesh was refined as needed(more will be discussed on this matter).

It should be noted that by using shell elements in the model, the small radius in the joint between the web and the flanges is ignored. The change in geometrical properties by neglecting this was deemed sufficiently small (less than 0.6% in area reduction). Since the column fails due to flexural buckling around its weak axis, the stiffness reduction due to this reduction is also deemed sufficiently small to be neglected. However, due to the way that shell elements are created, the flanges and the web overlap in a small area of magnitude $A_a = t_w \cdot t_f$ which in turn increases the cross-sectional area in the calculations. This is of special importance in very low-slenderness ($\bar{\lambda} \leq 0.2$) models since the ultimate load of the columns is controlled by yielding of the cross-section. The overlap in the web-flange intersection is schematized in figure 3.1.

3.1.3 Parameters of the Finite Element Model

Support Conditions

The columns were modeled as pin-ended columns. In order to achieve this, support plates were modeled at both ends. These support plates were given considerable stiffness, in order to not be deformed with very high loads and to distribute the load uniformly in the column's cross section. The plates were modeled with a linear support condition,

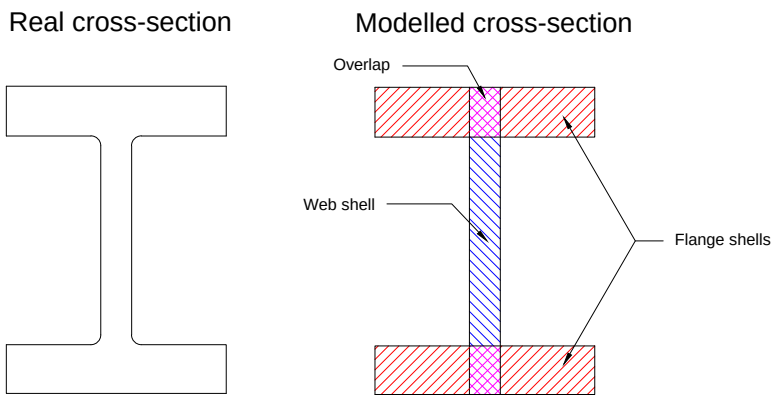

FIGURE 3.1: Overlap between flange and web shells in the finite element model.

aligned with the column's web, that allows for rotation around the column's z-z axis and restrains displacements in all directions. Figure 3.2 shows a modeled column with the support plates.

The choice for this support condition was in order to replicate the original tests from which the buckling curves were derived [9], which used pin-ended columns. The stiff plate solution was used in order to allow the rotation of the column without introducing excessive stress concentrations in the section's web at the supports. Without the plates, it was found that the applied load was unable to be distributed to the entire cross section, which led to premature failure due to yielding of the web.

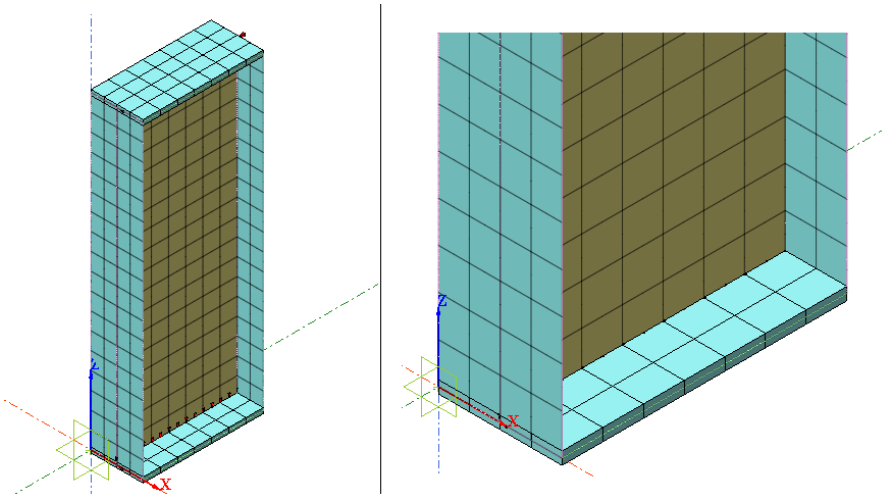

FIGURE 3.2: Modeling of support plates: Entire model(Left). Support plates closeup (Right).

Loading

The load was applied to the column as a vertical, uniform prescribed displacement in the support plates aligned with the column's web. The application of the load was chosen this way in order to allow the column to rotate in a way consistent with a pin-ended column. A uniformly distributed prescribed displacement across the entire cross-sectional area led to a restrained vertical displacement, which is another reason why the support plates were implemented. The prescribed displacement was increased with the length of the columns in order to obtain the full range of the load-displacement curve; columns in the slenderness range of $\bar{\lambda} \leq 0.5$ were applied a 5 mm vertical prescribed displacement while the columns in the range of $0.5 \leq \bar{\lambda} \leq 1.0$ were given a 10 mm displacement and the columns with $\bar{\lambda} \geq 1.0$ were given a 15 mm displacement.

Figure 3.3 shows a schematization of the application of the prescribed displacement along the axis of the column.

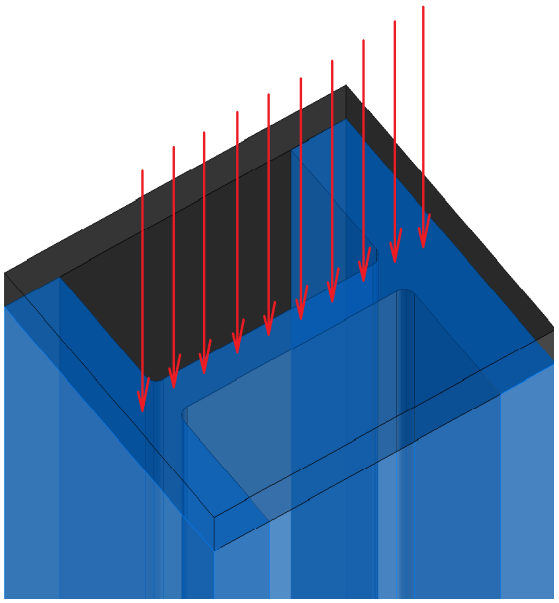

FIGURE 3.3: Application of the prescribed displacement on the column

Initial out-of-straightness

As discussed in section 2.1, one of the parameters that are considered in the imperfection factor α is the initial out-of-straightness of the column, which was determined to be $\frac{L}{1000}$ by Robertson in 1925 [9]. This initial deformation follows a half-sinusoidal shape with a maximum deformation at $\frac{L}{2}$. This deformation field coincides with the shape of the first eigenmode of a slender column, i.e. with a non-dimensional slendernes $\bar{\lambda} \geq 0.2$.

The application of this initial condition was performed during the analysis stage by considering a two-step analysis: a stability analysis and a non-linear analysis. During the stability analysis, the desired number of eigenmodes are calculated and a maximum prescribed displacement can be applied following the pattern of the desired eigenmode. Therefore, for each FEM a stability analysis was performed where the first buckling mode would be calculated and subsequently an imperfection of $\frac{L}{1000}$ was applied. This displacement field was then set as an initial condition for the subsequent non-linear analysis.

Figure 3.4 shows the deformed shape following the first buckling mode obtained using this method.

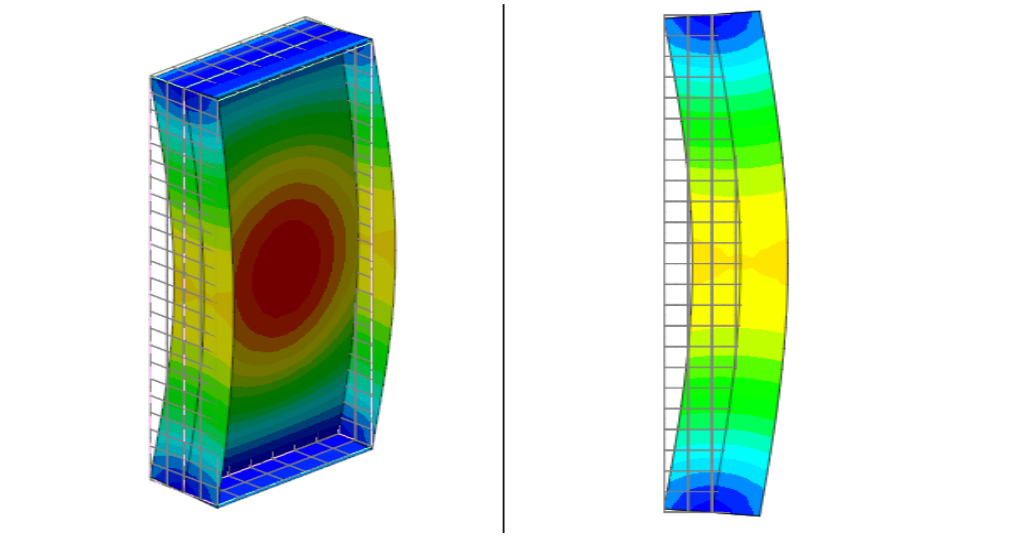

FIGURE 3.4: Initial out of straightness of a modeled column.

Residual Stresses

The final parameter for the input in the FEMs was an initial prestressing in the column's elements to model the residual stresses in the cross-section of each column. The magnitude and distribution of residual stresses in the cross-section of a rolled shape vary throughout literature. Figure 3.5 shows a comparison between the theoretical stress distribution in the cross-section and the 'Lehigh' stress distribution considered by the AISC code [7]. Figure 3.6 shows the comparison with the 'European' stress distribution given by the Swedish code BSK 99 and previously by the Dutch code NEN 6771 [17, 18]. It should be noted that while the Lehigh pattern assigns the same magnitude and distribution of residual stresses, the European pattern keeps the same distribution but varies the magnitude of the residual stresses based on the h/b ratio. This could be attributed to the fact that Deierlein and White consider the Lehigh pattern as representative of

"typical" wide-flange cross-sections. They also give the designer freedom to use residual stress patterns according to the cross-section being considered [19].

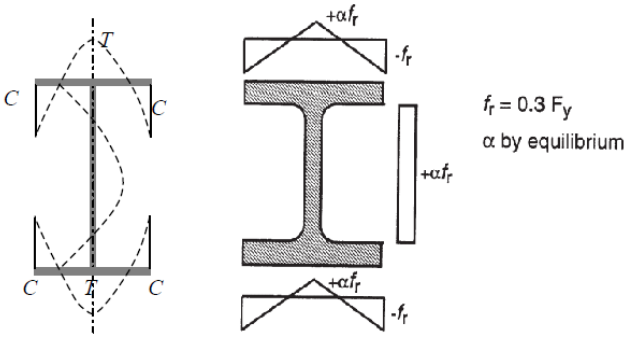

FIGURE 3.5: Theoretical residual stress distribution (Left) and Lehigh residual stress pattern (Right) for hot-rolled sections.

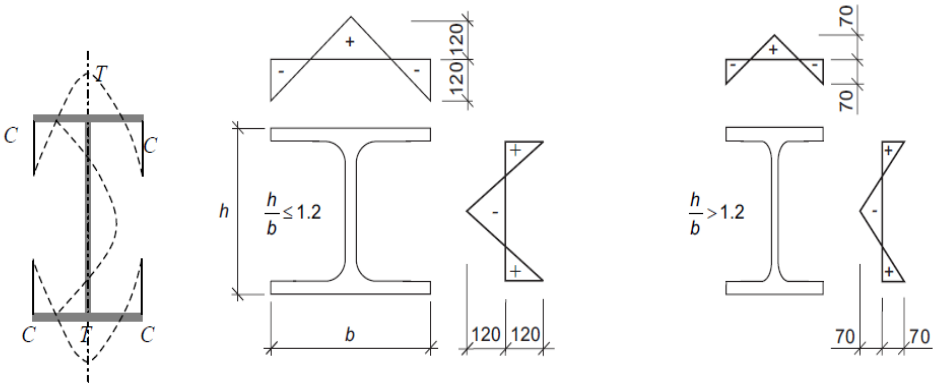

FIGURE 3.6: Theoretical residual stress distribution (Left) and the BSK 99/NEN6771 residual stress pattern (Right) for hot-rolled sections.

Different configurations of residual stress magnitude and distribution were tested in the model and it was found that for the selected cross-sections the closer fit to the Eurocode 1993-1-1 buckling curves was obtained by considering a combined approach; the Lehigh stress distribution pattern and the stress magnitude of the BSK 99/NEN 6671 codes.

The residual stresses were applied as an initial condition load case in the non-linear analysis of the model.

3.1.4 Analysis Parameters

As mentioned in the previous section, the analysis for the finite element model was performed in two steps: a stability analysis and a non-linear analysis. In the former, the

buckling mode is calculated and the initial imperfection of $\frac{L}{1000}$ is applied. The results of this stability analysis carry on as input for the non-linear analysis, which consists of two load cases:

1. Residual stresses: Applied as prestressing in the longitudinal direction of the column (σ_{zz}) in a single step. The results of this load application carry on as input for the next step.

2. Prescribed displacement: Applied as an incremental step loading. To ensure the interpolation between steps resulted in a smooth load-displacement graph the size of each step of load increase was set as 2.5% of the total prescribed displacement, resulting in a total of 40 steps. In cases where further precision was required the step size was reduced to 2.0% for a total of 50 steps.

The non-linear analysis considered physical and geometrical non-linearity. The material model used was an elasto-plastic stress-strain relationship with plasticity occurring at a stress equal to the yielding stress of the material f_y (275 or 460 N/mm^2). The iteration method chosen for the analysis was the Newthon-Rhapson method and the convergence norm for the iterations was a displacement controlled norm with a tolerance of 0.01 mm in relative displacement variation.

3.2 Results

Once the analysis for each FEM was finished, the vertical reaction of the nodes in the lower support were added up and plotted against the prescribed vertical displacement. The maximum reaction in this load-displacement graph was then taken as the value for the buckling resistance $N_{b,Rd}$ of the column. Figure 3.7 shows the load-displacement curve of the cross section for curve 'b' (457 x 191 x 161) with a non-dimensional slenderness $\bar{\lambda} = 1.0$ and a prescribed displacement of $\delta_{pres} = 15mm$.

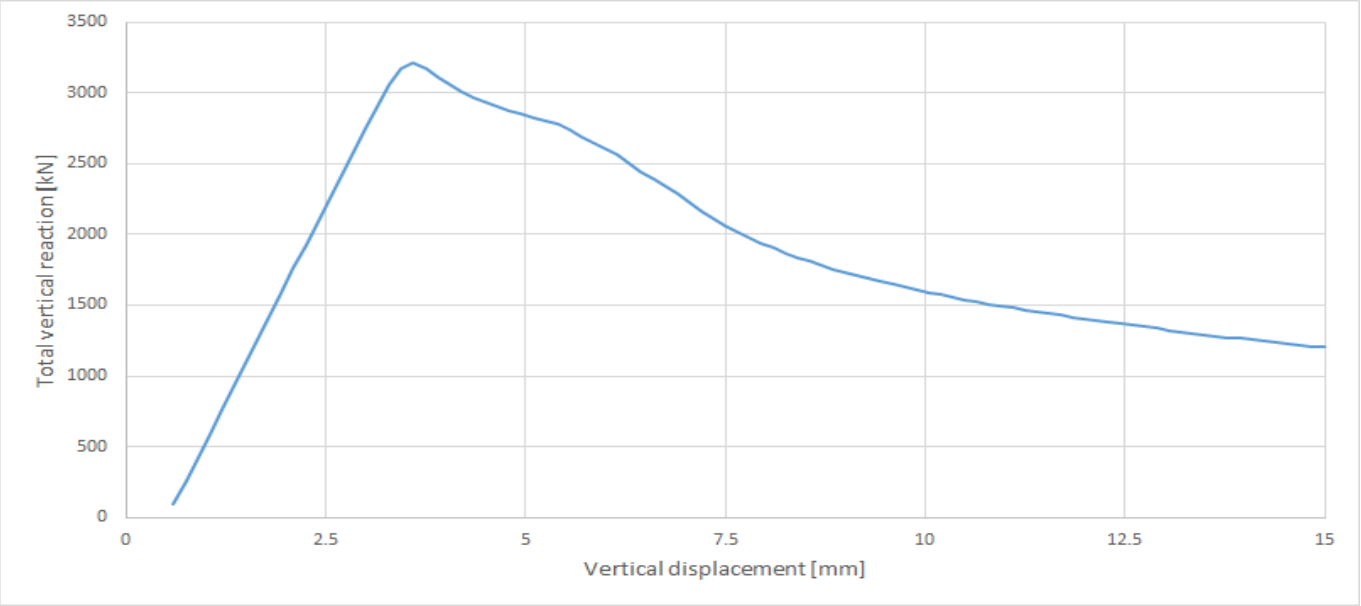

FIGURE 3.7: Load-displacement curve for 'b' cross-section with $\bar{\lambda} = 1.0$.

The load-displacement curve shown in figure 3.7 displays a linear relationship up until the maximum bearable load by the column, which occurs at a prescribed vertical displacement of 3.6 mm and has a magnitude of 3,218.6 kN. It is at this point where the column buckles due to compression yielding in the flanges. Figure 3.8 shows the deformation and stresses in the longitudinal direction (σ_{zz}) of the column at the point of the onset of buckling. It can be seen that the compression stresses in the flanges in the blue area have already exceeded the yielding stress ($275N/mm^2$) and thus the instability failure is triggered. The reason why figure 3.8 shows stresses higher than the yielding stress in the section is due to the linear interpolation (or extrapolation) between integration points. As the buckling load is reached and subsequently exceeded, the cross-section begins to plastify from the edge of the flanges towards the web. The finite element analysis calculates the normal stress in the elements of the edge of the flanges (which at this point is equal to the yield stress) and performs and extrapolation to determine the normal stress at the very edge of the flange. This overestimation of normal

stresses would be reduced with a finer mesh size near the edge of the column flange edges.

The magnitude of the vertical reaction at this point is therefore the buckling load $N_{b,Rd}$ of the column for $\bar{\lambda} = 1.0$. The buckling load divided by the squash load, $A \cdot f_y$ gives the buckling reduction factor χ. This analysis and post-processing is repeated for different values of $\bar{\lambda}$ to determine the buckling curve for each column.

The five types of cross sections, corresponding to each buckling curve, were modeled for 30 different values of $\bar{\lambda}$ and the results processed as it has just been described. The comparison between the Eurocode 1993-1-1 and the results from the finite element analysis are shown in figures 3.9 to 3.13

3.3 Discussion of the Results

The obtained buckling curves shown in figures 3.9 to 3.13 will be discussed separately to indicate the particularities found in each case.

3.3.1 Curves 'a_0' and 'a'

Shown in figure 3.9 and 3.10 respectively, the graphs shows an overall good agreement with the Eurocode buckling curves. However, there are some relatively significant differences in the medium slenderness range i.e. from $\bar{\lambda} = 0.6 - 1.1$ (particularly in curve 'a_0', with the largest variation occurring at $\bar{\lambda} = 1.0$ showing a buckling reduction factor of $\chi = 0.62$ compared to the EN 1993-1-1 value of 0.72. The models in the mentioned slenderness range were modified with a finer mesh and smaller step sizes for load application. This led to small improvements, yielding a higher buckling resistance, but the clear discrepancies in the mid-slenderness range remained.

As mentioned previously, due to this discrepancy, it was decided to model another cross-section suitable for the 'a_0 buckling curve. The results of the analysis are shown in figure 3.14.

A second cross-section was also considered for the 'a' buckling curve. The results of the analysis for this cross-section are shown in figure 3.15.

As it can be shown, the results of the additional cross-sections modeled are almost identical to those of the first sections; a good agreement is shown in the low-slenderness region ($\bar{\lambda} \leq 0.6$) and the high slenderness region ($\bar{\lambda} \geq 1.2$), with better agreement as the

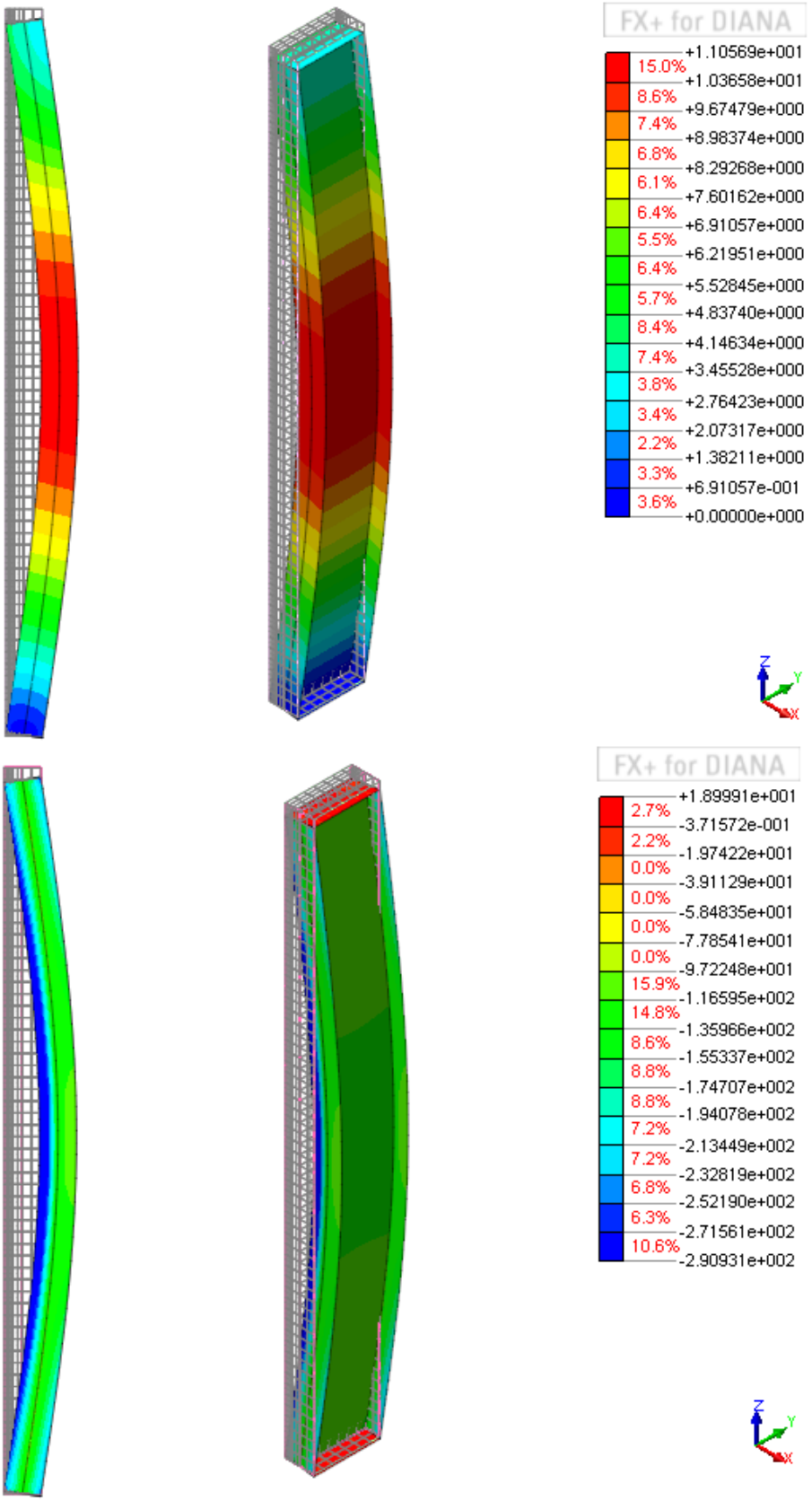

FIGURE 3.8: Displacement field in mm (Top) and stresses σ_{zz} in $\frac{N}{mm^2}$ at the onset of buckling (Bottom) for cross-section 'b' with $\bar{\lambda} = 1.0$ in N/mm^2.

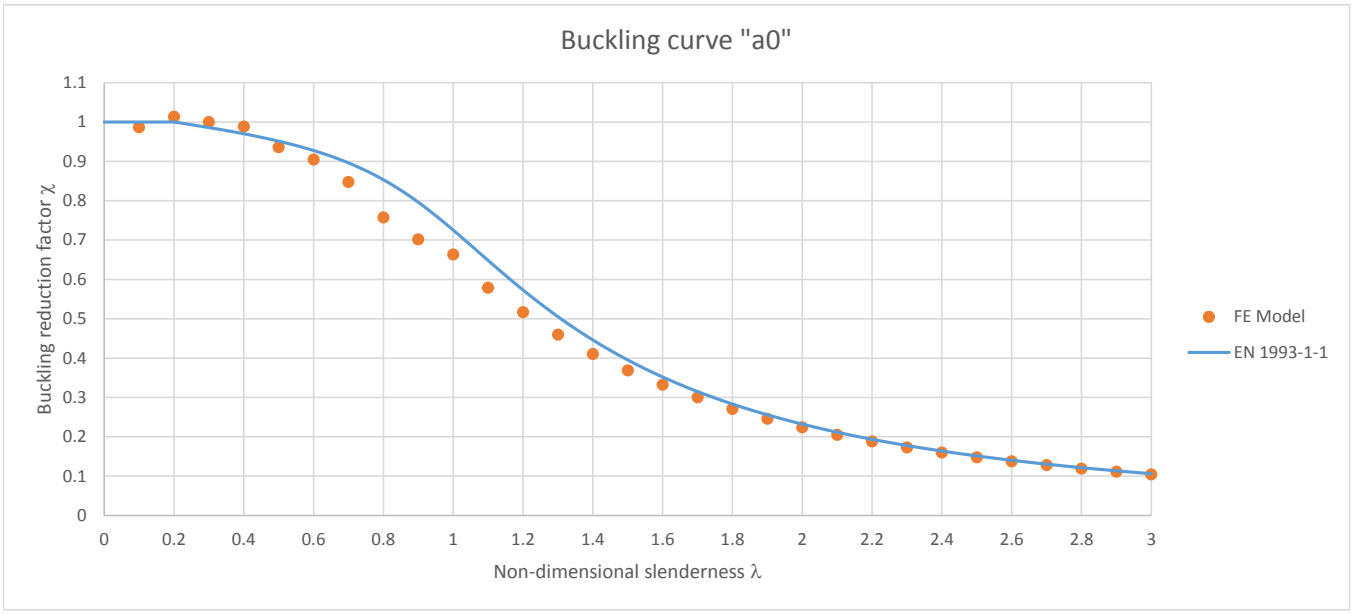

FIGURE 3.9: Comparison between EN 1993-1-1 and FEM results for buckling curve 'a0'.

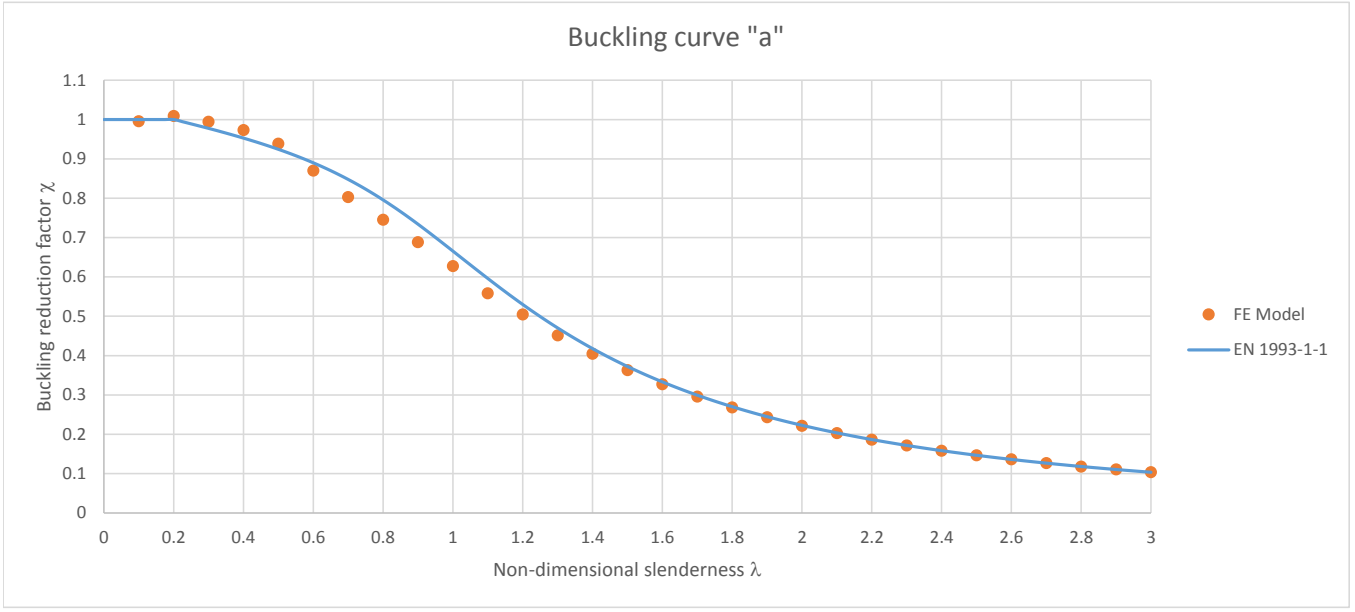

FIGURE 3.10: Comparison between EN 1993-1-1 and FEM results for buckling curve 'a'.

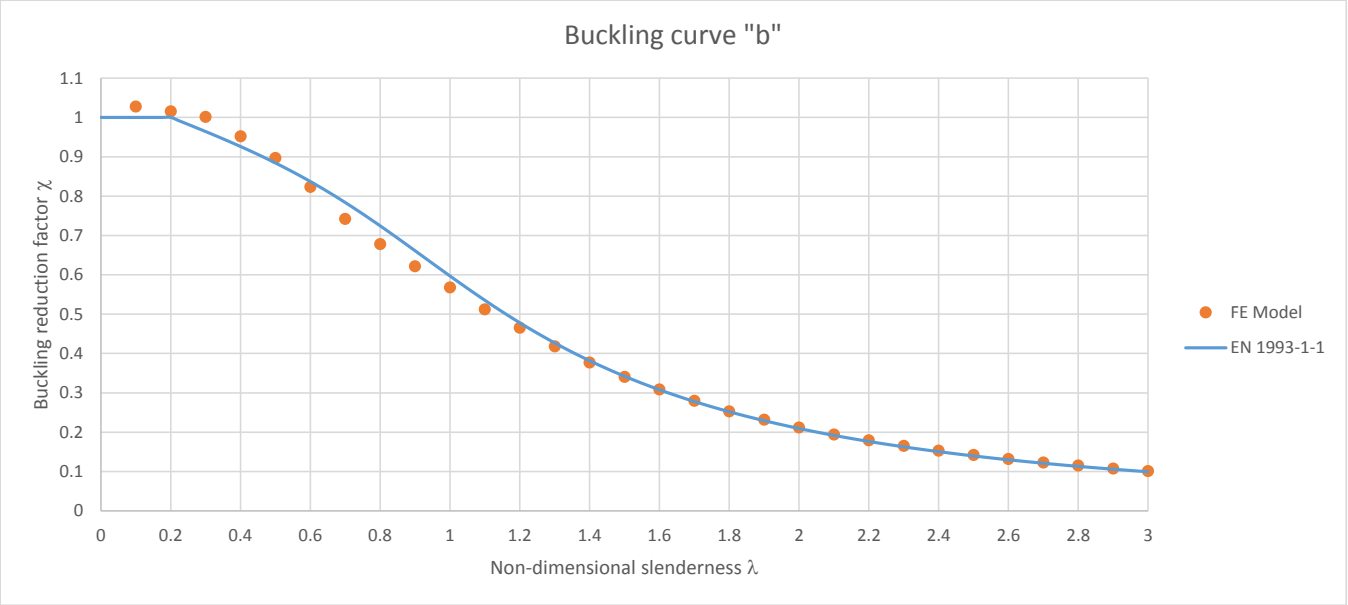

FIGURE 3.11: Comparison between EN 1993-1-1 and FEM results for buckling curve 'b'.

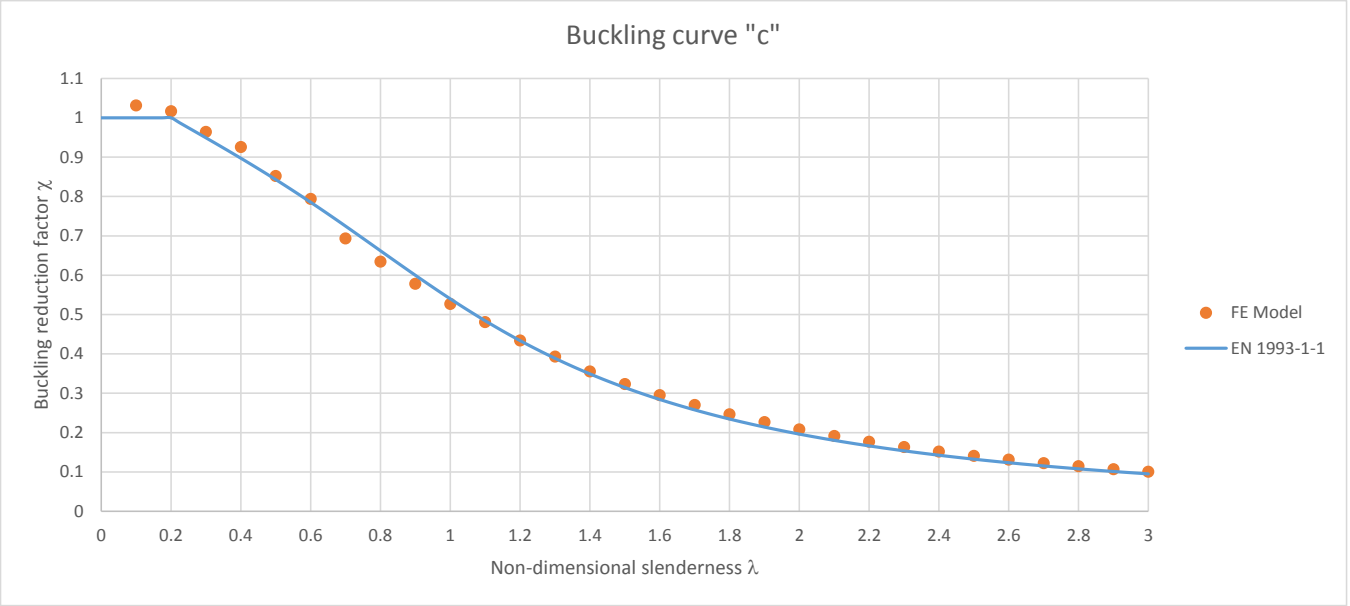

FIGURE 3.12: Comparison between EN 1993-1-1 and FEM results for buckling curve 'c'.

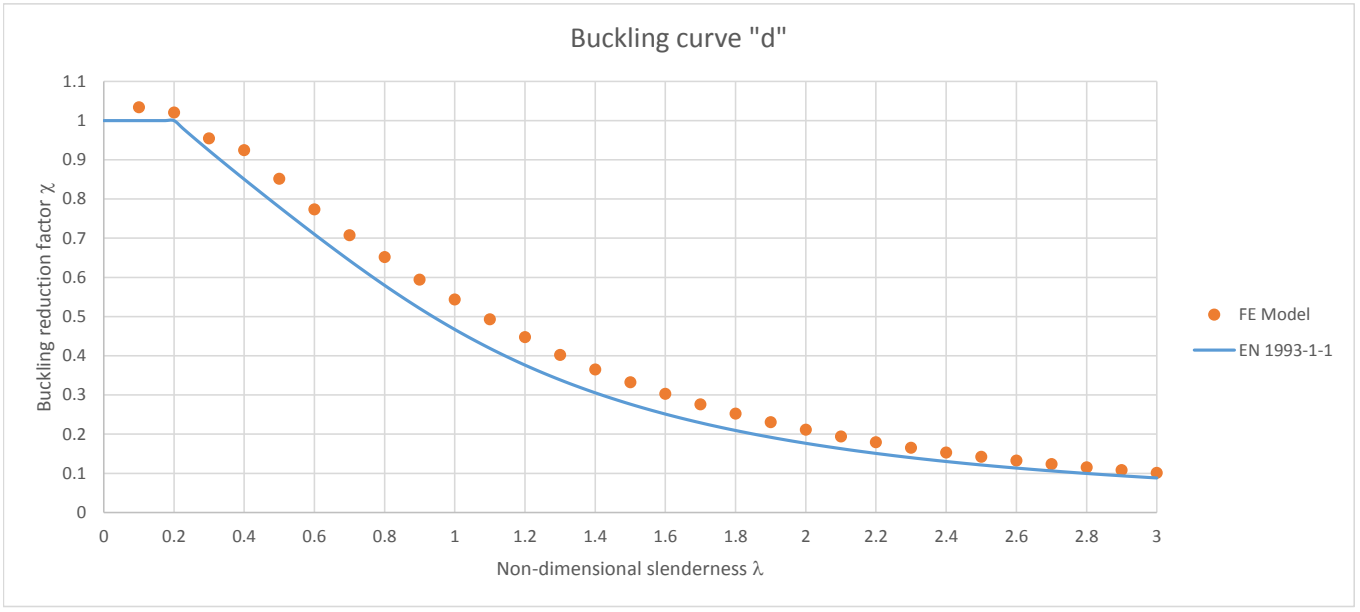

FIGURE 3.13: Comparison between EN 1993-1-1 and FEM results for buckling curve 'd'.

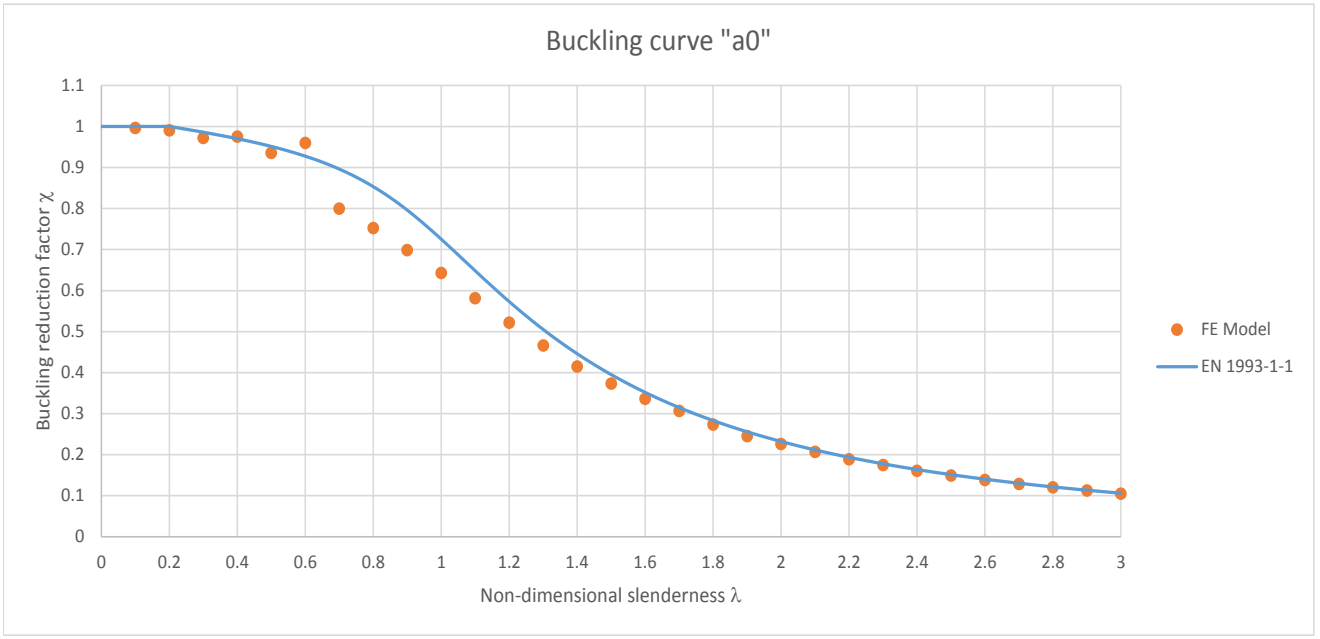

FIGURE 3.14: Comparison between EN 1993-1-1 and FEM results for buckling curve 'a_0' using a UKB 152 x 89 x 16 section.

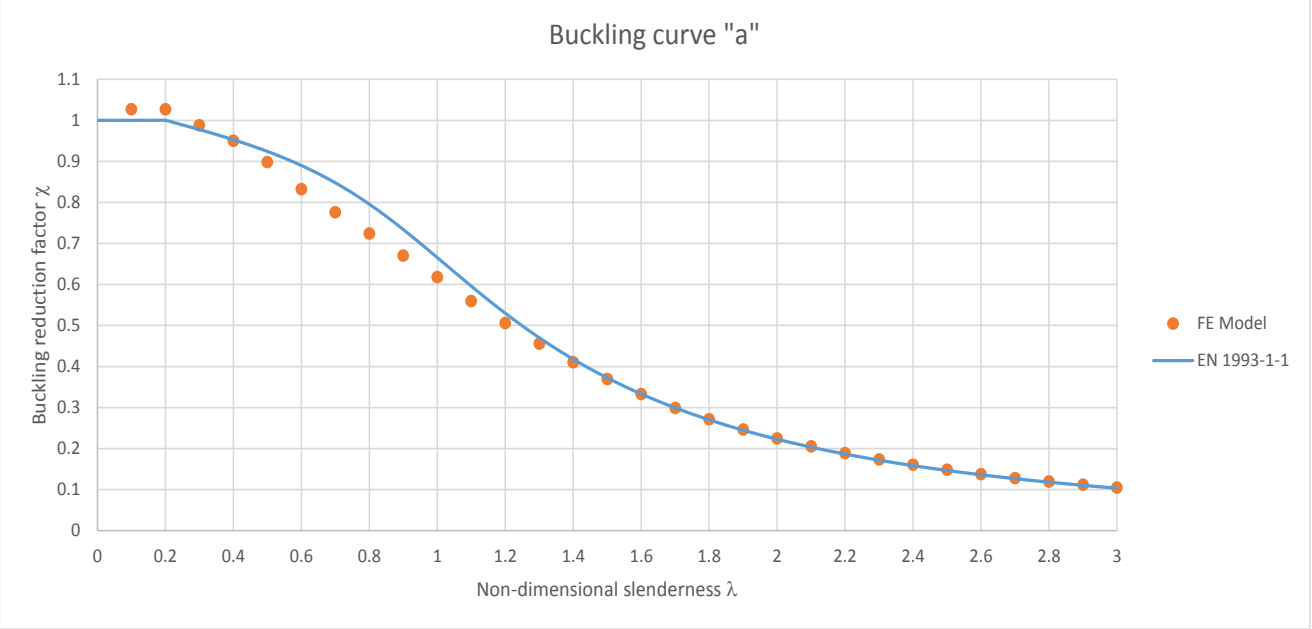

FIGURE 3.15: Comparison between EN 1993-1-1 and FEM results for buckling curve 'a' using a UKC 203 x 203 x 127 section.

non-dimensional slenderness increases, and a discrepancy in the mid-slenderness region ($0.6 \leq \bar{\lambda} \leq 1.1$). Upon careful inspection of the analysis results it was determined that the model was working properly and so the reasons for the mid-slenderness range discrepancy were assumed to be related to the residual stresses, the initial out-of-straightness and the steel grade.

It was found that in the original report by the ECCS, from which the buckling curves were derived, some high-strength steel I-shaped sections for buckling around the z-z axis were tested. The experimental tests showed that the resistance of these columns, with a yielding stress of 430 N/mm^2 or higher, were in-between buckling curves 'a' and 'b', with the higher discrepancy in the mid-slenderness range. Figure 3.16 extracted from the mentioned report shows these results by plotting the experimental results of an I-shaped cross-section with a yielding stress of 450 N/mm^2. Curve M21 shows the results for a section free of residual stresses, while curve M8 shows the results considering residual stresses [20].

It can be seen that the results in curve M8 are quite similar in shape to those obtained in the FEMs for curves 'a_0' and 'a'. From this we can conclude that the obtained results from the finite element analysis are in fact realistic for I-shaped columns.

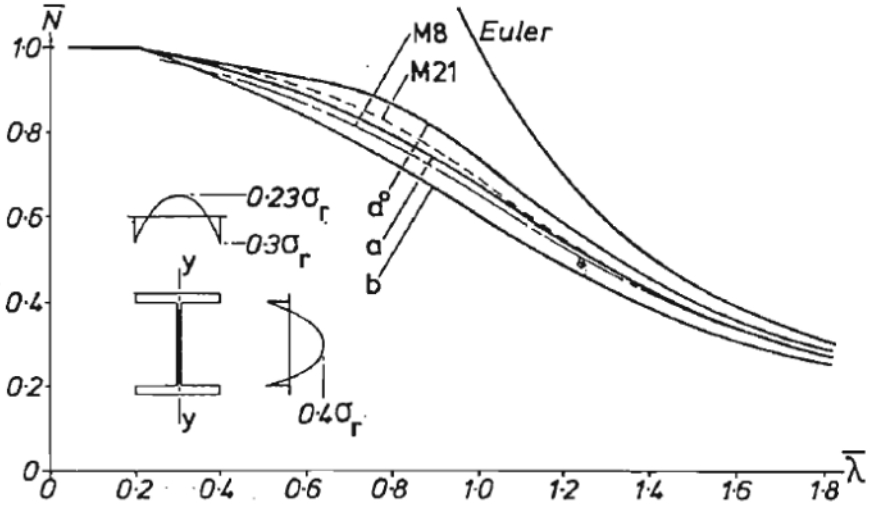

FIGURE 3.16: Experimental results on high-strength steel I-shaped cross sections [20]

In the original ECCS report, the 'a_0 buckling curve is only mentioned in a theoretical manner to describe the buckling behaviour of high-strength steel columns. No type of cross-section tested provided results that made the use of the 'a_0 buckling curve a reliable choice, not even high-strength circular sections. However, the ECCS manual makes the remark that in the future, more advanced manufacturing processes will allow design with the 'a_0' buckling curve for high-strength circular tubes. In the case of rolled I-sections, the ECCS recommendation is to use buckling curve 'b' for buckling around the z-z axis. [20].

It should be noted that steel grade S 460 is a fine grain structural steel. The grain refining process can be a thermal (e.g. rapid cooling) or a mechanical (e.g. cold forming) process, both of which have an influence in initial out-of-straightness and residual stresses [21]. A thermal grain refining process will lead to a more uniform cooling over time, which will reduce residual stresses in the section, which would normally arise from differential cooling after production. If cold forming is used, the cross-section will be straightened, minimizing its initial out-of-straightness. It is therefore likely that the residual stresses and the initial out-of-straightness considered in the models for curves 'a_0 and 'a' are above the real values for steel grade S 460, which would explain why the Eurocode 1993-1-1 allows for design of I-shaped rolled sections in this steel grade.

However, based on the FEM results, a material safety factor γ_{M1} greater than 1 would be recommended, at least for I-shaped columns bending about the z-z axis in the mid-slenderness range, unless specific material properties of the steel grade and cross-section are known and can be modeled.

3.3.2 Curves 'b' and 'c'

The results from the finite element analysis for buckling curves 'b' and 'c', shown in figures 3.11 and 3.12 respectively, show a very good agreement with the EN-1993-1-1 buckling curves, even in the medium slenderness range. In the case of curve 'b' the maximum difference between the FEM results and the Eurocode buckling curves was of 0.046 at a non-dimensional slenderness value of $\bar{\lambda} = 0.8$. For curve 'c' the maximum difference was of 0.0344 at $\bar{\lambda} = 0.7$.

From these findings it is concluded that the created finite element model is quite adequate for column cross-sections that can be classified in the buckling curves 'b' and 'c'.

3.3.3 Curve 'd'

The buckling reduction factor obtained for the cross-section corresponding to buckling curve 'd', shown in figure 3.13 display a good agreement with the shape of the buckling curve but with an offset, leading to the model over-estimating the column's resistance. The over-estimation in buckling resistance shown in the results of curve 'd' is most likely due to the remarkably high variation in residual stresses through the flange thickness. The Manual on Stability of Steel Structures, published by the European Convention for Constructional Steelwork in 1976, which is the origin of the Eurocode buckling curves, mentions that in thick-walled I-shaped members it was found that the residual stresses on the outside layer of the flanges (the face not in contact with the section's web) were completely in compression and almost close to the yielding stress near the tips. The residual stresses in the flanges decreased in the zone near the web [20]. Figure 3.17 shows how on the outside of two I-shaped sections the residual stresses are negative through the entire width while on the inside layer they decrease in magnitude and become tensile stresses in the web area.

Currently, this is somewhat managed in EN 1993-1-1, table 3.1, which gives yield stress values of different steel grades for different thicknesses up to 80 mm [10]. The FEM used considered the nominal value of the yield stress of steel grade S 275 ($f_y = 275 N/mm^2$), for which EN 1993-1-1 gives a value of $f_y = 255 N/mm^2$ for thicknesses of up to 80 mm. However, the Dutch standard NEN 6770 specifies a yield stress of 205 N/mm^2 for steel grade S 275 with a thickness greater than 100 mm [22]. A reduced yielding stress in the section would lead to a more premature failure in the model which would give a lower buckling reduction factor χ, resulting in a better fit to the Eurocode buckling

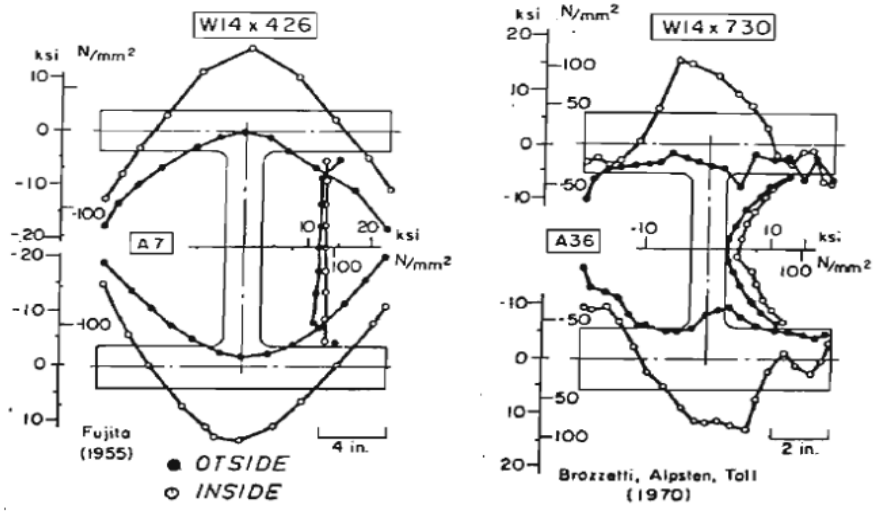

FIGURE 3.17: Residual stresses in thick-walled sections. [20]

curve. To confirm this, a second finite element model was created using the same cross-section but the reduced yielding stress recommended by the Dutch standard NEN 6770 for thicknesses greater than 100 mm ($f_y = 205N/mm^2$). The results are shown in figure 3.18.

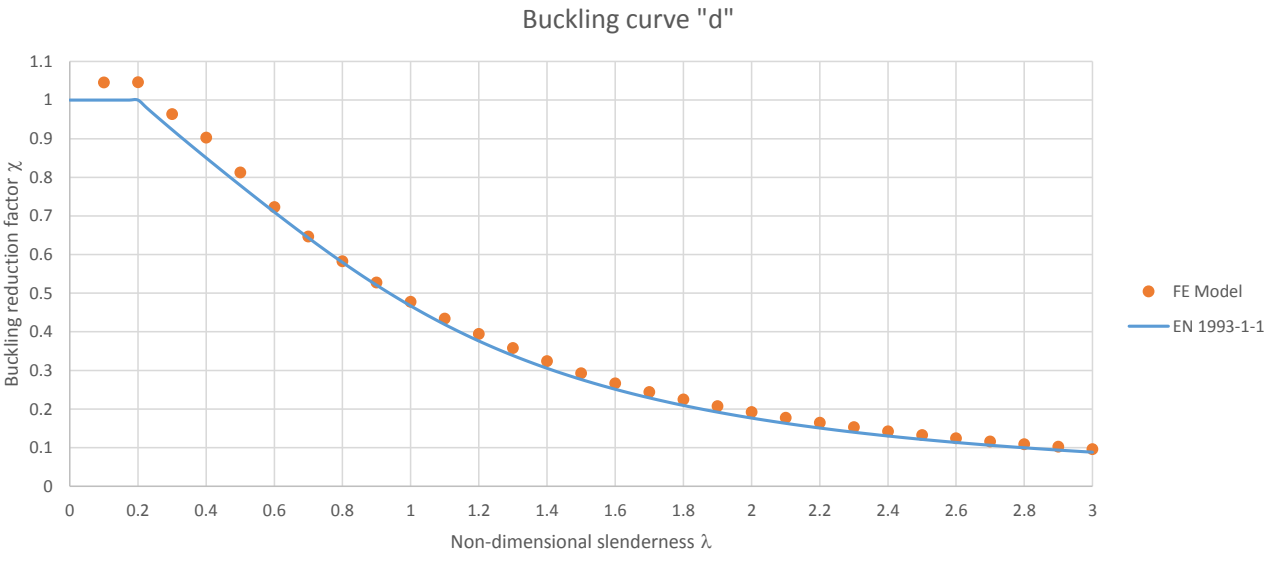

FIGURE 3.18: Comparison between EN 1993-1-1 and FEM results for buckling curve 'd' considering $f_y = 205N/mm^2$

As it can be seen from figure 3.18, the agreement with the Eurocode's 'd' buckling curve is remarkably improved by considering the lower yielding stress recommended by

the Dutch standard NEN 6770. From this we can conclude that, when analyzing the buckling behavior of thick-walled cross-sections, the reduction in yield stress should be taken into account. Also, given that the flanges of an I-shaped section make up a very large portion of the entire cross-sectional area (88 % in the case of the section used for this buckling curve) it is a good estimation to consider the yield stress in the flanges to be representative of the entire cross-section.

3.3.4 On Residual Stresses and Geometrical Imperfections

During the analysis of the finite element models just described it was found that the initial out-of-straightness and the residual stresses in the cross-section had a major influence on the buckling resistance of a column. However, there can be significant variation of these parameters in practice. The initial out-of-straightness half-sinusoidal shape with a maximum magnitude of $L/1000$, which is the one used for the derivation of the buckling curves is really a best-fit approximation to the shapes and magnitudes of initial imperfections found in the specimens during testing. In other words, it is unlikely that the shape and magnitude of the initial out-of-straightness of a column will correspond to that of a real column, but it has been determined to be a sufficiently accurate approximation for buckling resistance calculations [20].

Similarly as with geometrical imperfections, the estimation of residual stresses is an empirically-based approximation. The residual stress distribution for I-shaped sections recommended by the Swedish code BSK 99 and the Dutch standard NEN 6771 is a function of the h/b ratio that, while seeming like a somewhat gross generalization, has provided reasonably accurate results [17, 18]. However, this residual stress-distribution is not what one would find in every cross-section. Figure 3.19, extracted from the Manual on Stability of Steel Structures from which the buckling curves are derived, shows the various types of residual stress distributions found in the I-shaped specimens used during testing. It was found that not only is the magnitude of residual stresses a function of the h/b ratio, but it also depends on the t_w/t_f ratio. As such, a group of equations was suggested for calculations [20].

$$\begin{aligned}
\sigma_{c1} &= 165 \cdot [1 - \frac{h \cdot t_w}{2.4B \cdot t_f}] N/mm^2 \\
\sigma_{c2} &= 100 \cdot [1.5 + \frac{h \cdot t_w}{2.4B \cdot t_f}] N/mm^2 \\
\sigma_t &= 100 \cdot [0.7 + \frac{h \cdot t_w}{2B \cdot t_f}] N/mm^2
\end{aligned}$$

Where σ_{c1} is the compressive stress at the flange toes, σ_{c2} is the compressive stress in the center of the web and σ_t is the tensile stress at the web to flange junction.

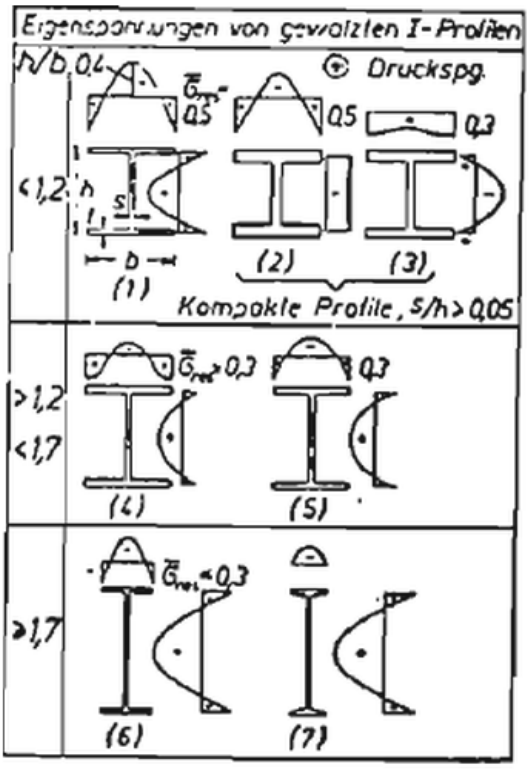

FIGURE 3.19: Residual stress distribution in I-shaped hot-rolled sections [20].

All of these variations and particularities in geometrical imperfections and residual stresses make it necessary to have a set standard for calculation with reasonable accuracy. Therefore, the Eurocode buckling curves can be thought of a statistically conservative design tool; providing reasonably accurate results for most cases while leaving some room for safety in the case of any particularities. A perfect fit with the EN 1993-1-1 buckling curves is technically impossible, but with the recommendations provided, a reasonable agreement can be achieved while some discrepancies should also be expected.

The influence of residual stresses and initial out-of-straightness is of particular importance in the buckling phenomena. One one hand, considering a symmetric residual stress distribution, a perfectly straight column under the action of a compressive load acting on its center of mass would, theoretically, never lead to instability, regardless of the length of the element. On the other hand, an imperfect column with no residual stresses would lead to higher buckling loads. This is due to the fact that the compressive residual stresses on the tips of the flanges lead to premature yielding, which leads to the onset of instability in the column. A section with no residual stresses would still buckle, as long as there is an initial out of straightness, but the premature yielding on the tip of

the flanges will not occur.

To illustrate the importance of the initial out-of-straightness and residual stresses in the buckling phenomena, an additional set of analyses was performed: a series of FEMs with the normally accepted imperfection of $\frac{L}{1000}$ but with no residual stresses. The results obtained were once again plotted with the Eurocode EN-1993-1-1 buckling curves as well as the results obtained with the normal residual stresses and are shown in figures 3.20 to 3.24.

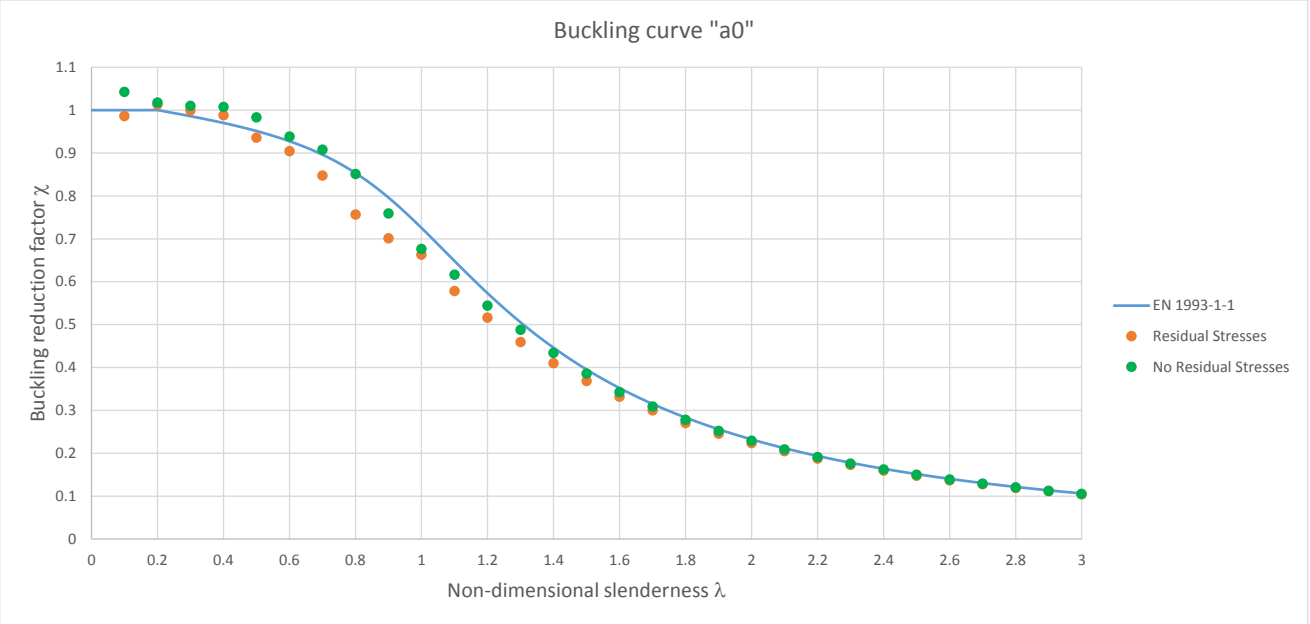

FIGURE 3.20: Comparison of FEMs with and without residual stresses for buckling curve 'a_0'.

A clear disagreement can be appreciated as one progresses from curve 'a_0' to curve 'd'. In the first curve, the points of the FEM with no residual stresses fit the buckling curve really well, but in curve 'd' there is a very clear overestimation of the buckling capacity. This can be related to the imperfection factor α, that takes into account the initial out-of-straightness, residual stresses and other imperfections in the calculations of buckling capacity of a column; while the value of this factor for curve 'a_0 is 0.13, the imperfection factor for curve 'd' is 0.76.

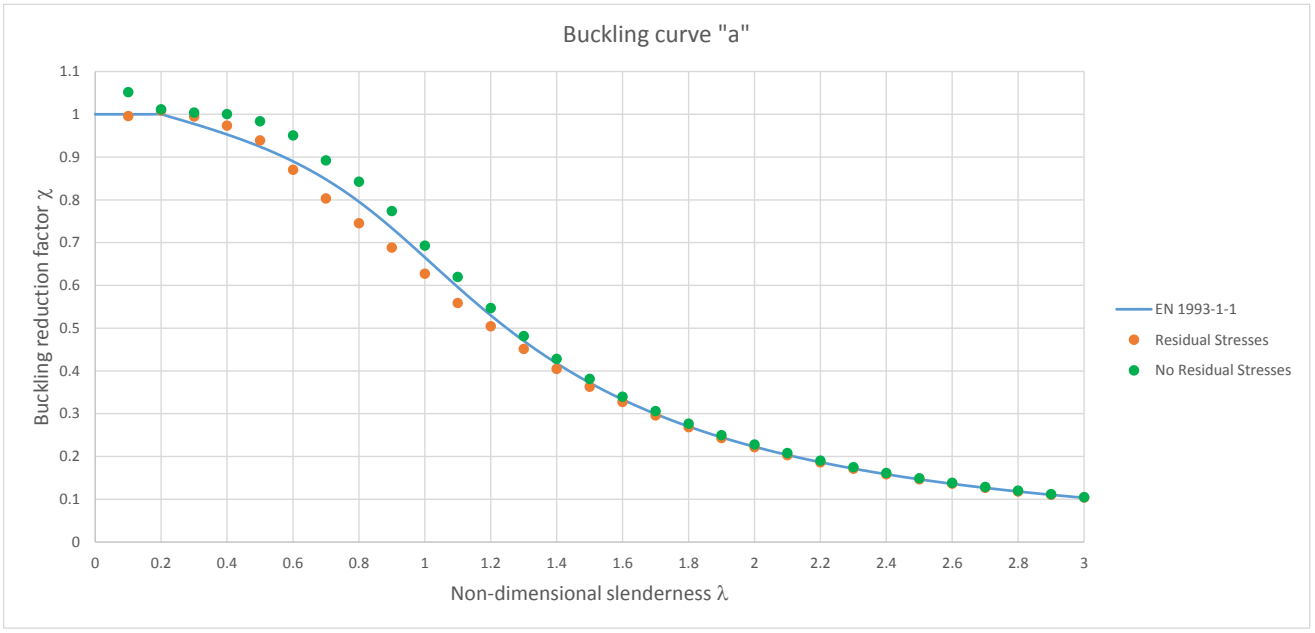

FIGURE 3.21: Comparison of FEMs with and without residual stresses for buckling curve 'a'.

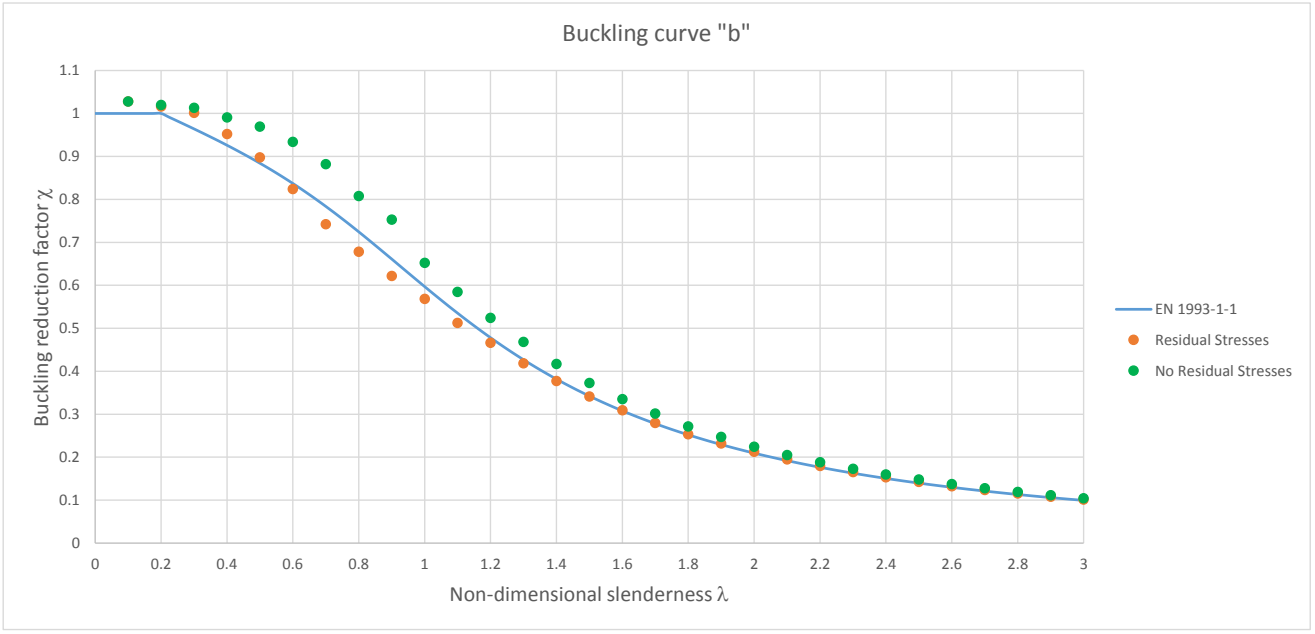

FIGURE 3.22: Comparison of FEMs with and without residual stresses for buckling curve 'b'.

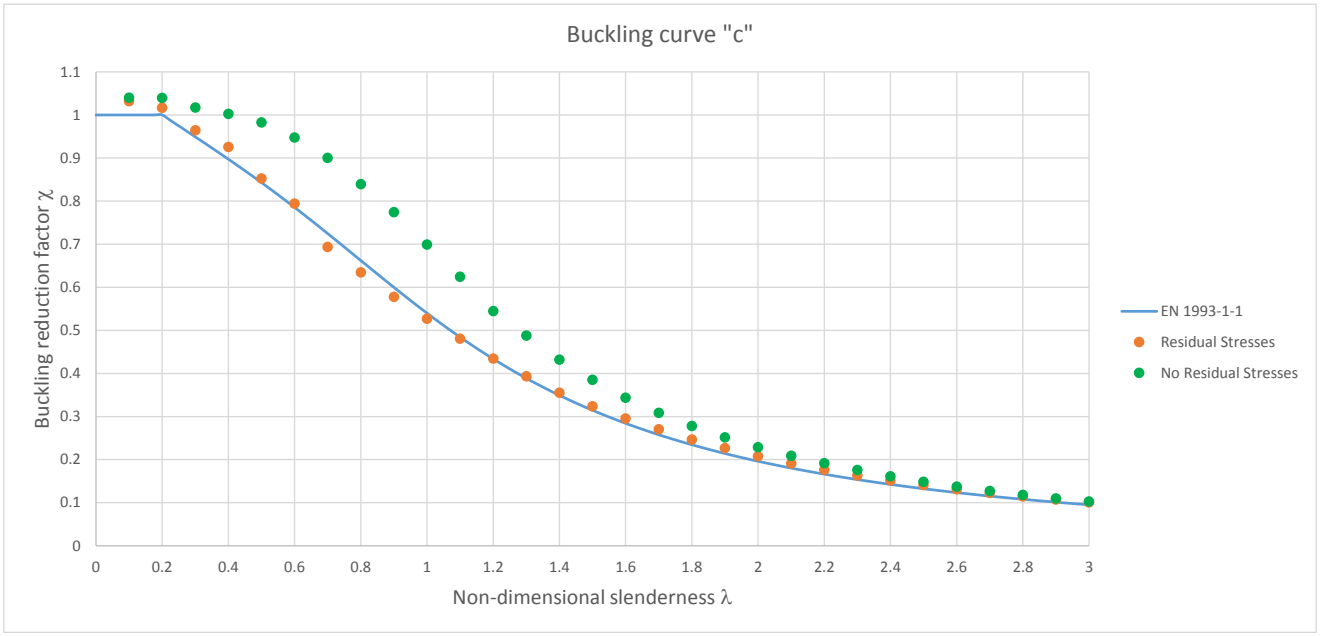

FIGURE 3.23: Comparison of FEMs with and without residual stresses for buckling curve 'c'.

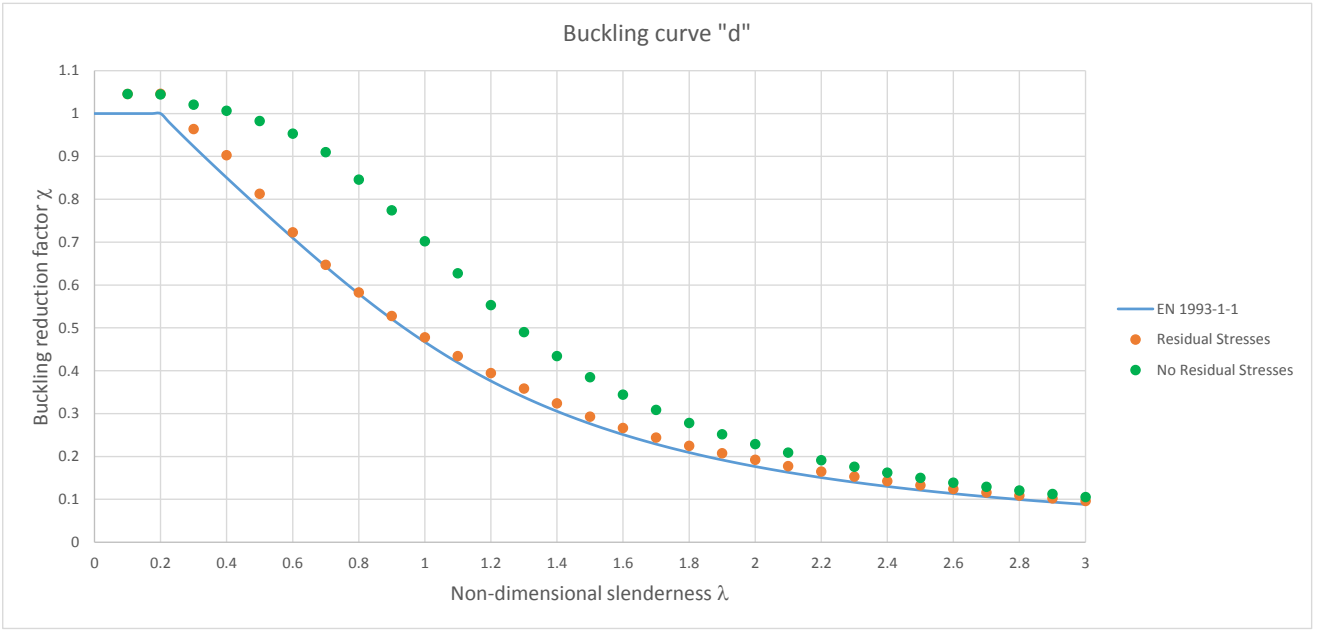

FIGURE 3.24: Comparison of FEMs with and without residual stresses for buckling curve 'd'.

3.4 Conclusions

- The results obtained with the finite element model show a reasonably good agreement with the Eurocode 1993-1-1 buckling curves for most cases.
- Buckling curves 'a_0 and 'a' for buckling about the z-z axis show the largest discrepancies with the FEM in the medium slenderness range ($0.6 \leq \bar{\lambda} \leq 1.1$) and special caution is recommended for design in these cases.The origin for the discrepancy is suspected to be the use of steel grade S 460, for which the geometrical imperfection and residual stress distributions considered in other steel grades may not apply.
- In the case of thick-walled I-shaped sections, as in those to be designed with buckling curve 'd', a reduction in yield stress corresponding to the flange thickness is necessary for an adequate estimation of load bearing capacity. The yield stress in the flanges can be considered representative of the entire cross-section.
- Geometrical imperfections and residual stresses have an important impact in the buckling resistance of a column. The real-life variation of both of these parameters have led to the acceptance of set standards, which also means that a small discrepancy in end results is to be expected. However, case-specific calculations can (and should) be used if further accuracy is required.
- Given the reasonable agreement with the Eurocode 1993-1-1 buckling curves, this finite element model is seemed acceptable for the description of the buckling phenomena at room temperatures.

Chapter 4

Mild Steel at Elevated Temperatures

4.1 Finite Element Model

A similar approach to the one considered in the room temperature analysis was applied for the elevated temperature study; a series of models of varying lengths with cross-sections assigned to buckling curves 'a_0' to 'd' were analyzed through a stability and a non-linear analysis, after which the maximum total vertical reaction the supports was registered as the buckling load for each model, $N_{b,fi,Rd}$. The results of each analysis were then plotted together with the buckling curves specified by EN 1993-1-2. The finite element models at elevated temperature considered the same cross-sections mentioned in table 3.2. The buckling reduction factor at elevated temperatures χ_{fi} was calculated from equation 2.4:

$$N_{b,fi,Rd} = \frac{\chi_{fi} \cdot A \cdot k_{y,\theta} \cdot f_y}{\gamma_{M,fi}}$$

A few considerations must be taken into account in the analysis at elevated temperatures, of which the relaxation of residual stresses and the increased non-linearity of the stress-strain relationship are of particular importance.

4.1.1 Relaxation of Residual Stresses

The effect of residual stresses is already considered in the Eurocode through the imperfection factor α that differentiates the buckling curves. Depending on the type of

cross section, a different buckling curve is considered in line with the corresponding residual stresses estimated to be generated during the manufacturing process (lower residual stresses in the section will correspond to a higher buckling reduction factor) [23]. This semi-empirical approach has been proven to be effective and acceptably accurate for room temperature design. However, there is no mention of how residual stresses should be considered at elevated temperatures in EN 1993-1-2. The problem with this is a potential over-conservative approach, since research has found that residual stresses in steel elements are greatly relaxed in elevated temperature conditions and failure is mainly determined by the decay in yielding strength and modulus of elasticity [24].

For the most part, residual stresses are neglected for elevated temperature design. However, advanced finite element models are able to take into account the level of residual stresses in an element, depending on how this stresses are first introduced. Takagi and Deierlein [25] proposed a simplified approach for residual stress modeling in their work, by setting the maximum residual stress at room temperature at a value of 69 MPa and reducing this stress through the yield strength reduction factor $k_{y,\theta}$ given by the Eurocode EN 1993-1-2 as temperature increased. Therefore, the residual stresses in the section decrease with the increase in temperature, although the difference in their results with and without residual stress consideration was minimal and only noticeable in members of intermediate slenderness. Yang and Hsu [26] evaluated the residual stresses in their test specimens as a percentage of the yield strength. They found that at room temperature, the maximum residual stresses in the section exceeded 20%, but by the time a temperature of 500,° C this value had dropped to less than 10%. They found no premature failure due to residual stresses at elevated temperature in any of the specimens and concluded that the effect of residual stresses in column resistance at elevated temperatures can be neglected.

In order to determine the importance of residual stresses at elevated temperatures it was decided to follow the Takagi and Deierlein approach, in which the residual stresses would be reduced by the yield strength reduction factor $k_{y,\theta}$. In order to have a basis for comparison, the whole range of analyses were performed with and without residual stresses.

4.1.2 Non-linearity of Stress-strain Relationship

Eurocode 1993-1-2 provides a series of formulations for the stress-strain relationships of carbon steel at elevated temperatures:

For $\varepsilon \leq \varepsilon_{p,\theta}$:

$$\sigma_\theta = \varepsilon \cdot E_{a,\theta} \tag{4.1}$$

For $\varepsilon_{p,\theta} < \varepsilon < \varepsilon_{y,\theta}$:

$$\sigma_\theta = f_{p,\theta} - c + \frac{b}{a}\sqrt{a^2 - (\varepsilon_{y,\theta} - \varepsilon)^2} \tag{4.2}$$

And for $\varepsilon_{y,\theta} \leq \varepsilon \leq \varepsilon_{t,\theta}$:

$$\sigma_\theta = f_{y,\theta} \tag{4.3}$$

Where:

$$\begin{aligned} a^2 = &\quad (\varepsilon_y, \theta - \varepsilon_{p,\theta})(\varepsilon_{y,\theta} - \varepsilon_{p,\theta} + c/E_{a,\theta}) \\ b^2 = &\quad c(\varepsilon_{y,\theta} - \varepsilon_{p,\theta})E_{a,\theta} + c^2 \\ c = &\quad \frac{(f_{y,\theta} - f_{p,\theta})^2}{(\varepsilon_{y,\theta} - \varepsilon_{p,\theta})E_{a,\theta} - 2(f_{y,\theta} - f_{p,\theta})} \end{aligned}$$

and:

$$\begin{aligned} \varepsilon_{p,\theta} = &\quad \frac{f_{p,\theta}}{E_{a,\theta}} \\ \varepsilon_{y,\theta} = &\quad 0.02 \\ \varepsilon_{t,\theta} = &\quad 0.15 \end{aligned}$$

Using the equations provided by EN-1993-1-2 the stress-strain relationships for different steel grades at different temperatures can be plotted. Figures 4.1 and 4.2 show the stress-strain relationships at different elevated temperatures for steel grades S275 and S460.

Currently, the Eurocode 1993-1-2 does not make any mention regarding the non-linearity of the stress-strain relationship and so it is unclear whether or not it has been considered in the derivation of the buckling curves at elevated temperatures.

If the non-linearity of the stress-strain relationship at elevated temperatures has been overlooked or ignored it would mean that the entire non-linear part of the stress-strain relationship is neglected, which could lead to un-conservative results. To address this problem in the finite element model, several points in the stress-strain relationships shown in figures 4.1 and 4.2 were specified as input in the material characterization of the finite element models. In order to determine just how important the curvature of the stress-strain relationship is at elevated temperatures two sets of columns, at 500 °C and 700,° C, were analyzed. It was decided to use these temperatures for the study because

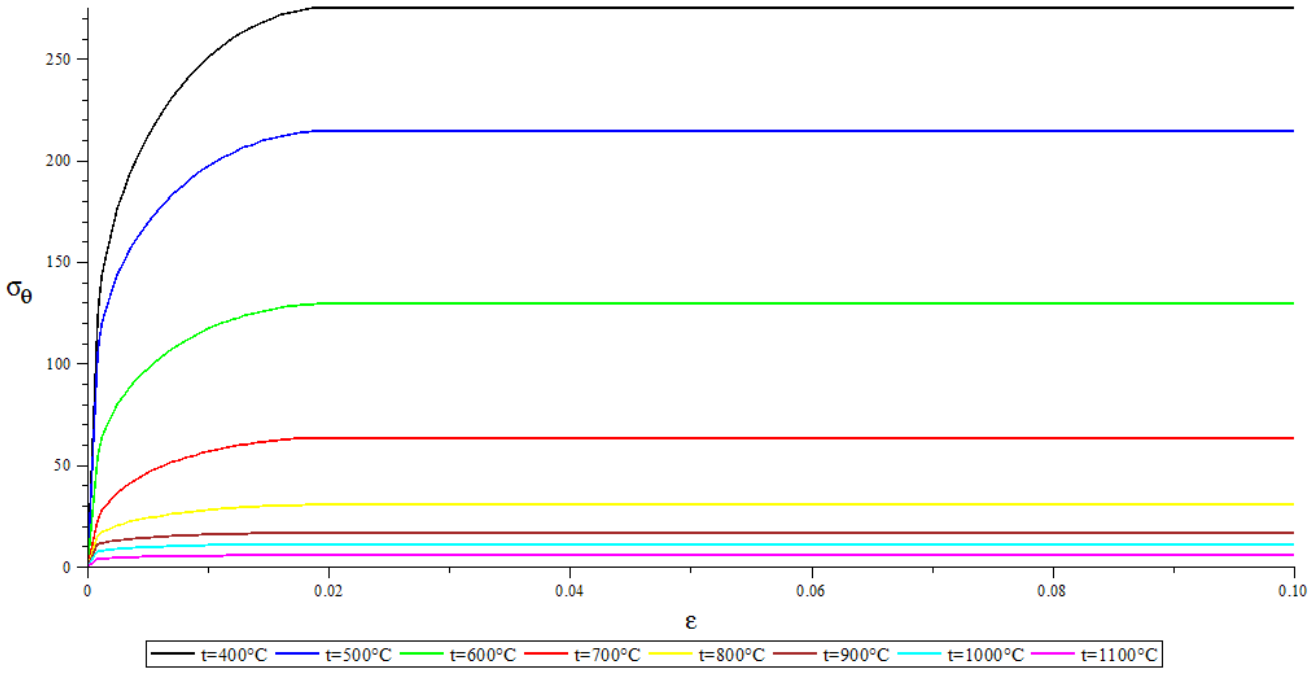

FIGURE 4.1: Stress-strain relationships at elevated temperatures for steel grade S275

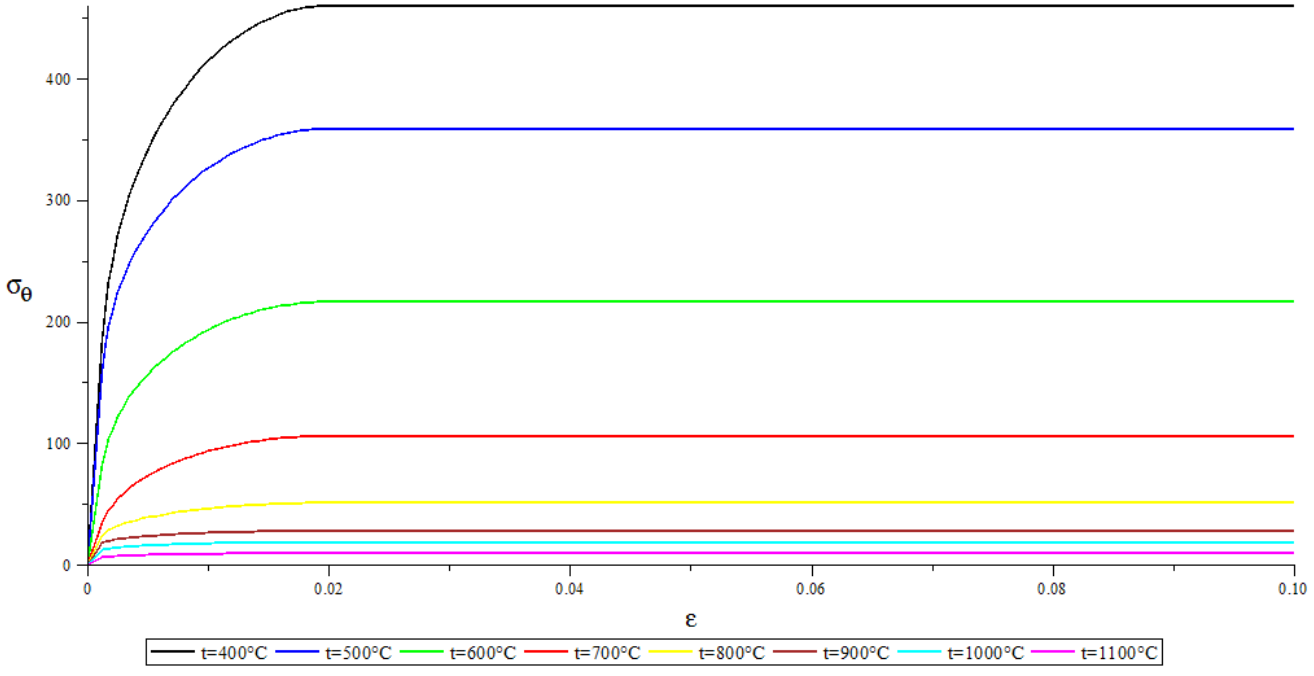

FIGURE 4.2: Stress-strain relationships at elevated temperatures for steel grade S460

the reduction in the yield stress of steel begins at 500 °C. The temperature at 700 °C was chosen to serve as a middle point in between the range of temperatures shown in figures 4.1 and 4.2.

To determine the importance of the consideration of a bi-linear stress-strain relationship in an elevated temperature analysis, an additional set of finite element models were created in the mid-slenderness range ($0.3 \leq \bar{\lambda} \leq 1.0$) where the highest discrepancy was expected.

4.1.3 Analysis Parameters

As in the analysis at room temperature, the analysis at elevated temperatures consisted in three steps:

1. Stability analysis determining the first eigenmode and applying an imperfection of $\frac{L}{100}$.
2. Applying the residual stresses considering the yield strength reduction factor at 500 °C or 700 °C, with values of 0.78 and 0.23 respectively.
3. Applying an incrementally increasing prescribed displacement in 40 steps (2.5% of the total prescribed displacement per step).

This analysis procedure mimics a steady-state testing methodology, where the specimen's temperature is kept at a constant level while the applied load is increased.

Upon termination of the analysis, the maximum total vertical reaction in the supports was measured and registered as the buckling load at elevated temperature $N_{b,fi,Rd}$, after which the buckling reduction factor at elevated temperature χ_{fi} was calculated using equation 2.4 and the result plotted against the buckling curves for elevated temperatures specified in Eurocode EN-1993-1-2.

4.2 Results at 500 °C

As in the analysis for room temperatures, the five cross-sections corresponding to each buckling curve were modeled for 30 different values of slenderness λ_θ. The values of the buckling load $N_{b,fi,Rd}$ were obtained and subsequently the corresponding values of the buckling reduction factors for elevated temperatures χ_{fi} were calculated. This procedure

was carried on for the cases of zero residual stresses and "relaxed" residual stresses. The results were then plotted against the buckling curves calculated using the provisions from Eurocode 1993-1-2. The obtained results are shown in figures 4.3 to 4.7.

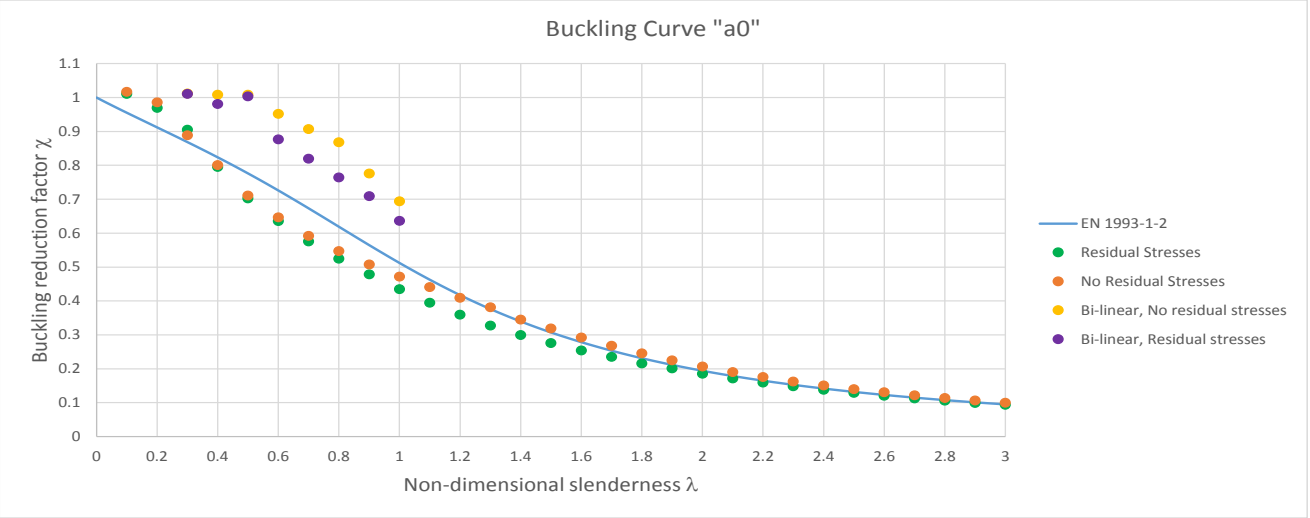

FIGURE 4.3: Comparison of FEMs with and without residual stresses at 500 °C for buckling curve 'a_0'.

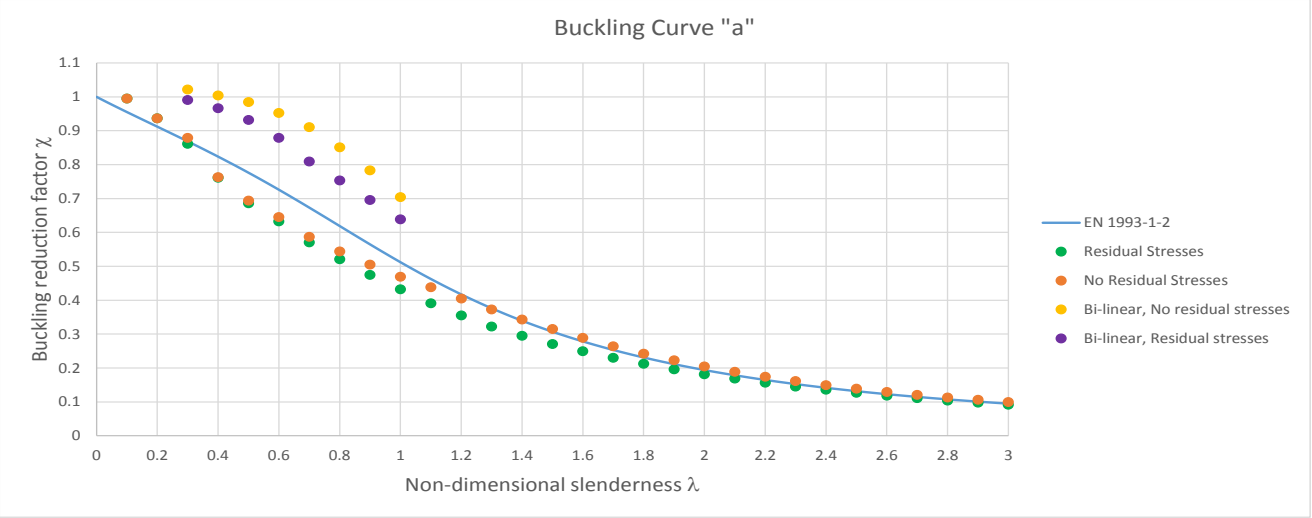

FIGURE 4.4: Comparison of FEMs with and without residual stresses at 500 °C for buckling curve 'b'.

As it can be seen from figures 4.3 to 4.7 the results from the finite element models show a lower buckling resistance than what is indicated by the corresponding buckling curves, particularly in the cases where residual stresses are considered. The FEM results for zero residual stresses have a relatively good agreement with the Eurocode buckling curves but still show a relative underestimation of buckling strength in the lower mid slenderness range ($0.4 \leq \lambda_\theta \leq 1.0$). However, it should be noted that the results have a closer fit to the Eurocode buckling curves as one progresses from buckling curve 'a_0'

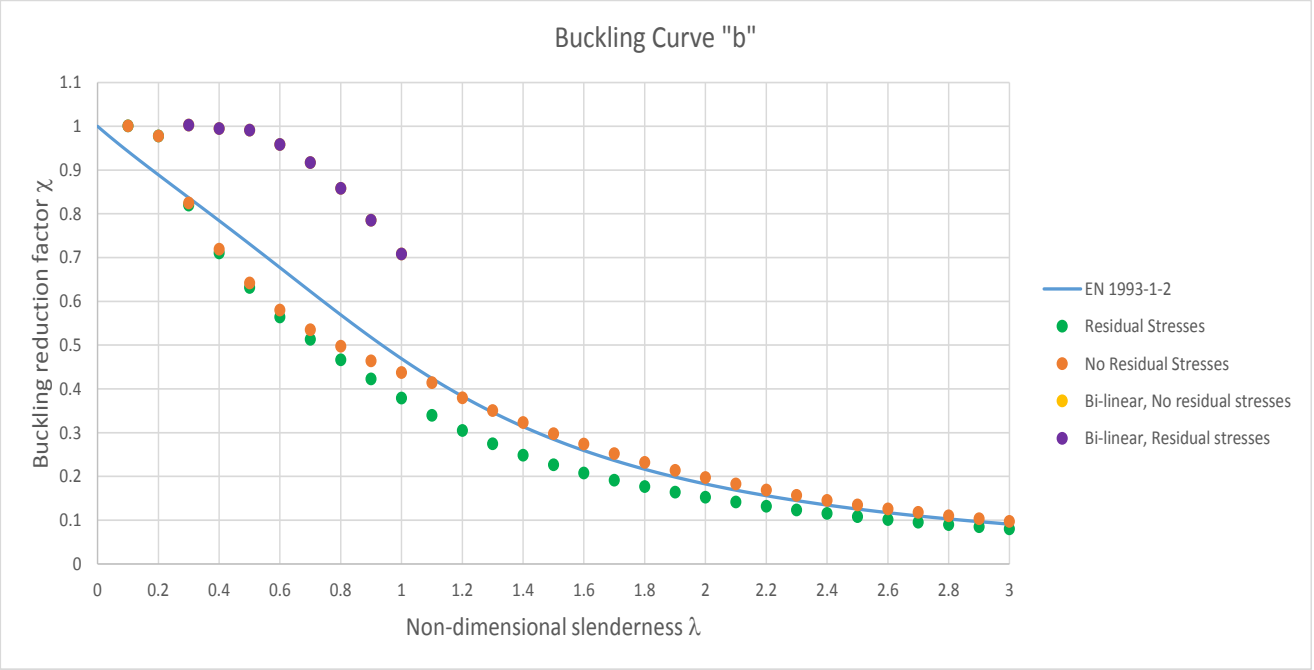

FIGURE 4.5: Comparison of FEMs with and without residual stresses at 500 °C for buckling curve 'c'.

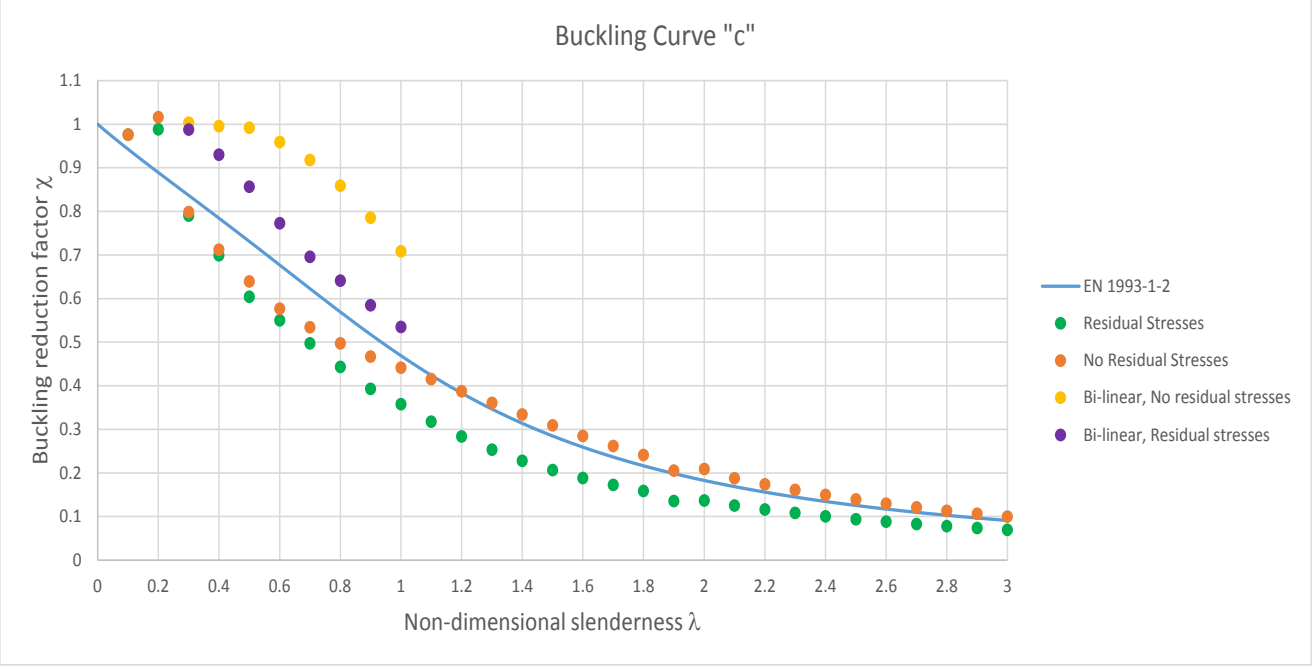

FIGURE 4.6: Comparison of FEMs with and without residual stresses at 500 °C for buckling curve 'c'.

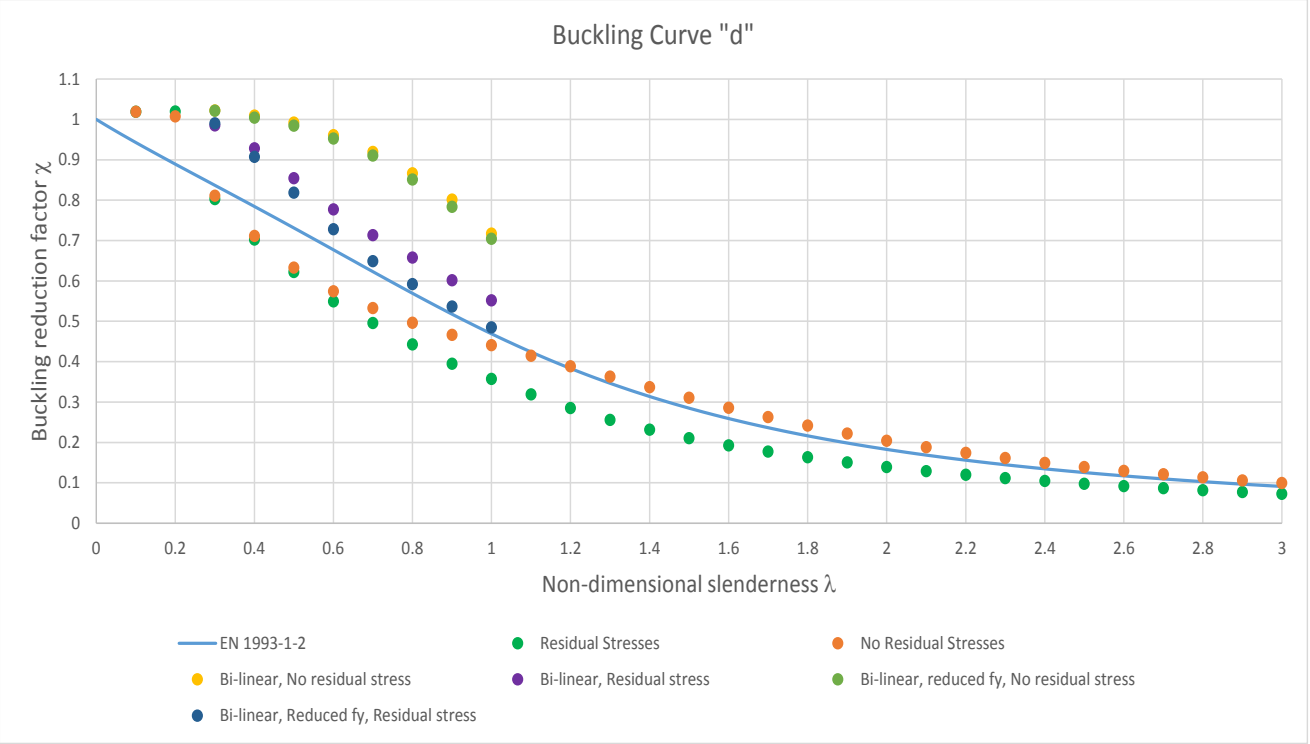

FIGURE 4.7: Comparison of FEMs with and without residual stresses at 500 °C for buckling curve 'd'.

to curve 'd'. The reason for these discrepancies can be due to a number of factors or a combination of them.

Eurocode 1993-1-2 makes no mention of the considerations that should be made for residual stresses for compression members at elevated temperatures. Given that the FEM results with zero residual stresses have a good agreement at low and high slenderness values it is possible that the Eurocode provisions disregard the effect of residual stresses at elevated temperatures or that they are considered to be very low.

The calculation procedure for elevated temperatures is quite similar to the one at room temperature. The mayor difference between both is that the calculations at elevated temperature consider the decay in mechanical properties (modulus of elasticity and yield stress). However, one factor that is not considered in this procedure is the increased non-linearity of the stress-strain relationship at elevated temperatures, which becomes more significant the higher the temperature is. At room temperature, the consideration of a bi-linear stress-strain relationship is quite reasonable, but at high temperatures, the deformation that a column would undergo while in the non-linear range of the stress-strain relationship might lead to a premature buckling failure that would account for the discrepancy in the results.

One other factor that could explain the difference in the results is the effective buckling length for the models of the columns. As in the room temperature analyses, a pin-ended column was considered. However, when a column that is part of a frame is considered, Eurocode 1993-1-2 mentions that the adjacency of cold compartments to that of a column exposed to a fire leads to increased rotational restraint in the supports [5]. This means that the effective buckling length of a column exposed to a fire is reduced by half, since the Eurocode assumes that the relative stiffness of the adjacent cold structure is sufficiently high to consider the column fix-ended. A fix-ended column would have a higher buckling resistance, which would account for the discrepancies in the results. However, the applicability of a reduced effective length is questionable in this case, given that individual columns are being analyzed, not columns as part of a frame. It is important to remember that the buckling curves at room temperature were obtained from experimental data on pin-ended columns, while the buckling curves at elevated temperatures are the product of the modification of the equation for the buckling load through the consideration of reduced mechanical properties.

4.3 Results at 700 °C

The results for the finite element models at 700,° C are shown in figures 4.8 to 4.12.

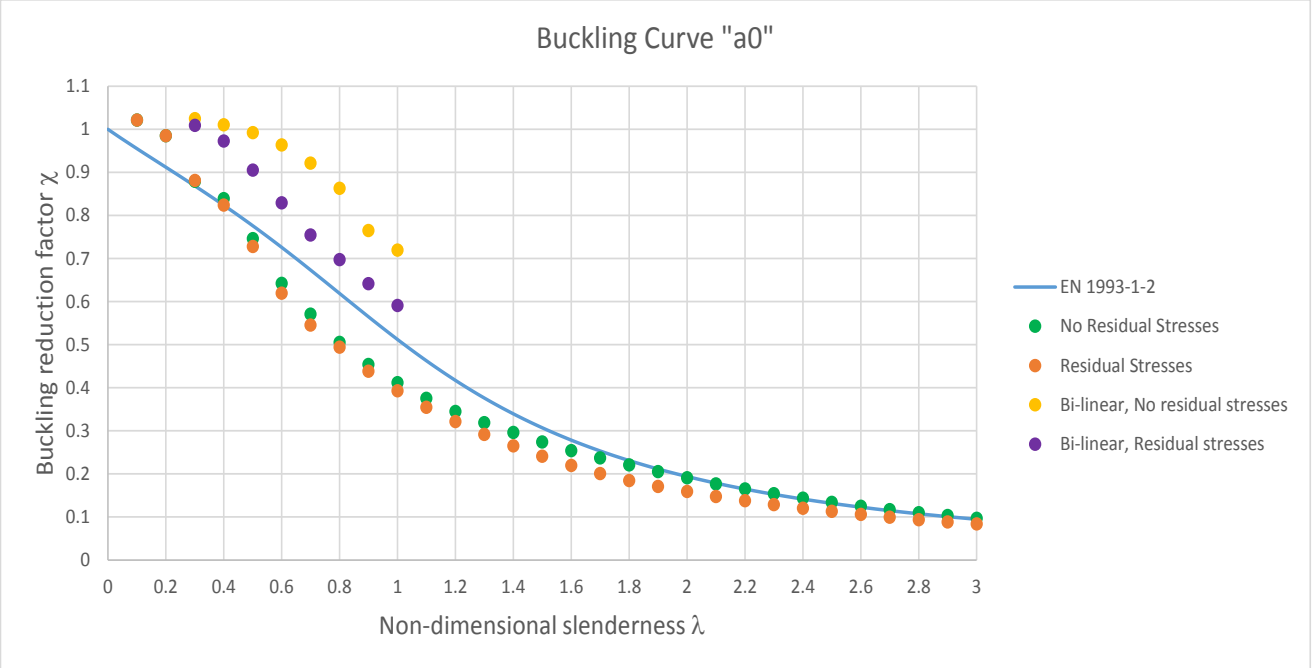

FIGURE 4.8: Comparison of FEMs with the EN 1993-1-2 provisions for buckling curve 'a_0' at 700 °C.

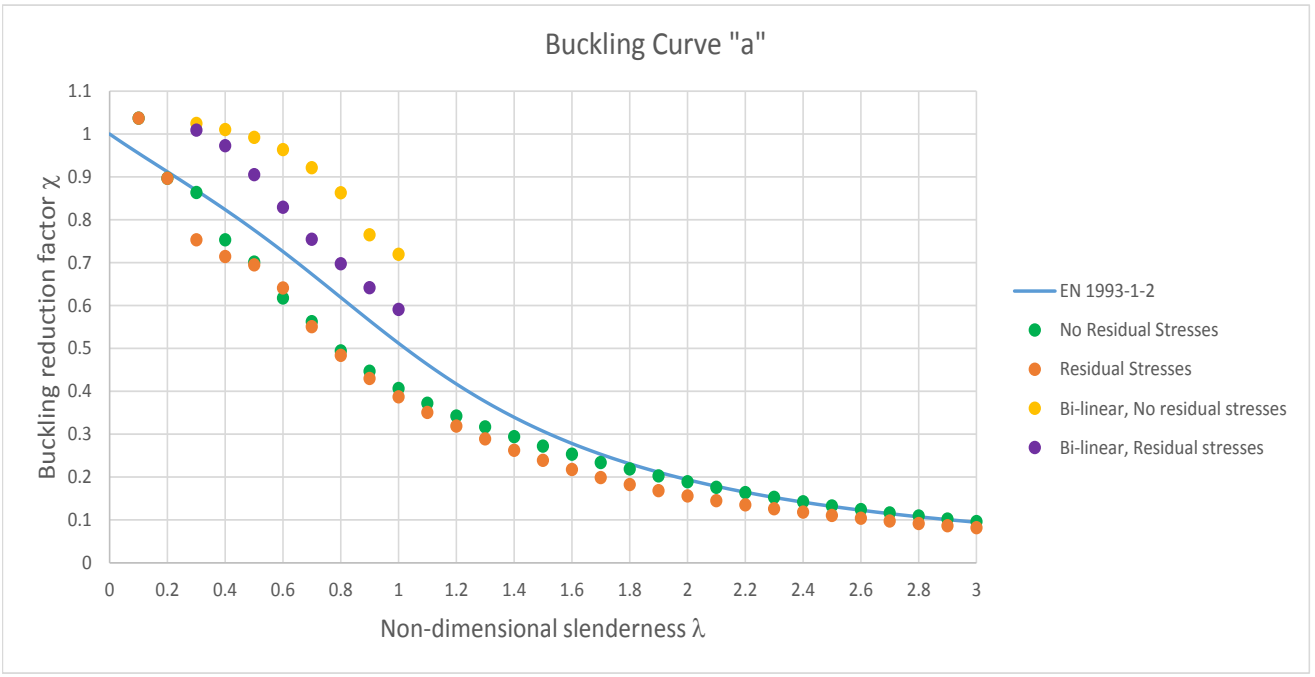

FIGURE 4.9: Comparison of FEMs with the EN 1993-1-2 provisions for buckling curve 'a' at 700 °C.

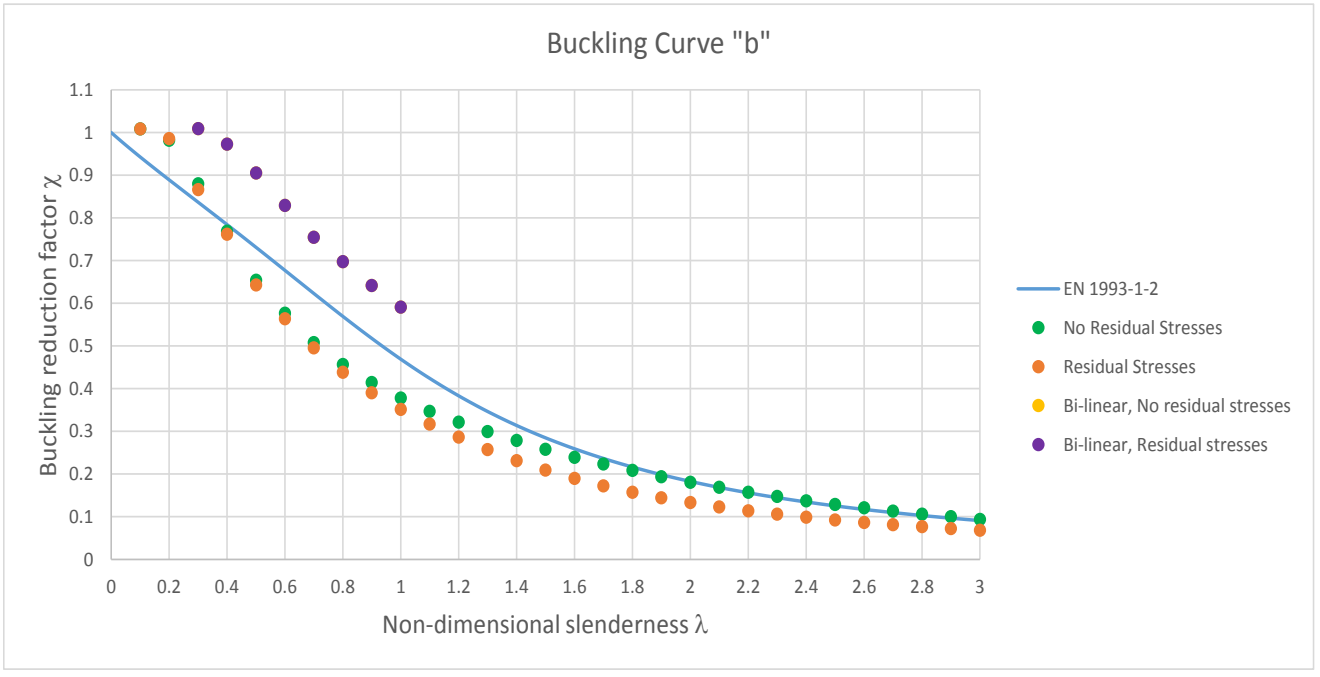

FIGURE 4.10: Comparison of FEMs with the EN 1993-1-2 provisions for buckling curve 'b' at 700 °C.

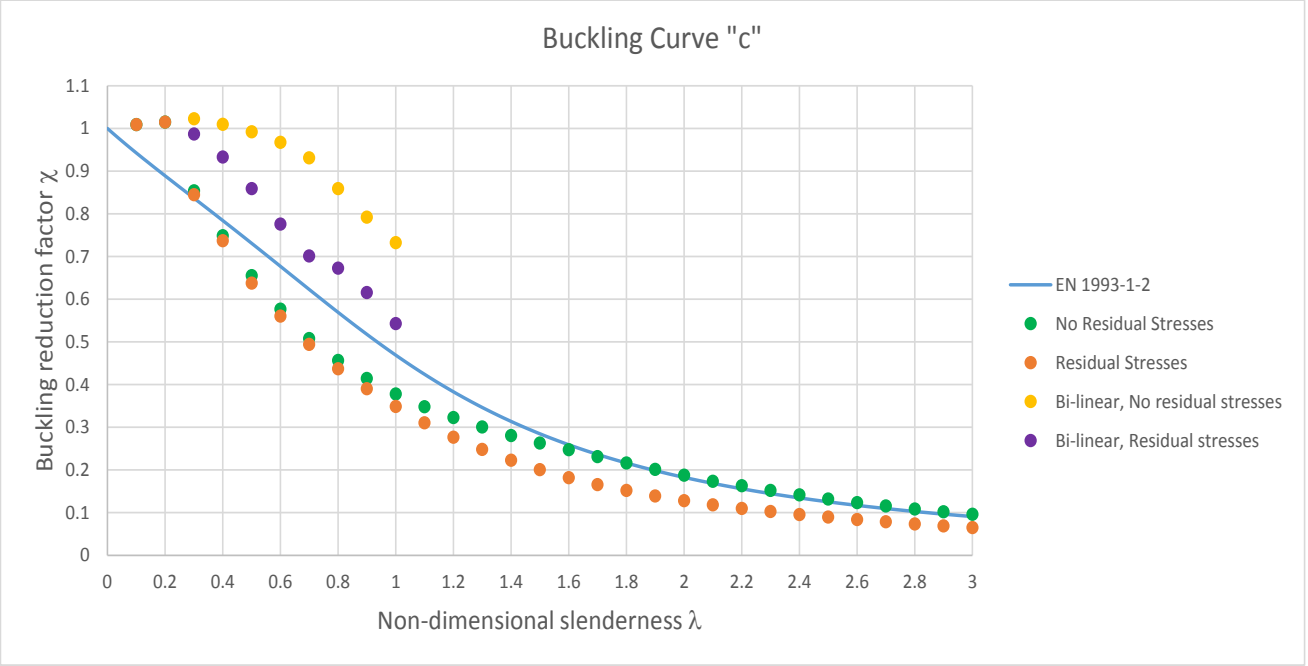

FIGURE 4.11: Comparison of FEMs with the EN 1993-1-2 provisions for buckling curve 'c' at 700 °C.

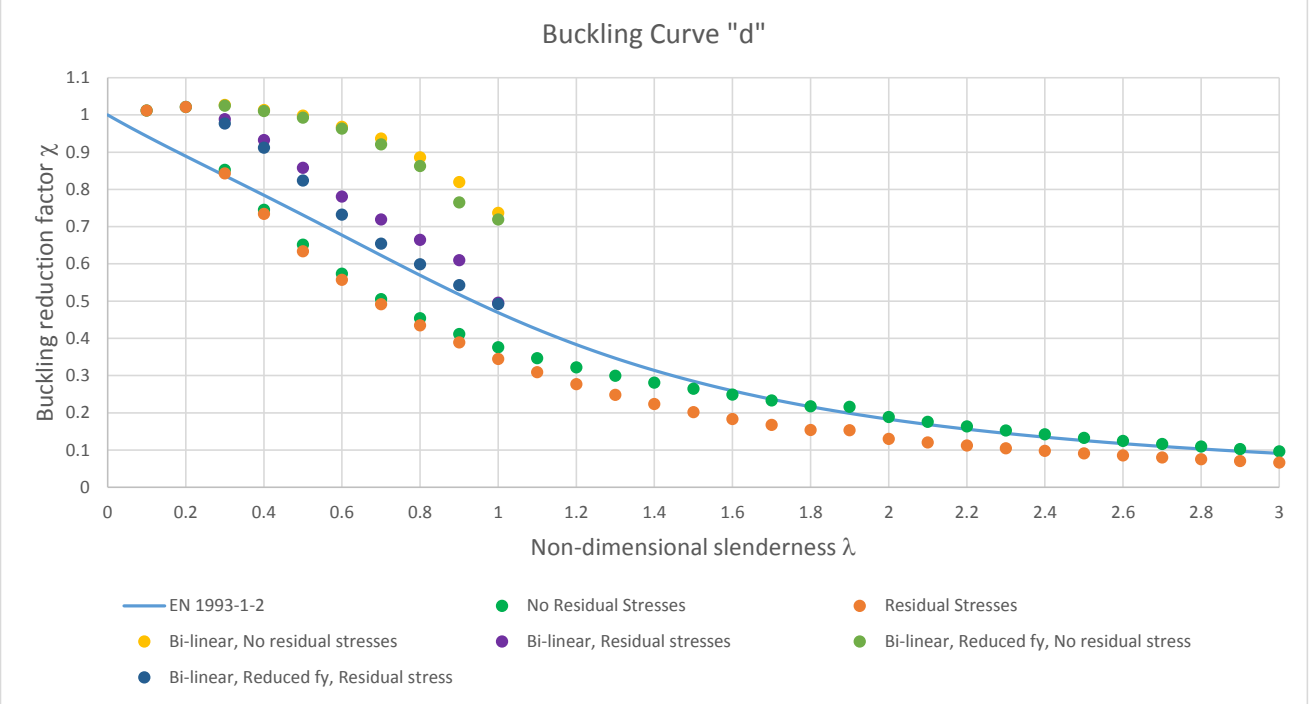

FIGURE 4.12: Comparison of FEMs with the EN 1993-1-2 provisions for buckling curve 'd' at 700 °C.

Similarly as in the analysis at 500,° C, the results show a reasonable agreement with the En 1993-1-2 buckling curves in the low and high slenderness ranges, but show a relative underestimation of buckling strength in the lower mid-slenderness region of the graph. The suspected reasons for this discrepancy are the same as in the analysis at 500 °C. A better agreement between both residual stress models is seen for the cross-section corresponding to the a_0 curve, while a progressively increasing discrepancy and better fit with the Eurocode buckling curve (particularly in the mid-slenderness range) is observed for cross-sections of curves "a" through "d". As in the case for the analysys at 500 °C this leads to a reasonable assumption that the Eurocode neglects residual stresses for elevated temperature calculations.

4.4 Comparison at different temperatures

From the obtained results from the finite element analysis a comparison between the constructed buckling curves of each cross-section was performed. The comparison between the finite element analysis results for room temperature, 500 °C and 700 °C is shown in figures 4.13 to 4.17. These figures include the results considering residual stresses (albeit reduced ones in the case of elevated temperatures).

As it can be observed from figures 4.13 to 4.17, the results obtained at elevated temperatures have no significant difference between 500,° C and 700,° C. This is due to the fact that the stress-strain relationship has little variation between the $\sigma/f_{y,\theta}$ ratio at different temperatures for any given strain. This means that while the mechanical properties of steel decay as temperature increases, they do so in a consistent way. This leads to very similar buckling curves for most temperature ranges, so while the buckling reduction factor for fire conditions $\chi_f i$ for a specific column has little variation with temperature, the column's buckling resistance will still be greatly reduced by the decay in its yielding strength. This also explains why the imperfection factor α at elevated temperatures is only dependent on the steel grade instead of the cross-section properties, as is the case for room temperature design.

To better illustrate this, the stress-strain relationships shown in figures 4.1 and 4.2 were normalized and are now shown as adimensional stress-strain curves in figures 4.18 and 4.19.Very little difference is seen between the normalized stress-strain curves between 400 °C and 1000 °C. The only perceivable difference can only be appreciated in the curves for 1100 °C. Up until this temperature, no significant difference between buckling curves should be expected.

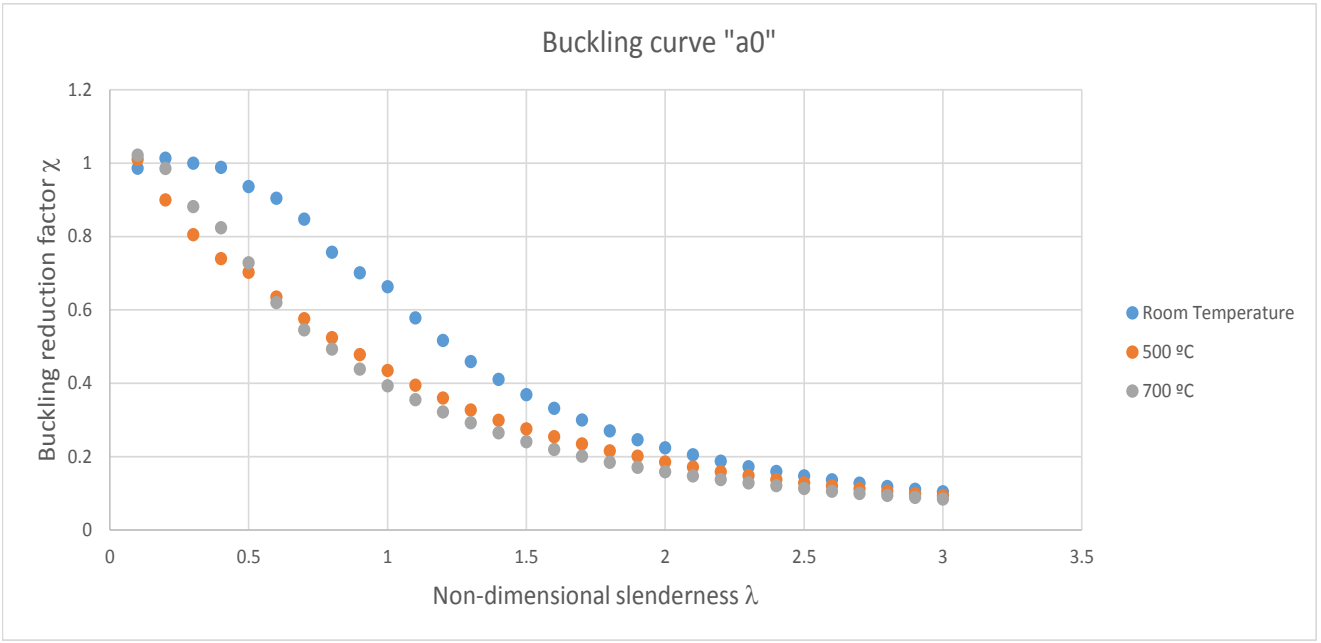

FIGURE 4.13: Comparison of FEA buckling curves at different temperatures for cross-section "a_0".

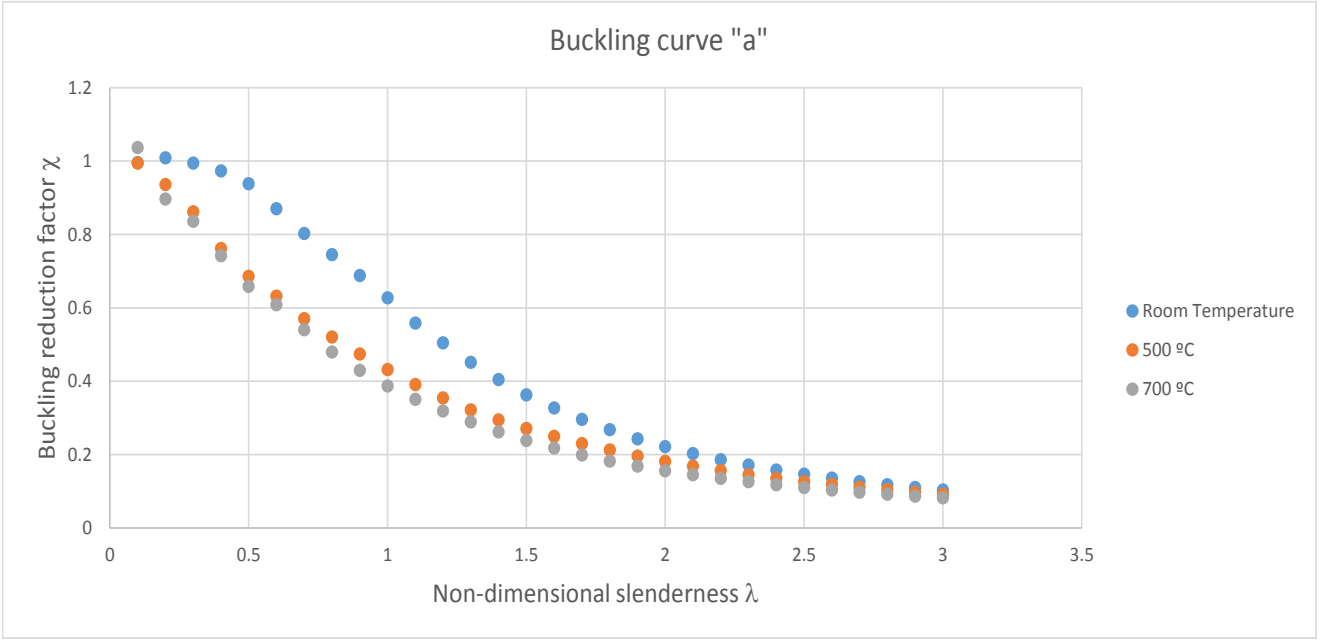

FIGURE 4.14: Comparison of FEA buckling curves at different temperatures for cross-section "a".

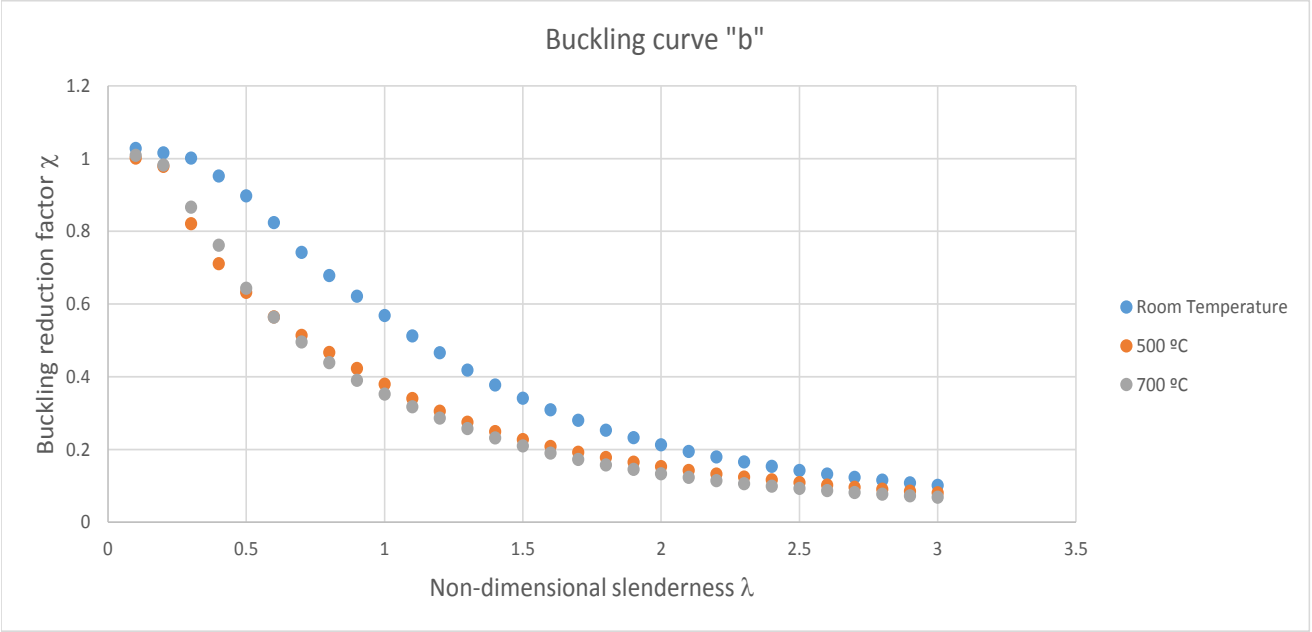

FIGURE 4.15: Comparison of FEA buckling curves at different temperatures for cross-section "b".

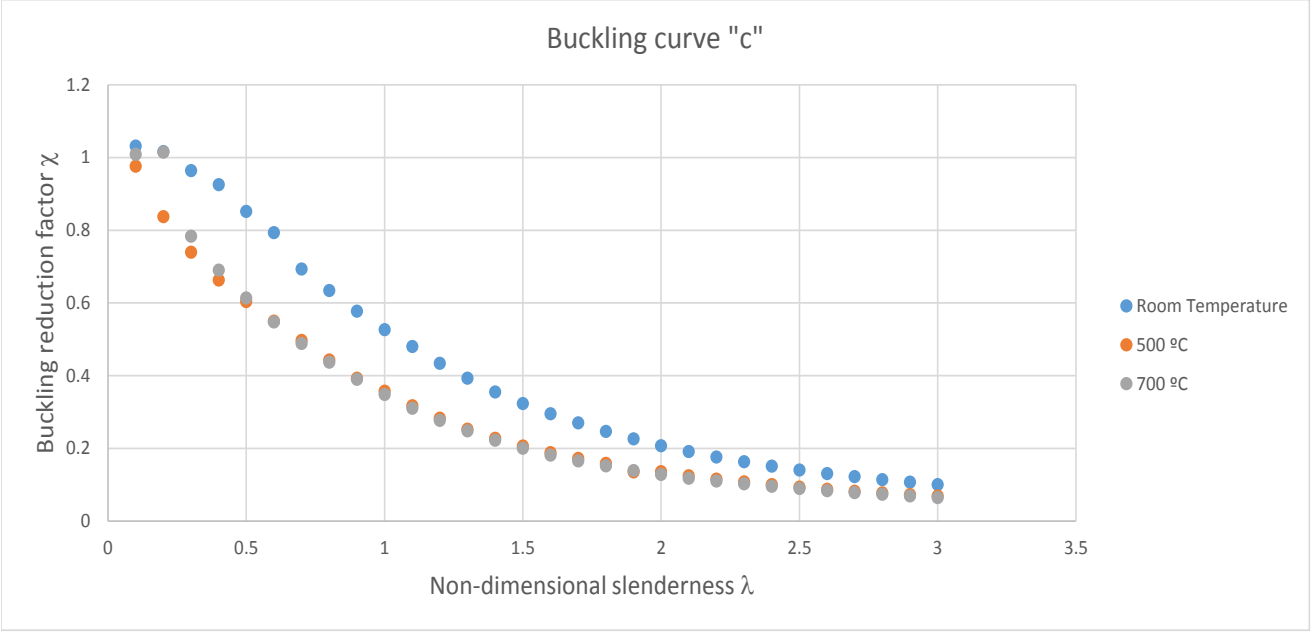

FIGURE 4.16: Comparison of FEA buckling curves at different temperatures for cross-section "c".

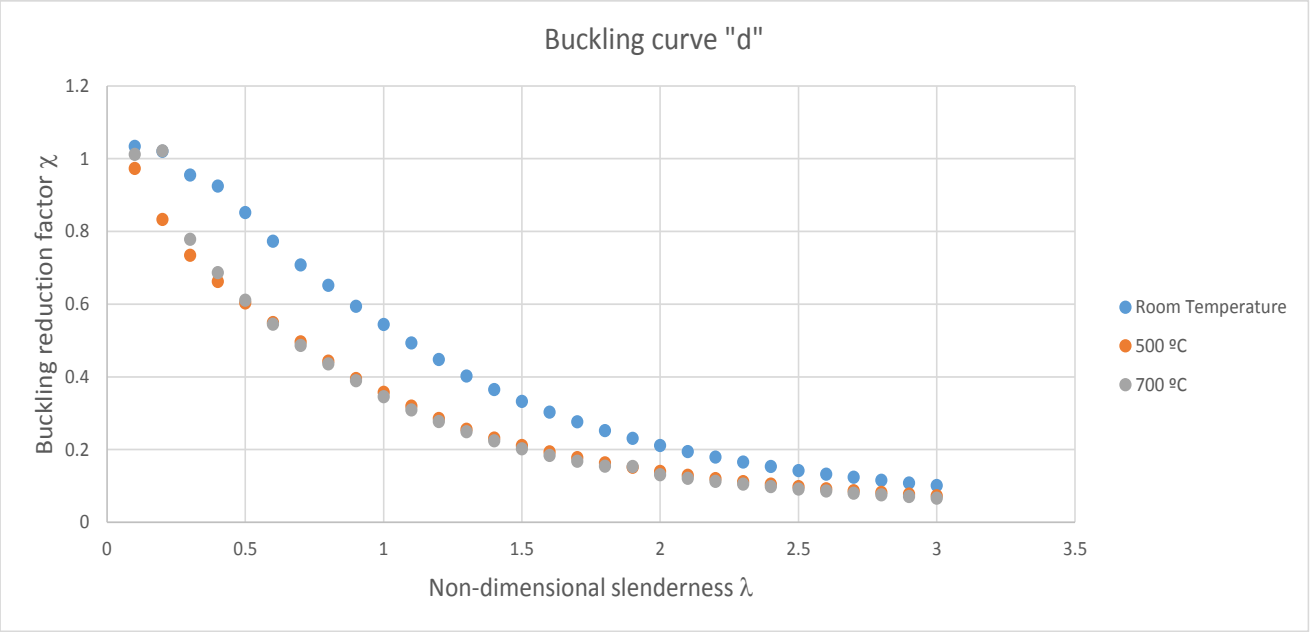

FIGURE 4.17: Comparison of FEA buckling curves at different temperatures for cross-section "d".

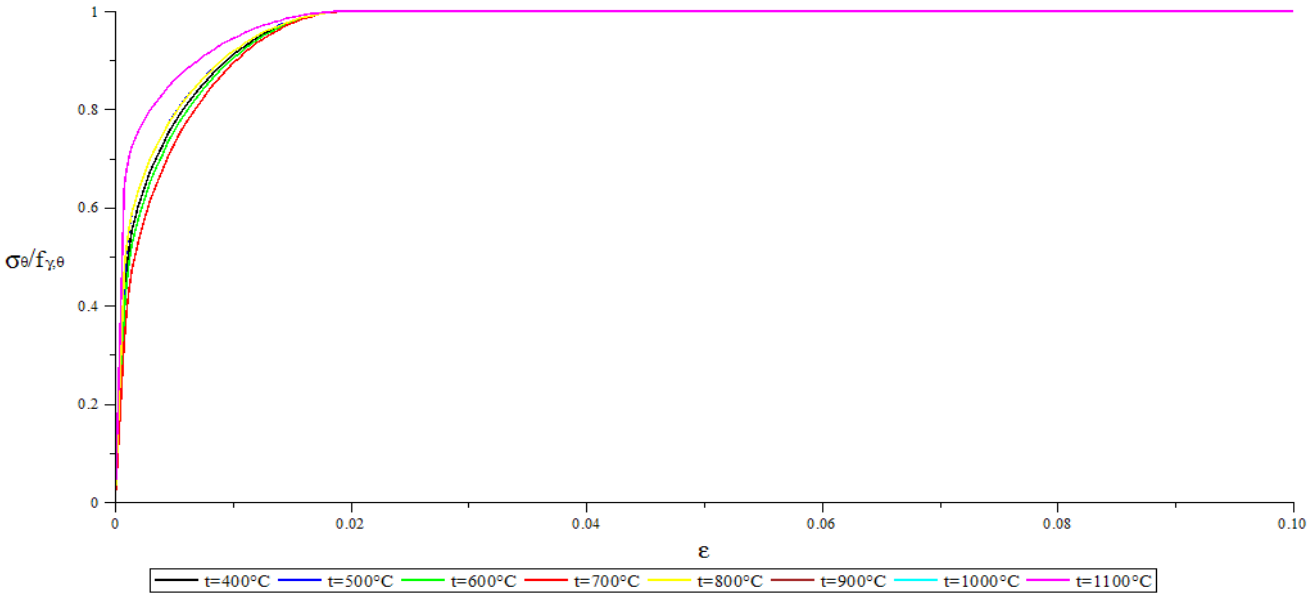

FIGURE 4.18: Normalized stress-strain relationships at elevated temperatures for steel grade S275

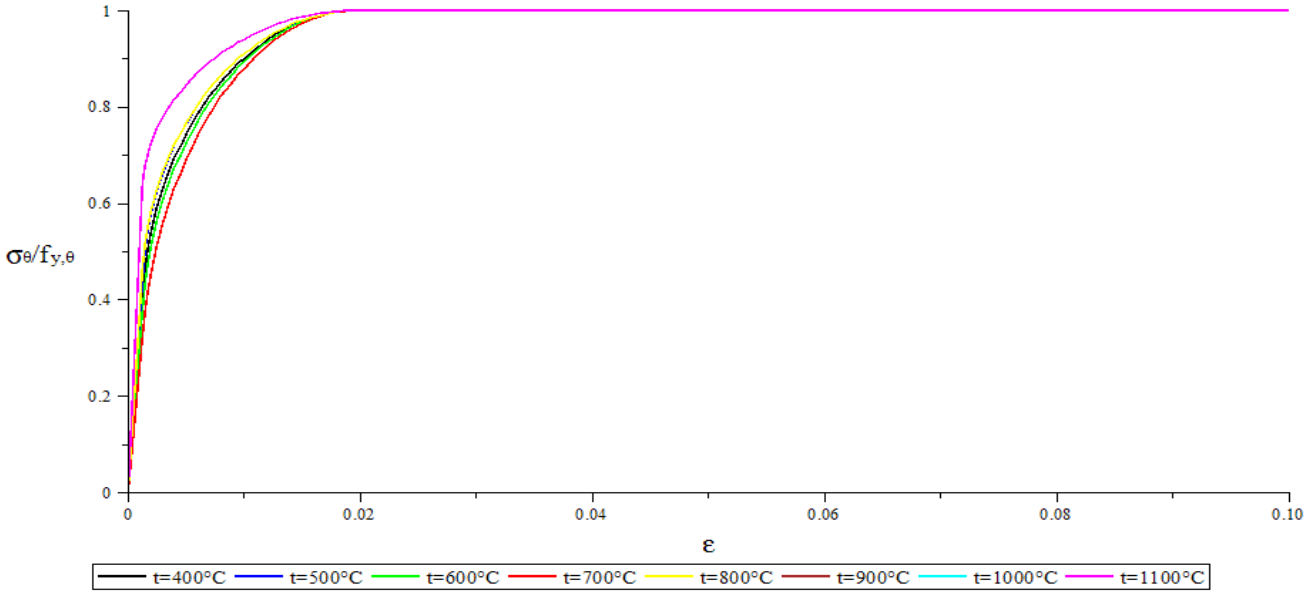

FIGURE 4.19: Normalized stress-strain relationships at elevated temperatures for steel grade S460

4.5 Summary and Conclusions

During this phase of the study a finite element analysis for axially loaded columns of variable slenderness with the cross-sections specified in table 3.2 at 500 °C and 700 °C was performed. The tasks described in this chapter can be summarized as follows:

- Finite element models with non-dimensional slenderness values ranging from 0.1 to 3.0 were created for the cross-sections corresponding to buckling curves "a_0" through "d" in EN 1993-1-1 for 500 °C and 700 °C. A total of 600 FEMs were created.
- Each model was created and analyzed as a pin-ended column under concentric axial load, which was introduced as a vertical prescribed displacement on top of the column.
- The mechanical properties of steel at each elevated temperature were specified in the way of an elevated temperature stress-strain relationship during the material characterization phase of pre-processing.
- Two sets of FEMs were analyzed: one considered a reduction of residual stresses proportional with temperature and a second one completely neglecting residual stresses.

- A stability analysis was performed to find the first buckling mode of each column followed by a non-linear analysis where the vertical prescribed displacement was applied.
- The buckling load found in these analyses was used to determine the buckling reduction factor in fire conditions $\chi_f i$
- The values of the factor χ_{fi} were plotted and buckling curves corresponding to each cross-section, temperature and residual stress state combination were created.
- The obtained buckling curves were compared between each other as well as with the Eurocode 1993-1-2 provisions.

Upon analysis and comparison of the obtained results the following initial conclusions can be drawn:

- A clear reduction in buckling capacity can be observed when comparing a room-temperature buckling curve to an elevated-temperature one for the same cross-section.
- For elevated temperatures, the cross-sectional classification has little meaning. This is due to the fact that at room temperature the curves are differentiated through the imperfection factor α, which has specific values depending on the geometrical properties of a cross-section; for elevated temperatures the imperfection factor α is only dependent on the nominal yield stress. This means that all cross-sections of the same steel grade will have the same elevated-temperature buckling curve, which is consistent with the results shown in figures 4.13 to 4.17. The reason for the change in the formulation of the imperfection factor α is probably due to the small variation in the $\sigma/f_{y,\theta}$ ratio at different temperatures. This is further illustrated through the normalized stress-strain relationships shown in figures 4.18 and 4.19.
- The buckling curves obtained from the finite element analysis show good agreement with the Eurocode provisions in the medium/high slenderness range but show discrepancies in the mid/low range. This discrepancy is likely due to the lack of consideration of the increasing non-linearity in the stress-strain relationship at elevated temperatures and the consideration of a uniform imperfection factor across all cross-sections in EN 1993-1-2.
- The consideration of a bi-linear stress-strain relationship produced higher values of the buckling reduction factor $\chi_f i$ in all cross-sections for both temperatures.

- A closer fit to the Eurocode provisions is observed on the buckling curve that neglects residual stresses, leading to the conclusion that EN 1993-1-2 is likely to completely disregard residual stresses at elevated temperatures.

From these findings it is hard to make a definitive statement on what the Eurocode considerations were for the formulation of the buckling curves at elevated temperatures, but looking at the plotted results at either temperature in can be seen that the Eurocode buckling curve in each case lies in-between the results with a non-linear stress-strain relationship with no residual stresses and the results with a bi-linear stress-strain relationship with no residual stresses. From this observation, the Eurocode buckling curves could be thought of a as an approximation of the buckling reduction factor χ_{fi} with no residual stresses. This approximation would be an average between the resistance given by a bi-linear and a non-linear stress-strain relationship.

Another aspect that should be noted on the obtained buckling curves is the fact that the low-slenderness "plateau" for non-dimensional slenderness values $\bar{\lambda} \leq 0.2$ shown in the room-temperature buckling curves is still present in the buckling curves at 700 °C, while the elevated temperature buckling curves created through the EN 1993-1-2 provisions have a negative slope at $\bar{\lambda} = 0$, completely disregarding the plateau. The result found through the finite element analysis is to be expected given that very stocky sections will not fail due to flexural buckling but instead will fail by plastic yielding of the cross-section. As in the room-temperature scenario, columns below this non-dimensional slenderness value will have a buckling reduction factor equal to one. The lack of consideration of this region in the buckling curves could also be a factor related to the discrepancy in the mid/low slenderness range between the FEA results and the Eurocode provisions. However, this behaviour is not shown so evidently in the obtained buckling curves at 500 °C

Chapter 5

Column Buckling Under the Effect of Thermal Gradients

5.1 Thermal gradients from literature

As discussed in section 2.4, Boon performed a detailed thermal analysis of steel columns under the effects of a thermal gradient produced by a pool fire [16]. Figures 5.1 and 5.2 show the temperature at different points in the cross-section for the cases when the thermal gradient was induced along the weak axis and the strong axis respectively. The figures show the temperature distributions for the cases of the maximum thermal gradient and maximum temperature during the fire.

These results were adapted to the cross-sections used in this study. To do so, the temperature distribution was normalized along the height or the width of the cross-section accordingly. The distribution was then approximated through a linear regression as it is shown in figures 5.3 and 5.4. The reason for this is because defining a linear temperature gradient prevents sudden spikes in stresses due to differential thermal expansion in-between the elements of the finite element model as opposed to simply specifying the temperatures at discrete points in the cross-section.

5.2 Finite Element Model

The construction of the finite element models for this stage was similar to what was done in previous chapters. However, due to the presence of a temperature gradient throughout the cross-section, some modifications were necessary.

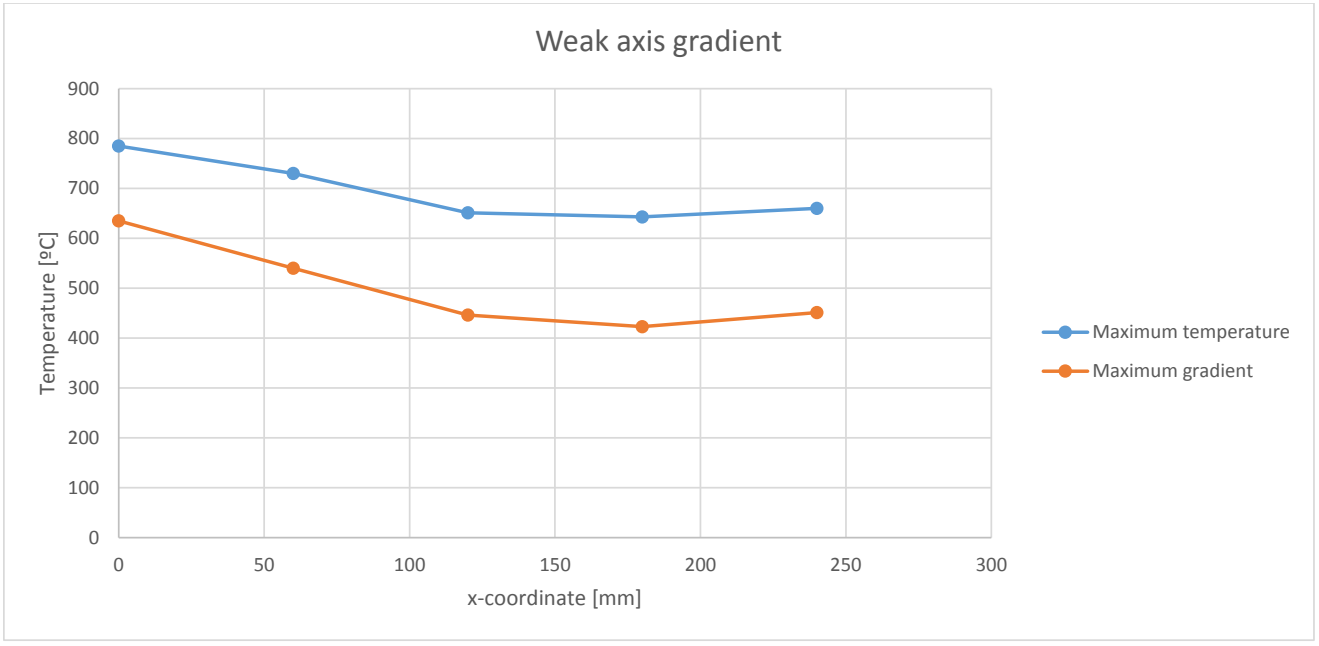

FIGURE 5.1: Temperature distribution along the weak axis.

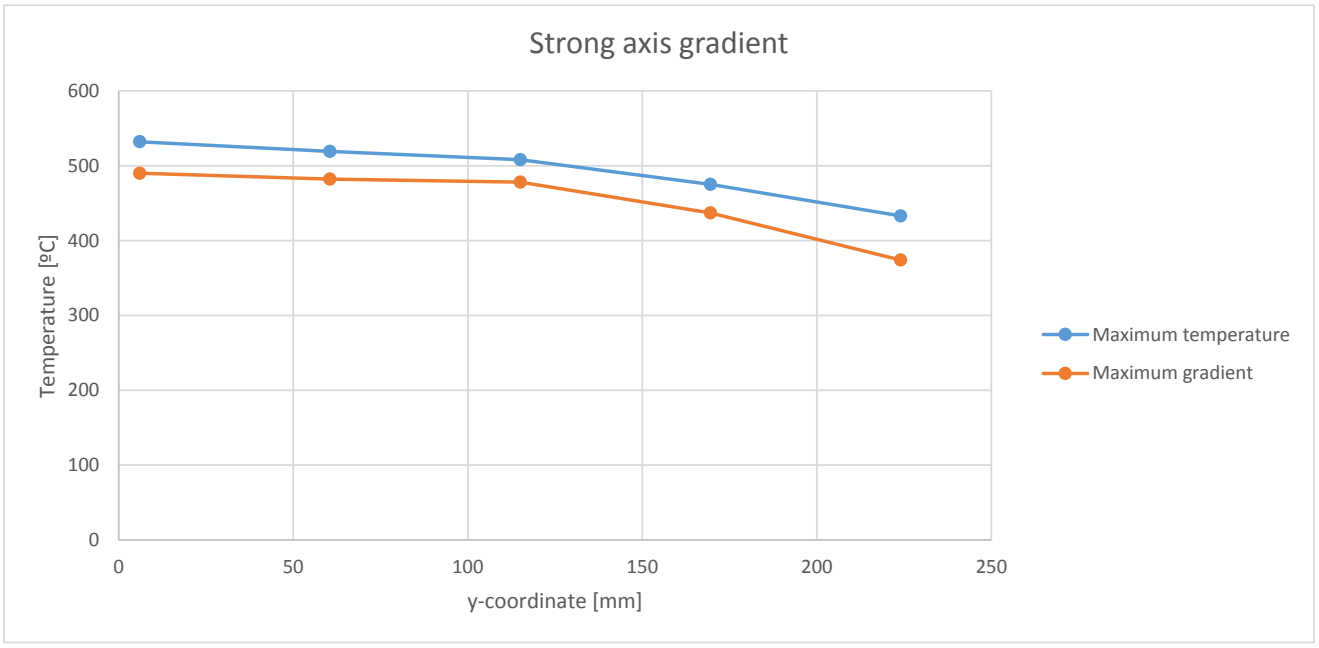

FIGURE 5.2: Temperature distribution along the strong axis.

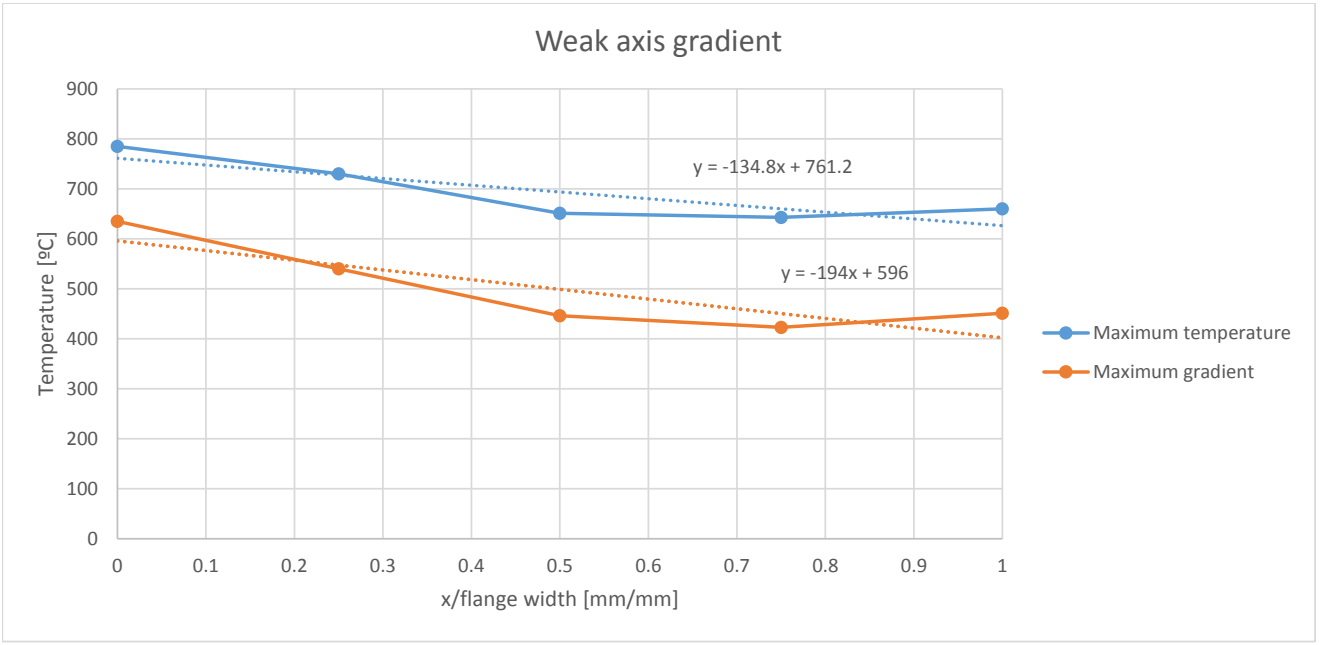

FIGURE 5.3: Temperature distribution normalized along the weak axis.

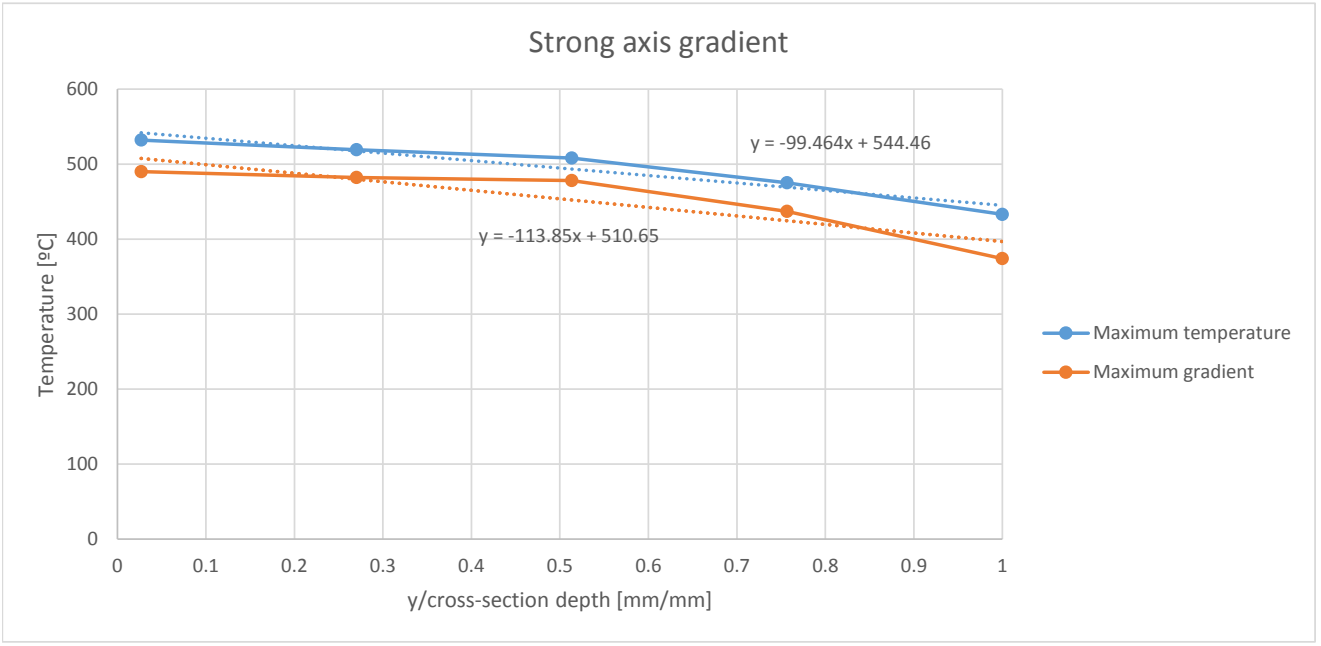

FIGURE 5.4: Temperature distribution normalized along the strong axis.

5.2.1 Definition of temperature-dependent material properties

The presence of a temperature gradient through the cross-section means that a single stress-strain relationship is not sufficient, but rather a set of various curves is required. The stress-strain relationships for mild steels at elevated temperatures can be derived through the provisions in Eurocode 1993-1-2 section 3.2 [10] as it was shown previously in figures 4.1 and 4.2. Using these derived stress-strain relationships at various temperatures, the mechanical behavior of steel is defined by specifying the modulus of elasticity (which is also temperature-dependent) to describe the linear portion of the stress-strain relationship before yielding and a set of equivalent plastic strains with corresponding stresses to describe the behavior after yielding. Combined, these two strain ranges constitute the full stress-strain relationship at a specific temperature. The stress-strain relationships for steel grades S460 and S275 were specified in this way for 300 °C, 400 °C...800 °C according to the maximum and minimum temperatures that were present in the models. The mechanical properties for any unspecified temperature in-between (e.g. at 350 °C) are determined automatically through linear interpolation.

The temperature-dependent modulus of elasticity in each model was defined according to the reduction factors from Eurocode 1993-1-2, previously shown in figure 2.2 [10]. Table 5.1 shows the values of Young's modulus used to describe the linear portion of the stress-strain relationship at various elevated temperatures.

TABLE 5.1: Young's modulus at various elevated temperatures.

Temperature	300 °C	400 °C	500 °C	600 °C	700 °C	800 °C
E [MPa]	168,000	147,000	126,000	65,100	27,300	18,900

Once the proportionality limit is reached (where the equivalent plastic strain is equal to $\varepsilon_p = 0$) the equivalent plastic strains and corresponding stresses are specified for each temperature. In the case of the stress-strain relationship of steel grade S275 at 300 °C the behavior is linear with a slope equal to 168,000 MPa up to a stress of 168.575 (the proportionality limit $f_{p,\theta}$ at 300 °C), which corresponds to a plastic strain of zero. Subsequent points in the stress-strain relationship are specified through plastic strain-stress pairs up to an equivalent plastic strain of 0.02. A total of 21 points were specified for this non-linear portion of each stress-strain relationship to provide as much accuracy as possible. This procedure was performed for steel grades S460, S275 and S275 with consideration for thick plates (as is the case of the "d" cross-section).

5.2.2 Application of the temperature gradients

The linear regression shown in each of the temperature distributions in figures 5.3 and 5.4 were used to define the temperature in the nodes for each finite element model. The equations used to determine these temperatures are as follow:

For the case of maximum gradient along the weak axis:

$$\theta = 596 - \frac{194 \cdot x}{b_f}$$

For the case of maximum temperature along the weak axis:

$$\theta = 761.2 - \frac{134.8 \cdot x}{b_f}$$

For the case of maximum gradient along the strong axis:

$$\theta = 510.65 - \frac{113.85 \cdot y}{h}$$

For the case of maximum temperature along the strong axis:

$$\theta = 544.46 - \frac{99.464 \cdot y}{h}$$

In each of the cases the mesh of the finite element models was also refined in the direction of the thermal gradient (i.e. it was refined along the strong axis for strong axis gradient and viceversa). Using the equations above and having refined the mesh in each corresponding direction the nodal temperatures were specified in the model. The temperature distributions for weak axis gradient are shown in figure 5.5 and the distributions for strong axis gradient are shown in figure 5.6.

5.2.3 Non-dimensional slenderness

Another aspect that had to be modified was the calculation of the length of each of the columns. In the case of a uniform temperature distribution, the column length was easily determined through equation 2.8:

$$\bar{\lambda_\theta} = \bar{\lambda}[\frac{k_{y,\theta}}{k_{E,\theta}}]^{0.5}$$

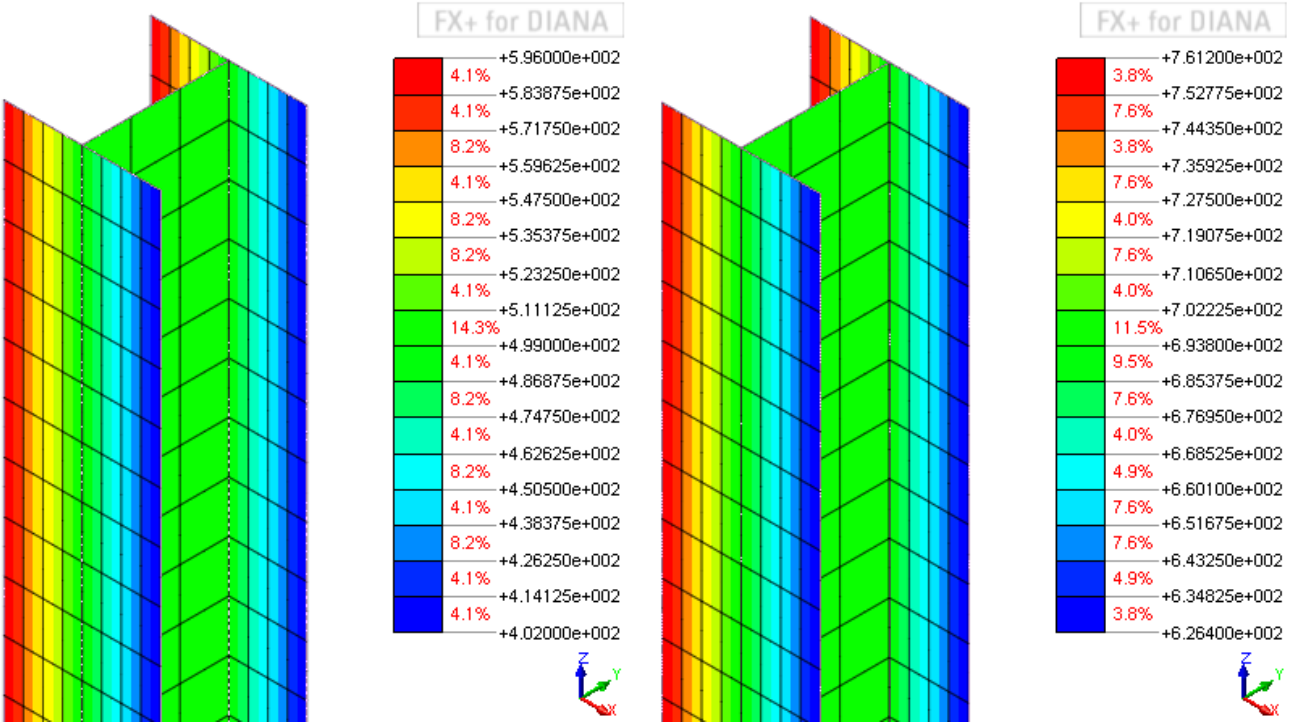

FIGURE 5.5: Maximum gradient distribution (left) and maximum temperature distribution (right) for weak axis thermal gradient.

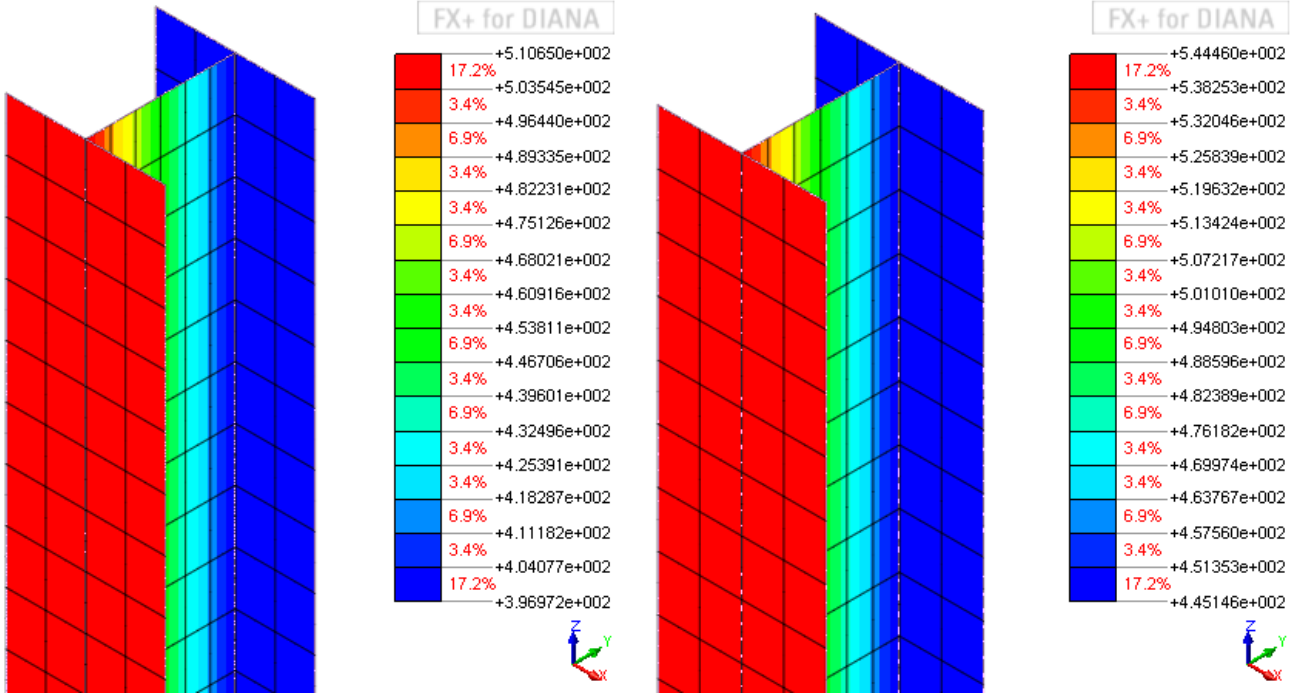

FIGURE 5.6: Maximum gradient distribution (left) and maximum temperature distribution (right) for strong axis thermal gradient.

...by using the corresponding values of the reduction factors $k_{y,\theta}$ and $k_{E,\theta}$. However, since the temperature in the cross-section is not uniform, the application of equation 2.8 is not as straightforward. The Eurocode 1993-1-2 gives no specific indication as to what temperature value to consider when calculating the non-dimensional slenderness of a column with a temperature gradient, but given that for the overall column resistance the highest temperature is to be taken, it stands to reason that this would also be the case in a non-uniform temperature scenario. As it has already been discussed, this approach can lead to an underestimation of the column's resistance. In order to obtain realistic results while maintaining simplicity in the construction of the finite element model and the final comparison, the non-dimensional slenderness was determined by considering a uniform temperature distribution throughout the cross-section using the average temperature from each gradient.

5.2.4 Analysis Parameters

The analysis of each of the finite element models created was performed through the following steps:

1. Stability analysis determining the first eigenmode and applying an imperfection equal to $\frac{L}{1000}$.
2. Application of the temperatures in each node of the model according to each temperature distribution.
3. Application of an incrementally increasing prescribed displacement up to the point of the onset of buckling.

Since in Chapter 4 it was found that residual stresses have little effect in the buckling resistance of columns at elevated temperatures it was decided not to include them in this stage of the study. Also, contrary to previous analyses, the step size of the incrementally increasing prescribed displacement was not kept at a constant 2.5% size. It frequently had to be increased in order to reach the onset of buckling.

Upon termination of the analysis, the maximum total vertical reaction in the supports was measured and registered as the buckling load $N_{b,fi,Rd}$, after which the buckling reduction factor χ_{fi} was determined through equation 2.4.

5.3 Results

Six values of non-dimensional slenderness were modeled for each cross-section: 0.2, 0.4, 0.6, 0.8, 1.5 and 2.5. These values were chosen in order to provide an overall assessment on the precision with which the Eurocode buckling curves and the buckling curves derived through finite element modeling are able to predict the buckling resistance of a column under the effect of a temperature gradient. The cross-sections were modeled for the temperature distributions shown in figures 5.3 and 5.4 for a total of 120 finite element models.

The buckling reduction factor for each of the six slenderness values mentioned were obtained for the four temperature distributions and plotted together with the finite element-derived buckling curve and the EN 1993-1-2 buckling curve for each of the cross-sections. The obtained results are shown in figures 5.7 to 5.11.

In figures 5.7 to 5.11 the temperature gradients 1 to 4 refer to:

- Temperature gradient 1: Maximum gradient along the strong axis.
- Temperature gradient 2: Gradient with maximum temperature along the strong axis.
- Temperature gradient 3: Maximum gradient along the weak axis.
- Temperature gradient 4: Gradient with maximum temperature along the weak axis.

The results from the models with temperature gradients along the strong axis show little variation within the two temperature distributions (i.e. Not much difference is appreciated between temperature gradient 1 and temperature gradient 2). The same can be observed for the case of a temperature gradient along the weak axis.

The results for strong axis gradient show that the Eurocode buckling curves overestimate the buckling reduction factor in almost all cases where the non-dimensional slenderness is not too high ($\bar{\lambda} \leq 1.5$). The same results appear to have very good agreement with the finite-element-derived buckling curve for most cases. The discrepancy for the results with a slenderness value of 2.5 is so small it can be safely neglected. The results for weak axis gradient show that both the Eurocode and the FEM-derived buckling curves overestimate the buckling reduction factor in all cases where the non-dimensional slenderness is not too high ($\bar{\lambda} \leq 1.5$). Once again, the discrepancy at very high slenderness values can be considered to be negligible.

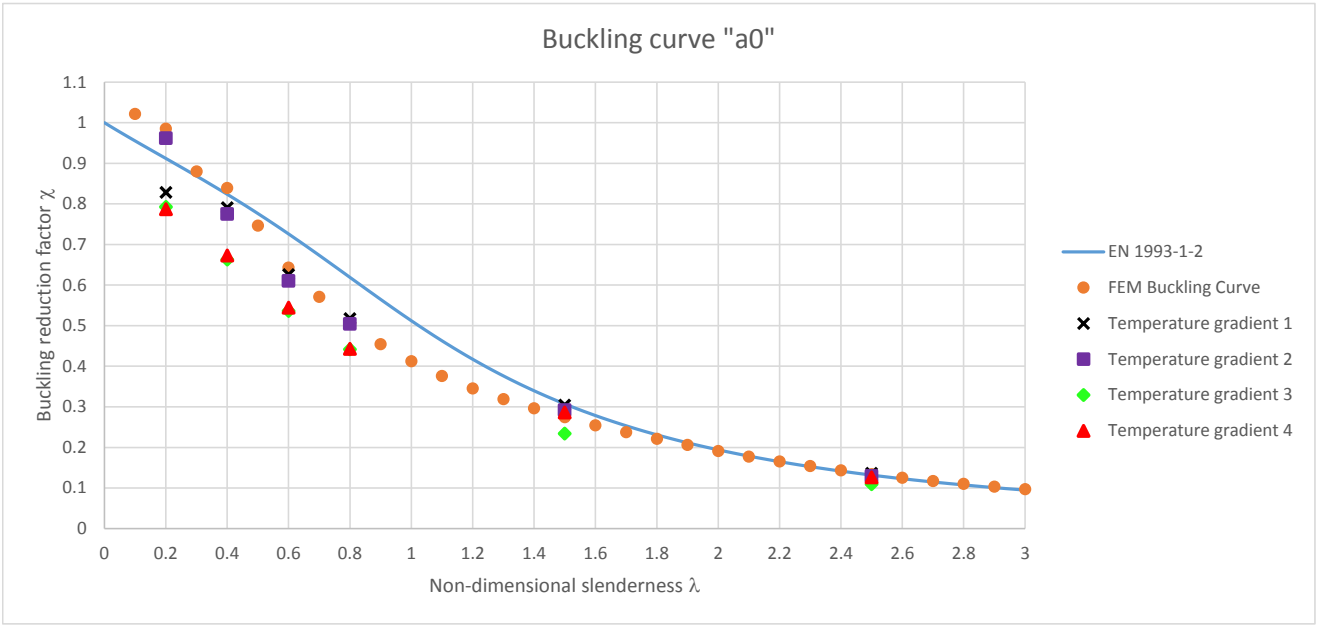

FIGURE 5.7: Comparison of FEM results with thermal gradients for cross-section "a_0"

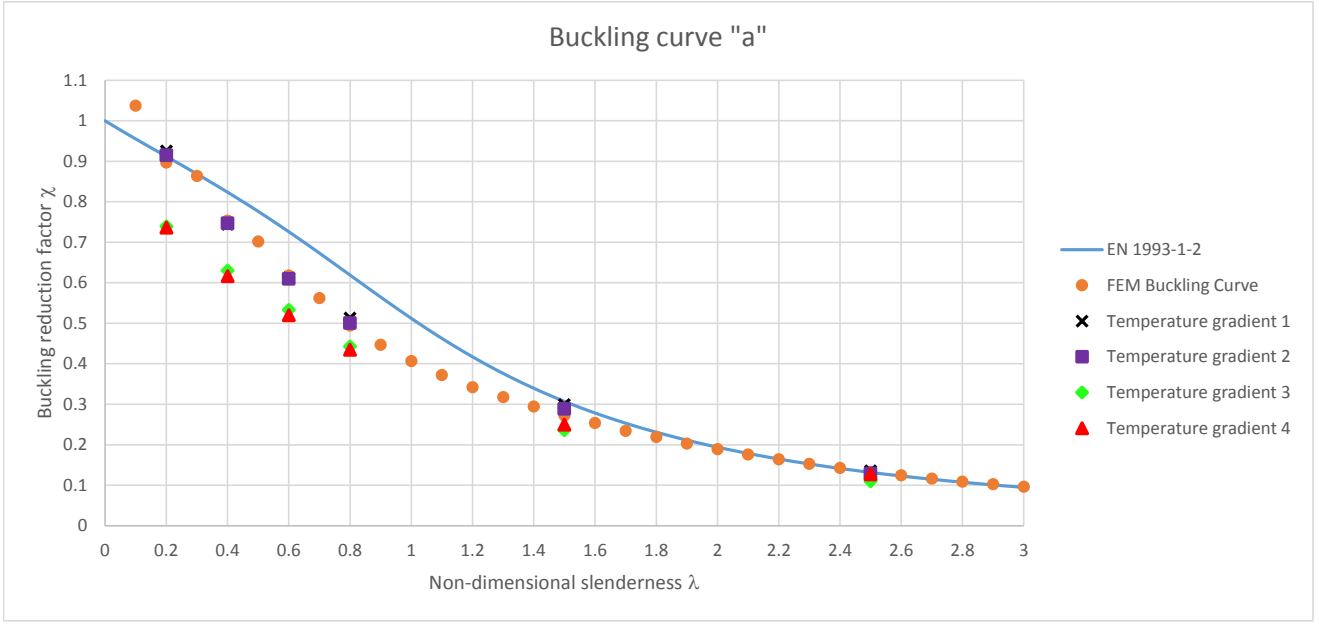

FIGURE 5.8: Comparison of FEM results with thermal gradients for cross-section "a"

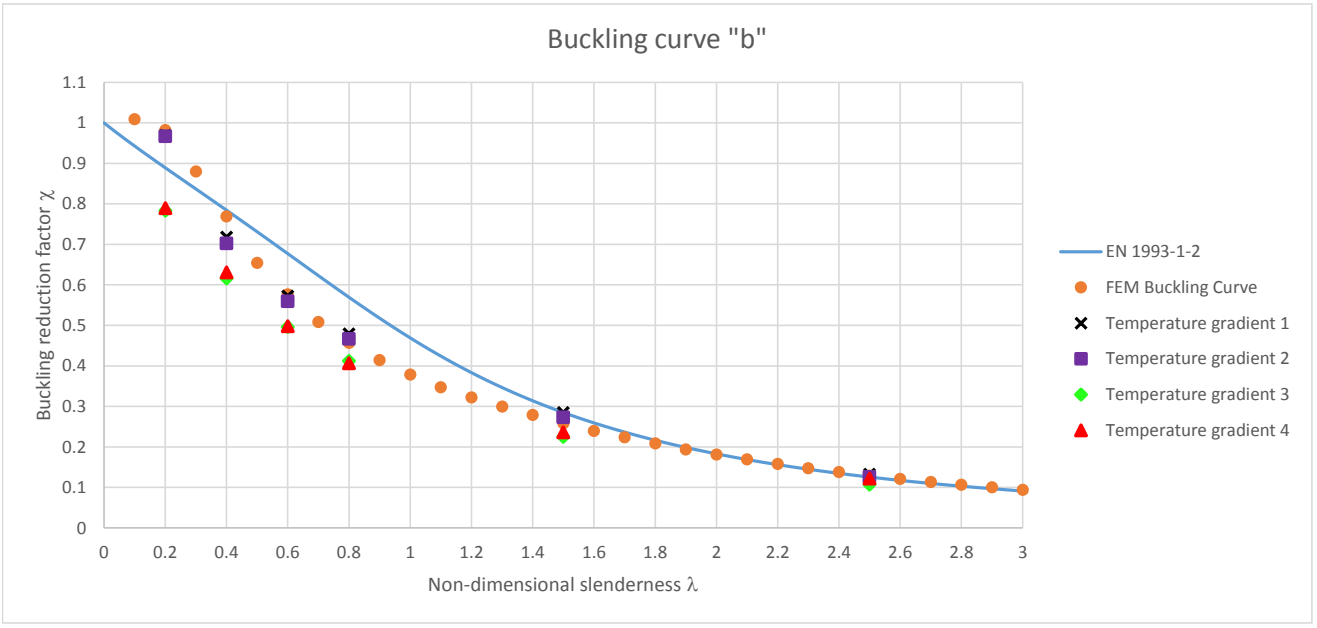

FIGURE 5.9: Comparison of FEM results with thermal gradients for cross-section "b"

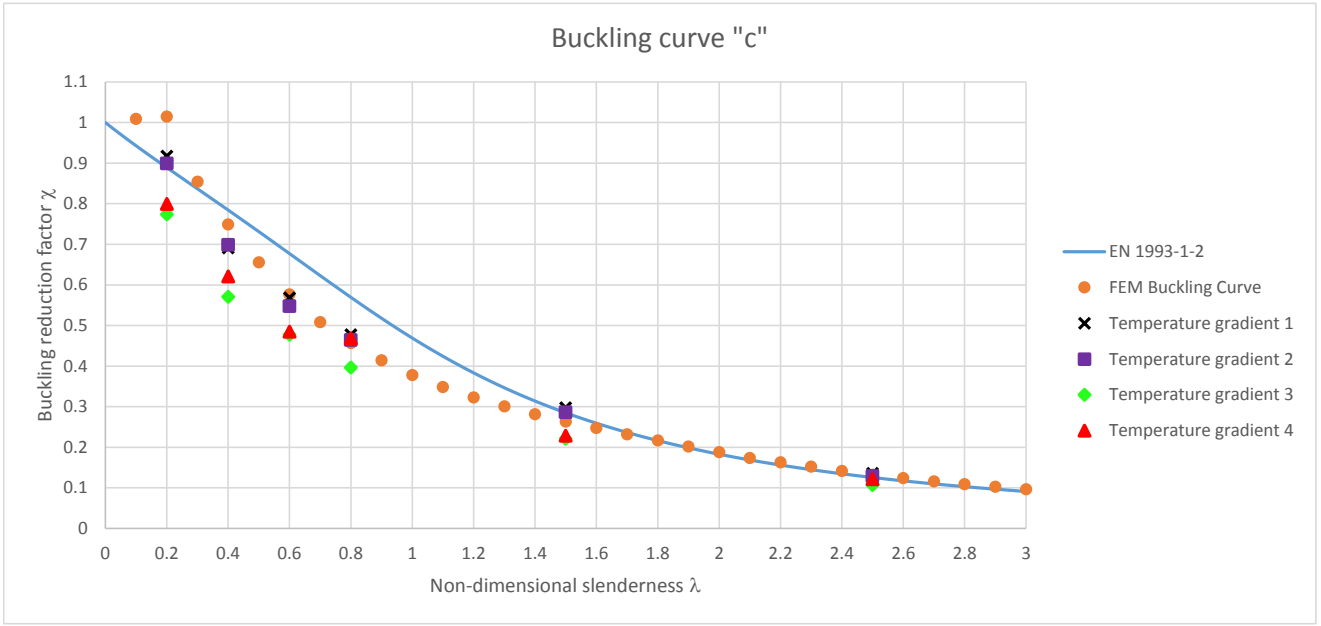

FIGURE 5.10: Comparison of FEM results with thermal gradients for cross-section "c"

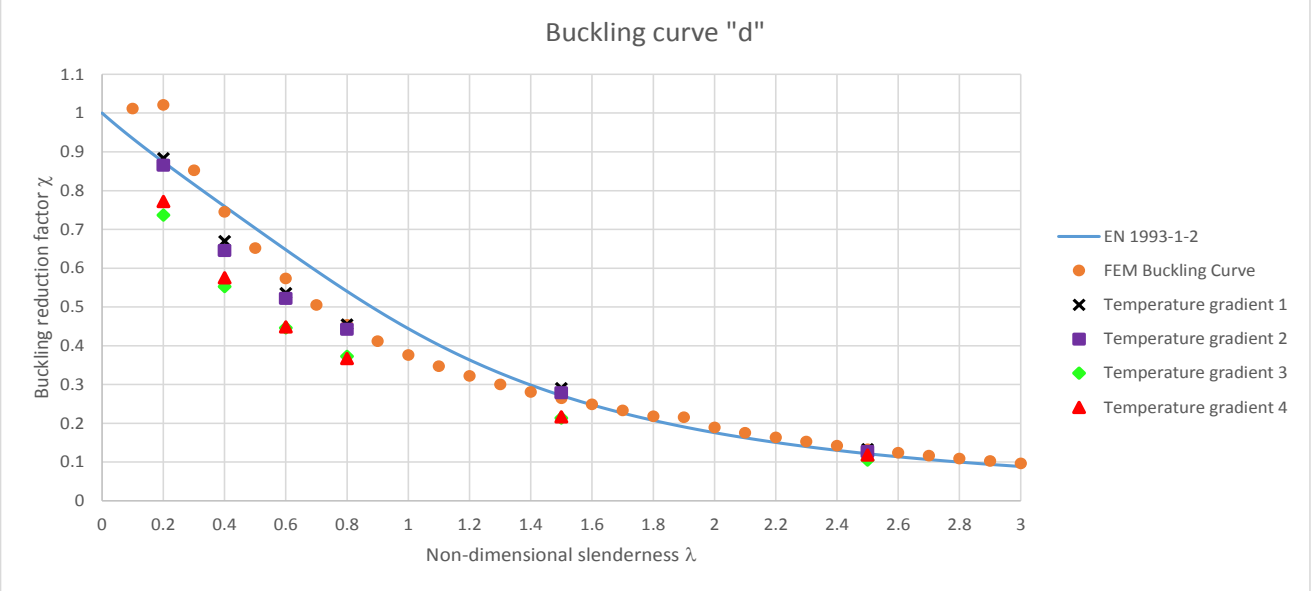

FIGURE 5.11: Comparison of FEM results with thermal gradients for cross-section "d"

The good agreement of the results with the FEM-buckling curve for the case of strong axis thermal gradient is due to the fact that in all cases where buckling took place ($\bar{\lambda} \geq 0.2$) the columns buckled around their weak axis. The direction of the thermal gradient shifts the location of the effective stiffness center along the strong axis, reducing the corresponding moment of inertia. However, even with this shift, the moment of inertia around the weak axis is still lower. This results in the column displaying a buckling behavior like a column with uniform temperature. In the case of a thermal gradient along the weak axis, the shift of the effective stiffness center leads to a decrease of the already low moment of inertia around the weak axis, further lowering the column's buckling resistance in this direction. This explains the discrepancy with the FEM-buckling curve, since the uniform temperature distribution consideration means no shift in the stiffness center. Regardless of this, the results still show a better agreement with the FEM-buckling curve than with the EN1993-1-2 buckling curve. This agreement improves as the non-dimensional slenderness increases.

It should also be noted that, opposed to the case of uniform temperature, the columns with a non-dimensional slenderness equal to 0.2 did not present a buckling reduction factor equal to 1.0. This is due to the fact that the temperature gradient will lead to uneven yielding along the cross-section (i.e. the parts at the highest temperature will yield first and the parts at the lowest temperature will yield last). When the first parts of the cross-section yield, stresses are redistributed in the direction opposite to the thermal gradient until the entire section has yielded. Therefore, even if the column fails

by yielding of the cross-section, whenever there is a temperature gradient present the column will never reach a buckling reduction factor equal to unity.

Figure 5.12 shows the buckling resistances of each of the models analyzed summarized in table form.

Cross-section	Temperature distribution	Non-dimensional slenderness					
		0.2	0.4	0.6	0.8	1.5	2.5
a0	1	6,947.96	6,629.78	5,245.05	4,336.46	2,548.79	1,138.75
	2	7,242.07	5,835.39	4,591.66	3,795.48	2,196.08	974.05
	3	5,857.92	4,895.97	3,961.60	3,263.34	1,730.73	807.82
	4	1,825.51	1,560.61	1,261.96	1,026.31	663.09	292.04
a	1	23,352.99	18,790.22	15,449.27	12,948.71	7,547.05	3,424.43
	2	20,718.37	16,922.33	13,808.09	11,337.74	6,528.89	2,917.10
	3	16,443.49	14,009.32	11,852.52	9,842.35	5,243.10	2,436.06
	4	5,137.95	4,303.04	3,631.39	3,036.35	1,741.70	884.61
b	1	4,860.26	3,598.83	2,869.48	2,401.46	1,427.36	663.96
	2	4,349.87	3,159.20	2,515.83	2,100.94	1,227.52	565.69
	3	3,460.50	2,719.58	2,192.40	1,819.37	992.98	470.17
	4	1,094.95	875.10	690.73	563.68	326.85	168.84
c	1	18,041.42	13,592.29	11,175.05	9,384.75	5,849.85	2,667.09
	2	15,874.17	12,330.96	9,657.90	8,195.59	5,046.01	2,272.19
	3	13,413.04	9,891.20	8,270.75	6,870.09	3,831.25	1,852.22
	4	4,349.32	3,375.77	2,638.51	2,549.18	1,241.88	658.21
d	1	16,931.19	12,826.73	10,262.54	8,711.85	5,564.27	2,555.74
	2	14,880.90	11,093.60	8,970.24	7,601.93	4,795.05	2,176.40
	3	12,441.72	9,328.32	7,529.15	6,289.01	3,597.35	1,766.07
	4	4,089.71	3,047.43	2,376.25	1,945.25	1,146.10	624.62

FIGURE 5.12: Buckling resistance of columns under the effect of thermal gradients (results in kN).

5.4 Comparison with construction codes EC3, AISC 2005 and AS 4100

The results from this stage were also compared with the AISC 2005 and AS 4100 codes to assess if either of them provided a more suitable alternative for the calculation of the buckling resistance of a column under the effect of thermal gradients.

The comparison between codes for a column under the action of temperature distribution 1 (maximum thermal gradient along the strong axis) is shown in figures 5.13 to 5.17.

For this temperature distribution it can be said that, for the most part, all construction codes have a reasonably good agreement with the FEM results, showing better agreement as the length of the column increases. Some overestimation and underestimation of buckling resistance is shown in different cross-sections in the mid-slenderness range, but this difference seems very low. The highest discrepancy between the FEM results and the building codes is seen at the lowest column length, where no buckling occurred. This is due to the consideration of all building codes that the entire section has a yielding strength corresponding to that of the highest temperature.

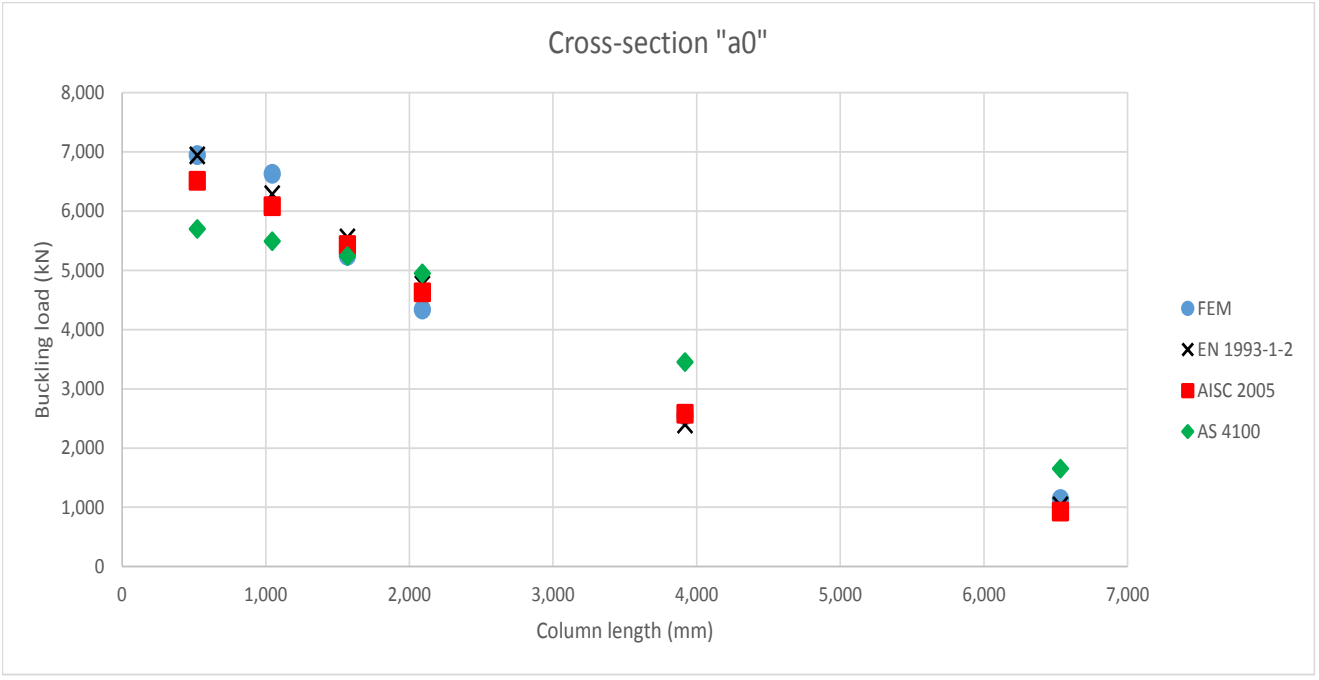

FIGURE 5.13: Comparison of FEM results with temperature distribution 1 for cross-section "a_0"

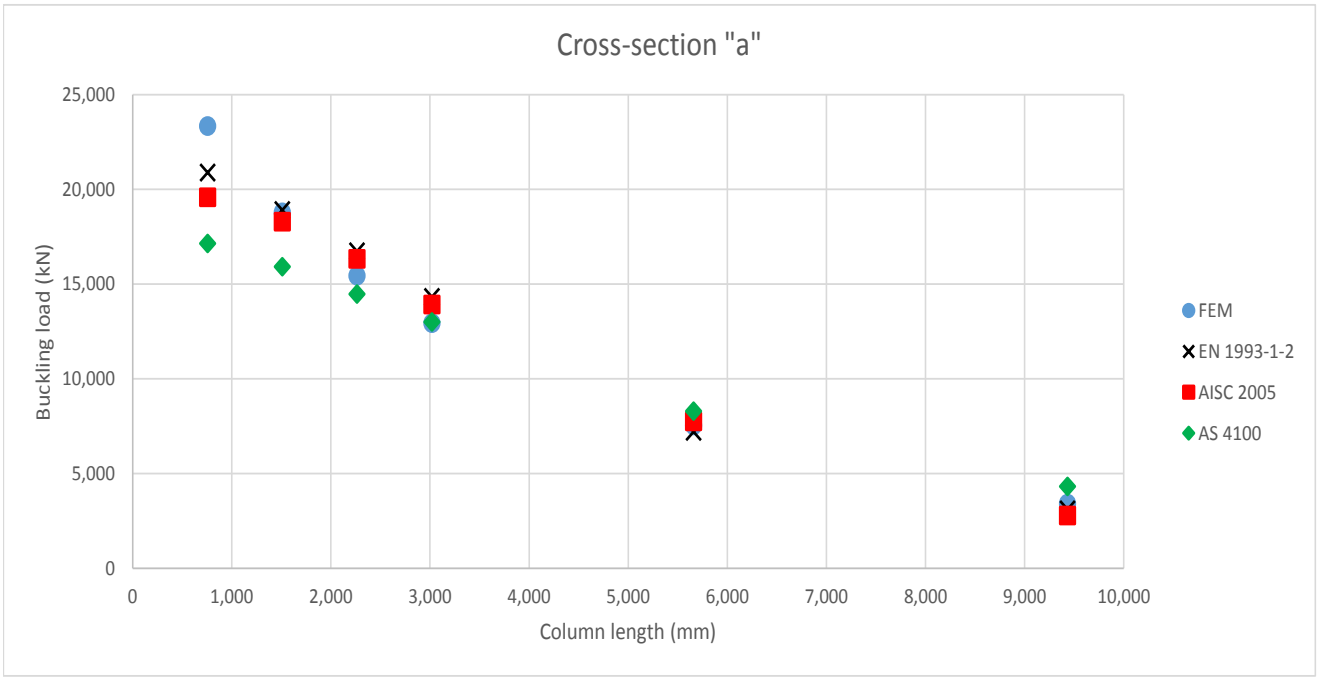

FIGURE 5.14: Comparison of FEM results with temperature distribution 1 for cross-section "a"

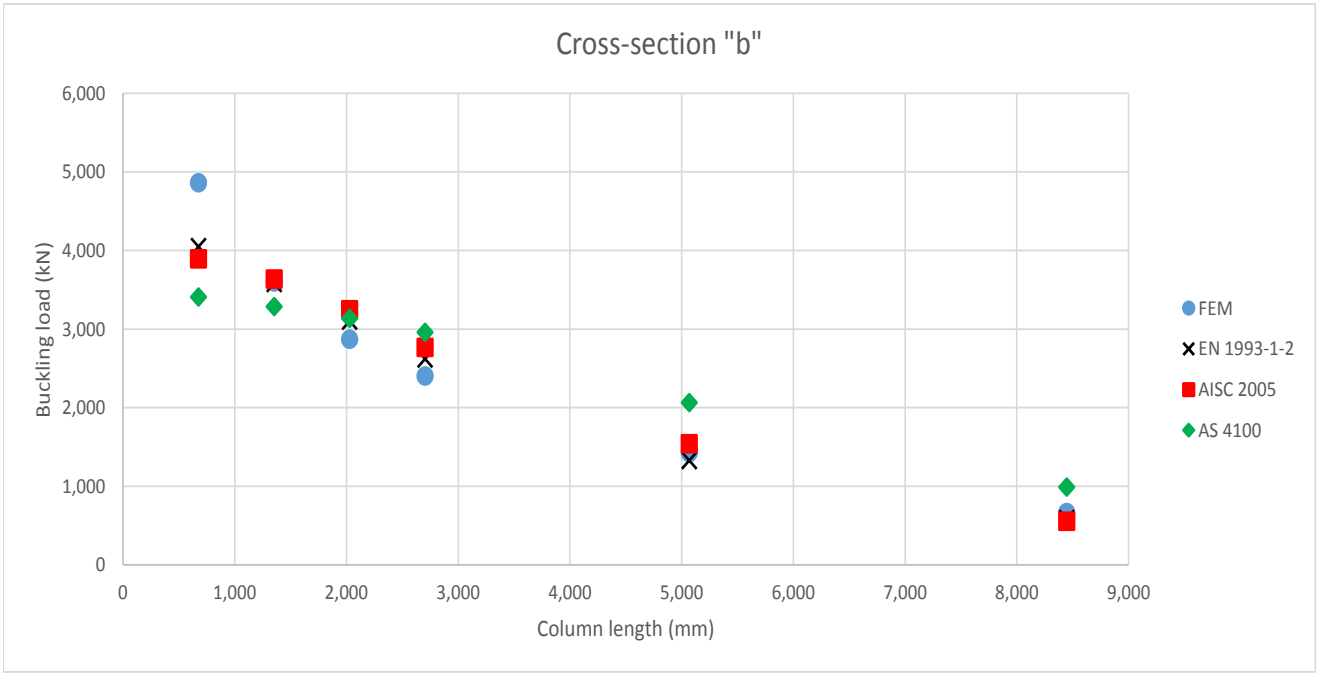

FIGURE 5.15: Comparison of FEM results with thermal gradients for cross-section "b"

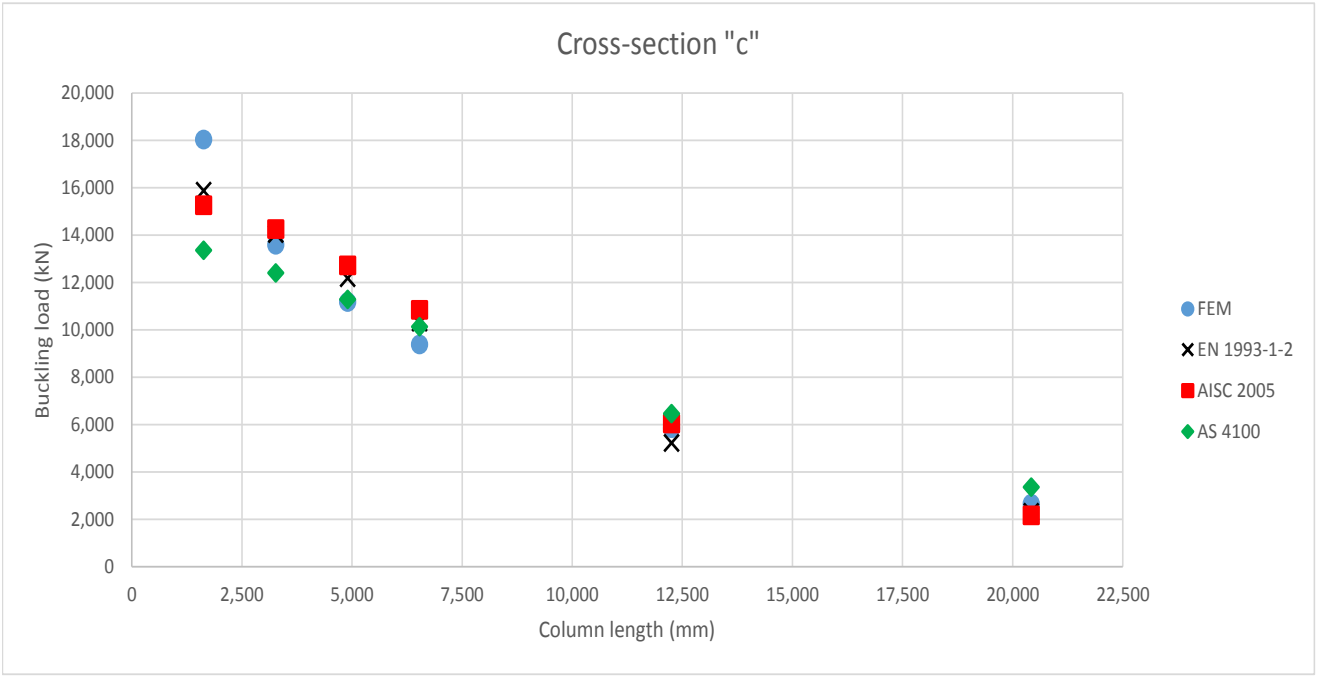

FIGURE 5.16: Comparison of FEM results with temperature distribution 1 for cross-section "c"

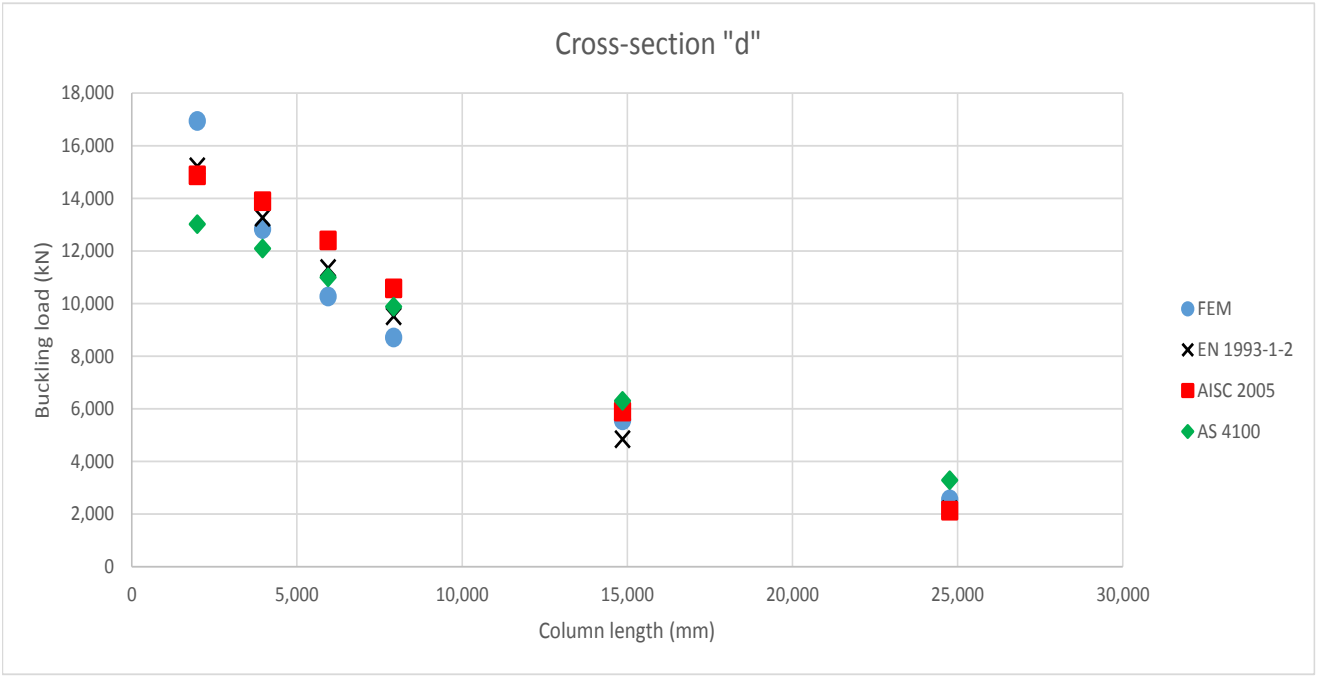

FIGURE 5.17: Comparison of FEM results with temperature distribution 1 for cross-section "d"

The comparison between codes for a column under the action of temperature distribution 2 (maximum temperature gradient along the strong axis) is shown in figures 5.18 to 5.22.

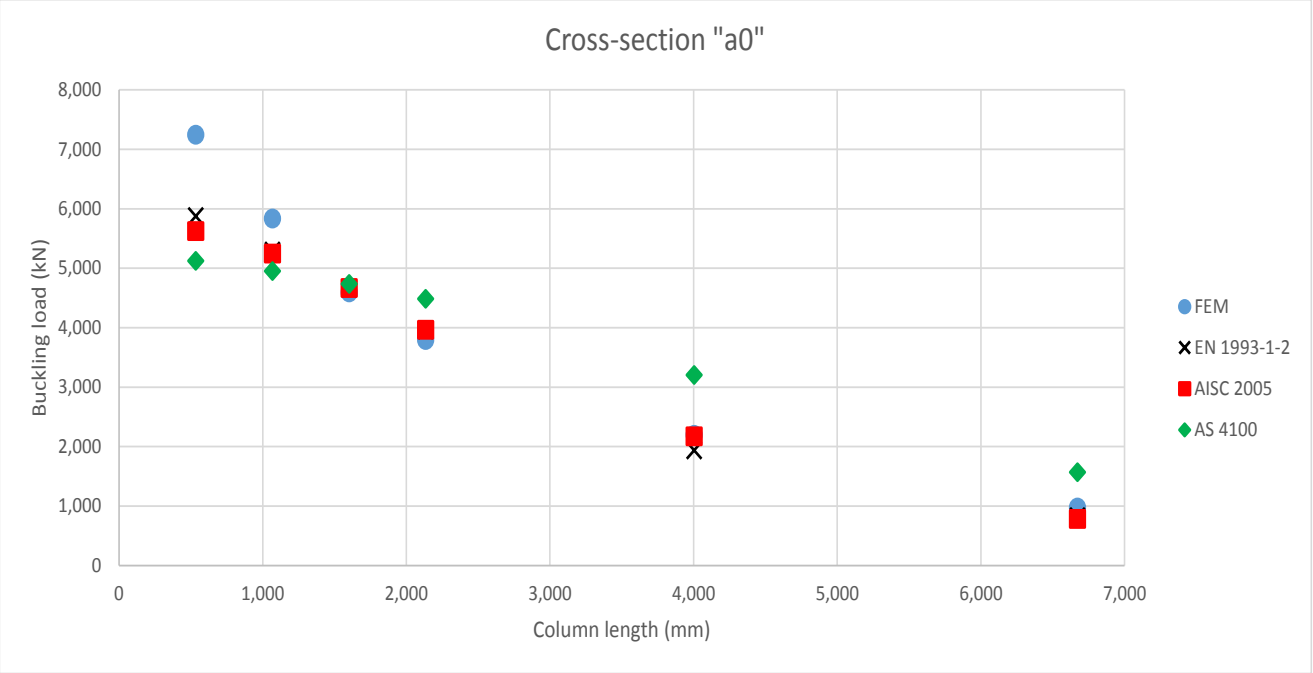

FIGURE 5.18: Comparison of FEM results with temperature distribution 2 for cross-section "a_0"

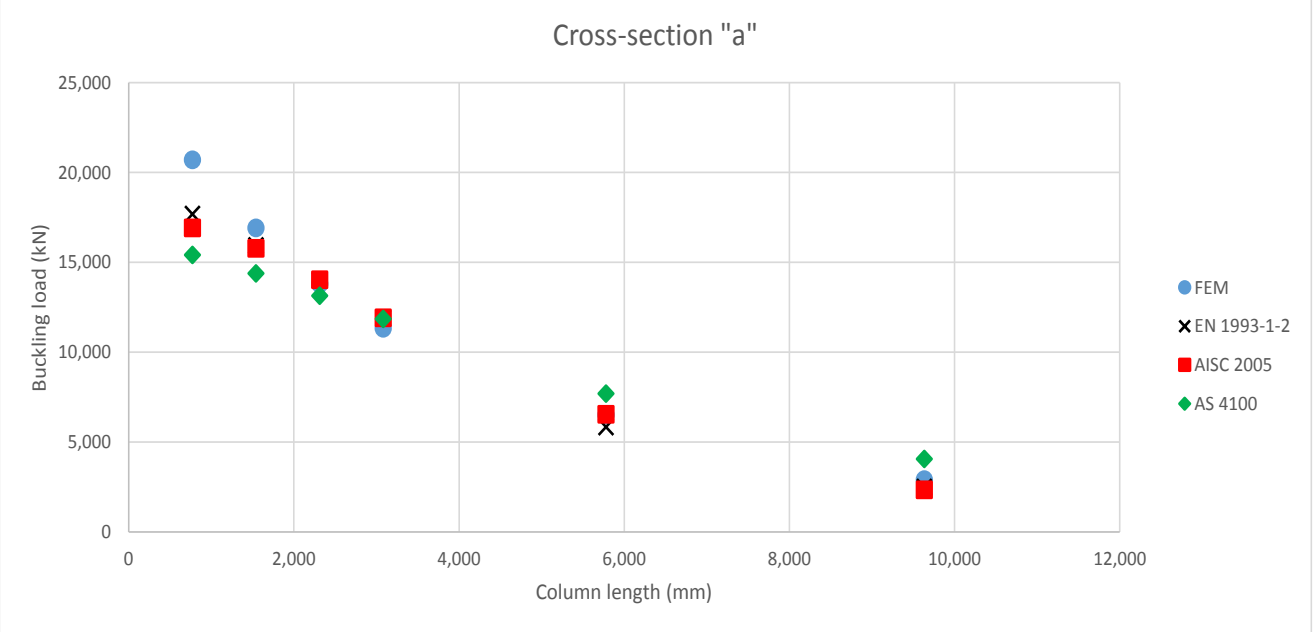

FIGURE 5.19: Comparison of FEM results with temperature distribution 2 for cross-section "a"

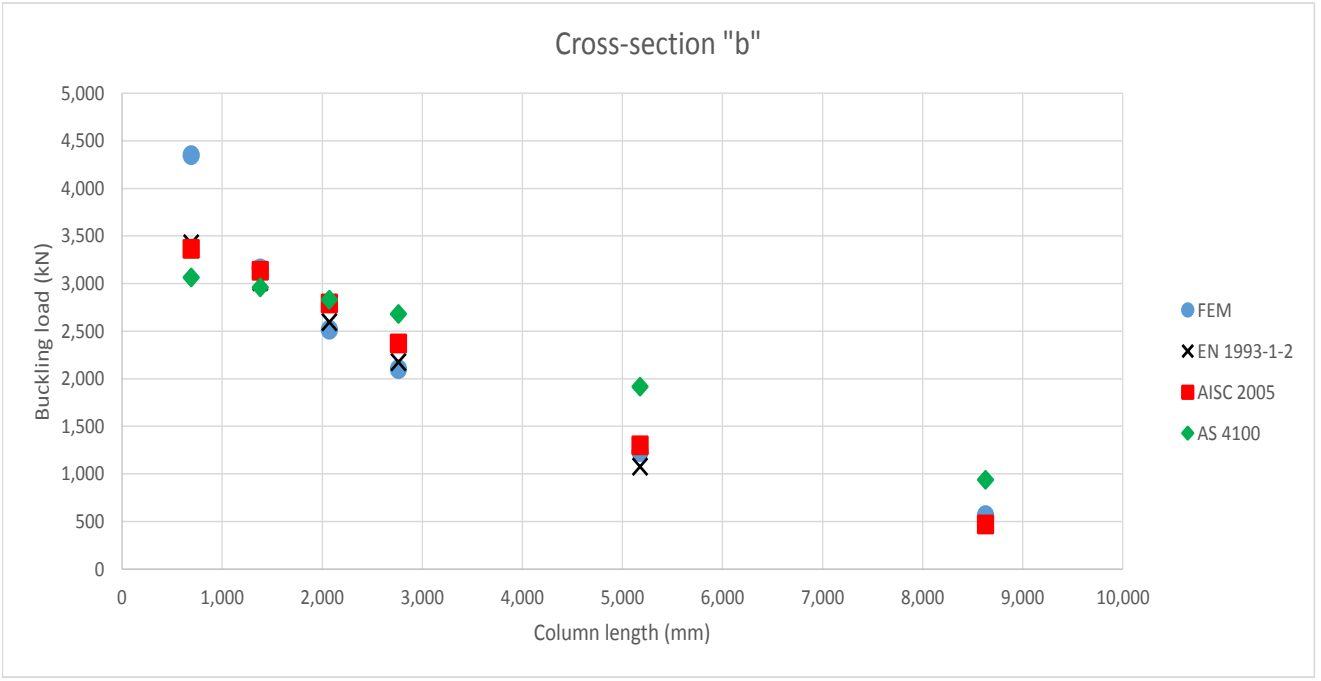

FIGURE 5.20: Comparison of FEM results with temperature distribution 2 for cross-section "b"

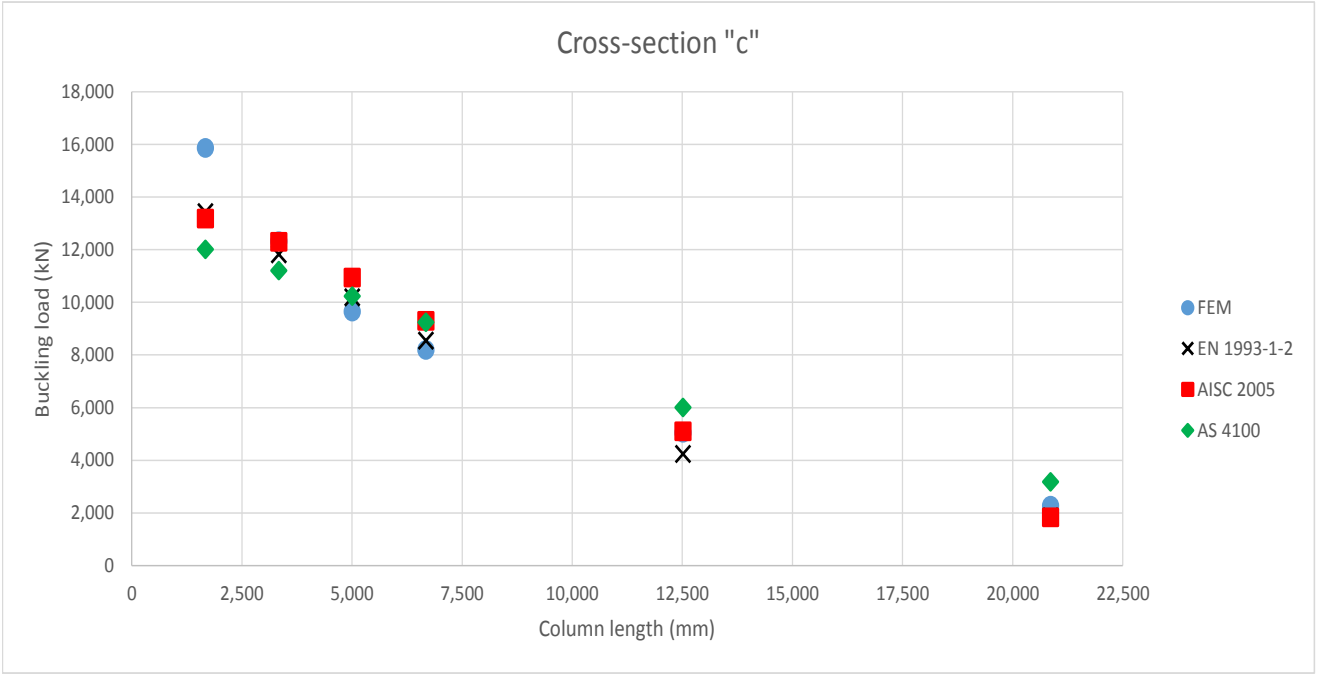

FIGURE 5.21: Comparison of FEM results with temperature distribution 2 for cross-section "c"

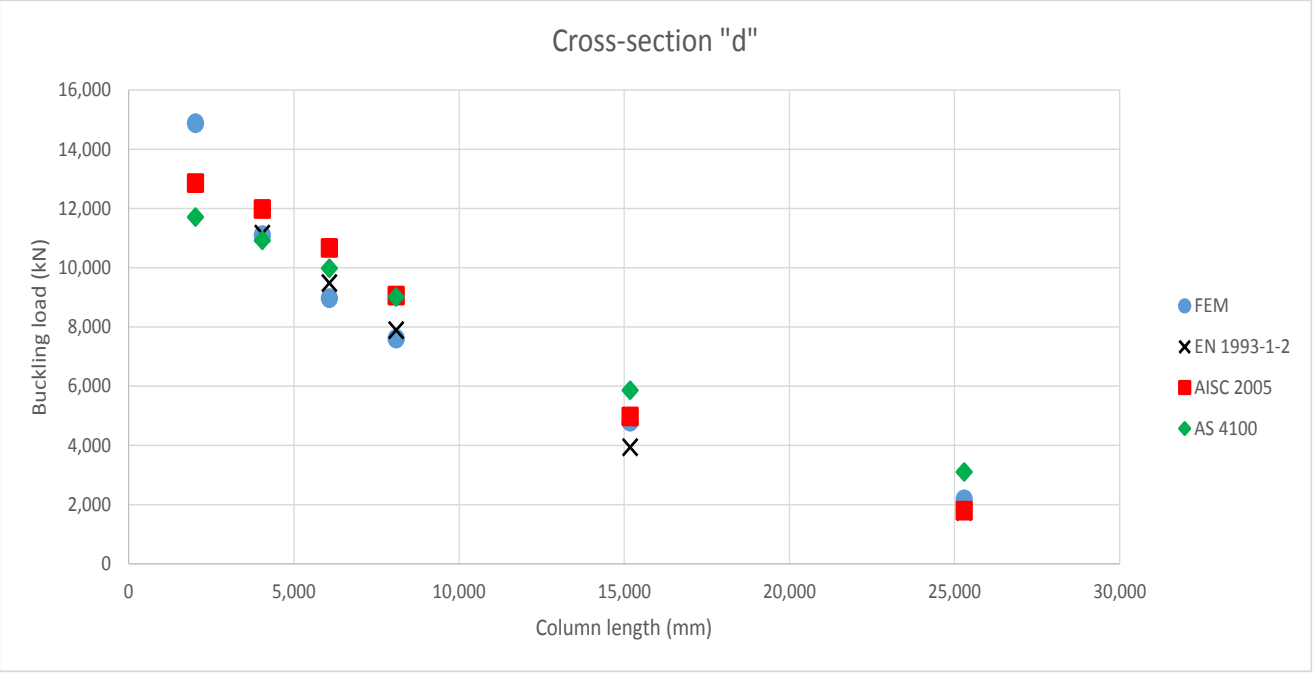

FIGURE 5.22: Comparison of FEM results with temperature distribution 2 for cross-section "d"

The comparison between codes for a column under the action of temperature distribution 3 (maximum thermal gradient along the weak axis) is shown in figures 5.18 to 5.22.

In this case, as in the case of temperature distribution 4, the discrepancy with all the codes is much larger for low-medium slenderness values. This is due to the shift in stiffness center that was discussed in the previous section. The calculations from EN 1993 and AISC codes overall underestimate the column's resistance in all cases. The AS 4100 standard has an overall better fit for temperature distribution 3 but it greatly overestimates the buckling resistance for temperature distribution 4.

The reason for the high discrepancy is due to the fact that the AS 4100 standard does not take the decay of Young's modulus into consideration for the calculations of column resistance, it only considers the yielding stress. The discrepancy with the finite element analysis results is much smaller for a gradient along the strong axis because in this case, as discussed in the previous section, the column behaves as a uniformly heated column buckling around its weak axis and the maximum temperature in temperature distributions 1 and 2 were 490 °C and 532 °C respectively, which means that the decay in the modulus of elasticity was not very critical and the difference between the AS 4100 calculations and the finite element model was therefore minimized. The discrepancy is much higher for a gradient along the weak axis due to the shift in stiffness center and the lack of consideration of the Young's modulus decay by the Australian standard.

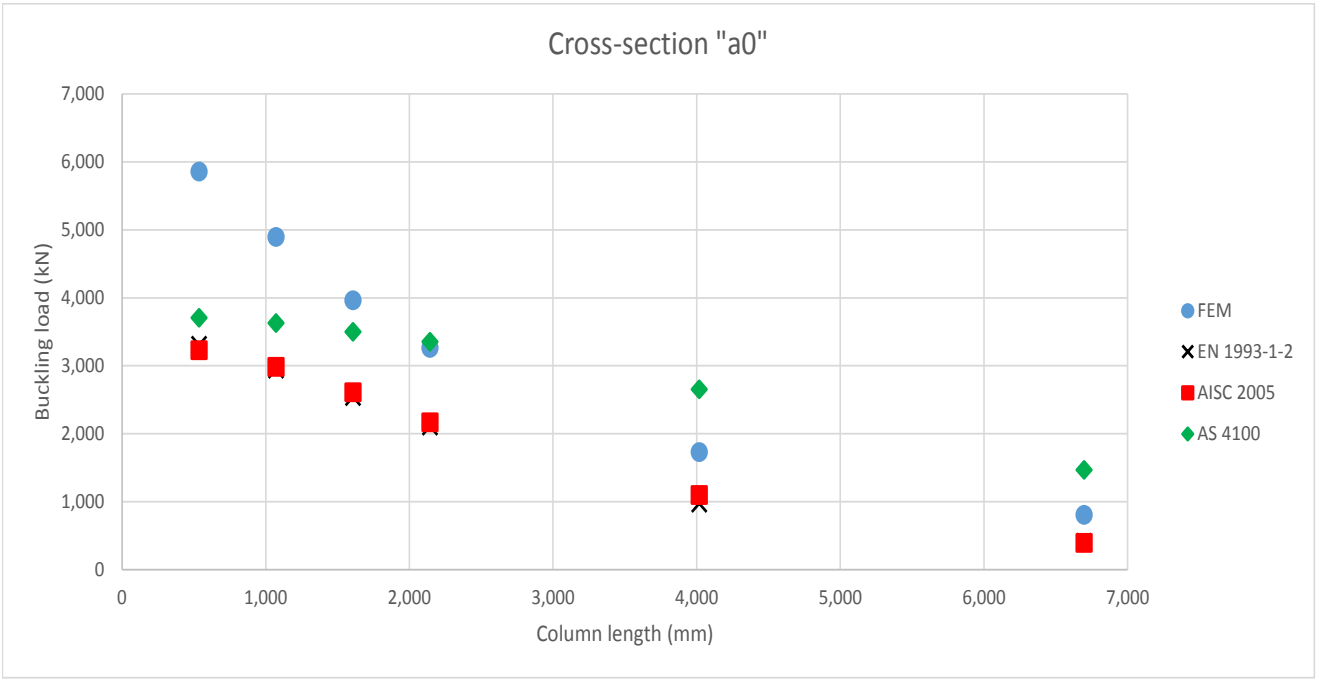

FIGURE 5.23: Comparison of FEM results with temperature distribution 3 for cross-section "a_0"

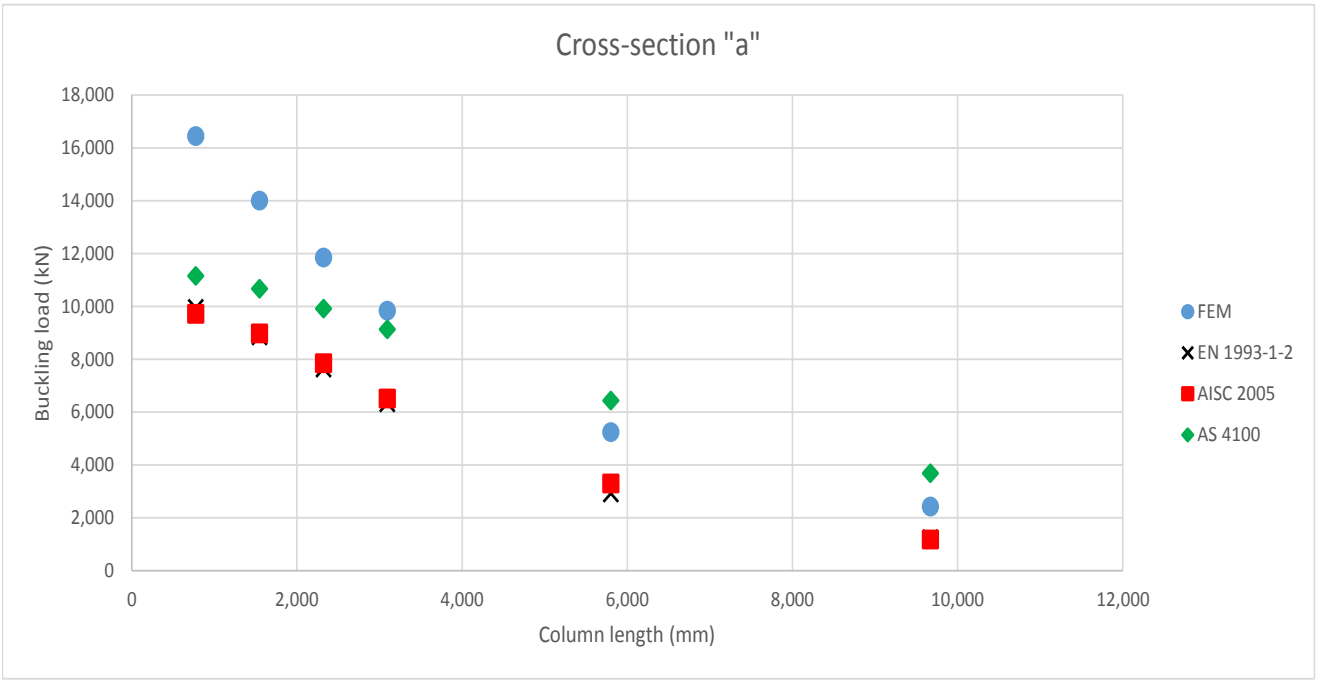

FIGURE 5.24: Comparison of FEM results with temperature distribution 3 for cross-section "a"

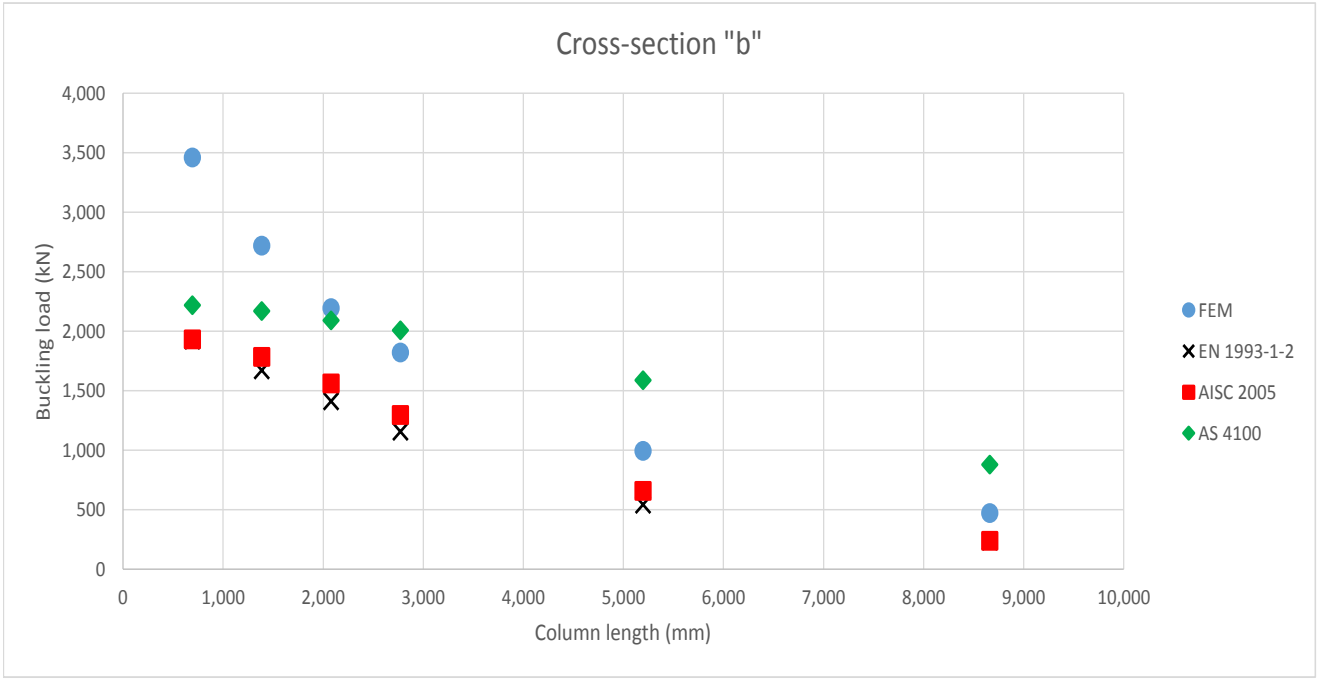

FIGURE 5.25: Comparison of FEM results with temperature distribution 3 for cross-section "b"

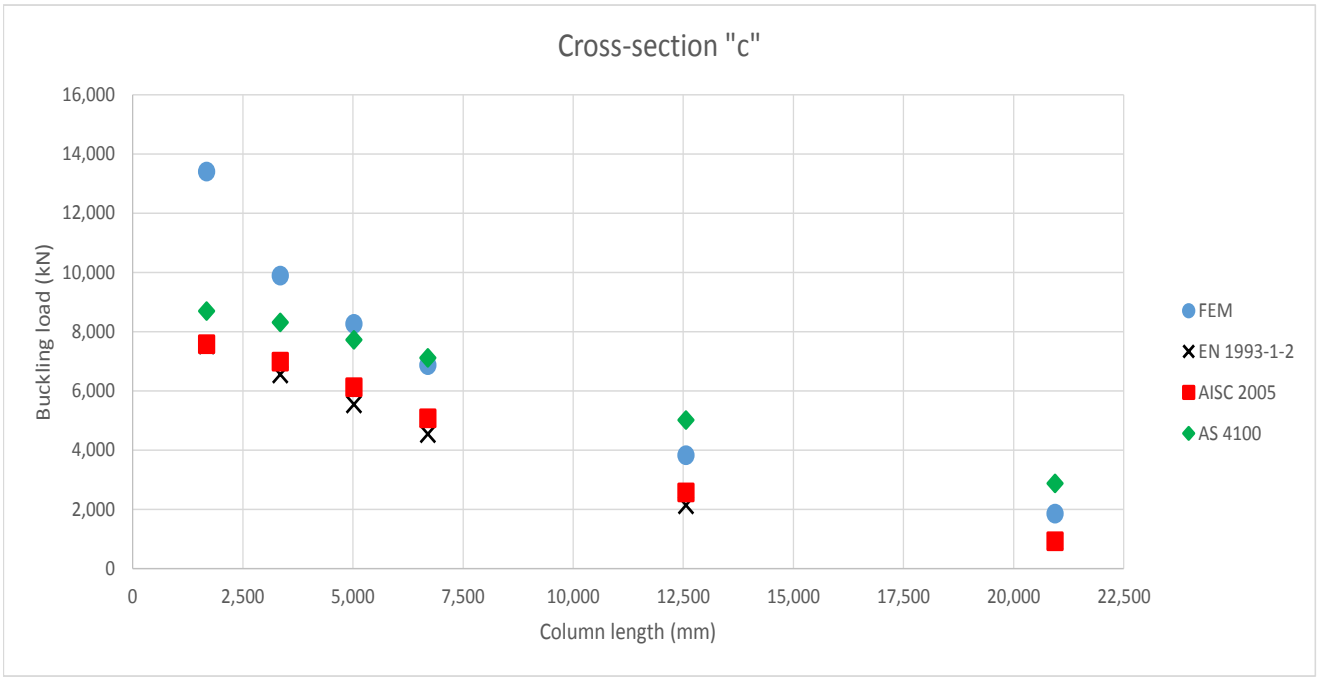

FIGURE 5.26: Comparison of FEM results with temperature distribution 3 for cross-section "c"

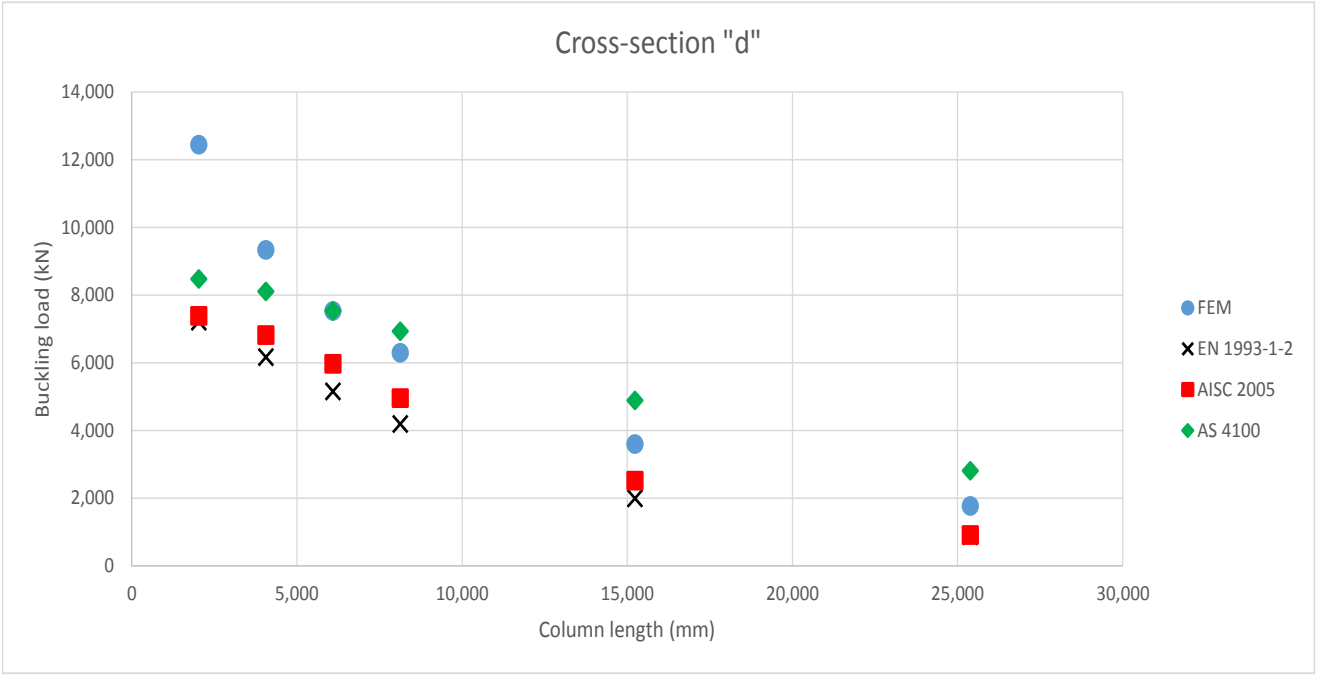

FIGURE 5.27: Comparison of FEM results with temperature distribution 3 for cross-section "d"

The comparison between codes for a column under the action of temperature distribution 4 (maximum temperature gradient along the weak axis) is shown in figures 5.28 to 5.32.

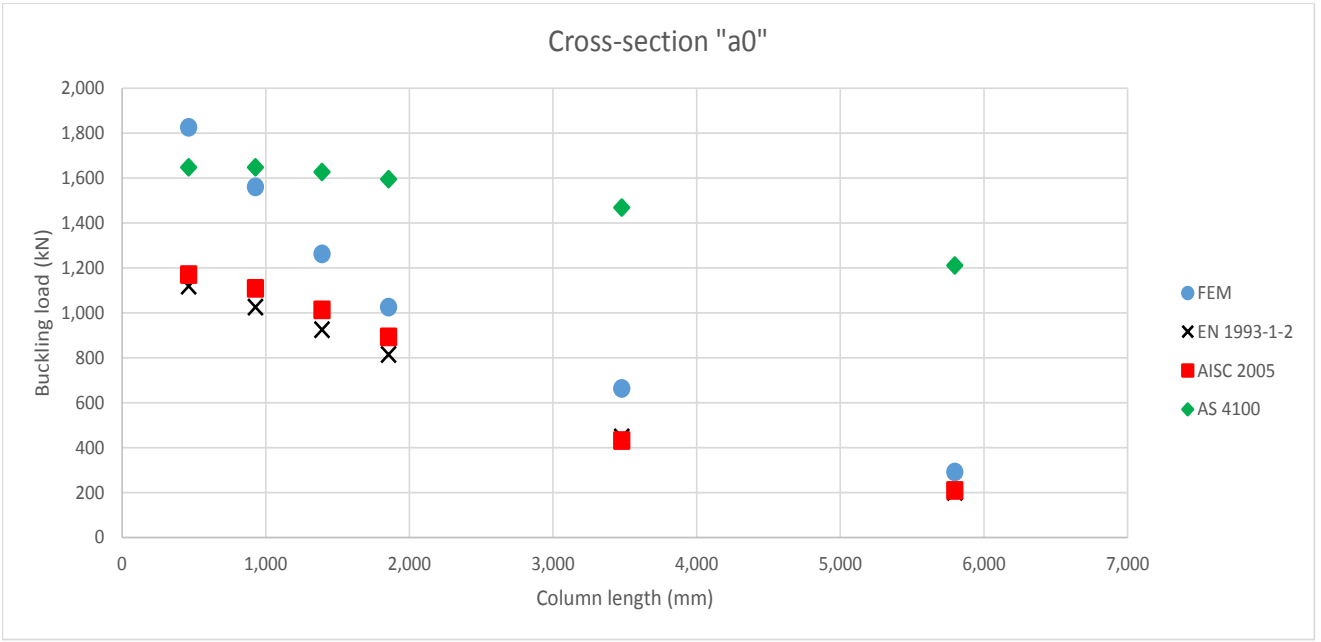

FIGURE 5.28: Comparison of FEM results with temperature distribution 4 for cross-section "a_0"

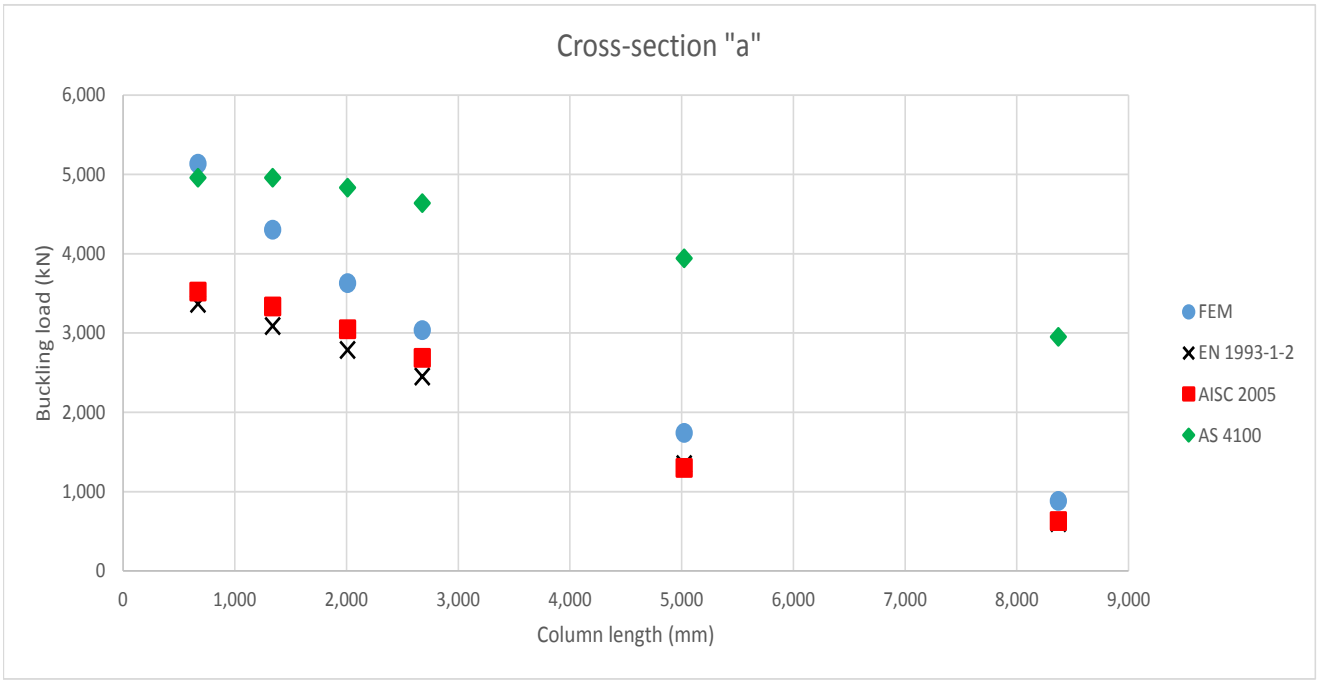

FIGURE 5.29: Comparison of FEM results with temperature distribution 4 for cross-section "a"

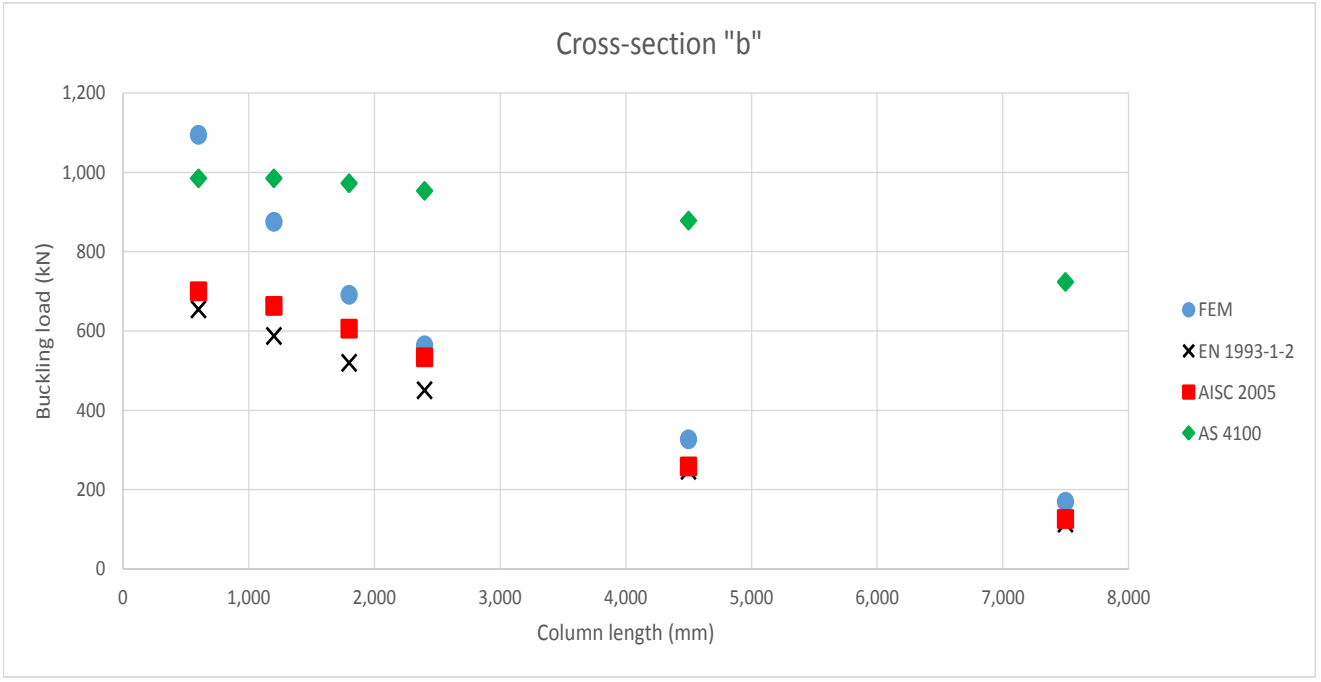

FIGURE 5.30: Comparison of FEM results with temperature distribution 4 for cross-section "b"

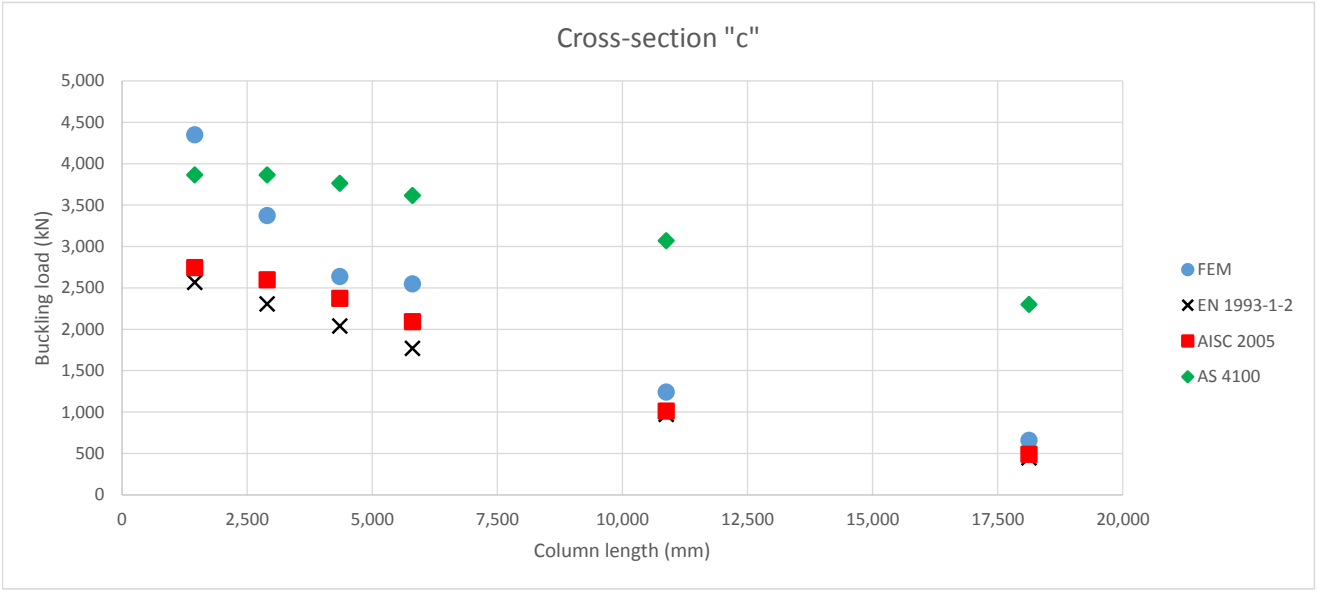

FIGURE 5.31: Comparison of FEM results with temperature distribution 4 for cross-section "c"

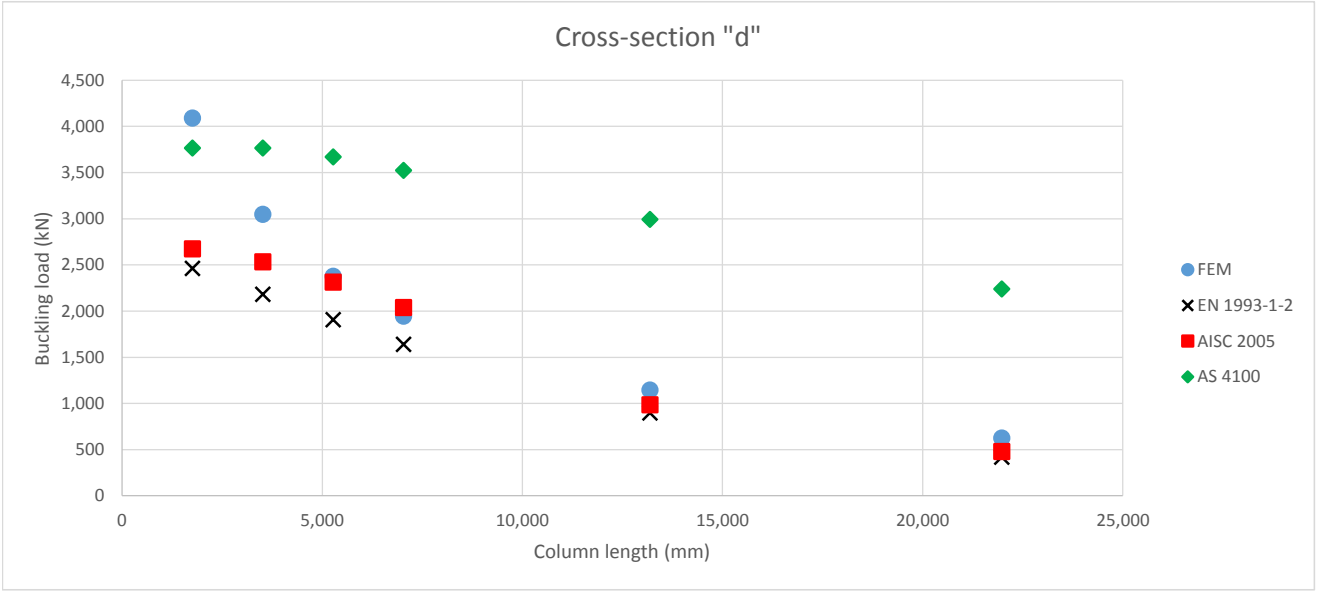

FIGURE 5.32: Comparison of FEM results with temperature distribution 4 for cross-section "d"

5.5 Summary and conclusions

During this stage of the study a finite element analysis on axially loaded columns under the effect of a thermal gradient was performed. Columns with the cross-sections specified in table 3.2 were analyzed for non-dimensional slenderness values equal to 0.2, 0.4, 0.6, 0.8, 1.5 and 2.5. Each model was analyzed under the effect of four different temperature distributions, two with a gradient along the strong axis, shown in figure 5.4, and two with a gradient along the weak axis, shown in figure 5.3. The tasks described in this chapter can be summarized as follows:

- The temperature distributions for strong axis gradient (Figure 5.2) and weak axis gradient (Figure 5.1) were normalized in order to be applied to the cross-sections of this study. The normalized temperature distributions are shown in figures 5.4 and 5.3.
- The material characterization for the finite element model was performed in order to consider multiple stress-strain relationships simultaneously. Stress-strain relationships for steel at elevated temperatures were specified for 300 °C, 400 °C, 500 °C, 600 °C, 700 °C and 800 °C in order to cover the temperature range of the thermal distributions that were to be applied.
- The finite element models for each cross-section and each temperature distribution were created by determining the column length corresponding to a uniformly heated cross-section at the average temperature for each thermal distribution.
- The FEMs were analyzed as pin-ended columns under concentric axial compression, which was introduced as a step-increasing prescribed displacement.
- A stability analysis was performed to find the first eigenmode of each column and apply an imperfection of $\frac{L}{1000}$ in the shape of that buckling shape. The nodal temperatures corresponding to each thermal gradient were then introduced. Finally, a non-linear analysis was carried out where the step-increasing vertical prescribed displacement was applied to the column.
- The buckling load resulting from the analysis was then registered and the corresponding buckling reduction factor χ_{fi} calculated.
- The obtained values of the buckling reduction factor χ_{fi} were compared to the Eurocode buckling curves and the FEM-derived buckling curves.
- The buckling loads for each case were also compared to the AISC 2005 and the AS 4100 standard provisions.

Upon analysis and comparison of the obtained results the following conclusions were drawn:

- For the temperature distributions considered, the magnitude of the gradient seems to be of little influence. Only the direction of the thermal gradient has a noticeable effect on the buckling behavior.
- The Eurocode 1993-1-2 buckling curves provide an overestimation of the buckling reduction factor χ_{fi} for I-shaped columns under the effect of thermal gradients for all cross-section types. This overestimation is more significant in the case of a thermal gradient along the weak axis of the cross-section.
- The FEM-derived buckling curves provide a good prediction of the buckling reduction factor χ_{fi} for the case of a thermal gradient along the strong axis. These buckling curves overestimate the buckling reduction factor for the case of a thermal gradient along the weak axis but still offer a more accurate prediction than the Eurocode buckling curves.
- Under the effect of a thermal gradient along the strong axis, the location of the stiffness center will move along the strong axis. This shift was however not sufficient to trigger buckling around the strong axis and in all cases weak axis buckling was observed. This meant that the columns behaved similarly to a uniformly heated column.
- Under the effect of a thermal gradient along the weak axis, the stiffness center shifted along the direction of the weak axis, further decreasing the cross-sections' bending capacity around this axis. This is why even the FEM-derived buckling curves overestimated buckling capacity for the case of weak axis thermal gradient.
- When comparing the buckling resistance obtained through finite element analysis to the predictions of EN3, AISC 2005 and AS 4100 it was found that overall, these construction codes provide a good prediction of buckling resistance for the case of a temperature gradient along the strong axis. The Eurocode and AISC standards underestimate buckling resistance for the case of a temperature gradient along the weak axis.
- The Australian standard AS 4100 can greatly overestimate buckling capacity due to the fact that it does not take into account the decay in modulus of Elasticity for column buckling calculations, as was the case with temperature distribution 4.

From these findings it can be stated that the buckling curves derived through finite element modeling offer a more accurate prediction of buckling resistance than the current

Eurocode provisions for the case of non-uniform temperature distribution when the average temperature is used to determine the non-dimensional slenderness of the column.

Chapter 6

Summary, Conclusions and Recommendations

The main aspects and conclusions of the work presented in this thesis are as follows:

- A finite element model (FEM) of a pin-ended column was created for 5 different I-shaped cross-sections corresponding to the EN 1993-1-1 classification into the buckling curves 'a_0', 'a', 'b', 'c' and 'd'. The model took into consideration initial imperfections and residual stresses as initial conditions.
- This model was analyzed under the effect of a vertical, concentric compression load. The resulting buckling resistance was then compared to that calculated through the Eurocode 1993-1-1 buckling curves in order to validate the FEM.
- Upon finding an acceptable agreement with the Eurocode provisions, the FEMs were modified to be analyzed at 500 °C and 700 °C. The stress-strain relationship of steel was modified at both temperatures in order to simulate the decay in mechanical properties as well as the non-linearity of the stress-strain curve that develops at elevated temperatures.
- The buckling resistances these models was compared with the Eurocode 1993-1-2 showing some discrepancy at the mid-slenderness range. It was also found that residual stresses are greatly relaxed and can be neglected at elevated temperatures.
- The results from this stage were used to build new buckling curves that would serve as a basis for comparison for the last part of the study.
- The FEMs were then analyzed under the effect of a linear thermal gradient in the cross-section along the weak and strong axis. A stress-strain-temperature

dependency was specified to determine the mechanical behavior of all elements at different temperatures. Four different temperature distributions were applied.

- It was found that the results of this last stage had a better agreement with the FEM-derived buckling curves than with the Eurocode provisions. The results were also compared to the AISC 2005 and AS 4100 codes.

From the findings in chapter 5 it can be concluded that the Eurocode provisions underestimate buckling resistance at elevated temperatures for a column under the effect of a thermal gradient along its weak axis. The Eurocode equations provide an over-conservative estimation of buckling resistance in the mid-slenderness range due to the fact that it determines it by considering a uniform temperature distribution using only the maximum temperature in the cross-section. This approach would become more and more conservative as the thermal gradient in the cross-section increases due to the Eurocode only considering the maximum temperature. This could represent much higher construction costs in the form of bigger cross-sections and excessive fire protection, especially in the case of perimeter columns, where the maximum thermal gradients are expected during a fire.

The following recommendations on this topic are provided:

- Further research, particularly in the form of full-size experiments, should be carried out in order to verify the findings and conclusions in this thesis.
- A wider spectrum of temperature distributions should be analyzed as well as the effect of a temperature gradient along the length of the column in buckling resistance. Further, the effect of temperature gradients through the cross-section simultaneous to gradients along the length of the element can be studied.
- The difference with, and effect of, different support conditions as well as the case of columns as part of a frame can be studied.
- An analytic or experimental modification of the Perry-Robertson approach can be researched in order to provide a more accurate prediction of buckling resistance in the case of thermal gradients. A possible way to accomplish this is to find values for the η factor that are dependent on the element's length and it's average or maximum temperature.
- Further research on the same topic can be carried out considering different cross-sections (angles, circular or rectangular hollow sections, channels, etc.).

- A revision on the current Eurocode provisions for calculations at elevated temperatures is necessary. The current design approach, which considers an over-conservative fire curve and, as it was found in this thesis, also an over-conservative buckling resistance, could be providing a simplified calculation method at a very high economic cost. An amendment to EN 1993-1-2 providing guidelines for elevated temperature design in the presence of thermal gradients would be ideal.

Bibliography

[1] J. A. Purkiss, *Fire Safety Engineering: Design of Structures.* Butterworth-Heinemann, second ed., 1996.

[2] A. H. Buchanan, *Structural design for fire safety.* Wiley, 2001.

[3] T. Z. Harmathy and W. W. Stanzak, "Elevated-temperature tensile and creep properties of some structural and prestressing steels," *ASTM Special Technical Publication*, no. 464, pp. 186–208, 1970.

[4] T. Z. Harmathy, *Fire Safety Design & Concrete.* New York: John Wiley & Sons, Inc., 1st ed., 1993.

[5] European Comitee For Standarization, "Eurocode 3: Design of steel structures - Part 1-2: General rules - Structural fire design," 2005.

[6] B. Kirby and R. R. Preston, "High Temperature Properties of Hot-rolled , Structural Steels for Use in Fire Engineering Design Studies," *Fire Safety Journal*, vol. 13, pp. 27–37, 1988.

[7] American Institute of Steel Construction, "Specification for Structural Steel Buildings," 2005.

[8] British Standards Institution, "Structural use of steelwork in building. Part 8: Code of practice for fire resistant design.," 1998.

[9] R. Narayanan, V. Kalyanaraman, A. Santhakumar, S. Seetharaman, S. Satish Kumar, S. Arul Jayachandran, and R. Senthil, "Design of axially loaded columns," 2011.

[10] European Comitee For Standarization, "Eurocode 3: Design of Steel Structures - Part 1 - 1: General rules and rules for buildings," 2005.

[11] AS 4100, "Australian Standards: Steel structures," 1998.

[12] V. Kodur, M. Dwaikat, and R. Fike, "High-Temperature Properties of Steel for Fire Resistance Modeling of Structures," *Journal of Materials in Civil Engineering*, vol. 22, pp. 423–434, May 2010.

[13] A. Agarwal, L. Choe, and A. H. Varma, "Fire design of steel columns: Effects of thermal gradients," *Journal of Constructional Steel Research*, vol. 93, pp. 107–118, Feb. 2014.

[14] A. O. Olawale, *Collapse Behaviour of Steel Columns in Fire*. PhD thesis, University of Sheffield, 1988.

[15] M. Dwaikat, V. Kodur, S. Quiel, and M. Garlock, "Experimental behavior of steel beam–columns subjected to fire-induced thermal gradients," *Journal of Constructional Steel Research*, vol. 67, pp. 30–38, Jan. 2011.

[16] W. Boon, *The Influence of Thermal Gradients in Steel Columns due to Pool Fires*. PhD thesis, Delft University of Technology, 2014.

[17] The Netherlands Standarization Institute, "NEN 67771: Technische Grondslagen voor Bouwconstructies- TGB 1990 - Staalconstructies - Stabiliteit," 2000.

[18] National Board of Housing Living and Planning, "Swedish Regulations for Steel Structures, BSK 99," 2003.

[19] G. G. Deierlein and D. White, "Strength Assessment with Spread-of-Plasticity Analysis," in *Guide to Stability Design Criteria for Metal Structures* (R. D. Ziemian, ed.), ch. Frame Stab, pp. 740–741, John Wiley & Sons, Inc., sixth ed., 2010.

[20] European Convention For Constructional Steelwork, "Manual on Stability of Steel Structures," tech. rep., 1976.

[21] ESDEP Working Group, *The European Steel Design Education Programme*. 1994.

[22] The Netherlands Standarization Institute, "NEN 6770: TGB 1990 - Staalconstructies - Basiseisen en basisrekenregels voor overwegend statisch belaste constructies," 1997.

[23] F. Joannides and A. Weller, *Structural steel design to BS 5950. Pt I.* Thomas Telford Publishing, 2002.

[24] K.-C. Yang, H.-H. Lee, and O. Chan, "Experimental study of fire-resistant steel H-columns at elevated temperature," *Journal of Constructional Steel Research*, vol. 62, pp. 544–553, June 2006.

[25] J. Takagi and G. G. Deierlein, "Strength design criteria for steel members at elevated temperatures," *Journal of Constructional Steel Research*, vol. 63, pp. 1036–1050, Aug. 2007.

[26] K.-C. Yang and R. Hsu, "Structural behavior of centrally loaded steel columns at elevated temperature," *Journal of Constructional Steel Research*, vol. 65, pp. 2062–2068, Oct. 2009.

Appendix A

Results for room temperature

FEM: Mild steel at room temperature

Curve a0

Section: UKB 457 x 191 x 161

f_y 460 N/mm²

Buckling about the z-z axis

Web class 1

Flange class 1

Section properties:

Depth of the section	h	492	mm
Width of the section	b	199.4	mm
Web thickness	t_w	18	mm
Flange thickness	t_f	32	mm
Root radius	r	10.2	mm
Depth between fillets	d	407.6	mm
Second moment of area	I_{zz}	42500000	mm^4
Radius of gyration	r_{zz}	45.5	mm
Area of section	A	20600	mm²

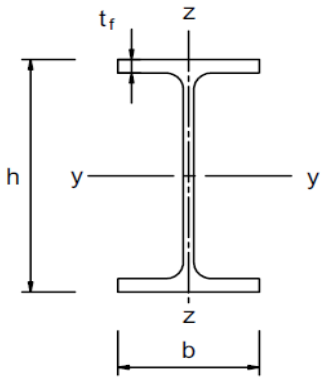

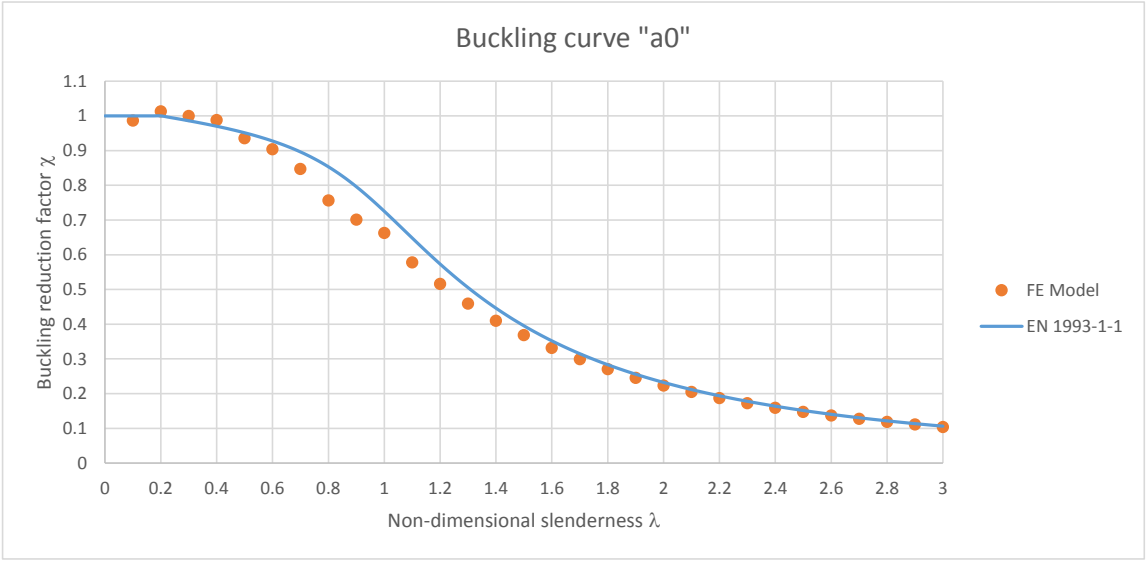

λ	L_{cr} (mm)	N_b (kN)	χ_{FEM}	$\chi_{EN3-1-1}$
0.1	305.42	9,348.14	0.986507	1
0.2	610.84	9,602.90	1.013392	1
0.3	916.26	9,473.56	0.999742	0.985935
0.4	1221.68	9,365.47	0.988335	0.970142
0.5	1527.10	8,868.13	0.935852	0.951321
0.6	1832.52	8,570.28	0.90442	0.927584
0.7	2137.94	8,030.98	0.847508	0.896148
0.8	2443.36	7,172.25	0.756886	0.853345
0.9	2748.78	6,646.39	0.701391	0.796054
1	3054.20	6,283.00	0.663044	0.725344
1.1	3359.62	5,481.63	0.578475	0.648248
1.2	3665.04	4,894.51	0.516516	0.5732
1.3	3970.46	4,352.84	0.459354	0.505291
1.4	4275.88	3,888.56	0.410359	0.446102
1.5	4581.30	3,492.46	0.368558	0.395336
1.6	4886.72	3,145.78	0.331973	0.352005
1.7	5192.14	2,842.41	0.299959	0.314993
1.8	5497.56	2,563.67	0.270543	0.28327
1.9	5802.98	2,328.34	0.245709	0.255949
2	6108.40	2,121.64	0.223897	0.232299
2.1	6413.82	1,941.61	0.204897	0.211715
2.2	6719.24	1,779.61	0.187802	0.193706
2.3	7024.66	1,637.51	0.172806	0.177871
2.4	7330.08	1,511.93	0.159553	0.163879
2.5	7635.50	1,400.15	0.147758	0.151461
2.6	7940.92	1,299.36	0.137121	0.140391
2.7	8246.34	1,209.30	0.127617	0.130484
2.8	8551.76	1,127.77	0.119013	0.121584
2.9	8857.18	1,054.81	0.111314	0.113559
3	9162.60	988.32	0.104298	0.1063

FEM: Mild steel at room temperature

Curve a0

Section: UKB 152 x 89 x 16

f_y 460 N/mm²

Buckling about the z-z axis

Web class 1

Flange class 1

Section properties:

Depth of the section	h	152.4	mm
Width of the section	b	88.7	mm
Web thickness	t_w	4.5	mm
Flange thickness	t_f	7.7	mm
Root radius	r	7.6	mm
Depth between fillets	d	121.8	mm
Second moment of area	I_{zz}	898000	mm^4
Radius of gyration	r_{zz}	21	mm
Area of section	A	2030	mm²

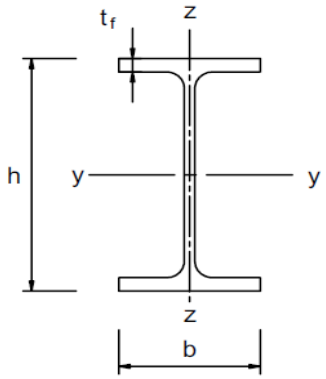

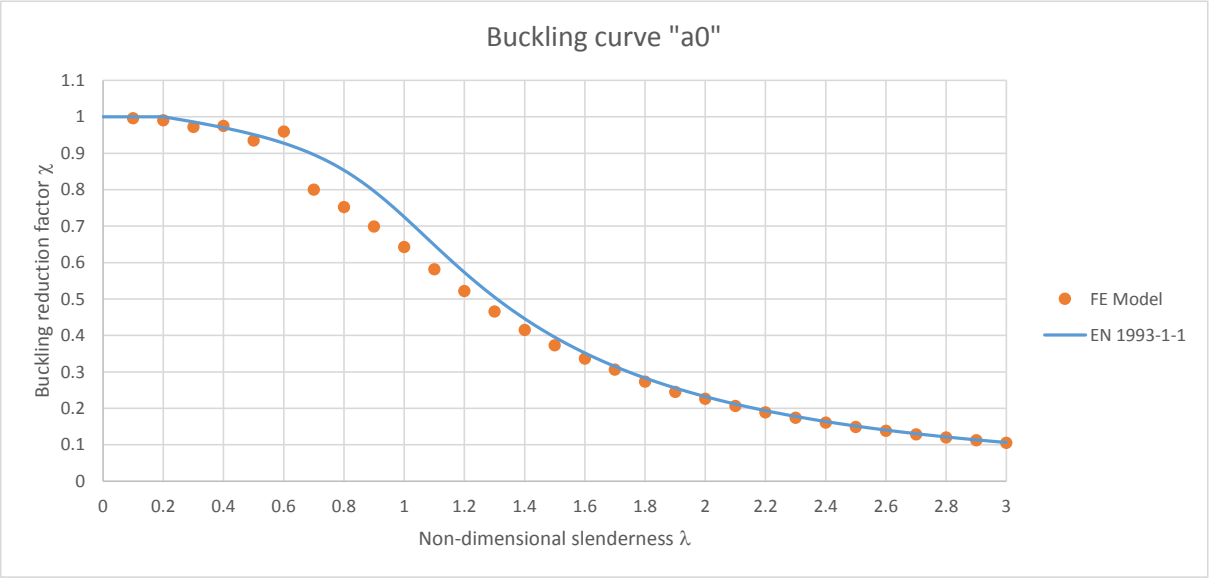

λ	L_{cr} (mm)	N_b (kN)	χ_{FEM}	$\chi_{EN3-1-1}$
0.1	140.96	929.97	0.995895	1
0.2	281.92	924.57	0.990112	1
0.3	422.88	907.51	0.971851	0.985935
0.4	563.84	910.51	0.975063	0.970142
0.5	704.80	872.99	0.934884	0.951321
0.6	845.76	895.82	0.959325	0.927584
0.7	986.72	746.72	0.799662	0.896148
0.8	1127.68	702.46	0.752263	0.853345
0.9	1268.64	652.34	0.698584	0.796054
1	1409.60	599.97	0.6425	0.725344
1.1	1550.56	542.77	0.581249	0.648248
1.2	1691.52	486.96	0.521478	0.5732
1.3	1832.48	435.02	0.465861	0.505291
1.4	1973.44	387.40	0.414865	0.446102
1.5	2114.40	348.13	0.372811	0.395336
1.6	2255.36	313.91	0.336161	0.352005
1.7	2396.32	286.09	0.306368	0.314993
1.8	2537.28	254.86	0.272927	0.28327
1.9	2678.24	228.77	0.244984	0.255949
2	2819.20	210.75	0.225694	0.232299
2.1	2960.16	192.94	0.206616	0.211715
2.2	3101.12	176.03	0.18851	0.193706
2.3	3242.08	162.76	0.174295	0.177871
2.4	3383.04	149.75	0.16037	0.163879
2.5	3524.00	139.13	0.148991	0.151461
2.6	3664.96	128.95	0.138094	0.140391
2.7	3805.92	119.94	0.128439	0.130484
2.8	3946.88	111.98	0.119917	0.121584
2.9	4087.84	104.72	0.112147	0.113559
3	4228.80	98.14	0.105093	0.1063

FEM: Mild steel at room temperature

Curve a

Section: UKB 1016 x 305 x 487

f_y 460 N/mm²

Buckling about the z-z axis

Web class 3

Flange class 1

Section properties:

Depth of the section	h	1036.3	mm
Width of the section	b	308.5	mm
Web thickness	t_w	30	mm
Flange thickness	t_f	54.1	mm
Root radius	r	30	mm
Depth between fillets	d	868.1	mm
Second moment of area	I_{zz}	267000000	mm^4
Radius of gyration	r_{zz}	65.7	mm
Area of section	A	62000	mm²

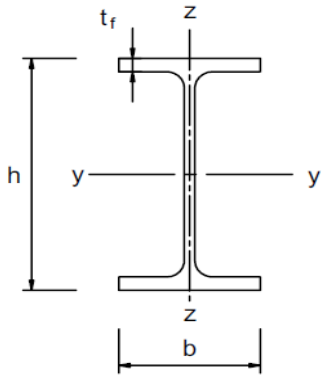

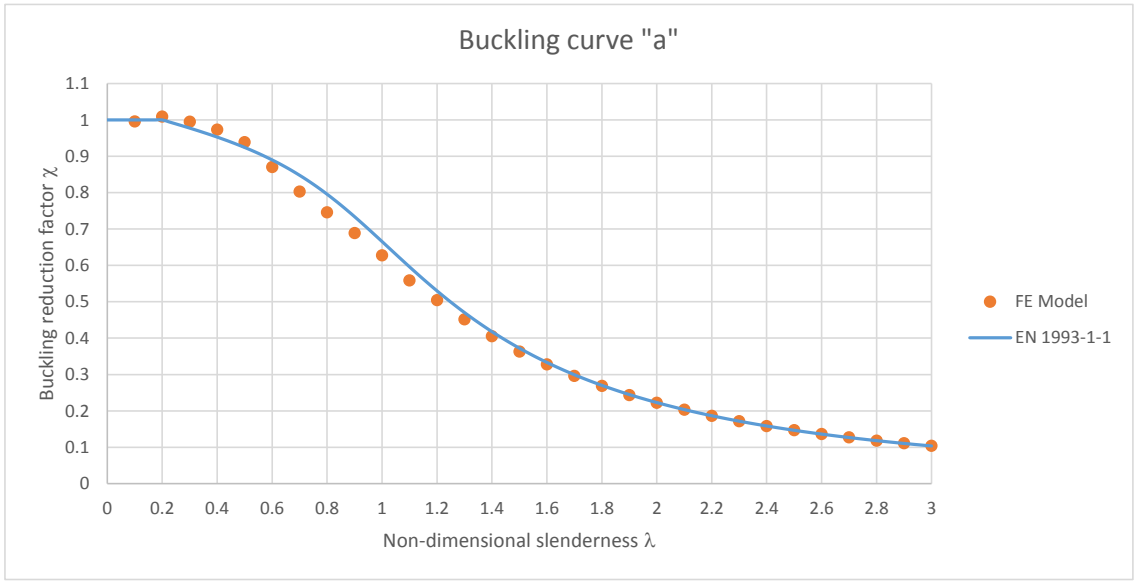

λ	L_{cr} (mm)	N_b (kN)	χ_{FEM}	$\chi_{EN3-1-1}$
0.1	441.01	28,408.71	0.996098	1
0.2	882.02	28,782.66	1.00921	1
0.3	1323.03	28,374.56	0.9949	0.977493
0.4	1764.04	27,763.76	0.973484	0.952785
0.5	2205.05	26,781.05	0.939027	0.924273
0.6	2646.06	24,817.43	0.870176	0.889995
0.7	3087.07	22,906.63	0.803178	0.84774
0.8	3528.08	21,265.60	0.745638	0.795703
0.9	3969.09	19,640.30	0.68865	0.733941
1	4410.10	17,898.50	0.627577	0.665603
1.1	4851.11	15,934.57	0.558716	0.596008
1.2	5292.12	14,390.67	0.504582	0.529996
1.3	5733.13	12,879.67	0.451601	0.470339
1.4	6174.14	11,550.80	0.405007	0.4179
1.5	6615.15	10,361.40	0.363303	0.372437
1.6	7056.16	9,339.96	0.327488	0.33323
1.7	7497.17	8,451.87	0.296349	0.299434
1.8	7938.18	7,658.08	0.268516	0.270239
1.9	8379.19	6,944.56	0.243498	0.24493
2	8820.20	6,333.98	0.222089	0.222895
2.1	9261.21	5,799.70	0.203356	0.203624
2.2	9702.22	5,322.55	0.186625	0.186692
2.3	10143.23	4,898.96	0.171773	0.171749
2.4	10584.24	4,520.39	0.158499	0.158503
2.5	11025.25	4,190.53	0.146933	0.146713
2.6	11466.26	3,888.35	0.136338	0.136176
2.7	11907.27	3,619.67	0.126917	0.126724
2.8	12348.28	3,376.56	0.118393	0.118215
2.9	12789.29	3,158.87	0.11076	0.110528
3	13230.30	2,961.07	0.103824	0.103563

FEM: Mild steel at room temperature

Curve a

Section: UKC 203 x 203 x 127

f_y 460 N/mm²

Buckling about the z-z axis

Web class 1

Flange class 1

Section properties:

Depth of the section	h	241.4	mm
Width of the section	b	213.9	mm
Web thickness	t_w	18.1	mm
Flange thickness	t_f	30.1	mm
Root radius	r	10.2	mm
Depth between fillets	d	160.8	mm
Second moment of area	I_{zz}	49200000	mm^4
Radius of gyration	r_{zz}	55	mm
Area of section	A	16200	mm²

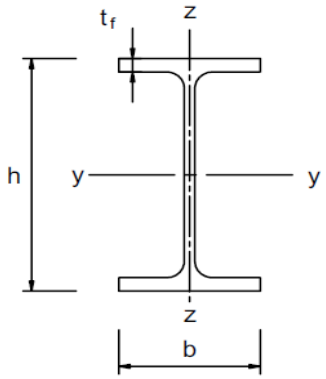

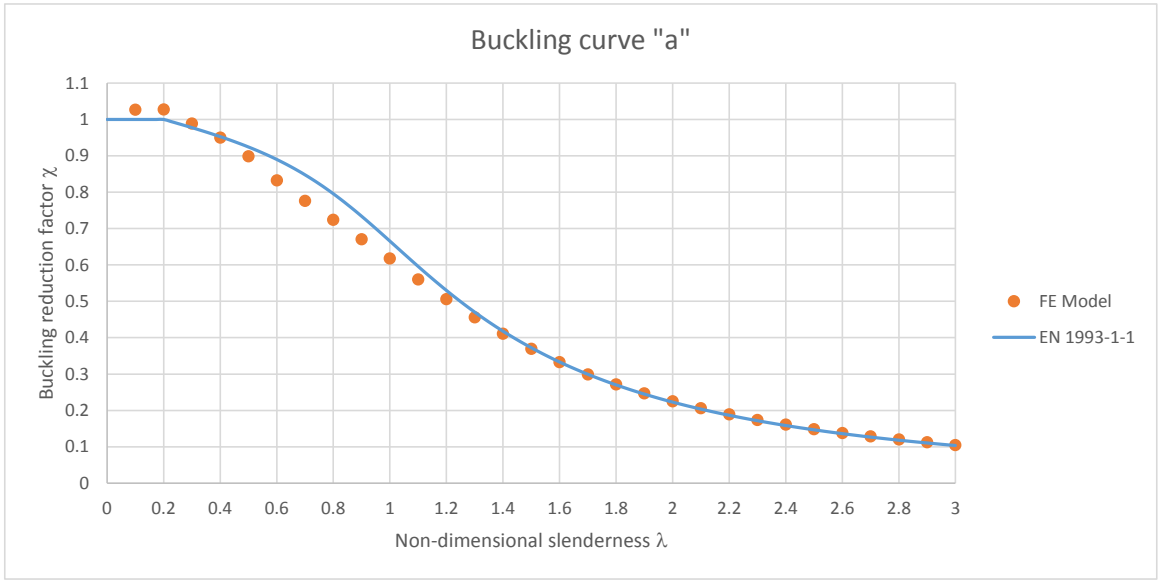

λ	L_{cr} (mm)	N_b (kN)	χ_{FEM}	$\chi_{EN3-1-1}$
0.1	369.18	7,653.98	1.027104	1
0.2	738.36	7,656.48	1.027439	1
0.3	1107.54	7,366.35	0.988507	0.977493
0.4	1476.72	7,082.01	0.950351	0.952785
0.5	1845.90	6,696.35	0.898597	0.924273
0.6	2215.08	6,202.71	0.832355	0.889995
0.7	2584.26	5,782.75	0.775999	0.84774
0.8	2953.44	5,396.59	0.72418	0.795703
0.9	3322.62	4,997.44	0.670617	0.733941
1	3691.80	4,604.11	0.617835	0.665603
1.1	4060.98	4,171.73	0.559814	0.596008
1.2	4430.16	3,770.88	0.506022	0.529996
1.3	4799.34	3,400.14	0.456272	0.470339
1.4	5168.52	3,060.04	0.410633	0.4179
1.5	5537.70	2,754.23	0.369597	0.372437
1.6	5906.88	2,480.83	0.332908	0.33323
1.7	6276.06	2,228.23	0.299012	0.299434
1.8	6645.24	2,025.11	0.271754	0.270239
1.9	7014.42	1,840.30	0.246953	0.24493
2	7383.60	1,677.88	0.225158	0.222895
2.1	7752.78	1,533.50	0.205784	0.203624
2.2	8121.96	1,407.64	0.188894	0.186692
2.3	8491.14	1,296.34	0.173959	0.171749
2.4	8860.32	1,197.51	0.160696	0.158503
2.5	9229.50	1,107.81	0.14866	0.146713
2.6	9598.68	1,029.35	0.138131	0.136176
2.7	9967.86	958.00	0.128556	0.126724
2.8	10337.04	893.75	0.119934	0.118215
2.9	10706.22	835.77	0.112154	0.110528
3	11075.40	782.79	0.105044	0.103563

FEM: Mild steel at room temperature

Curve b

Section: UKB 457 x 191 x 161

f_y 275 N/mm²

Buckling about the z-z axis

Web class 1

Flange class 1

Section properties:

Depth of the section	h	492	mm
Width of the section	b	199.4	mm
Web thickness	t_w	18	mm
Flange thickness	t_f	32	mm
Root radius	r	10.2	mm
Depth between fillets	d	407.6	mm
Second moment of area	I_{zz}	42500000	mm^4
Radius of gyration	r_{zz}	45.5	mm
Area of section	A	20600	mm²

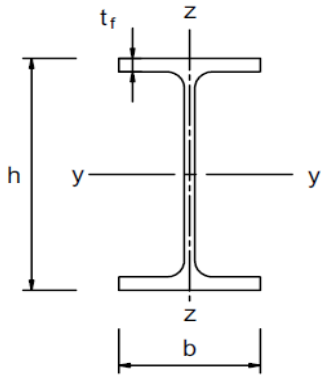

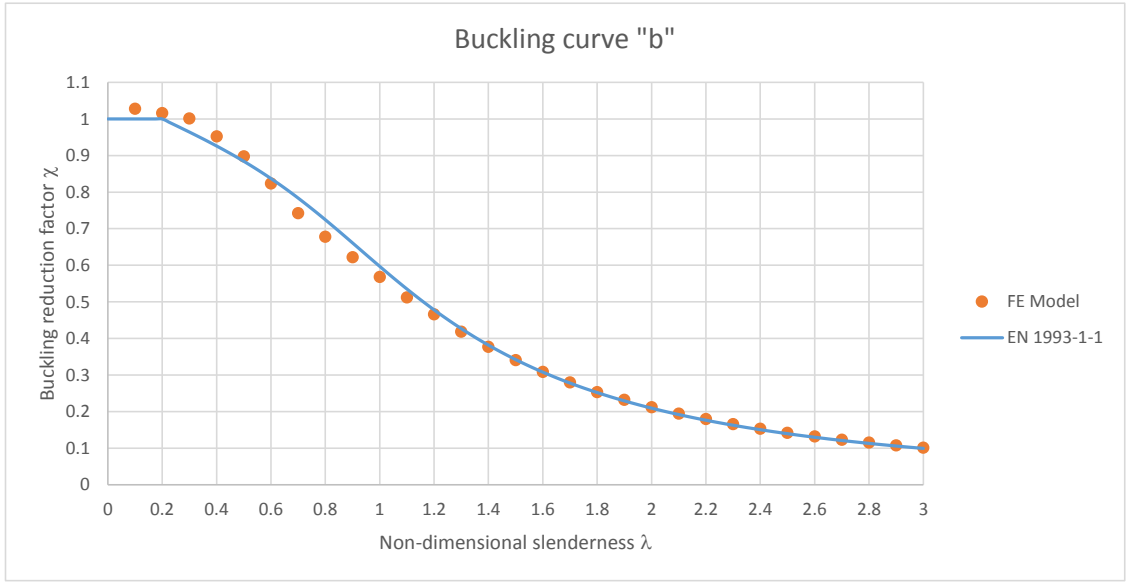

λ	L_{cr} (mm)	N_b (kN)	χ_{FEM}	$\chi_{EN3-1-1}$
0.1	395.01	5,822.01	1.027715	1
0.2	790.02	5,754.90	1.01587	1
0.3	1185.03	5,672.93	1.0014	0.964106
0.4	1580.04	5,393.29	0.952036	0.926073
0.5	1975.05	5,084.00	0.89744	0.884215
0.6	2370.06	4,666.68	0.823775	0.837059
0.7	2765.07	4,203.39	0.741993	0.78371
0.8	3160.08	3,841.50	0.678111	0.724454
0.9	3555.09	3,521.60	0.621641	0.661182
1	3950.10	3,218.58	0.568151	0.597023
1.1	4345.11	2,902.34	0.512328	0.535223
1.2	4740.12	2,639.29	0.465894	0.478126
1.3	5135.13	2,370.14	0.418383	0.426882
1.4	5530.14	2,136.48	0.377136	0.381698
1.5	5925.15	1,930.90	0.340847	0.342235
1.6	6320.16	1,749.27	0.308786	0.307904
1.7	6715.17	1,584.15	0.279637	0.278054
1.8	7110.18	1,433.28	0.253006	0.252059
1.9	7505.19	1,313.64	0.231886	0.229357
2	7900.20	1,201.88	0.212159	0.209461
2.1	8295.21	1,101.33	0.19441	0.191958
2.2	8690.22	1,016.89	0.179504	0.176499
2.3	9085.23	936.70	0.165348	0.162791
2.4	9480.24	867.61	0.153152	0.150589
2.5	9875.25	805.49	0.142187	0.139685
2.6	10270.26	748.88	0.132194	0.129907
2.7	10665.27	697.97	0.123207	0.121108
2.8	11060.28	652.13	0.115116	0.113163
2.9	11455.29	610.69	0.107801	0.105968
3	11850.30	573.03	0.101154	0.099432

FEM: Mild steel at room temperature

Curve c

Section: UKC 356 x 406 x 634

f_y 275 N/mm²

Buckling about the z-z axis

Web class 1

Flange class 1

Section properties:

Depth of the section	h	474.6	mm
Width of the section	b	424	mm
Web thickness	t_w	47.6	mm
Flange thickness	t_f	77	mm
Root radius	r	15.2	mm
Depth between fillets	d	290.2	mm
Second moment of area	I_{zz}	981000000	mm^4
Radius of gyration	r_{zz}	110	mm
Area of section	A	80800	mm²

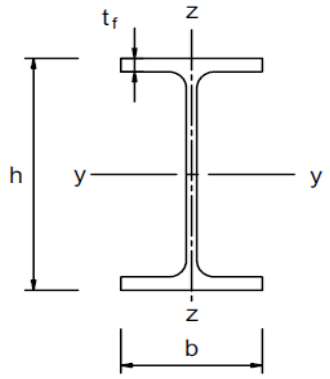

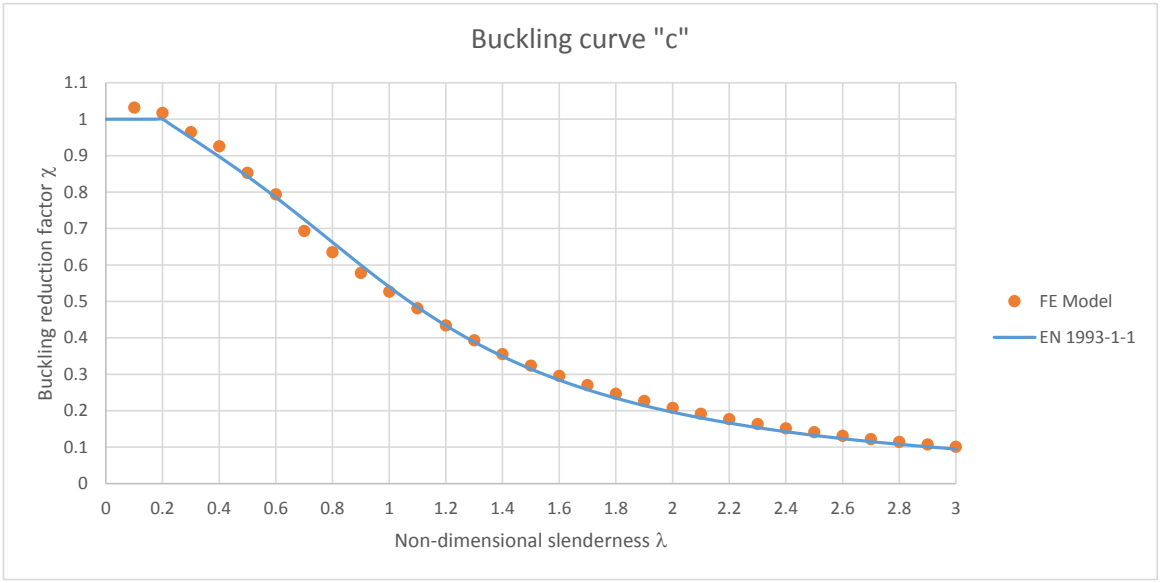

λ	L_{cr} (mm)	N_b (kN)	χ_{FEM}	$\chi_{EN3-1-1}$
0.1	954.96	22,925.11	1.031733	1
0.2	1909.92	22,593.47	1.016808	1
0.3	2864.88	21,426.89	0.964307	0.949148
0.4	3819.84	20,566.95	0.925605	0.897321
0.5	4774.80	18,941.31	0.852444	0.842991
0.6	5729.76	17,639.30	0.793848	0.785385
0.7	6684.72	15,404.75	0.693283	0.724689
0.8	7639.68	14,099.90	0.634559	0.662155
0.9	8594.64	12,839.70	0.577844	0.599831
1	9549.60	11,704.49	0.526755	0.539939
1.1	10504.56	10,684.78	0.480863	0.484247
1.2	11459.52	9,647.48	0.43418	0.433769
1.3	12414.48	8,736.39	0.393177	0.388818
1.4	13369.44	7,896.43	0.355375	0.349219
1.5	14324.40	7,190.76	0.323616	0.314535
1.6	15279.36	6,562.16	0.295327	0.28422
1.7	16234.32	6,001.17	0.27008	0.257719
1.8	17189.28	5,480.77	0.246659	0.234512
1.9	18144.24	5,031.96	0.226461	0.214134
2	19099.20	4,617.80	0.207822	0.196184
2.1	20054.16	4,250.38	0.191286	0.180316
2.2	21009.12	3,922.17	0.176515	0.16624
2.3	21964.08	3,627.26	0.163243	0.153707
2.4	22919.04	3,364.45	0.151416	0.142508
2.5	23874.00	3,126.27	0.140696	0.132466
2.6	24828.96	2,911.65	0.131038	0.123432
2.7	25783.92	2,716.72	0.122265	0.115279
2.8	26738.88	2,541.11	0.114361	0.107897
2.9	27693.84	2,381.37	0.107172	0.101195
3	28648.80	2,236.27	0.100642	0.095092

FEM: Mild steel at room temperature

Curve d

Section: UKC 356 x 406 x 634 *With a thicker flange of t_f = 110 mm

f_y 275 N/mm²

Buckling about the z-z axis

Web class 1

Flange class 1

Section properties:

Depth of the section	h	474.6	mm
Width of the section	b	424	mm
Web thickness	t_w	47.6	mm
Flange thickness	t_f	110	mm
Root radius	r	15.2	mm
Depth between fillets	d	224.2	mm
Second moment of area	I_{zz}	1400237632	mm^4
Radius of gyration	r_{zz}	115.152798	mm
Area of section	A	105597.286	mm²

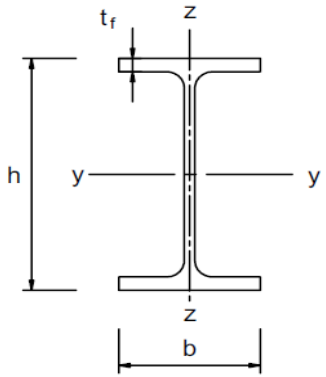

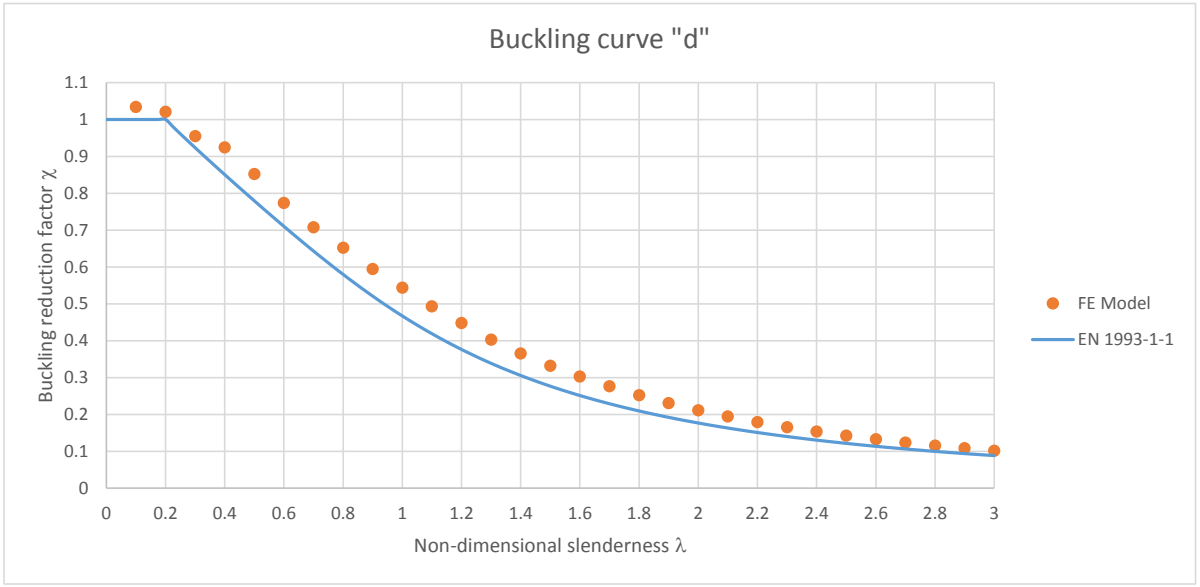

λ	L_{cr} (mm)	N_b (kN)	χ_{FEM}	$\chi_{EN3-1-1}$
0.1	999.70	30,023.30	1.033887	1
0.2	1999.40	29,627.97	1.020273	1
0.3	2999.10	27,725.05	0.954744	0.923456
0.4	3998.80	26,833.71	0.924049	0.850385
0.5	4998.50	24,729.84	0.851601	0.77932
0.6	5998.20	22,447.60	0.773009	0.710031
0.7	6997.90	20,537.73	0.70724	0.643145
0.8	7997.60	18,923.25	0.651644	0.579716
0.9	8997.30	17,250.17	0.594029	0.52079
1	9997.00	15,788.81	0.543706	0.467091
1.1	10996.70	14,305.47	0.492625	0.418916
1.2	11996.40	12,995.67	0.447521	0.37618
1.3	12996.10	11,680.16	0.40222	0.338539
1.4	13995.80	10,597.40	0.364933	0.305512
1.5	14995.50	9,638.20	0.331902	0.27657
1.6	15995.20	8,781.65	0.302406	0.251197
1.7	16994.90	8,009.84	0.275828	0.228915
1.8	17994.60	7,315.41	0.251915	0.209298
1.9	18994.30	6,687.36	0.230287	0.191977
2	19994.00	6,129.72	0.211084	0.176633
2.1	20993.70	5,633.42	0.193993	0.162994
2.2	21993.40	5,200.44	0.179083	0.15083
2.3	22993.10	4,796.06	0.165158	0.139944
2.4	23992.80	4,441.32	0.152942	0.130171
2.5	24992.50	4,122.89	0.141976	0.121367
2.6	25992.20	3,837.41	0.132145	0.113413
2.7	26991.90	3,578.72	0.123237	0.106205
2.8	27991.60	3,345.51	0.115207	0.099654
2.9	28991.30	3,133.42	0.107903	0.093685
3	29991.00	2,929.26	0.100872	0.088231

FEM: Mild steel at room temperature

Curve d

Section: UKC 356 x 406 x 634 *With a thicker flange of t_f = 110 mm

f_y 205 N/mm²

Buckling about the z-z axis

Web class 1

Flange class 1

Section properties:

Depth of the section	h	474.6	mm
Width of the section	b	424	mm
Web thickness	t_w	47.6	mm
Flange thickness	t_f	110	mm
Root radius	r	15.2	mm
Depth between fillets	d	224.2	mm
Second moment of area	I_{zz}	1400237632	mm^4
Radius of gyration	r_{zz}	115.152798	mm
Area of section	A	105597.286	mm²

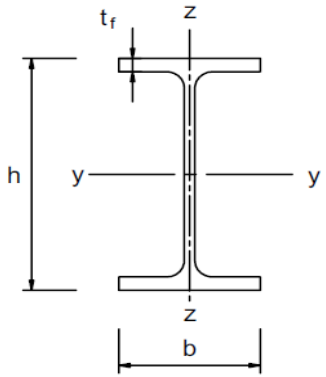

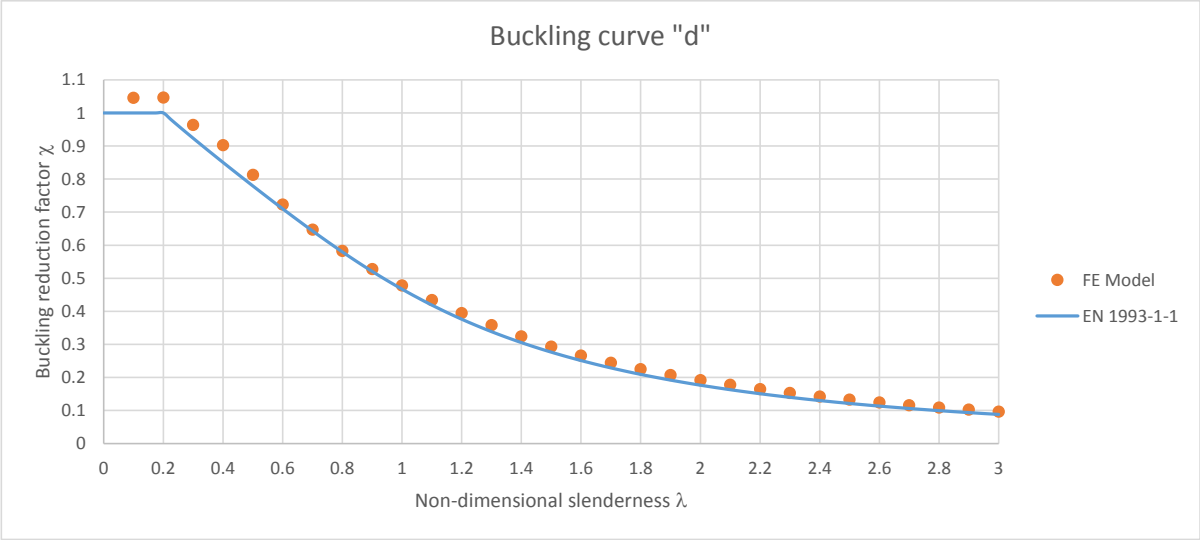

λ	L_{cr} (mm)	N_b (kN)	χ_{FEM}	$\chi_{EN3-1-1}$
0.1	1157.86	22,639.26	1.045817	1
0.2	2315.72	22,644.92	1.046078	1
0.3	3473.58	20,862.43	0.963736	0.923456
0.4	4631.44	19,538.40	0.902573	0.850385
0.5	5789.30	17,594.14	0.812758	0.77932
0.6	6947.16	15,650.40	0.722967	0.710031
0.7	8105.02	14,007.44	0.647071	0.643145
0.8	9262.88	12,614.89	0.582743	0.579716
0.9	10420.74	11,425.72	0.527809	0.52079
1	11578.60	10,346.46	0.477953	0.467091
1.1	12736.46	9,394.62	0.433983	0.418916
1.2	13894.32	8,544.49	0.394711	0.37618
1.3	15052.18	7,755.26	0.358253	0.338539
1.4	16210.04	7,013.34	0.32398	0.305512
1.5	17367.90	6,343.01	0.293014	0.27657
1.6	18525.76	5,763.58	0.266248	0.251197
1.7	19683.62	5,285.90	0.244181	0.228915
1.8	20841.48	4,868.47	0.224898	0.209298
1.9	21999.34	4,491.68	0.207493	0.191977
2	23157.20	4,156.14	0.191992	0.176633
2.1	24315.06	3,842.17	0.177488	0.162994
2.2	25472.92	3,566.17	0.164739	0.15083
2.3	26630.78	3,313.77	0.153079	0.139944
2.4	27788.64	3,082.47	0.142394	0.130171
2.5	28946.50	2,874.89	0.132805	0.121367
2.6	30104.36	2,685.71	0.124066	0.113413
2.7	31262.22	2,514.16	0.116141	0.106205
2.8	32420.08	2,358.01	0.108928	0.099654
2.9	33577.94	2,214.05	0.102278	0.093685
3	34735.80	2,083.19	0.096233	0.088231

FEM: Mild steel at room temperature

Curve a0

Section: UKB 457 x 191 x 161

f_y 460 N/mm²

Buckling about the z-z axis

Web class 1

Flange class 1

Section properties:

Depth of the section	h	492	mm
Width of the section	b	199.4	mm
Web thickness	t_w	18	mm
Flange thickness	t_f	32	mm
Root radius	r	10.2	mm
Depth between fillets	d	407.6	mm
Second moment of area	I_{zz}	42500000	mm^4
Radius of gyration	r_{zz}	45.5	mm
Area of section	A	20600	mm²

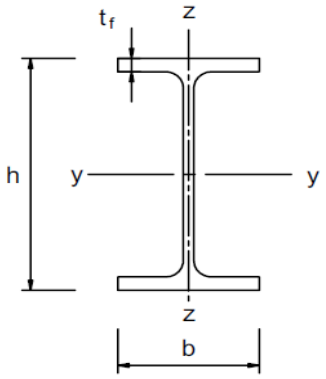

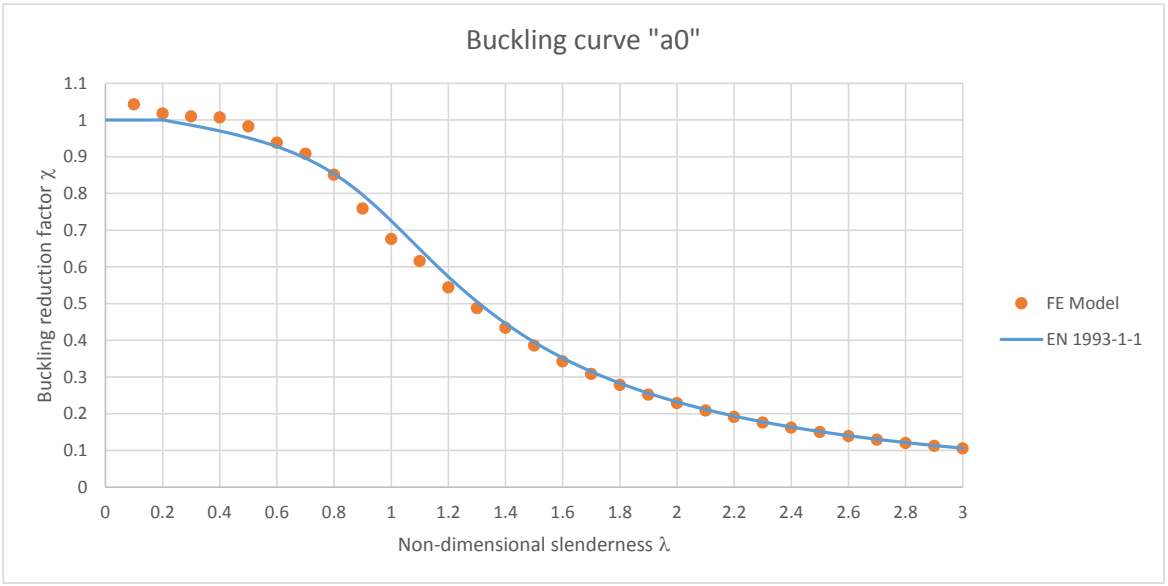

λ	L_{cr} (mm)	N_b (kN)	χ_{FEM}	$\chi_{EN3\text{-}1\text{-}1}$
0.1	305.42	9,880.07	1.042641	1
0.2	610.84	9,643.86	1.017714	1
0.3	916.26	9,570.26	1.009947	0.985935
0.4	1221.68	9,548.03	1.007602	0.970142
0.5	1527.10	9,315.13	0.983023	0.951321
0.6	1832.52	8,891.78	0.938348	0.927584
0.7	2137.94	8,604.41	0.908021	0.896148
0.8	2443.36	8,063.39	0.850927	0.853345
0.9	2748.78	7,192.11	0.758981	0.796054
1	3054.20	6,407.73	0.676206	0.725344
1.1	3359.62	5,841.50	0.616452	0.648248
1.2	3665.04	5,155.81	0.544091	0.5732
1.3	3970.46	4,624.32	0.488004	0.505291
1.4	4275.88	4,112.88	0.434031	0.446102
1.5	4581.30	3,654.82	0.385692	0.395336
1.6	4886.72	3,249.16	0.342883	0.352005
1.7	5192.14	2,926.93	0.308879	0.314993
1.8	5497.56	2,637.81	0.278367	0.28327
1.9	5802.98	2,389.54	0.252167	0.255949
2	6108.40	2,171.94	0.229205	0.232299
2.1	6413.82	1,980.46	0.208997	0.211715
2.2	6719.24	1,813.51	0.191379	0.193706
2.3	7024.66	1,667.39	0.17596	0.177871
2.4	7330.08	1,537.18	0.162219	0.163879
2.5	7635.50	1,421.68	0.15003	0.151461
2.6	7940.92	1,318.30	0.13912	0.140391
2.7	8246.34	1,225.07	0.129281	0.130484
2.8	8551.76	1,142.84	0.120603	0.121584
2.9	8857.18	1,067.77	0.112682	0.113559
3	9162.60	999.80	0.105509	0.1063

FEM: Mild steel at room temperature

Curve a

Section: UKB 1016 x 305 x 487

f_y 460 N/mm²

Buckling about the z-z axis

Web class 3

Flange class 1

Section properties:

Depth of the section	h	1036.3	mm
Width of the section	b	308.5	mm
Web thickness	t_w	30	mm
Flange thickness	t_f	54.1	mm
Root radius	r	30	mm
Depth between fillets	d	868.1	mm
Second moment of area	I_{zz}	267000000	mm^4
Radius of gyration	r_{zz}	65.7	mm
Area of section	A	62000	mm²

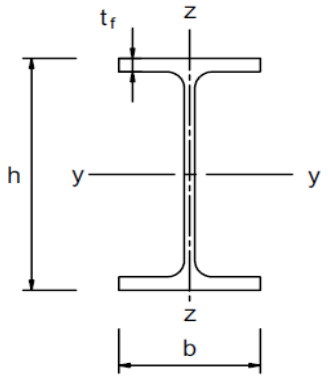

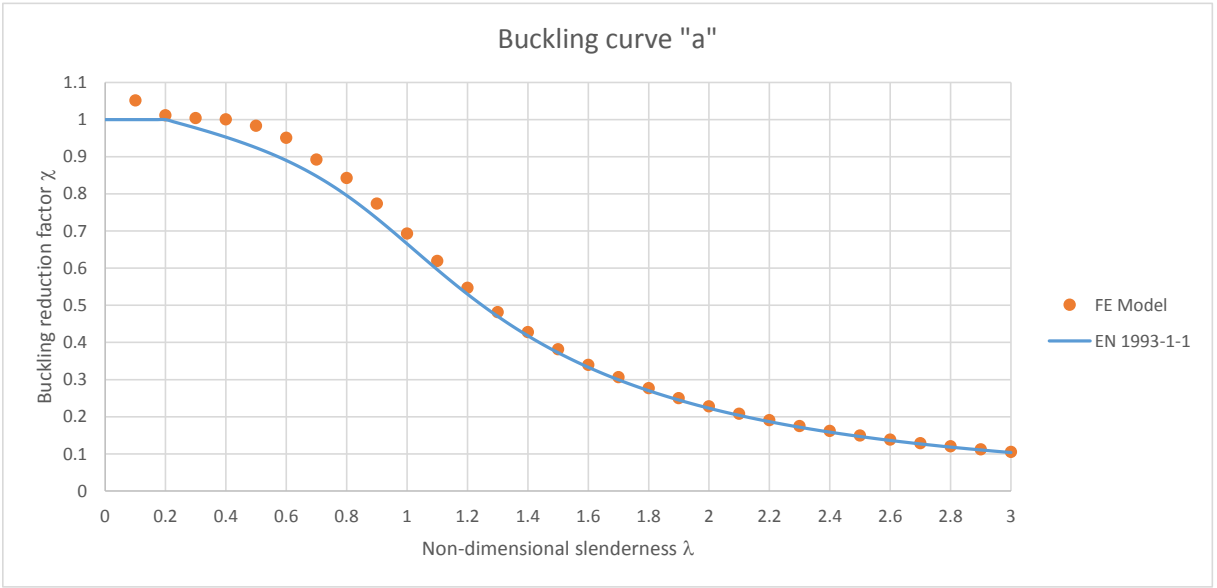

λ	L_{cr} (mm)	N_b (kN)	χ_{FEM}	$\chi_{EN3-1-1}$
0.1	441.01	29,997.49	1.051806	1
0.2	882.02	28,853.01	1.011676	1
0.3	1323.03	28,629.10	1.003825	0.977493
0.4	1764.04	28,535.43	1.000541	0.952785
0.5	2205.05	28,053.27	0.983635	0.924273
0.6	2646.06	27,117.09	0.95081	0.889995
0.7	3087.07	25,445.18	0.892187	0.84774
0.8	3528.08	24,030.31	0.842578	0.795703
0.9	3969.09	22,076.52	0.774072	0.733941
1	4410.10	19,765.59	0.693043	0.665603
1.1	4851.11	17,672.90	0.619667	0.596008
1.2	5292.12	15,605.43	0.547175	0.529996
1.3	5733.13	13,741.96	0.481836	0.470339
1.4	6174.14	12,208.49	0.428068	0.4179
1.5	6615.15	10,883.68	0.381616	0.372437
1.6	7056.16	9,690.14	0.339767	0.33323
1.7	7497.17	8,737.56	0.306366	0.299434
1.8	7938.18	7,896.58	0.276879	0.270239
1.9	8379.19	7,121.59	0.249705	0.24493
2	8820.20	6,500.74	0.227936	0.222895
2.1	9261.21	5,932.43	0.20801	0.203624
2.2	9702.22	5,433.27	0.190508	0.186692
2.3	10143.23	4,995.75	0.175166	0.171749
2.4	10584.24	4,608.70	0.161595	0.158503
2.5	11025.25	4,261.03	0.149405	0.146713
2.6	11466.26	3,952.42	0.138584	0.136176
2.7	11907.27	3,678.81	0.128991	0.126724
2.8	12348.28	3,428.50	0.120214	0.118215
2.9	12789.29	3,205.45	0.112393	0.110528
3	13230.30	3,001.72	0.10525	0.103563

FEM: Mild steel at room temperature

Curve b

Section: UKB 457 x 191 x 161

f_y 275 N/mm²

Buckling about the z-z axis

Web class 1

Flange class 1

Section properties:

Depth of the section	h	492	mm
Width of the section	b	199.4	mm
Web thickness	t_w	18	mm
Flange thickness	t_f	32	mm
Root radius	r	10.2	mm
Depth between fillets	d	407.6	mm
Second moment of area	I_{zz}	42500000	mm^4
Radius of gyration	r_{zz}	45.5	mm
Area of section	A	20600	mm²

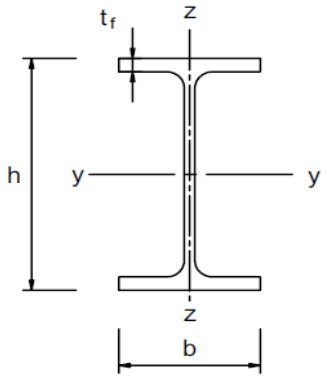

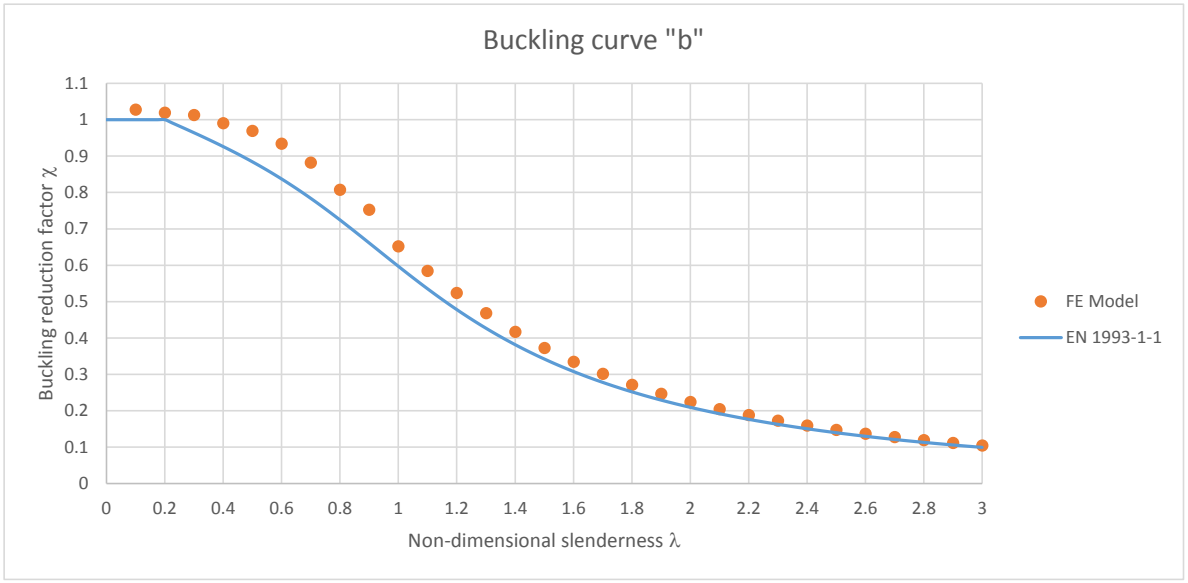

λ	L_{cr} (mm)	N_b (kN)	χ_{FEM}	$\chi_{EN3-1-1}$
0.1	395.01	5,822.01	1.027715	1
0.2	790.02	5,774.37	1.019306	1
0.3	1185.03	5,738.04	1.012893	0.964106
0.4	1580.04	5,610.69	0.990413	0.926073
0.5	1975.05	5,490.46	0.96919	0.884215
0.6	2370.06	5,289.38	0.933694	0.837059
0.7	2765.07	4,995.62	0.881839	0.78371
0.8	3160.08	4,573.77	0.807373	0.724454
0.9	3555.09	4,263.73	0.752645	0.661182
1	3950.10	3,692.71	0.651846	0.597023
1.1	4345.11	3,310.74	0.58442	0.535223
1.2	4740.12	2,967.64	0.523856	0.478126
1.3	5135.13	2,651.56	0.468059	0.426882
1.4	5530.14	2,361.73	0.416898	0.381698
1.5	5925.15	2,111.18	0.372671	0.342235
1.6	6320.16	1,896.40	0.334757	0.307904
1.7	6715.17	1,706.69	0.301269	0.278054
1.8	7110.18	1,536.96	0.271308	0.252059
1.9	7505.19	1,397.63	0.246714	0.229357
2	7900.20	1,270.14	0.224208	0.209461
2.1	8295.21	1,159.21	0.204627	0.191958
2.2	8690.22	1,064.83	0.187966	0.176499
2.3	9085.23	979.34	0.172876	0.162791
2.4	9480.24	903.44	0.159478	0.150589
2.5	9875.25	836.35	0.147635	0.139685
2.6	10270.26	776.13	0.137004	0.129907
2.7	10665.27	721.93	0.127438	0.121108
2.8	11060.28	673.52	0.118891	0.113163
2.9	11455.29	629.65	0.111148	0.105968
3	11850.30	590.01	0.10415	0.099432

FEM: Mild steel at room temperature

Curve c

Section: UKC 356 x 406 x 634

f_y 275 N/mm²

Buckling about the z-z axis

Web class 1

Flange class 1

Section properties:

Depth of the section	h	474.6	mm
Width of the section	b	424	mm
Web thickness	t_w	47.6	mm
Flange thickness	t_f	77	mm
Root radius	r	15.2	mm
Depth between fillets	d	290.2	mm
Second moment of area	I_{zz}	981000000	mm^4
Radius of gyration	r_{zz}	110	mm
Area of section	A	80800	mm²

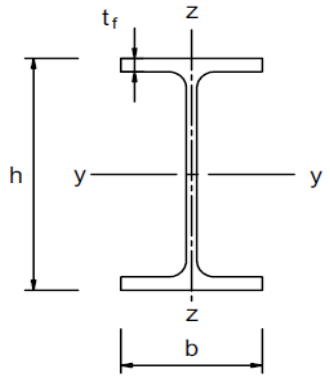

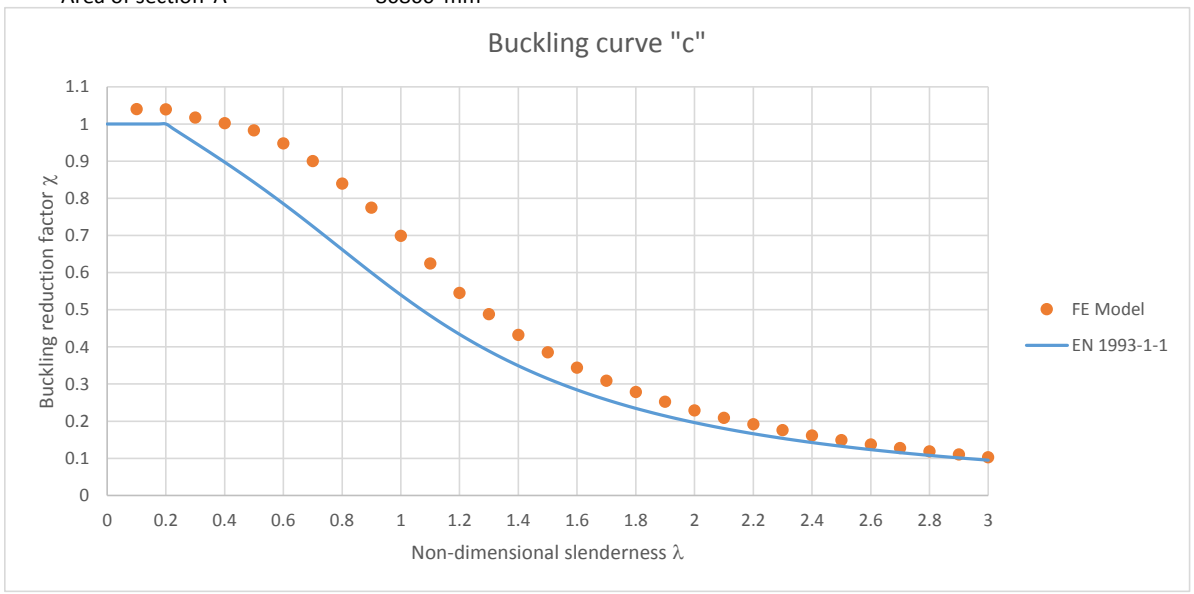

λ	L_{cr} (mm)	N_b (kN)	χ_{FEM}	$\chi_{EN3-1-1}$
0.1	954.96	23,111.04	1.040101	1
0.2	1909.92	23,095.34	1.039394	1
0.3	2864.88	22,601.64	1.017176	0.949148
0.4	3819.84	22,268.47	1.002181	0.897321
0.5	4774.80	21,834.12	0.982634	0.842991
0.6	5729.76	21,050.42	0.947364	0.785385
0.7	6684.72	20,002.26	0.900192	0.724689
0.8	7639.68	18,644.46	0.839084	0.662155
0.9	8594.64	17,208.95	0.77448	0.599831
1	9549.60	15,528.50	0.698852	0.539939
1.1	10504.56	13,872.36	0.624319	0.484247
1.2	11459.52	12,103.98	0.544734	0.433769
1.3	12414.48	10,835.78	0.487659	0.388818
1.4	13369.44	9,601.36	0.432104	0.349219
1.5	14324.40	8,554.32	0.384983	0.314535
1.6	15279.36	7,635.69	0.343641	0.28422
1.7	16234.32	6,854.33	0.308476	0.257719
1.8	17189.28	6,176.79	0.277983	0.234512
1.9	18144.24	5,593.69	0.251741	0.214134
2	19099.20	5,083.50	0.22878	0.196184
2.1	20054.16	4,641.76	0.2089	0.180316
2.2	21009.12	4,252.31	0.191373	0.16624
2.3	21964.08	3,906.69	0.175819	0.153707
2.4	22919.04	3,585.04	0.161343	0.142508
2.5	23874.00	3,301.33	0.148575	0.132466
2.6	24828.96	3,049.65	0.137248	0.123432
2.7	25783.92	2,825.37	0.127154	0.115279
2.8	26738.88	2,624.99	0.118136	0.107897
2.9	27693.84	2,444.88	0.110031	0.101195
3	28648.80	2,282.60	0.102727	0.095092

FEM: Mild steel at room temperature

Curve d

Section: UKC 356 x 406 x 634

f_y 275 N/mm²

Buckling about the z-z axis

Web class 1

Flange class 1

Section properties:

Depth of the section	h	474.6	mm
Width of the section	b	424	mm
Web thickness	t_w	47.6	mm
Flange thickness	t_f	110	mm
Root radius	r	15.2	mm
Depth between fillets	d	224.2	mm
Second moment of area	I_{zz}	1400237632	mm^4
Radius of gyration	r_{zz}	115.152798	mm
Area of section	A	105597.286	mm²

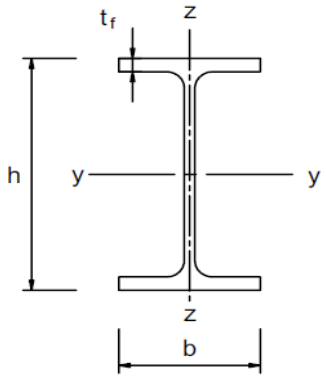

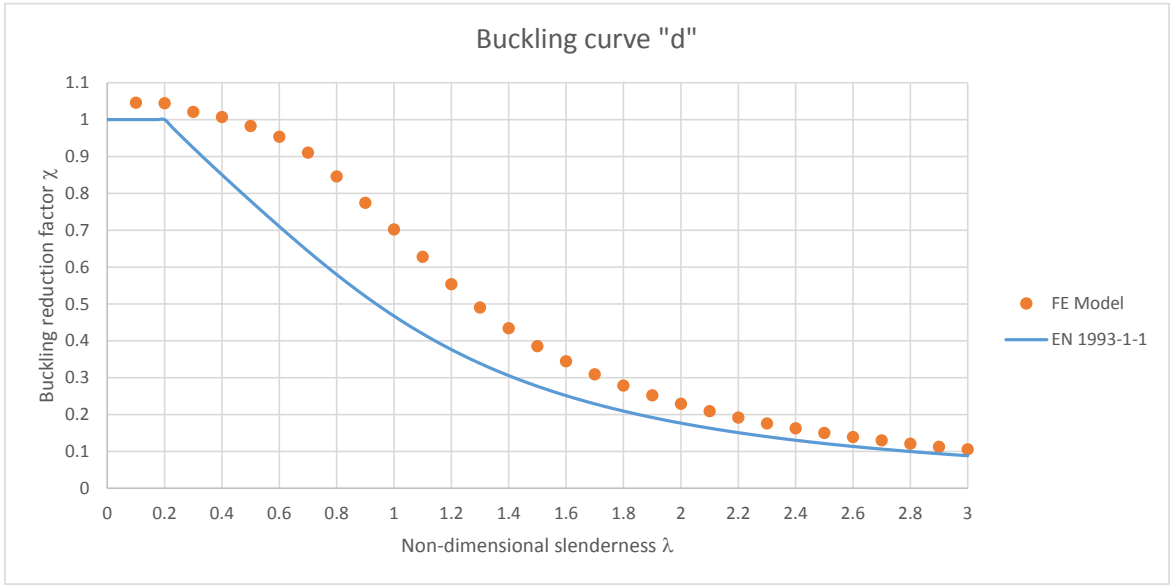

λ	L_{cr} (mm)	N_b (kN)	χ_{FEM}	$\chi_{EN3-1-1}$
0.1	999.70	30,357.21	1.045385	1
0.2	1999.40	30,332.13	1.044522	1
0.3	2999.10	29,646.63	1.020916	0.923456
0.4	3998.80	29,233.44	1.006687	0.850385
0.5	4998.50	28,539.91	0.982805	0.77932
0.6	5998.20	27,675.42	0.953035	0.710031
0.7	6997.90	26,428.65	0.910101	0.643145
0.8	7997.60	24,566.72	0.845983	0.579716
0.9	8997.30	22,488.02	0.774401	0.52079
1	9997.00	20,384.65	0.701969	0.467091
1.1	10996.70	18,217.88	0.627354	0.418916
1.2	11996.40	16,065.14	0.553222	0.37618
1.3	12996.10	14,228.77	0.489984	0.338539
1.4	13995.80	12,609.40	0.434219	0.305512
1.5	14995.50	11,180.22	0.385004	0.27657
1.6	15995.20	9,990.40	0.344031	0.251197
1.7	16994.90	8,968.86	0.308853	0.228915
1.8	17994.60	8,078.58	0.278195	0.209298
1.9	18994.30	7,313.41	0.251846	0.191977
2	19994.00	6,645.06	0.22883	0.176633
2.1	20993.70	6,065.70	0.208879	0.162994
2.2	21993.40	5,553.31	0.191235	0.15083
2.3	22993.10	5,106.32	0.175842	0.139944
2.4	23992.80	4,706.34	0.162068	0.130171
2.5	24992.50	4,352.89	0.149897	0.121367
2.6	25992.20	4,038.71	0.139077	0.113413
2.7	26991.90	3,756.59	0.129363	0.106205
2.8	27991.60	3,502.23	0.120603	0.099654
2.9	28991.30	3,271.98	0.112674	0.093685
3	29991.00	3,064.57	0.105532	0.088231

Appendix B

Results for elevated temperatures

FEM: Mild steel at 500 degrees C

Curve a0

Section:	UKB 457 x 191 x 161	
f_y	460	N/mm²
E	210000	N/mm²
$k_{y,\theta}$	0.78	
$k_{E,\theta}$	0.6	

Section properties:

Depth of the section	h	492	mm
Width of the section	b	199.4	mm
Web thickness	t_w	18	mm
Flange thickness	t_f	32	mm
Root radius	r	10.2	mm
Depth between fillets	d	407.6	mm
Second moment of area	I_{zz}	42500000	mm^4
Radius of gyration	r_{zz}	45.5	mm
Area of section	A	20600	mm²

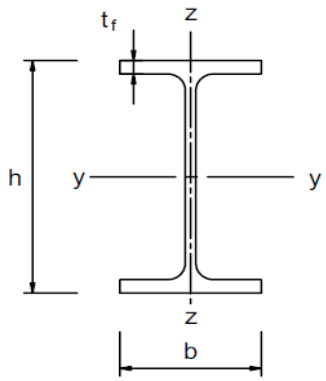

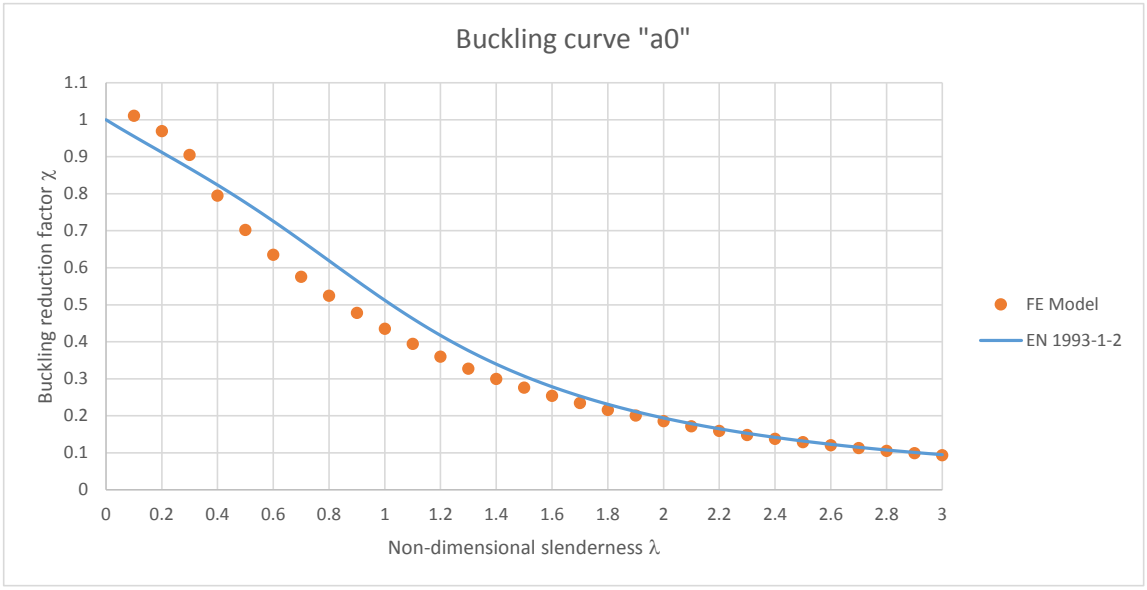

λ_θ	L_{cr} (mm)	N_b (kN)	χ_{FEM}	$\chi_{EN3-1-1}$
0.1	267.87	7,470.51	1.010719	0.955195
0.2	535.74	7,165.58	0.969465	0.912046
0.3	803.60	6,692.30	0.905432	0.868661
0.4	1071.47	5,879.40	0.79545	0.823693
0.5	1339.34	5,191.20	0.702341	0.776259
0.6	1607.21	4,696.95	0.635471	0.726011
0.7	1875.07	4,256.72	0.57591	0.673258
0.8	2142.94	3,877.49	0.524603	0.618999
0.9	2410.81	3,535.93	0.478392	0.564756
1	2678.68	3,215.93	0.435098	0.512191
1.1	2946.54	2,917.27	0.394691	0.462714
1.2	3214.41	2,658.75	0.359714	0.417245
1.3	3482.28	2,421.00	0.327548	0.376195
1.4	3750.15	2,213.89	0.299527	0.339575
1.5	4018.02	2,039.63	0.275951	0.307143
1.6	4285.88	1,877.99	0.254081	0.278527
1.7	4553.75	1,736.37	0.234922	0.25331
1.8	4821.62	1,594.46	0.215721	0.231076
1.9	5089.49	1,486.74	0.201148	0.211443
2	5357.35	1,372.09	0.185636	0.194065
2.1	5625.22	1,267.68	0.171511	0.178641
2.2	5893.09	1,175.57	0.159049	0.164909
2.3	6160.96	1,096.33	0.148328	0.152647
2.4	6428.82	1,019.73	0.137964	0.141662
2.5	6696.69	951.79	0.128772	0.131791
2.6	6964.56	889.70	0.120372	0.122893
2.7	7232.43	832.42	0.112621	0.114848
2.8	7500.30	780.65	0.105618	0.107554
2.9	7768.16	733.69	0.099264	0.100923
3	8036.03	690.90	0.093475	0.094878

FEM: Mild steel at 500 degrees C

Curve a

Section:	UKB 1016 x 305 x 487	
f_y	460	N/mm²
E	210000	N/mm²
$k_{y,\theta}$	0.78	
$k_{E,\theta}$	0.6	

Section properties:

Depth of the section	h	1036.3	mm
Width of the section	b	308.5	mm
Web thickness	t_w	30	mm
Flange thickness	t_f	54.1	mm
Root radius	r	30	mm
Depth between fillets	d	868.1	mm
Second moment of area	I_{zz}	267000000	mm^4
Radius of gyration	r_{zz}	65.7	mm
Area of section	A	62000	mm²

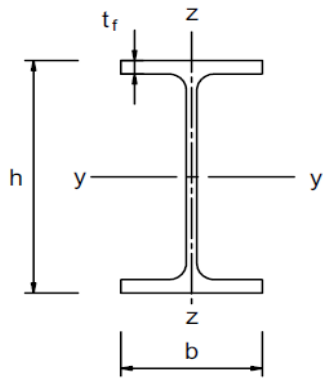

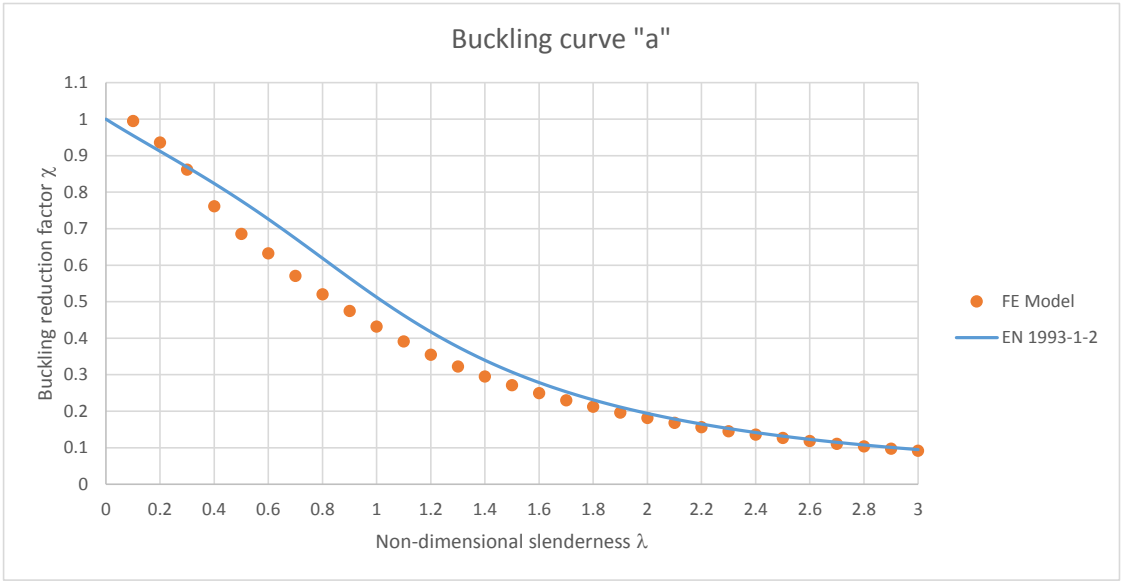

λ_θ	L_{cr} (mm)	N_b (kN)	χ_{FEM}	$\chi_{EN3-1-1}$
0.1	386.79	22,136.89	0.995113	0.955195
0.2	773.58	20,834.23	0.936555	0.912046
0.3	1160.37	19,170.55	0.861768	0.868661
0.4	1547.16	16,943.41	0.761652	0.823693
0.5	1933.95	15,257.05	0.685846	0.776259
0.6	2320.73	14,072.81	0.632611	0.726011
0.7	2707.52	12,697.75	0.570798	0.673258
0.8	3094.31	11,583.94	0.52073	0.618999
0.9	3481.10	10,559.28	0.474668	0.564756
1	3867.89	9,618.71	0.432387	0.512191
1.1	4254.68	8,703.71	0.391255	0.462714
1.2	4641.47	7,897.13	0.354997	0.417245
1.3	5028.26	7,172.42	0.32242	0.376195
1.4	5415.05	6,567.35	0.29522	0.339575
1.5	5801.84	6,032.91	0.271196	0.307143
1.6	6188.63	5,558.10	0.249852	0.278527
1.7	6575.42	5,126.01	0.230428	0.25331
1.8	6962.20	4,734.02	0.212807	0.231076
1.9	7348.99	4,372.13	0.196539	0.211443
2	7735.78	4,046.55	0.181903	0.194065
2.1	8122.57	3,751.62	0.168645	0.178641
2.2	8509.36	3,485.16	0.156668	0.164909
2.3	8896.15	3,238.28	0.145569	0.152647
2.4	9282.94	3,024.25	0.135948	0.141662
2.5	9669.73	2,820.99	0.126811	0.131791
2.6	10056.52	2,640.14	0.118681	0.122893
2.7	10443.31	2,471.32	0.111093	0.114848
2.8	10830.10	2,318.19	0.104209	0.107554
2.9	11216.89	2,178.40	0.097925	0.100923
3	11603.67	2,049.95	0.092151	0.094878

FEM: Mild steel at 500 degrees C

Curve b

Section:	UKB 457 x 191 x 161	
f_y	275	N/mm²
E	210000	N/mm²
$k_{y,\theta}$	0.78	
$k_{E,\theta}$	0.6	

Section properties:

Depth of the section	h	492	mm
Width of the section	b	199.4	mm
Web thickness	t_w	18	mm
Flange thickness	t_f	32	mm
Root radius	r	10.2	mm
Depth between fillets	d	407.6	mm
Second moment of area	I_{zz}	42500000	mm^4
Radius of gyration	r_{zz}	45.5	mm
Area of section	A	20600	mm²

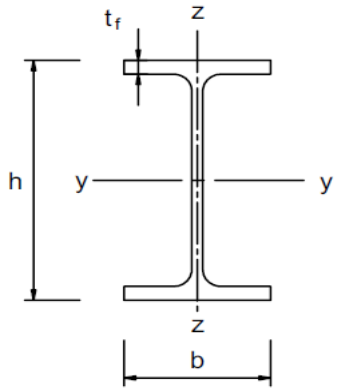

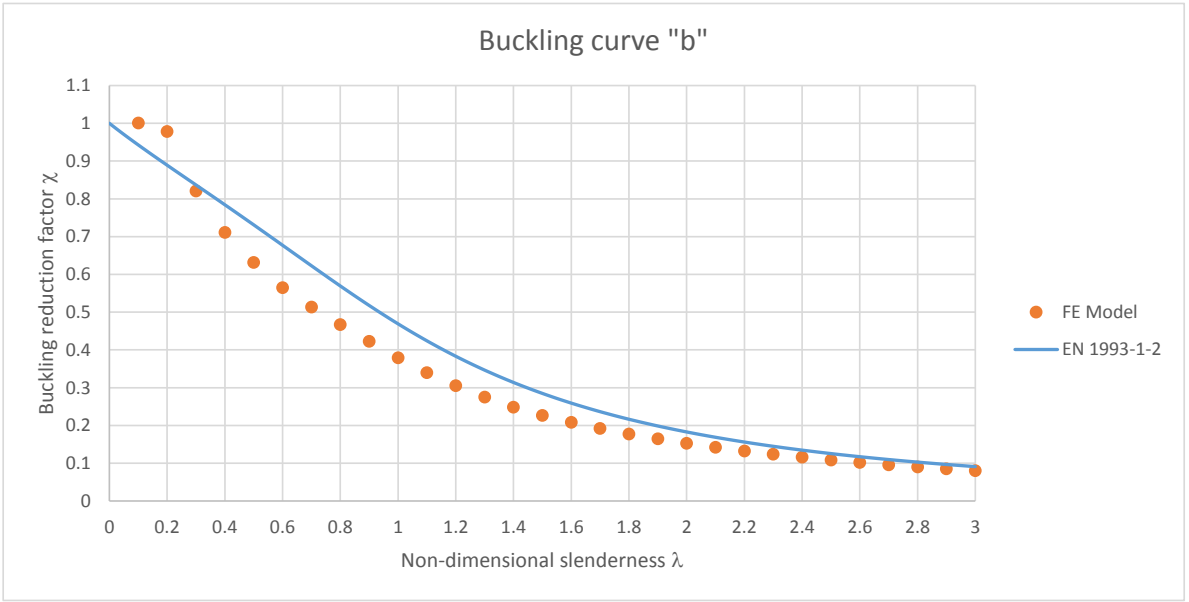

λ_θ	L_{cr} (mm)	N_b (kN)	χ_{FEM}	$\chi_{EN3-1-1}$
0.1	346.44	4,423.47	1.00108	0.94281
0.2	692.89	4,322.56	0.978243	0.8892
0.3	1039.33	3,625.95	0.820592	0.836859
0.4	1385.78	3,141.70	0.711001	0.784411
0.5	1732.22	2,792.01	0.631862	0.731187
0.6	2078.66	2,494.66	0.564569	0.677166
0.7	2425.11	2,270.61	0.513864	0.622903
0.8	2771.55	2,062.89	0.466854	0.569381
0.9	3117.99	1,868.41	0.422841	0.51776
1	3464.44	1,676.63	0.379441	0.469092
1.1	3810.88	1,501.16	0.339729	0.424132
1.2	4157.33	1,349.30	0.305362	0.383268
1.3	4503.77	1,214.20	0.274787	0.346569
1.4	4850.21	1,098.89	0.248692	0.31387
1.5	5196.66	1,002.28	0.226827	0.284872
1.6	5543.10	920.31	0.208276	0.259215
1.7	5889.55	847.98	0.191907	0.236522
1.8	6235.99	783.27	0.177263	0.216435
1.9	6582.43	727.37	0.164611	0.198625
2	6928.88	675.56	0.152887	0.182797
2.1	7275.32	627.63	0.14204	0.168694
2.2	7621.77	585.42	0.132486	0.156093
2.3	7968.21	547.08	0.12381	0.144802
2.4	8314.65	511.94	0.115857	0.134653
2.5	8661.10	478.88	0.108377	0.125506
2.6	9007.54	451.10	0.10209	0.117237
2.7	9353.98	424.09	0.095976	0.109741
2.8	9700.43	399.58	0.090429	0.102929
2.9	10046.87	377.35	0.085398	0.09672
3	10393.32	355.78	0.080516	0.091048

FEM: Mild steel at 500 degrees C

Curve c

Section:	UKC 356 x 406 x 634	
f_y	275	N/mm²
E	210000	N/mm²
$k_{y,\theta}$	0.78	
$k_{E,\theta}$	0.6	

Section properties:

Depth of the section	h	474.6	mm
Width of the section	b	424	mm
Web thickness	t_w	47.6	mm
Flange thickness	t_f	77	mm
Root radius	r	15.2	mm
Depth between fillets	d	290.2	mm
Second moment of area	I_{zz}	981000000	mm^4
Radius of gyration	r_{zz}	110	mm
Area of section	A	80800	mm²

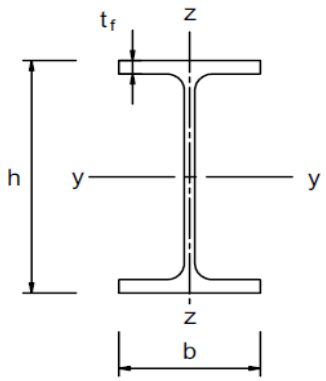

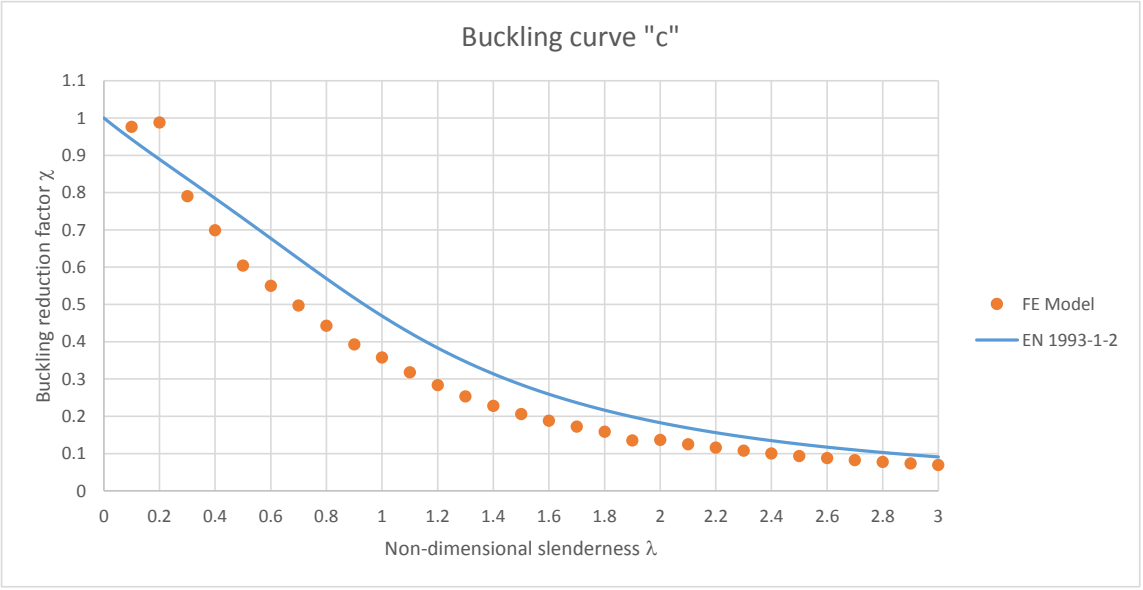

λ_θ	L_{cr} (mm)	N_b (kN)	χ_{FEM}	$\chi_{EN3-1-1}$
0.1	837.56	16,921.63	0.976345	0.94281
0.2	1675.11	17,127.31	0.988213	0.8892
0.3	2512.67	13,702.01	0.79058	0.836859
0.4	3350.23	12,123.40	0.699497	0.784411
0.5	4187.78	10,471.90	0.604208	0.731187
0.6	5025.34	9,536.16	0.550218	0.677166
0.7	5862.90	8,614.84	0.49706	0.622903
0.8	6700.45	7,681.75	0.443222	0.569381
0.9	7538.01	6,812.77	0.393084	0.51776
1	8375.57	6,198.16	0.357622	0.469092
1.1	9213.12	5,507.86	0.317793	0.424132
1.2	10050.68	4,914.05	0.283531	0.383268
1.3	10888.24	4,389.95	0.253292	0.346569
1.4	11725.79	3,948.59	0.227826	0.31387
1.5	12563.35	3,579.14	0.20651	0.284872
1.6	13400.91	3,264.75	0.18837	0.259215
1.7	14238.46	2,991.45	0.172601	0.236522
1.8	15076.02	2,749.35	0.158632	0.216435
1.9	15913.58	2,350.46	0.135617	0.198625
2	16751.13	2,366.09	0.136519	0.182797
2.1	17588.69	2,166.65	0.125012	0.168694
2.2	18426.25	2,011.01	0.116032	0.156093
2.3	19263.80	1,869.88	0.107888	0.144802
2.4	20101.36	1,741.74	0.100495	0.134653
2.5	20938.92	1,626.43	0.093842	0.125506
2.6	21776.47	1,524.04	0.087934	0.117237
2.7	22614.03	1,432.65	0.082661	0.109741
2.8	23451.59	1,349.51	0.077864	0.102929
2.9	24289.14	1,273.46	0.073476	0.09672
3	25126.70	1,203.42	0.069435	0.091048

FEM: Mild steel at 500 degrees C

Curve d

Section: UKC 356 x 406 x 634 *With a thicker flange of t_f = 110 mm

f_y	275	N/mm²
E	210000	N/mm²
$k_{y,\theta}$	0.78	
$k_{E,\theta}$	0.6	

Section properties:

Depth of the section	h	474.6	mm
Width of the section	b	424	mm
Web thickness	t_w	47.6	mm
Flange thickness	t_f	110	mm
Root radius	r	15.2	mm
Depth between fillets	d	224.2	mm
Second moment of area	I_{zz}	1400237632	mm^4
Radius of gyration	r_{zz}	115.152798	mm
Area of section	A	105597.286	mm²

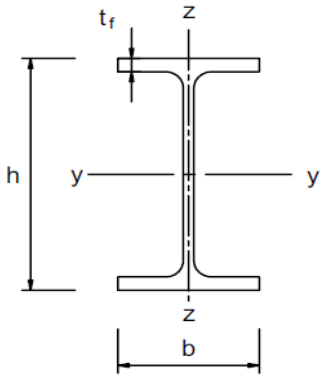

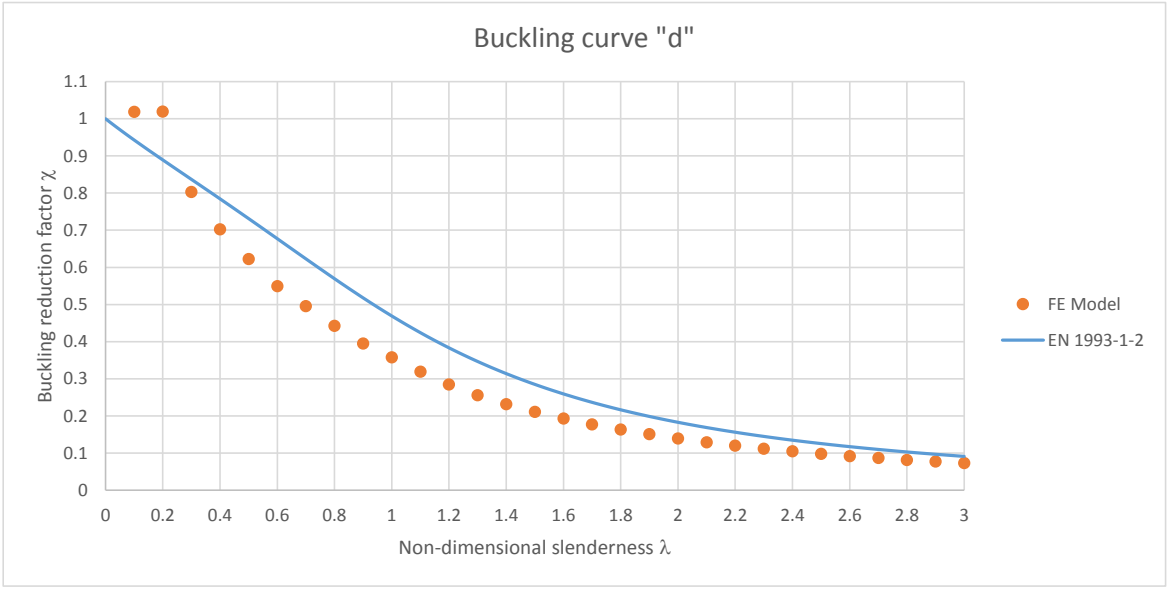

λ_θ	L_{cr} (mm)	N_b (kN)	χ_{FEM}	$\chi_{EN3-1-1}$
0.1	876.79	23,075.03	1.018737	0.94281
0.2	1753.58	23,089.22	1.019364	0.8892
0.3	2630.37	18,186.63	0.80292	0.836859
0.4	3507.16	15,914.34	0.702601	0.784411
0.5	4383.95	14,092.59	0.622172	0.731187
0.6	5260.74	12,440.25	0.549223	0.677166
0.7	6137.54	11,230.25	0.495803	0.622903
0.8	7014.33	10,027.15	0.442688	0.569381
0.9	7891.12	8,942.98	0.394823	0.51776
1	8767.91	8,096.39	0.357447	0.469092
1.1	9644.70	7,230.41	0.319215	0.424132
1.2	10521.49	6,455.53	0.285005	0.383268
1.3	11398.28	5,793.63	0.255783	0.346569
1.4	12275.07	5,241.28	0.231397	0.31387
1.5	13151.86	4,771.75	0.210668	0.284872
1.6	14028.65	4,371.56	0.192999	0.259215
1.7	14905.44	4,017.27	0.177358	0.236522
1.8	15782.23	3,699.40	0.163324	0.216435
1.9	16659.03	3,413.32	0.150694	0.198625
2	17535.82	3,155.85	0.139327	0.182797
2.1	18412.61	2,921.74	0.128991	0.168694
2.2	19289.40	2,711.29	0.119701	0.156093
2.3	20166.19	2,528.77	0.111642	0.144802
2.4	21042.98	2,366.01	0.104457	0.134653
2.5	21919.77	2,218.69	0.097953	0.125506
2.6	22796.56	2,084.36	0.092022	0.117237
2.7	23673.35	1,961.00	0.086576	0.109741
2.8	24550.14	1,848.07	0.08159	0.102929
2.9	25426.93	1,743.83	0.076988	0.09672
3	26303.72	1,647.56	0.072738	0.091048

FEM: Mild steel at 500 degrees C

Curve a0

Section:	UKB 457 x 191 x 161	
f_y	460	N/mm²
E	210000	N/mm²
$k_{y,\theta}$	0.78	
$k_{E,\theta}$	0.6	

Section properties:

Depth of the section	h	492	mm
Width of the section	b	199.4	mm
Web thickness	t_w	18	mm
Flange thickness	t_f	32	mm
Root radius	r	10.2	mm
Depth between fillets	d	407.6	mm
Second moment of area	I_{zz}	42500000	mm^4
Radius of gyration	r_{zz}	45.5	mm
Area of section	A	20600	mm²

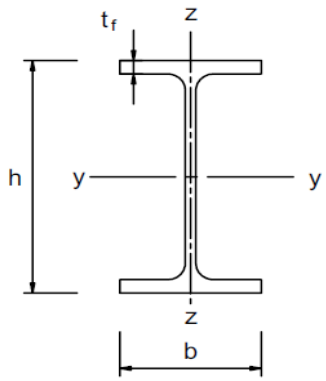

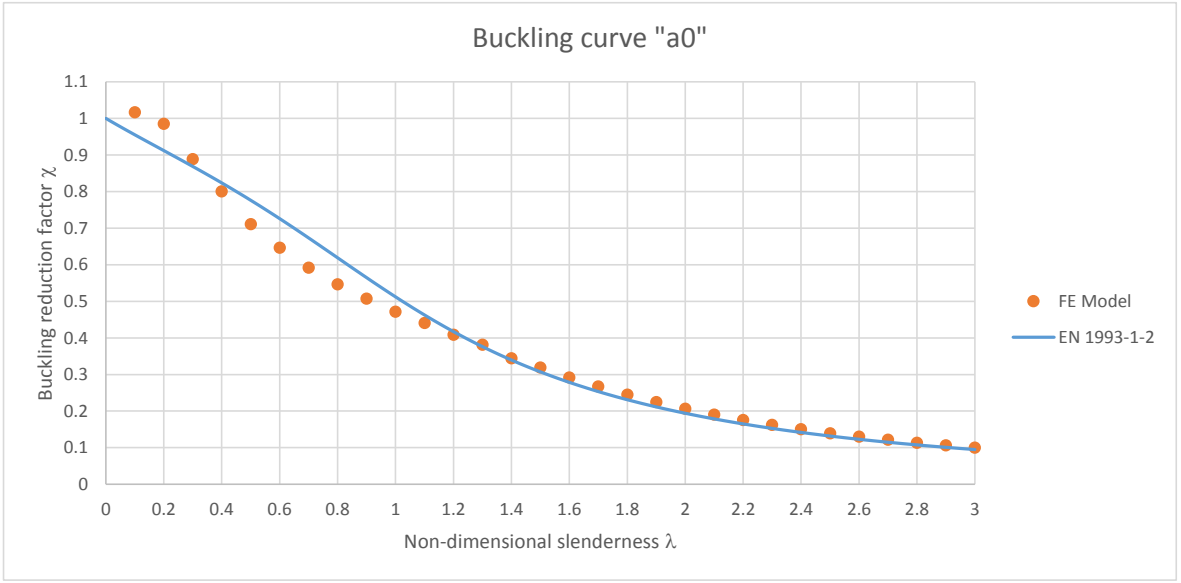

λ_θ	L_{cr} (mm)	N_b (kN)	χ_{FEM}	$\chi_{EN3-1-1}$
0.1	267.87	7,515.36	1.016787	0.955195
0.2	535.74	7,285.27	0.985657	0.912046
0.3	803.60	6,568.18	0.888639	0.868661
0.4	1071.47	5,918.39	0.800726	0.823693
0.5	1339.34	5,255.49	0.711039	0.776259
0.6	1607.21	4,780.62	0.646792	0.726011
0.7	1875.07	4,374.59	0.591858	0.673258
0.8	2142.94	4,042.15	0.546881	0.618999
0.9	2410.81	3,753.00	0.50776	0.564756
1	2678.68	3,486.72	0.471734	0.512191
1.1	2946.54	3,260.26	0.441095	0.462714
1.2	3214.41	3,024.13	0.409148	0.417245
1.3	3482.28	2,818.69	0.381354	0.376195
1.4	3750.15	2,547.82	0.344706	0.339575
1.5	4018.02	2,357.87	0.319007	0.307143
1.6	4285.88	2,158.72	0.292063	0.278527
1.7	4553.75	1,978.52	0.267683	0.25331
1.8	4821.62	1,813.13	0.245307	0.231076
1.9	5089.49	1,663.87	0.225112	0.211443
2	5357.35	1,528.84	0.206844	0.194065
2.1	5625.22	1,407.53	0.190432	0.178641
2.2	5893.09	1,298.82	0.175724	0.164909
2.3	6160.96	1,201.06	0.162497	0.152647
2.4	6428.82	1,112.33	0.150493	0.141662
2.5	6696.69	1,033.01	0.13976	0.131791
2.6	6964.56	964.47	0.130487	0.122893
2.7	7232.43	899.52	0.1217	0.114848
2.8	7500.30	840.35	0.113695	0.107554
2.9	7768.16	788.39	0.106665	0.100923
3	8036.03	739.67	0.100074	0.094878

FEM: Mild steel at 500 degrees C

Curve a

Section:	UKB 1016 x 305 x 487	
f_y	460	N/mm²
E	210000	N/mm²
$k_{y,\theta}$	0.78	
$k_{E,\theta}$	0.6	

Section properties:

Depth of the section	h	1036.3	mm
Width of the section	b	308.5	mm
Web thickness	t_w	30	mm
Flange thickness	t_f	54.1	mm
Root radius	r	30	mm
Depth between fillets	d	868.1	mm
Second moment of area	I_{zz}	267000000	mm^4
Radius of gyration	r_{zz}	65.7	mm
Area of section	A	62000	mm²

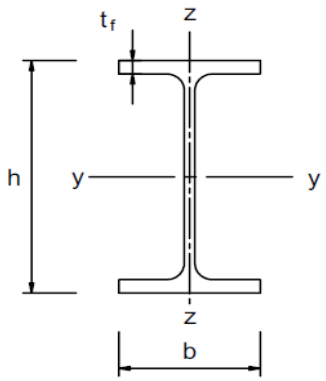

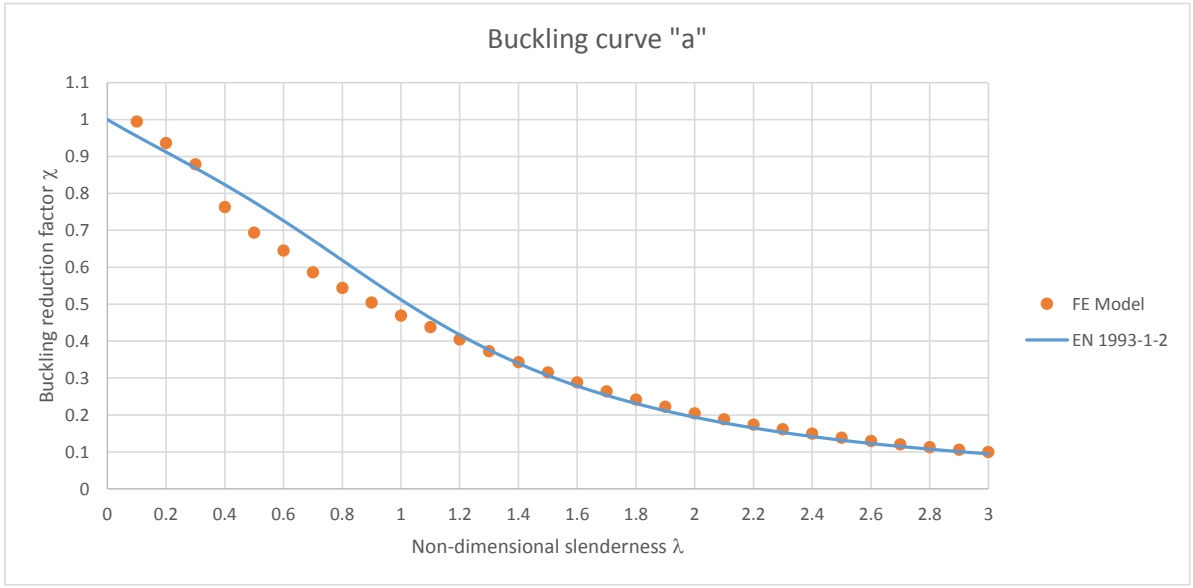

λ_θ	L_{cr} (mm)	N_b (kN)	χ_{FEM}	$\chi_{EN3-1-1}$
0.1	386.79	22,136.89	0.995113	0.955195
0.2	773.58	20,834.23	0.936555	0.912046
0.3	1160.37	19,556.02	0.879096	0.868661
0.4	1547.16	16,978.85	0.763245	0.823693
0.5	1933.95	15,441.88	0.694155	0.776259
0.6	2320.73	14,360.54	0.645545	0.726011
0.7	2707.52	13,055.50	0.58688	0.673258
0.8	3094.31	12,105.06	0.544155	0.618999
0.9	3481.10	11,236.01	0.505089	0.564756
1	3867.89	10,446.19	0.469585	0.512191
1.1	4254.68	9,751.65	0.438363	0.462714
1.2	4641.47	9,011.82	0.405106	0.417245
1.3	5028.26	8,301.45	0.373173	0.376195
1.4	5415.05	7,637.89	0.343344	0.339575
1.5	5801.84	7,015.35	0.315359	0.307143
1.6	6188.63	6,426.35	0.288882	0.278527
1.7	6575.42	5,883.20	0.264466	0.25331
1.8	6962.20	5,393.08	0.242434	0.231076
1.9	7348.99	4,954.48	0.222717	0.211443
2	7735.78	4,556.74	0.204838	0.194065
2.1	8122.57	4,197.42	0.188685	0.178641
2.2	8509.36	3,881.28	0.174474	0.164909
2.3	8896.15	3,589.86	0.161374	0.152647
2.4	9282.94	3,329.38	0.149665	0.141662
2.5	9669.73	3,092.90	0.139034	0.131791
2.6	10056.52	2,882.77	0.129588	0.122893
2.7	10443.31	2,692.31	0.121027	0.114848
2.8	10830.10	2,517.88	0.113185	0.107554
2.9	11216.89	2,361.47	0.106155	0.100923
3	11603.67	2,217.35	0.099676	0.094878

FEM: Mild steel at 500 degrees C

Curve b

Section:	UKB 457 x 191 x 161	
f_y	275	N/mm²
E	210000	N/mm²
$k_{y,\theta}$	0.78	
$k_{E,\theta}$	0.6	

Section properties:

Depth of the section	h	492	mm
Width of the section	b	199.4	mm
Web thickness	t_w	18	mm
Flange thickness	t_f	32	mm
Root radius	r	10.2	mm
Depth between fillets	d	407.6	mm
Second moment of area	I_{zz}	42500000	mm^4
Radius of gyration	r_{zz}	45.5	mm
Area of section	A	20600	mm²

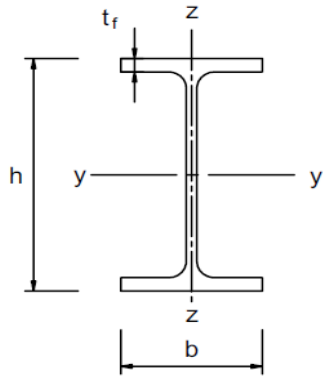

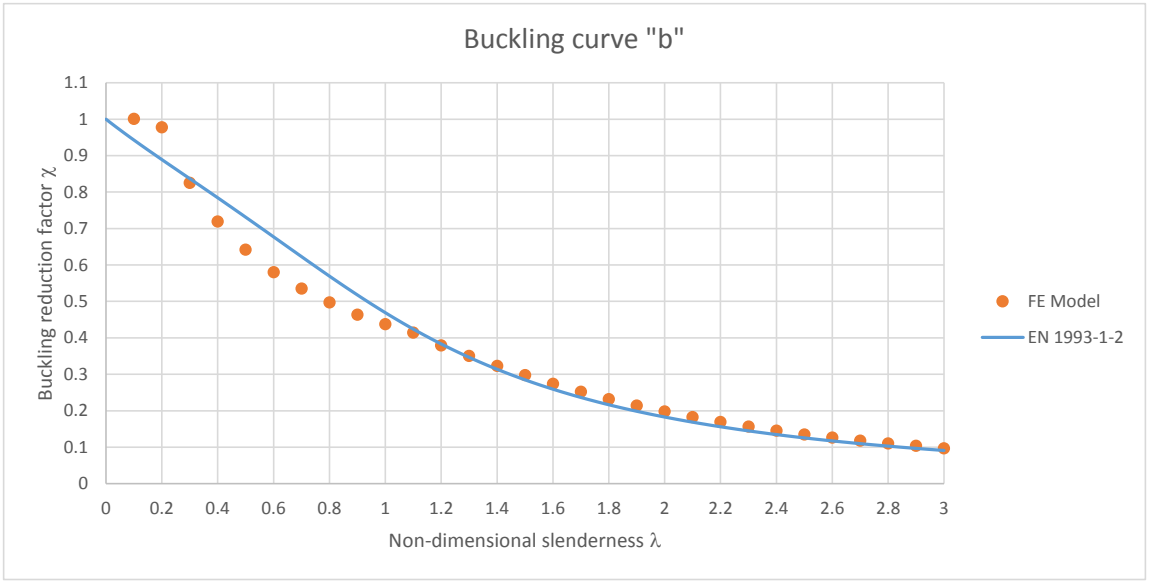

λ_θ	L_{cr} (mm)	N_b (kN)	χ_{FEM}	$\chi_{EN3-1-1}$
0.1	346.44	4,423.47	1.00108	0.94281
0.2	692.89	4,322.56	0.978243	0.8892
0.3	1039.33	3,646.90	0.825333	0.836859
0.4	1385.78	3,178.35	0.719294	0.784411
0.5	1732.22	2,838.37	0.642354	0.731187
0.6	2078.66	2,565.06	0.580502	0.677166
0.7	2425.11	2,366.20	0.535496	0.622903
0.8	2771.55	2,198.90	0.497635	0.569381
0.9	3117.99	2,050.91	0.464143	0.51776
1	3464.44	1,934.04	0.437695	0.469092
1.1	3810.88	1,831.54	0.414498	0.424132
1.2	4157.33	1,678.08	0.379768	0.383268
1.3	4503.77	1,550.86	0.350976	0.346569
1.4	4850.21	1,428.86	0.323366	0.31387
1.5	5196.66	1,316.40	0.297917	0.284872
1.6	5543.10	1,212.83	0.274477	0.259215
1.7	5889.55	1,115.88	0.252536	0.236522
1.8	6235.99	1,026.26	0.232253	0.216435
1.9	6582.43	946.41	0.214183	0.198625
2	6928.88	874.61	0.197934	0.182797
2.1	7275.32	808.43	0.182956	0.168694
2.2	7621.77	747.78	0.169231	0.156093
2.3	7968.21	692.99	0.156832	0.144802
2.4	8314.65	643.76	0.14569	0.134653
2.5	8661.10	598.07	0.13535	0.125506
2.6	9007.54	558.48	0.126391	0.117237
2.7	9353.98	522.42	0.118229	0.109741
2.8	9700.43	488.31	0.110511	0.102929
2.9	10046.87	459.01	0.103879	0.09672
3	10393.32	430.53	0.097433	0.091048

FEM: Mild steel at 500 degrees C

Curve c

Section:	UKC 356 x 406 x 634	
f_y	275	N/mm²
E	210000	N/mm²
$k_{y,\theta}$	0.78	
$k_{E,\theta}$	0.6	

Section properties:

Depth of the section	h	474.6	mm
Width of the section	b	424	mm
Web thickness	t_w	47.6	mm
Flange thickness	t_f	77	mm
Root radius	r	15.2	mm
Depth between fillets	d	290.2	mm
Second moment of area	I_{zz}	981000000	mm^4
Radius of gyration	r_{zz}	110	mm
Area of section	A	80800	mm²

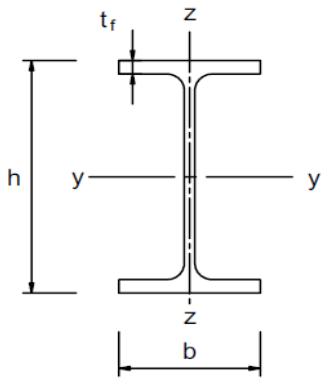

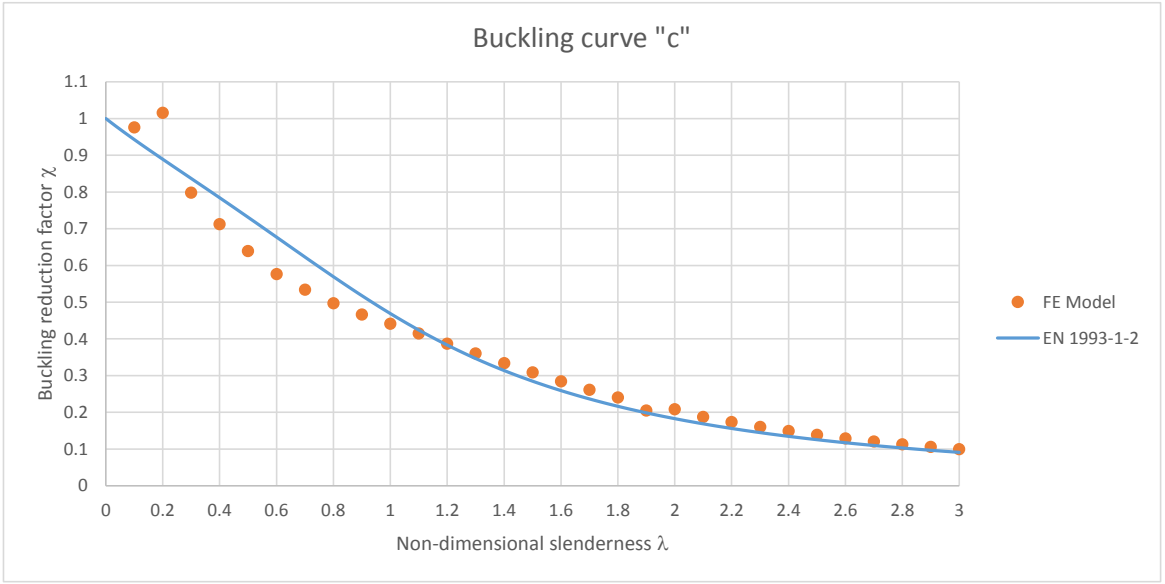

λ_θ	L_{cr} (mm)	N_b (kN)	χ_{FEM}	$\chi_{EN3-1-1}$
0.1	837.56	16,921.63	0.976345	0.94281
0.2	1675.11	17,608.14	1.015956	0.8892
0.3	2512.67	13,831.71	0.798063	0.836859
0.4	3350.23	12,346.38	0.712362	0.784411
0.5	4187.78	11,083.31	0.639486	0.731187
0.6	5025.34	9,997.85	0.576857	0.677166
0.7	5862.90	9,259.47	0.534254	0.622903
0.8	6700.45	8,622.41	0.497496	0.569381
0.9	7538.01	8,092.06	0.466896	0.51776
1	8375.57	7,648.71	0.441316	0.469092
1.1	9213.12	7,193.61	0.415057	0.424132
1.2	10050.68	6,713.05	0.38733	0.383268
1.3	10888.24	6,251.40	0.360694	0.346569
1.4	11725.79	5,792.04	0.33419	0.31387
1.5	12563.35	5,358.60	0.309181	0.284872
1.6	13400.91	4,932.28	0.284583	0.259215
1.7	14238.46	4,537.99	0.261833	0.236522
1.8	15076.02	4,175.78	0.240934	0.216435
1.9	15913.58	3,557.32	0.20525	0.198625
2	16751.13	3,616.23	0.20865	0.182797
2.1	17588.69	3,255.40	0.187831	0.168694
2.2	18426.25	3,008.79	0.173601	0.156093
2.3	19263.80	2,786.24	0.16076	0.144802
2.4	20101.36	2,587.00	0.149265	0.134653
2.5	20938.92	2,406.94	0.138876	0.125506
2.6	21776.47	2,243.95	0.129472	0.117237
2.7	22614.03	2,096.54	0.120966	0.109741
2.8	23451.59	1,962.35	0.113224	0.102929
2.9	24289.14	1,839.97	0.106163	0.09672
3	25126.70	1,728.64	0.099739	0.091048

FEM: Mild steel at 500 degrees C

Curve d

Section: UKC 356 x 406 x 634 *With a thicker flange of t_f = 110 mm

f_y	275	N/mm²
E	210000	N/mm²
$k_{y,\theta}$	0.78	
$k_{E,\theta}$	0.6	

Section properties:

Depth of the section	h	474.6	mm
Width of the section	b	424	mm
Web thickness	t_w	47.6	mm
Flange thickness	t_f	110	mm
Root radius	r	15.2	mm
Depth between fillets	d	224.2	mm
Second moment of area	I_{zz}	1400237632	mm^4
Radius of gyration	r_{zz}	115.152798	mm
Area of section	A	105597.286	mm²

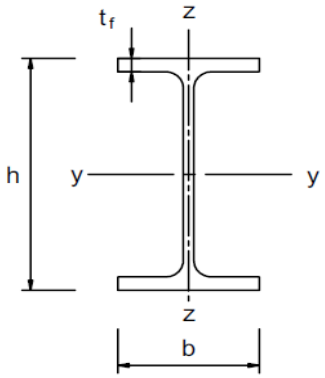

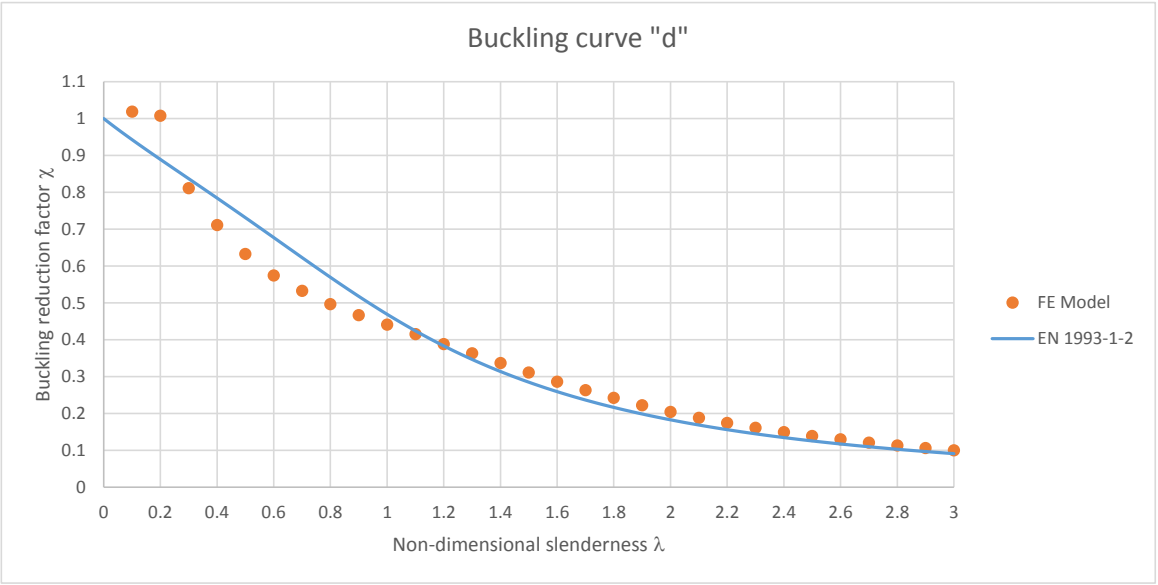

λ_θ	L_{cr} (mm)	N_b (kN)	χ_{FEM}	$\chi_{EN3-1-1}$
0.1	876.79	23,075.03	1.018737	0.94281
0.2	1753.58	22,817.66	1.007375	0.8892
0.3	2630.37	18,371.10	0.811064	0.836859
0.4	3507.16	16,109.22	0.711204	0.784411
0.5	4383.95	14,333.84	0.632823	0.731187
0.6	5260.74	13,007.01	0.574245	0.677166
0.7	6137.54	12,061.98	0.532523	0.622903
0.8	7014.33	11,243.46	0.496386	0.569381
0.9	7891.12	10,571.84	0.466735	0.51776
1	8767.91	9,992.11	0.441141	0.469092
1.1	9644.70	9,401.74	0.415076	0.424132
1.2	10521.49	8,797.86	0.388416	0.383268
1.3	11398.28	8,227.89	0.363253	0.346569
1.4	12275.07	7,626.08	0.336683	0.31387
1.5	13151.86	7,045.63	0.311057	0.284872
1.6	14028.65	6,478.13	0.286002	0.259215
1.7	14905.44	5,960.43	0.263147	0.236522
1.8	15782.23	5,482.89	0.242063	0.216435
1.9	16659.03	5,032.92	0.222198	0.198625
2	17535.82	4,631.20	0.204462	0.182797
2.1	18412.61	4,268.21	0.188437	0.168694
2.2	19289.40	3,943.77	0.174113	0.156093
2.3	20166.19	3,652.25	0.161243	0.144802
2.4	21042.98	3,389.54	0.149644	0.134653
2.5	21919.77	3,152.17	0.139165	0.125506
2.6	22796.56	2,937.87	0.129704	0.117237
2.7	23673.35	2,743.67	0.12113	0.109741
2.8	24550.14	2,567.90	0.11337	0.102929
2.9	25426.93	2,407.32	0.10628	0.09672
3	26303.72	2,261.45	0.09984	0.091048

FEM: Mild steel at 700 degrees C

Curve a0

Section:	UKB 457 x 191 x 161	
f_y	460	N/mm²
E	210000	N/mm²
$k_{y,\theta}$	0.23	
$k_{E,\theta}$	0.13	

Section properties:

Depth of the section	h	492	mm
Width of the section	b	199.4	mm
Web thickness	t_w	18	mm
Flange thickness	t_f	32	mm
Root radius	r	10.2	mm
Depth between fillets	d	407.6	mm
Second moment of area	I_{zz}	42500000	mm^4
Radius of gyration	r_{zz}	45.5	mm
Area of section	A	20600	mm²

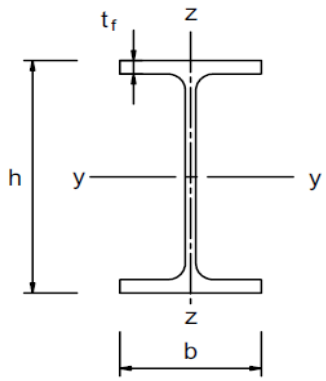

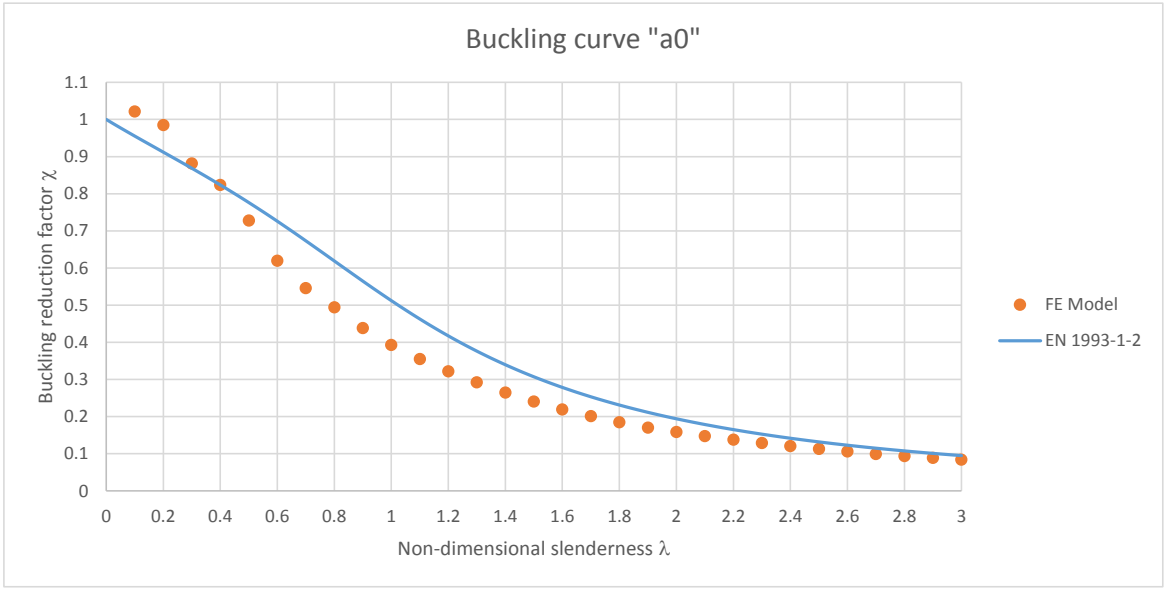

λ_θ	L_{cr} (mm)	N_b (kN)	χ_{FEM}	$\chi_{EN3-1-1}$
0.1	229.61	2,226.94	1.021774	0.955195
0.2	459.23	2,147.60	0.985375	0.912046
0.3	688.84	1,921.42	0.881598	0.868661
0.4	918.46	1,796.23	0.824154	0.823693
0.5	1148.07	1,586.85	0.728088	0.776259
0.6	1377.69	1,350.46	0.619625	0.726011
0.7	1607.30	1,189.64	0.545835	0.673258
0.8	1836.92	1,077.89	0.494565	0.618999
0.9	2066.53	955.82	0.438554	0.564756
1	2296.15	856.24	0.392863	0.512191
1.1	2525.76	773.66	0.354976	0.462714
1.2	2755.38	701.35	0.321796	0.417245
1.3	2984.99	636.63	0.292103	0.376195
1.4	3214.61	577.66	0.265047	0.339575
1.5	3444.22	525.35	0.241043	0.307143
1.6	3673.84	478.74	0.219658	0.278527
1.7	3903.45	438.40	0.201147	0.25331
1.8	4133.07	403.01	0.184909	0.231076
1.9	4362.68	372.19	0.17077	0.211443
2	4592.29	346.64	0.159046	0.194065
2.1	4821.91	322.25	0.147854	0.178641
2.2	5051.52	300.10	0.137692	0.164909
2.3	5281.14	280.72	0.128803	0.152647
2.4	5510.75	263.10	0.120719	0.141662
2.5	5740.37	246.28	0.113001	0.131791
2.6	5969.98	231.27	0.106112	0.122893
2.7	6199.60	217.11	0.099618	0.114848
2.8	6429.21	204.96	0.094043	0.107554
2.9	6658.83	193.60	0.088828	0.100923
3	6888.44	183.48	0.084184	0.094878

FEM: Mild steel at 700 degrees C

Curve a

Section:	UKB 1016 x 305 x 487	
f_y	460	N/mm²
E	210000	N/mm²
$k_{y,\theta}$	0.23	
$k_{E,\theta}$	0.13	

Section properties:

Depth of the section	h	1036.3	mm
Width of the section	b	308.5	mm
Web thickness	t_w	30	mm
Flange thickness	t_f	54.1	mm
Root radius	r	30	mm
Depth between fillets	d	868.1	mm
Second moment of area	I_{zz}	267000000	mm^4
Radius of gyration	r_{zz}	65.7	mm
Area of section	A	62000	mm²

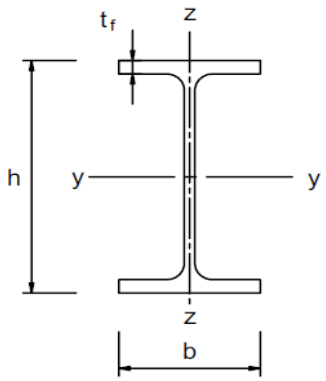

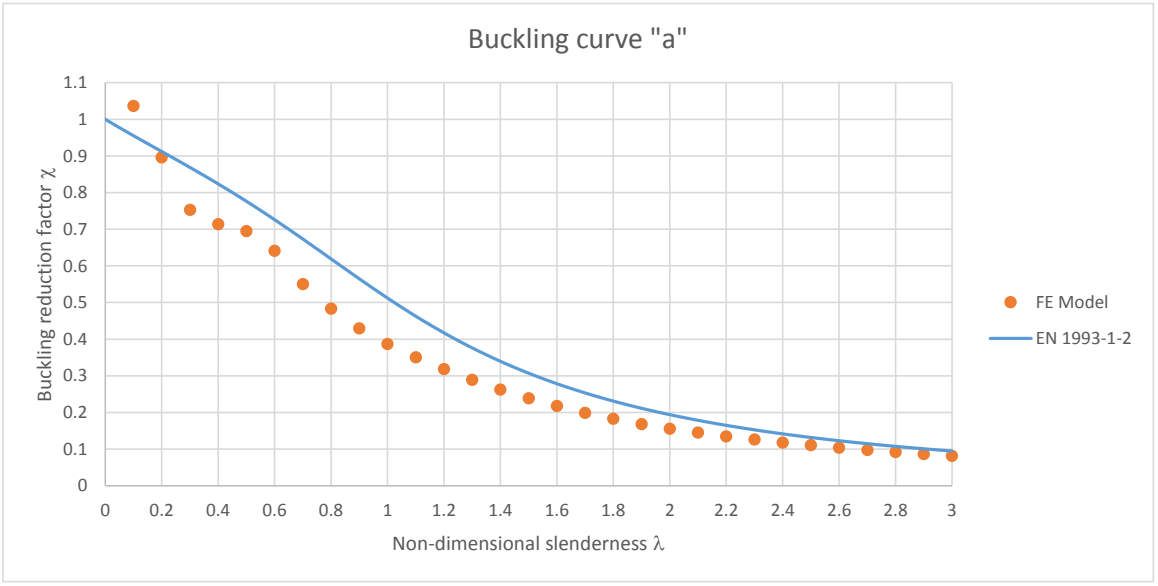

λ_θ	L_{cr} (mm)	N_b (kN)	χ_{FEM}	$\chi_{EN3-1-1}$
0.1	331.55	6,802.95	1.037098	0.955195
0.2	663.11	5,881.62	0.896643	0.912046
0.3	994.66	4,941.27	0.753289	0.868661
0.4	1326.21	4,685.17	0.714247	0.823693
0.5	1657.77	4,560.24	0.695201	0.776259
0.6	1989.32	4,205.22	0.641079	0.726011
0.7	2320.88	3,612.37	0.550699	0.673258
0.8	2652.43	3,173.07	0.483729	0.618999
0.9	2983.98	2,820.13	0.429924	0.564756
1	3315.54	2,541.76	0.387486	0.512191
1.1	3647.09	2,302.51	0.351014	0.462714
1.2	3978.64	2,091.18	0.318796	0.417245
1.3	4310.20	1,898.12	0.289365	0.376195
1.4	4641.75	1,722.75	0.262631	0.339575
1.5	4973.30	1,567.41	0.23895	0.307143
1.6	5304.86	1,429.52	0.217927	0.278527
1.7	5636.41	1,306.87	0.19923	0.25331
1.8	5967.96	1,200.04	0.182944	0.231076
1.9	6299.52	1,106.17	0.168634	0.211443
2	6631.07	1,024.95	0.156252	0.194065
2.1	6962.63	952.02	0.145133	0.178641
2.2	7294.18	887.40	0.135283	0.164909
2.3	7625.73	828.85	0.126357	0.152647
2.4	7957.29	776.33	0.11835	0.141662
2.5	8288.84	728.00	0.110983	0.131791
2.6	8620.39	683.01	0.104124	0.122893
2.7	8951.95	641.38	0.097778	0.114848
2.8	9283.50	604.14	0.0921	0.107554
2.9	9615.05	570.50	0.086971	0.100923
3	9946.61	539.09	0.082183	0.094878

FEM: Mild steel at 700 degrees C

Curve b

Section:	UKB 457 x 191 x 161	
f_y	275	N/mm²
E	210000	N/mm²
$k_{y,\theta}$	0.23	
$k_{E,\theta}$	0.13	

Section properties:

Depth of the section	h	492	mm
Width of the section	b	199.4	mm
Web thickness	t_w	18	mm
Flange thickness	t_f	32	mm
Root radius	r	10.2	mm
Depth between fillets	d	407.6	mm
Second moment of area	I_{zz}	42500000	mm^4
Radius of gyration	r_{zz}	45.5	mm
Area of section	A	20600	mm²

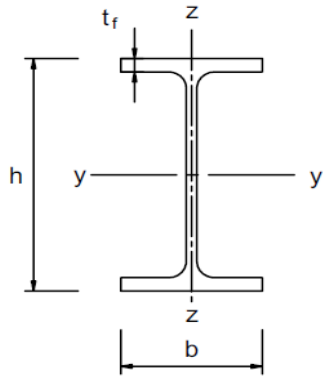

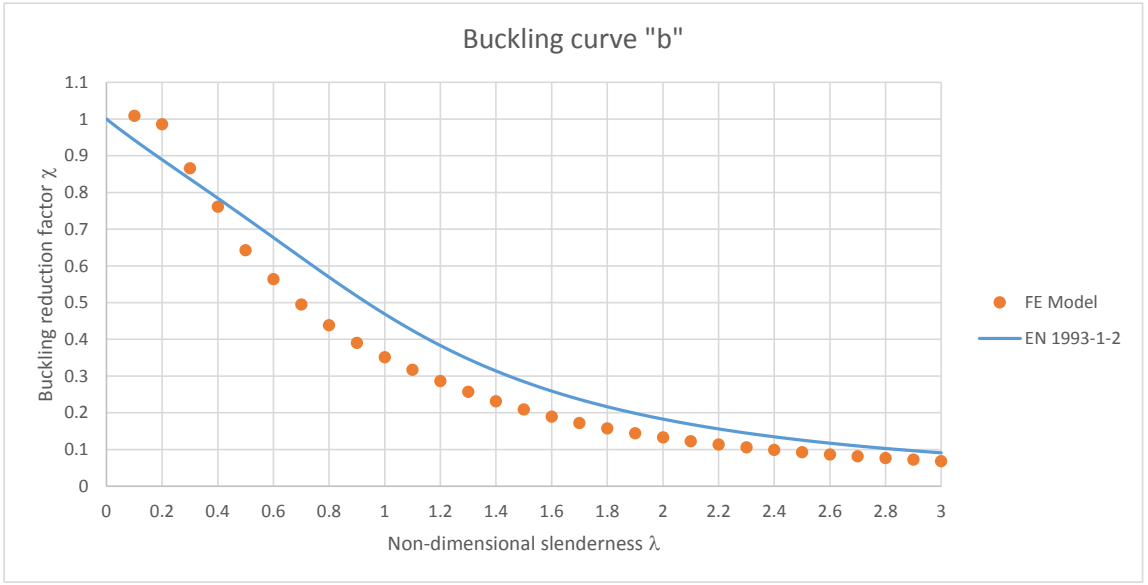

λ_θ	L_{cr} (mm)	N_b (kN)	χ_{FEM}	$\chi_{EN3-1-1}$
0.1	296.97	1,314.28	1.008693	0.94281
0.2	593.94	1,284.57	0.985892	0.8892
0.3	890.91	1,128.50	0.866112	0.836859
0.4	1187.88	992.19	0.761498	0.784411
0.5	1484.85	837.94	0.643113	0.731187
0.6	1781.82	734.83	0.563977	0.677166
0.7	2078.79	645.54	0.495445	0.622903
0.8	2375.76	571.23	0.438412	0.569381
0.9	2672.73	508.45	0.39023	0.51776
1	2969.70	458.36	0.351783	0.469092
1.1	3266.67	413.44	0.317312	0.424132
1.2	3563.64	373.21	0.286432	0.383268
1.3	3860.61	335.38	0.257398	0.346569
1.4	4157.58	301.70	0.23155	0.31387
1.5	4454.55	272.87	0.209422	0.284872
1.6	4751.52	247.00	0.189569	0.259215
1.7	5048.49	224.83	0.172558	0.236522
1.8	5345.46	205.09	0.157407	0.216435
1.9	5642.43	188.49	0.144664	0.198625
2	5939.40	173.45	0.133122	0.182797
2.1	6236.37	160.17	0.122925	0.168694
2.2	6533.34	148.34	0.113848	0.156093
2.3	6830.31	138.00	0.105914	0.144802
2.4	7127.28	128.86	0.098902	0.134653
2.5	7424.25	120.65	0.092595	0.125506
2.6	7721.22	113.14	0.086835	0.117237
2.7	8018.19	106.33	0.081608	0.109741
2.8	8315.16	100.07	0.076799	0.102929
2.9	8612.13	94.30	0.072376	0.09672
3	8909.09	89.02	0.068322	0.091048

FEM: Mild steel at 700 degrees C

Curve c

Section:	UKC 356 x 406 x 634	
f_y	275	N/mm²
E	210000	N/mm²
$k_{y,\theta}$	0.23	
$k_{E,\theta}$	0.13	

Section properties:

Depth of the section	h	474.6	mm
Width of the section	b	424	mm
Web thickness	t_w	47.6	mm
Flange thickness	t_f	77	mm
Root radius	r	15.2	mm
Depth between fillets	d	290.2	mm
Second moment of area	I_{zz}	981000000	mm^4
Radius of gyration	r_{zz}	110	mm
Area of section	A	80800	mm²

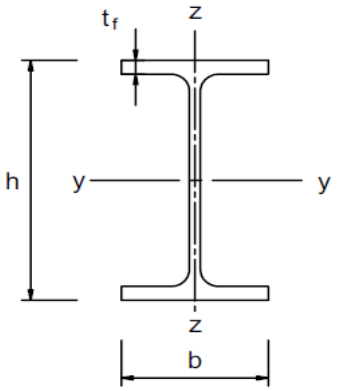

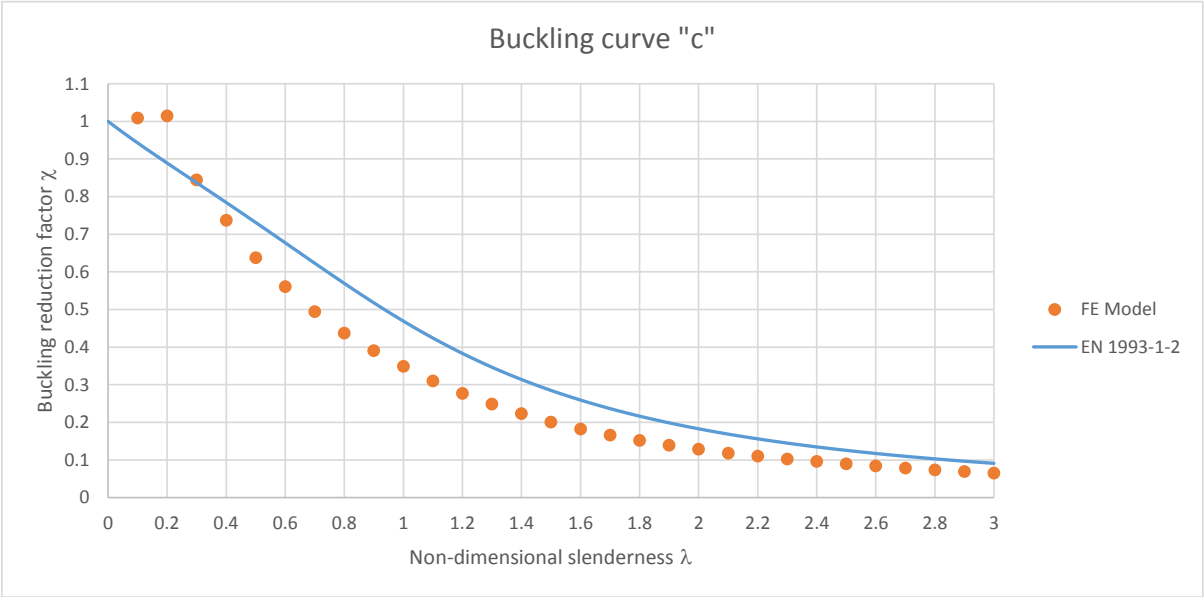

λ_θ	L_{cr} (mm)	N_b (kN)	χ_{FEM}	$\chi_{EN3-1-1}$
0.1	717.95	5,157.03	1.009086	0.94281
0.2	1435.90	5,186.37	1.014825	0.8892
0.3	2153.85	4,316.79	0.844674	0.836859
0.4	2871.80	3,766.90	0.737076	0.784411
0.5	3589.75	3,259.52	0.637796	0.731187
0.6	4307.69	2,865.42	0.560681	0.677166
0.7	5025.64	2,525.10	0.494091	0.622903
0.8	5743.59	2,234.25	0.43718	0.569381
0.9	6461.54	1,995.64	0.39049	0.51776
1	7179.49	1,782.23	0.348732	0.469092
1.1	7897.44	1,585.97	0.31033	0.424132
1.2	8615.39	1,415.23	0.276921	0.383268
1.3	9333.34	1,269.24	0.248354	0.346569
1.4	10051.29	1,139.53	0.222973	0.31387
1.5	10769.24	1,026.37	0.200832	0.284872
1.6	11487.18	930.48	0.182069	0.259215
1.7	12205.13	848.27	0.165982	0.236522
1.8	12923.08	776.38	0.151915	0.216435
1.9	13641.03	712.90	0.139494	0.198625
2	14358.98	656.52	0.128463	0.182797
2.1	15076.93	604.71	0.118324	0.168694
2.2	15794.88	563.47	0.110255	0.156093
2.3	16512.83	524.66	0.102662	0.144802
2.4	17230.78	489.87	0.095853	0.134653
2.5	17948.73	458.39	0.089693	0.125506
2.6	18666.67	429.55	0.084052	0.117237
2.7	19384.62	402.45	0.078747	0.109741
2.8	20102.57	377.22	0.073811	0.102929
2.9	20820.52	354.22	0.069311	0.09672
3	21538.47	332.99	0.065157	0.091048

FEM: Mild steel at 700 degrees C

Curve d

Section: UKC 356 x 406 x 634 *With a thicker flange of t_f = 110 mm

f_y	275	N/mm²
E	210000	N/mm²
$k_{y,\theta}$	0.23	
$k_{E,\theta}$	0.13	

Section properties:

Depth of the section	h	474.6	mm
Width of the section	b	424	mm
Web thickness	t_w	47.6	mm
Flange thickness	t_f	110	mm
Root radius	r	15.2	mm
Depth between fillets	d	224.2	mm
Second moment of area	I_{zz}	1400237632	mm^4
Radius of gyration	r_{zz}	115.152798	mm
Area of section	A	105597.286	mm²

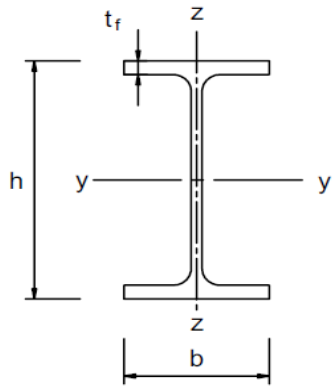

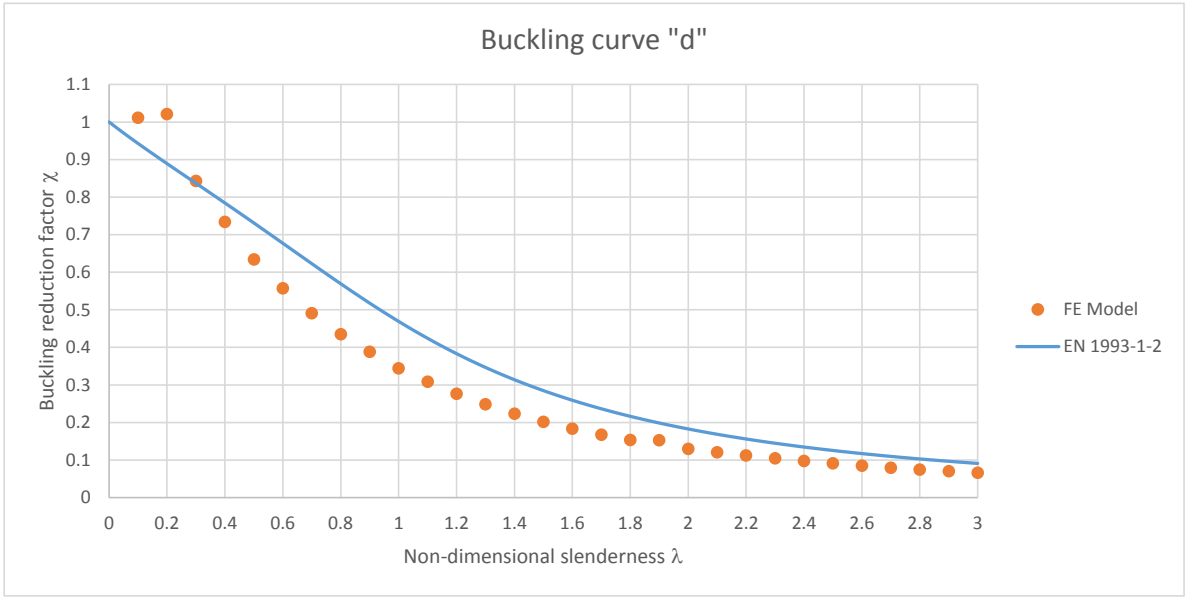

λ_θ	L_{cr} (mm)	N_b (kN)	χ_{FEM}	$\chi_{EN3-1-1}$
0.1	751.58	6,757.55	1.011756	0.94281
0.2	1503.16	6,820.49	1.02118	0.8892
0.3	2254.74	5,630.78	0.843053	0.836859
0.4	3006.32	4,903.07	0.7341	0.784411
0.5	3757.90	4,234.65	0.634022	0.731187
0.6	4509.48	3,723.32	0.557464	0.677166
0.7	5261.06	3,282.61	0.49148	0.622903
0.8	6012.64	2,905.87	0.435074	0.569381
0.9	6764.22	2,596.70	0.388784	0.51776
1	7515.80	2,302.40	0.344721	0.469092
1.1	8267.38	2,062.81	0.308849	0.424132
1.2	9018.96	1,847.63	0.276631	0.383268
1.3	9770.54	1,659.90	0.248524	0.346569
1.4	10522.13	1,492.32	0.223433	0.31387
1.5	11273.71	1,348.49	0.2019	0.284872
1.6	12025.29	1,225.74	0.18352	0.259215
1.7	12776.87	1,119.03	0.167544	0.236522
1.8	13528.45	1,025.81	0.153587	0.216435
1.9	14280.03	1,021.17	0.152892	0.198625
2	15031.61	869.90	0.130243	0.182797
2.1	15783.19	806.20	0.120706	0.168694
2.2	16534.77	749.67	0.112242	0.156093
2.3	17286.35	698.54	0.104587	0.144802
2.4	18037.93	652.24	0.097655	0.134653
2.5	18789.51	609.96	0.091325	0.125506
2.6	19541.09	570.46	0.085411	0.117237
2.7	20292.67	533.92	0.07994	0.109741
2.8	21044.25	500.88	0.074992	0.102929
2.9	21795.83	470.42	0.070432	0.09672
3	22547.41	442.55	0.06626	0.091048

FEM: Mild steel at 700 degrees C

Curve a

Section:	UKB 1016 x 305 x 487	
f_y	460	N/mm²
E	210000	N/mm²
$k_{y,\theta}$	0.23	
$k_{E,\theta}$	0.13	

Section properties:

Depth of the section	h	1036.3	mm
Width of the section	b	308.5	mm
Web thickness	t_w	30	mm
Flange thickness	t_f	54.1	mm
Root radius	r	30	mm
Depth between fillets	d	868.1	mm
Second moment of area	I_{zz}	267000000	mm^4
Radius of gyration	r_{zz}	65.7	mm
Area of section	A	62000	mm²

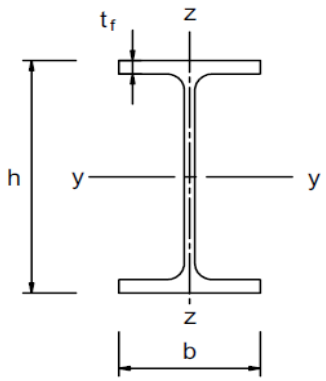

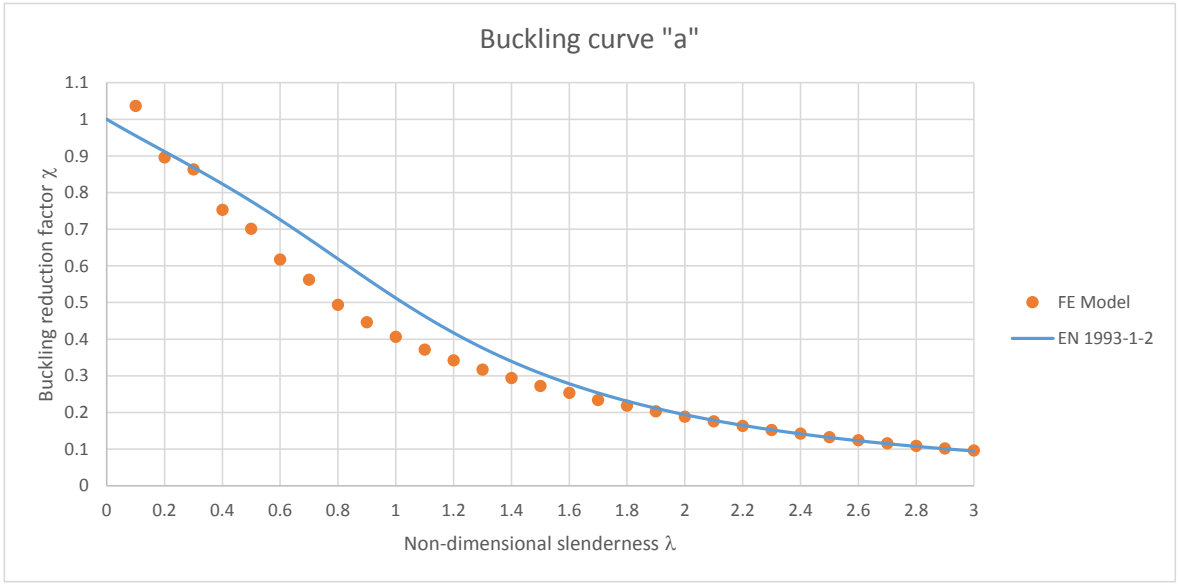

λ_θ	L_{cr} (mm)	N_b (kN)	χ_{FEM}	$\chi_{EN3-1-1}$
0.1	331.55	6,802.95	1.037098	0.955195
0.2	663.11	5,881.62	0.896643	0.912046
0.3	994.66	5,666.00	0.863772	0.868661
0.4	1326.21	4,940.00	0.753095	0.823693
0.5	1657.77	4,602.62	0.701662	0.776259
0.6	1989.32	4,051.60	0.61766	0.726011
0.7	2320.88	3,687.85	0.562206	0.673258
0.8	2652.43	3,241.46	0.494156	0.618999
0.9	2983.98	2,931.26	0.446866	0.564756
1	3315.54	2,668.41	0.406795	0.512191
1.1	3647.09	2,440.06	0.371983	0.462714
1.2	3978.64	2,245.07	0.342258	0.417245
1.3	4310.20	2,081.29	0.317289	0.376195
1.4	4641.75	1,931.63	0.294475	0.339575
1.5	4973.30	1,787.02	0.272428	0.307143
1.6	5304.86	1,664.37	0.25373	0.278527
1.7	5636.41	1,536.89	0.234297	0.25331
1.8	5967.96	1,435.54	0.218846	0.231076
1.9	6299.52	1,332.29	0.203106	0.211443
2	6631.07	1,240.39	0.189095	0.194065
2.1	6962.63	1,154.57	0.176012	0.178641
2.2	7294.18	1,074.81	0.163853	0.164909
2.3	7625.73	1,001.57	0.152687	0.152647
2.4	7957.29	935.13	0.142559	0.141662
2.5	8288.84	871.72	0.132893	0.131791
2.6	8620.39	814.92	0.124234	0.122893
2.7	8951.95	762.77	0.116283	0.114848
2.8	9283.50	715.54	0.109083	0.107554
2.9	9615.05	672.27	0.102486	0.100923
3	9946.61	632.40	0.096408	0.094878

FEM: Mild steel at 700 degrees C

Curve a

Section:	UKB 1016 x 305 x 487	
f_y	460	N/mm²
E	210000	N/mm²
$k_{y,\theta}$	0.23	
$k_{E,\theta}$	0.13	

Section properties:

Depth of the section	h	1036.3	mm
Width of the section	b	308.5	mm
Web thickness	t_w	30	mm
Flange thickness	t_f	54.1	mm
Root radius	r	30	mm
Depth between fillets	d	868.1	mm
Second moment of area	I_{zz}	267000000	mm^4
Radius of gyration	r_{zz}	65.7	mm
Area of section	A	62000	mm²

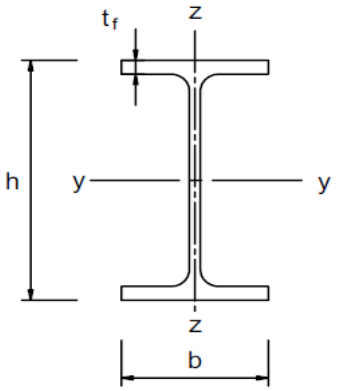

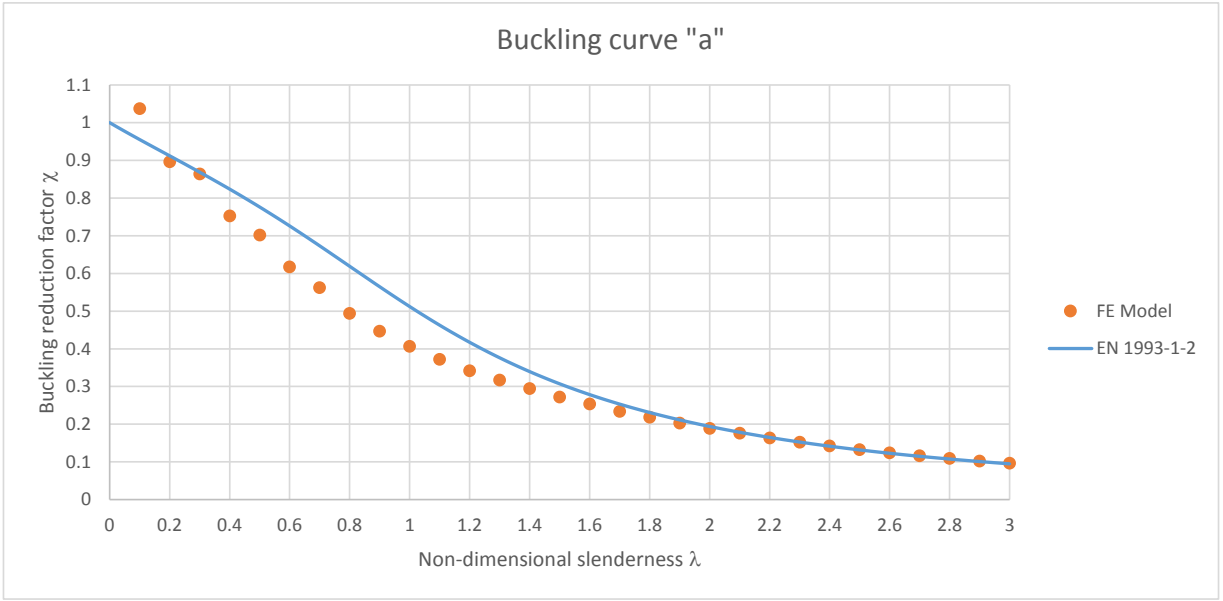

λ_θ	L_{cr} (mm)	N_b (kN)	χ_{FEM}	$\chi_{EN3-1-1}$
0.1	331.55	6,802.95	1.037098	0.955195
0.2	663.11	5,881.62	0.896643	0.912046
0.3	994.66	5,666.00	0.863772	0.868661
0.4	1326.21	4,940.00	0.753095	0.823693
0.5	1657.77	4,602.62	0.701662	0.776259
0.6	1989.32	4,051.60	0.61766	0.726011
0.7	2320.88	3,687.85	0.562206	0.673258
0.8	2652.43	3,241.46	0.494156	0.618999
0.9	2983.98	2,931.26	0.446866	0.564756
1	3315.54	2,668.41	0.406795	0.512191
1.1	3647.09	2,440.06	0.371983	0.462714
1.2	3978.64	2,245.07	0.342258	0.417245
1.3	4310.20	2,081.29	0.317289	0.376195
1.4	4641.75	1,931.63	0.294475	0.339575
1.5	4973.30	1,787.02	0.272428	0.307143
1.6	5304.86	1,664.37	0.25373	0.278527
1.7	5636.41	1,536.89	0.234297	0.25331
1.8	5967.96	1,435.54	0.218846	0.231076
1.9	6299.52	1,332.29	0.203106	0.211443
2	6631.07	1,240.39	0.189095	0.194065
2.1	6962.63	1,154.57	0.176012	0.178641
2.2	7294.18	1,074.81	0.163853	0.164909
2.3	7625.73	1,001.57	0.152687	0.152647
2.4	7957.29	935.13	0.142559	0.141662
2.5	8288.84	871.72	0.132893	0.131791
2.6	8620.39	814.92	0.124234	0.122893
2.7	8951.95	762.77	0.116283	0.114848
2.8	9283.50	715.54	0.109083	0.107554
2.9	9615.05	672.27	0.102486	0.100923
3	9946.61	632.40	0.096408	0.094878

FEM: Mild steel at 700 degrees C

Curve b

Section:	UKB 457 x 191 x 161		*Suitable for change to fy = 265 Mpa
f_y	275	N/mm²	
E	210000	N/mm²	
$k_{y,\theta}$	0.23		
$k_{E,\theta}$	0.13		

Section properties:

Depth of the section	h	492	mm
Width of the section	b	199.4	mm
Web thickness	t_w	18	mm
Flange thickness	t_f	32	mm
Root radius	r	10.2	mm
Depth between fillets	d	407.6	mm
Second moment of area	I_{zz}	42500000	mm^4
Radius of gyration	r_{zz}	45.5	mm
Area of section	A	20600	mm²

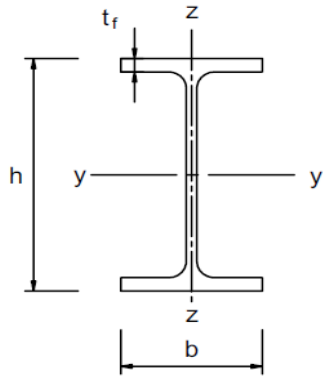

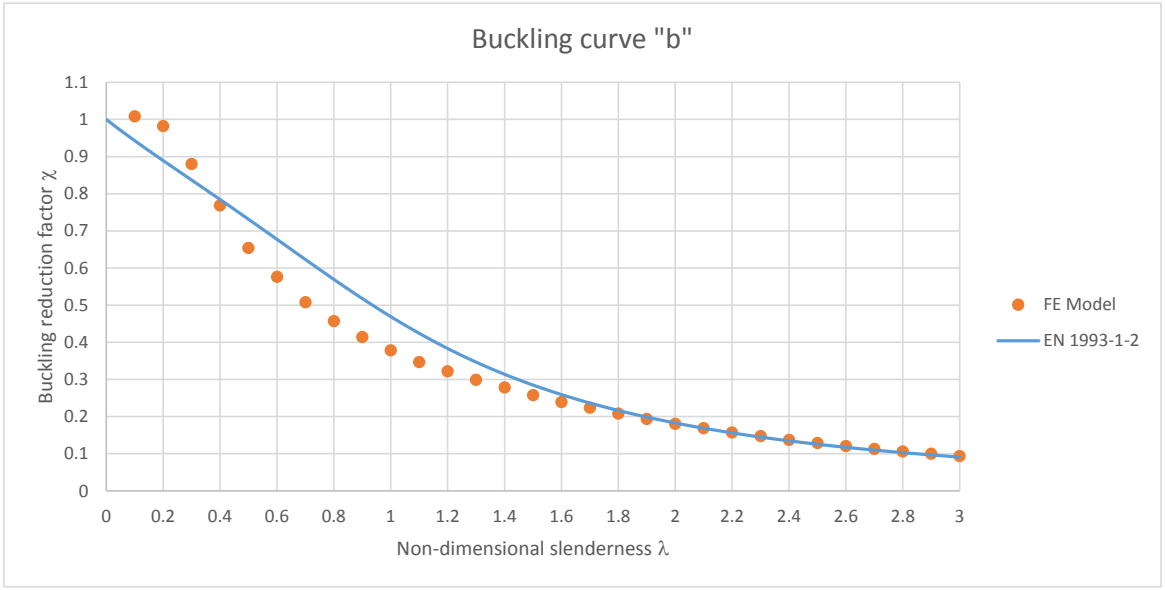

λ_θ	L_{cr} (mm)	N_b (kN)	χ_{FEM}	$\chi_{EN3-1-1}$
0.1	296.97	1,314.28	1.008693	0.94281
0.2	593.94	1,279.77	0.982212	0.8892
0.3	890.91	1,146.66	0.880049	0.836859
0.4	1187.88	1,001.51	0.768651	0.784411
0.5	1484.85	852.18	0.654042	0.731187
0.6	1781.82	751.34	0.576645	0.677166
0.7	2078.79	662.07	0.50813	0.622903
0.8	2375.76	595.34	0.45692	0.569381
0.9	2672.73	539.72	0.41423	0.51776
1	2969.70	492.90	0.378293	0.469092
1.1	3266.67	452.20	0.347058	0.424132
1.2	3563.64	419.43	0.321906	0.383268
1.3	3860.61	390.22	0.299486	0.346569
1.4	4157.58	363.24	0.278781	0.31387
1.5	4454.55	336.44	0.258215	0.284872
1.6	4751.52	311.67	0.239207	0.259215
1.7	5048.49	291.71	0.223888	0.236522
1.8	5345.46	271.74	0.208557	0.216435
1.9	5642.43	252.41	0.193718	0.198625
2	5939.40	235.85	0.181011	0.182797
2.1	6236.37	220.04	0.168879	0.168694
2.2	6533.34	205.25	0.157525	0.156093
2.3	6830.31	192.06	0.147404	0.144802
2.4	7127.28	179.24	0.137567	0.134653
2.5	7424.25	167.75	0.128744	0.125506
2.6	7721.22	157.33	0.120748	0.117237
2.7	8018.19	147.53	0.113229	0.109741
2.8	8315.16	138.54	0.106325	0.102929
2.9	8612.13	130.29	0.099997	0.09672
3	8909.09	122.57	0.094074	0.091048

FEM: Mild steel at 700 degrees C

Curve c

Section:	UKC 356 x 406 x 634	
f_y	275	N/mm²
E	210000	N/mm²
$k_{y,\theta}$	0.23	
$k_{E,\theta}$	0.13	

Section properties:

Depth of the section	h	474.6	mm
Width of the section	b	424	mm
Web thickness	t_w	47.6	mm
Flange thickness	t_f	77	mm
Root radius	r	15.2	mm
Depth between fillets	d	290.2	mm
Second moment of area	I_{zz}	981000000	mm^4
Radius of gyration	r_{zz}	110	mm
Area of section	A	80800	mm²

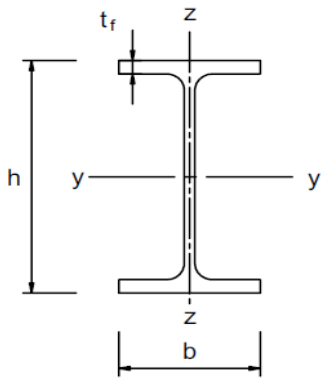

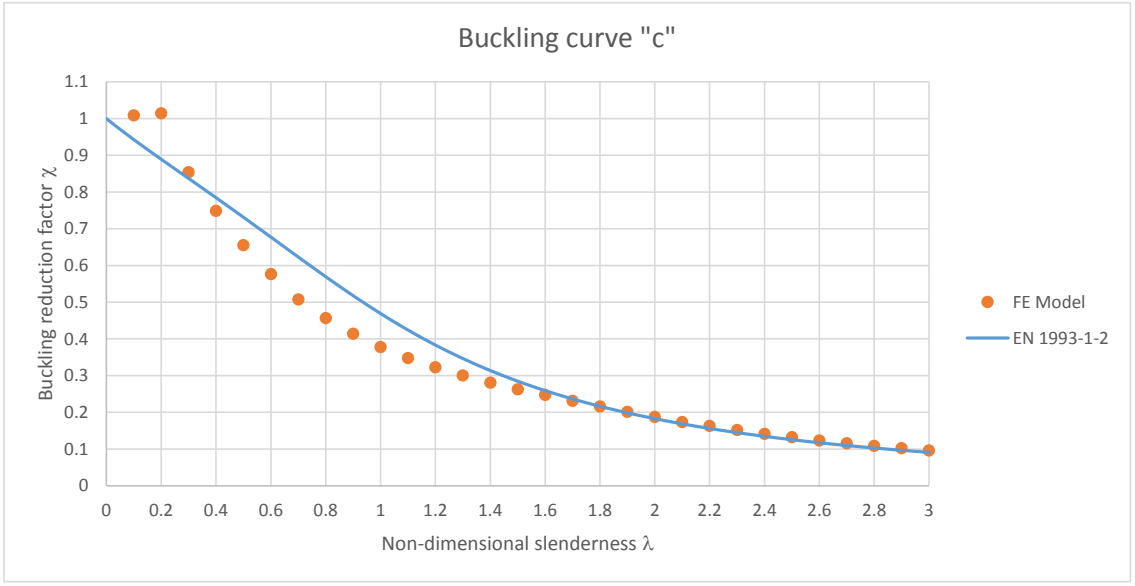

λ_θ	L_{cr} (mm)	N_b (kN)	χ_{FEM}	$\chi_{EN3-1-1}$
0.1	717.95	5,157.03	1.009086	0.94281
0.2	1435.90	5,186.37	1.014825	0.8892
0.3	2153.85	4,365.62	0.854228	0.836859
0.4	2871.80	3,826.94	0.748824	0.784411
0.5	3589.75	3,348.57	0.65522	0.731187
0.6	4307.69	2,947.32	0.576708	0.677166
0.7	5025.64	2,595.86	0.507937	0.622903
0.8	5743.59	2,333.16	0.456534	0.569381
0.9	6461.54	2,117.25	0.414286	0.51776
1	7179.49	1,932.20	0.378078	0.469092
1.1	7897.44	1,779.59	0.348216	0.424132
1.2	8615.39	1,649.85	0.32283	0.383268
1.3	9333.34	1,537.61	0.300867	0.346569
1.4	10051.29	1,436.25	0.281034	0.31387
1.5	10769.24	1,345.58	0.263292	0.284872
1.6	11487.18	1,264.44	0.247416	0.259215
1.7	12205.13	1,183.92	0.231659	0.236522
1.8	12923.08	1,106.05	0.216423	0.216435
1.9	13641.03	1,031.74	0.201882	0.198625
2	14358.98	960.75	0.187992	0.182797
2.1	15076.93	886.96	0.173554	0.168694
2.2	15794.88	833.11	0.163017	0.156093
2.3	16512.83	776.65	0.151969	0.144802
2.4	17230.78	723.98	0.141662	0.134653
2.5	17948.73	676.67	0.132405	0.125506
2.6	18666.67	632.92	0.123845	0.117237
2.7	19384.62	593.25	0.116082	0.109741
2.8	20102.57	556.67	0.108925	0.102929
2.9	20820.52	523.53	0.10244	0.09672
3	21538.47	492.80	0.096426	0.091048

FEM: Mild steel at 700 degrees C

Curve d

Section: UKC 356 x 406 x 634 *With a thicker flange of t_f = 110 mm

f_y	275	N/mm²
E	210000	N/mm²
$k_{y,\theta}$	0.23	
$k_{E,\theta}$	0.13	

Section properties:

Depth of the section	h	474.6	mm
Width of the section	b	424	mm
Web thickness	t_w	47.6	mm
Flange thickness	t_f	110	mm
Root radius	r	15.2	mm
Depth between fillets	d	224.2	mm
Second moment of area	I_{zz}	1400237632	mm^4
Radius of gyration	r_{zz}	115.152798	mm
Area of section	A	105597.286	mm²

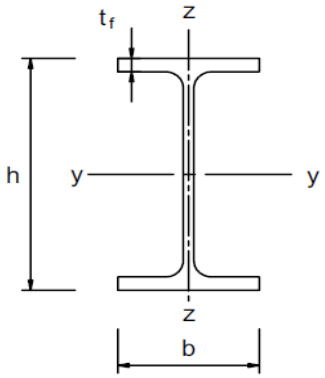

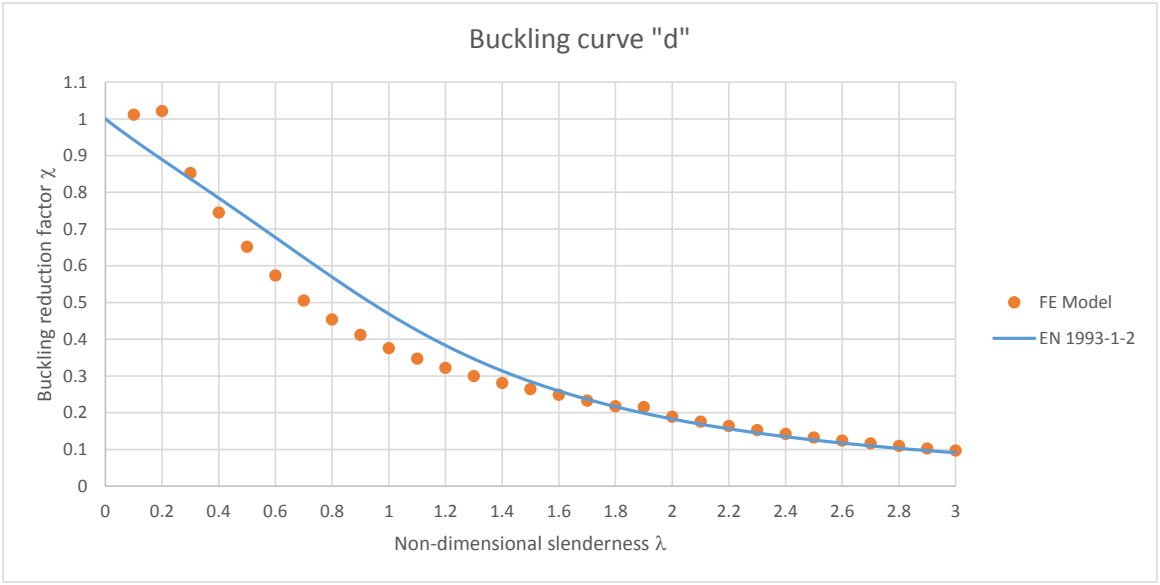

λ_θ	L_{cr} (mm)	N_b (kN)	χ_{FEM}	$\chi_{EN3-1-1}$
0.1	751.58	6,757.55	1.011756	0.94281
0.2	1503.16	6,820.49	1.02118	0.8892
0.3	2254.74	5,693.44	0.852436	0.836859
0.4	3006.32	4,978.88	0.745449	0.784411
0.5	3757.90	4,353.12	0.651759	0.731187
0.6	4509.48	3,831.48	0.573658	0.677166
0.7	5261.06	3,374.86	0.505291	0.622903
0.8	6012.64	3,031.91	0.453944	0.569381
0.9	6764.22	2,751.47	0.411957	0.51776
1	7515.80	2,510.63	0.375898	0.469092
1.1	8267.38	2,317.37	0.346962	0.424132
1.2	9018.96	2,149.34	0.321804	0.383268
1.3	9770.54	2,002.64	0.299841	0.346569
1.4	10522.13	1,876.31	0.280925	0.31387
1.5	11273.71	1,765.47	0.264331	0.284872
1.6	12025.29	1,662.59	0.248927	0.259215
1.7	12776.87	1,556.82	0.233091	0.236522
1.8	13528.45	1,454.51	0.217773	0.216435
1.9	14280.03	1,441.12	0.215767	0.198625
2	15031.61	1,262.51	0.189026	0.182797
2.1	15783.19	1,173.31	0.175671	0.168694
2.2	16534.77	1,093.46	0.163716	0.156093
2.3	17286.35	1,019.04	0.152573	0.144802
2.4	18037.93	949.57	0.142171	0.134653
2.5	18789.51	886.89	0.132787	0.125506
2.6	19541.09	829.94	0.12426	0.117237
2.7	20292.67	777.41	0.116396	0.109741
2.8	21044.25	729.45	0.109215	0.102929
2.9	21795.83	685.73	0.102669	0.09672
3	22547.41	645.50	0.096646	0.091048

Appendix C

Results for columns with thermal gradients

FEM: Strong axis gradient - maximum gradient

Curve a0

Section:	UKB 457 x 191 x 161	
f_y	460	N/mm²
E	210000	N/mm²
Av. Temp	452.2	
$k_{y,\theta}$	0.88516	
$k_{E,\theta}$	0.6478	

Section properties:

Depth of the section	h	492	mm
Width of the section	b	199.4	mm
Web thickness	t_w	18	mm
Flange thickness	t_f	32	mm
Root radius	r	10.2	mm
Depth between fillets	d	407.6	mm
Second moment of area	I_{zz}	42500000	mm^4
Radius of gyration	r_{zz}	45.5	mm
Area of section	A	20600	mm²

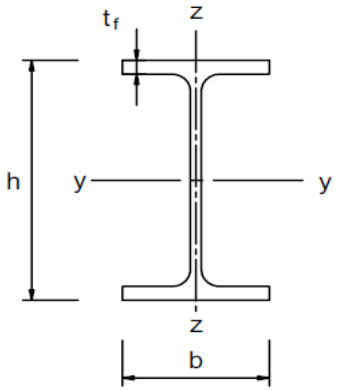

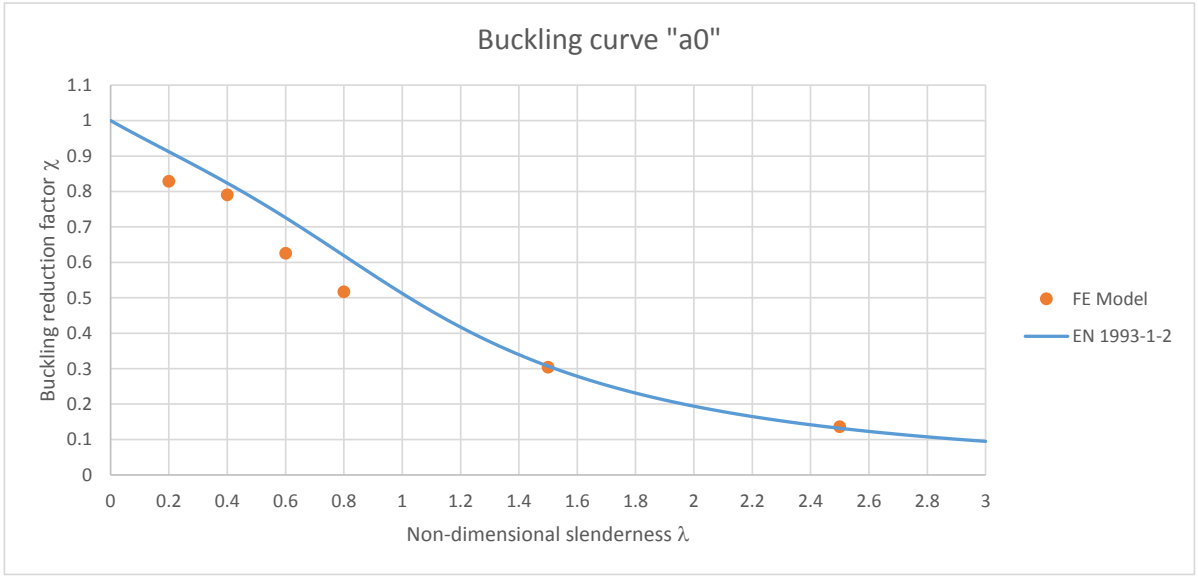

λ_θ	L_{cr} (mm)	N_b (kN)	χ_{FEM}	$\chi_{EN3-1-1}$
0.1	261.28	-		0.955195
0.2	522.55	6,947.96	0.828344	0.912046
0.3	783.83	-		0.868661
0.4	1045.11	6,629.78	0.79041	0.823693
0.5	1306.39	-		0.776259
0.6	1567.66	5,245.05	0.62532	0.726011
0.7	1828.94	-		0.673258
0.8	2090.22	4,336.46	0.516998	0.618999
0.9	2351.50	-		0.564756
1	2612.77	-		0.512191
1.1	2874.05	-		0.462714
1.2	3135.33	-		0.417245
1.3	3396.60	-		0.376195
1.4	3657.88	-		0.339575
1.5	3919.16	2,548.79	0.303869	0.307143
1.6	4180.44	-		0.278527
1.7	4441.71	-		0.25331
1.8	4702.99	-		0.231076
1.9	4964.27	-		0.211443
2	5225.54	-		0.194065
2.1	5486.82	-		0.178641
2.2	5748.10	-		0.164909
2.3	6009.38	-		0.152647
2.4	6270.65	-		0.141662
2.5	6531.93	1,138.75	0.135763	0.131791
2.6	6793.21	-		0.122893
2.7	7054.49	-		0.114848
2.8	7315.76	-		0.107554
2.9	7577.04	-		0.100923
3	7838.32	-		0.094878

FEM: Strong axis gradient - maximum gradient

Curve a

Section:	UKB 1016 x 305 x 487	
f_y	460	N/mm²
E	210000	N/mm²
Av. Temp	452.2	
$k_{y,\theta}$	0.88516	
$k_{E,\theta}$	0.6478	

Section properties:

Depth of the section	h	1036.3	mm
Width of the section	b	308.5	mm
Web thickness	t_w	30	mm
Flange thickness	t_f	54.1	mm
Root radius	r	30	mm
Depth between fillets	d	868.1	mm
Second moment of area	I_{zz}	267000000	mm^4
Radius of gyration	r_{zz}	65.7	mm
Area of section	A	62000	mm²

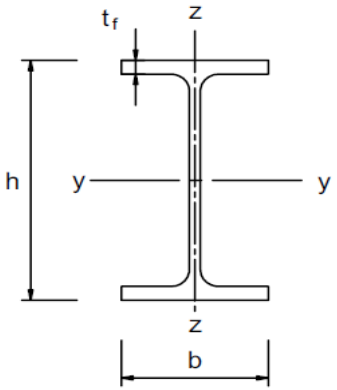

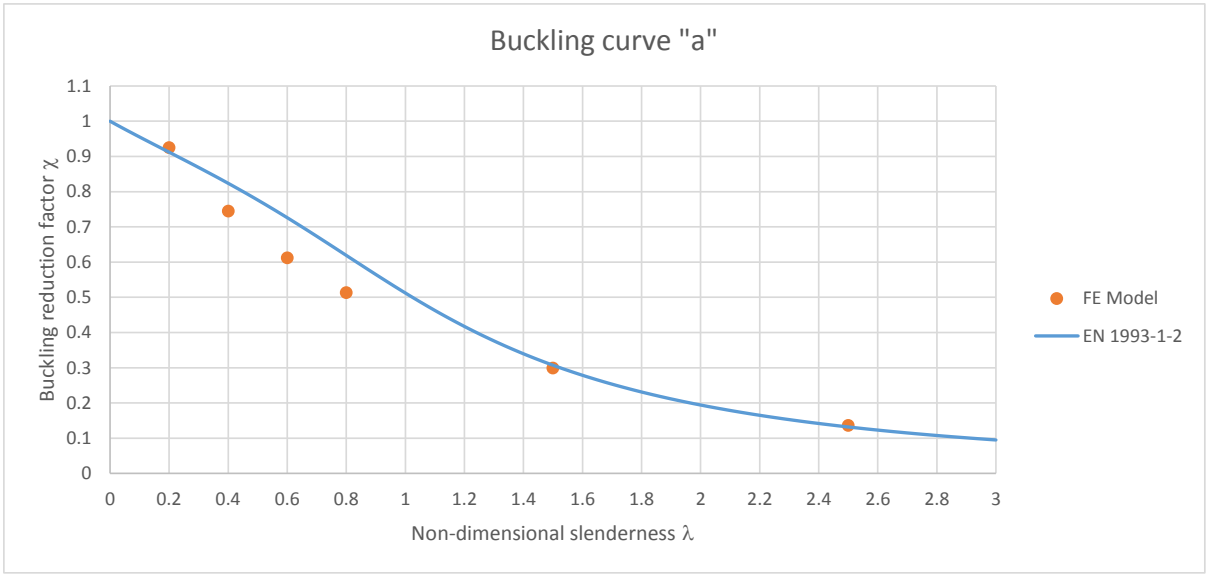

λ_θ	L_{cr} (mm)	N_b (kN)	χ_{FEM}	$\chi_{EN3-1-1}$
0.1	377.27	-		0.955195
0.2	754.55	23,352.99	0.925063	0.912046
0.3	1131.82	-		0.868661
0.4	1509.09	18,790.22	0.744321	0.823693
0.5	1886.36	-		0.776259
0.6	2263.64	15,449.27	0.611979	0.726011
0.7	2640.91	-		0.673258
0.8	3018.18	12,948.71	0.512926	0.618999
0.9	3395.46	-		0.564756
1	3772.73	-		0.512191
1.1	4150.00	-		0.462714
1.2	4527.27	-		0.417245
1.3	4904.55	-		0.376195
1.4	5281.82	-		0.339575
1.5	5659.09	7,547.05	0.298955	0.307143
1.6	6036.37	-		0.278527
1.7	6413.64	-		0.25331
1.8	6790.91	-		0.231076
1.9	7168.18	-		0.211443
2	7545.46	-		0.194065
2.1	7922.73	-		0.178641
2.2	8300.00	-		0.164909
2.3	8677.28	-		0.152647
2.4	9054.55	-		0.141662
2.5	9431.82	3,424.43	0.135649	0.131791
2.6	9809.09	-		0.122893
2.7	10186.37	-		0.114848
2.8	10563.64	-		0.107554
2.9	10940.91	-		0.100923
3	11318.19	-		0.094878

FEM: Strong axis gradient - maximum gradient

Curve b

Section:	UKB 457 x 191 x 161	
f_y	275	N/mm²
E	210000	N/mm²
Av. Temp	452.2	
$k_{y,\theta}$	0.88516	
$k_{E,\theta}$	0.6478	

Section properties:

Depth of the section	h	492	mm
Width of the section	b	199.4	mm
Web thickness	t_w	18	mm
Flange thickness	t_f	32	mm
Root radius	r	10.2	mm
Depth between fillets	d	407.6	mm
Second moment of area	I_{zz}	42500000	mm^4
Radius of gyration	r_{zz}	45.5	mm
Area of section	A	20600	mm²

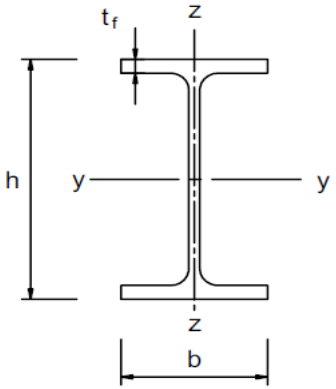

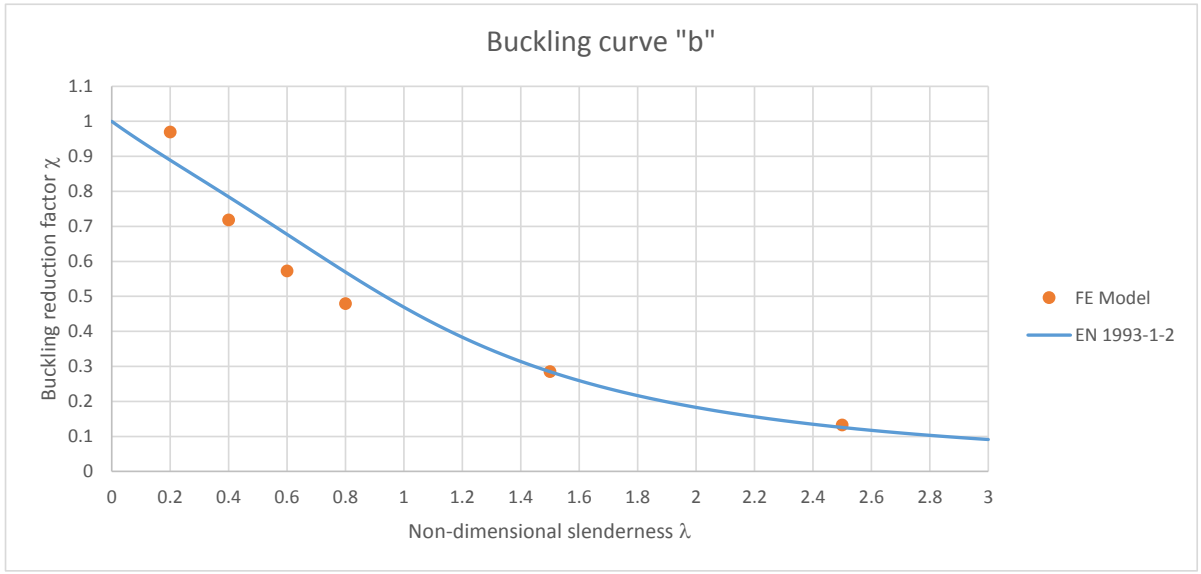

λ_θ	L_{cr} (mm)	N_b (kN)	χ_{FEM}	$\chi_{EN3-1-1}$
0.1	337.92	-		0.94281
0.2	675.84	4,860.26	0.969255	0.8892
0.3	1013.76	-		0.836859
0.4	1351.68	3,598.83	0.717695	0.784411
0.5	1689.60	-		0.731187
0.6	2027.52	2,869.48	0.572245	0.677166
0.7	2365.44	-		0.622903
0.8	2703.36	2,401.46	0.47891	0.569381
0.9	3041.28	-		0.51776
1	3379.20	-		0.469092
1.1	3717.12	-		0.424132
1.2	4055.04	-		0.383268
1.3	4392.96	-		0.346569
1.4	4730.88	-		0.31387
1.5	5068.80	1,427.36	0.28465	0.284872
1.6	5406.72	-		0.259215
1.7	5744.64	-		0.236522
1.8	6082.56	-		0.216435
1.9	6420.48	-		0.198625
2	6758.40	-		0.182797
2.1	7096.32	-		0.168694
2.2	7434.24	-		0.156093
2.3	7772.16	-		0.144802
2.4	8110.08	-		0.134653
2.5	8448.00	663.96	0.132411	0.125506
2.6	8785.93	-		0.117237
2.7	9123.85	-		0.109741
2.8	9461.77	-		0.102929
2.9	9799.69	-		0.09672
3	10137.61	-		0.091048

FEM: Strong axis gradient - maximum gradient

Curve c

Section:	UKC 356 x 406 x 634	
f_y	275	N/mm²
E	210000	N/mm²
Av. Temp	452.2	
$k_{y,\theta}$	0.88516	
$k_{E,\theta}$	0.6478	

Section properties:

Depth of the section	h	474.6	mm
Width of the section	b	424	mm
Web thickness	t_w	47.6	mm
Flange thickness	t_f	77	mm
Root radius	r	15.2	mm
Depth between fillets	d	290.2	mm
Second moment of area	I_{zz}	981000000	mm^4
Radius of gyration	r_{zz}	110	mm
Area of section	A	80800	mm²

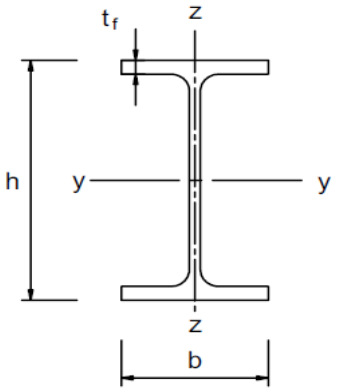

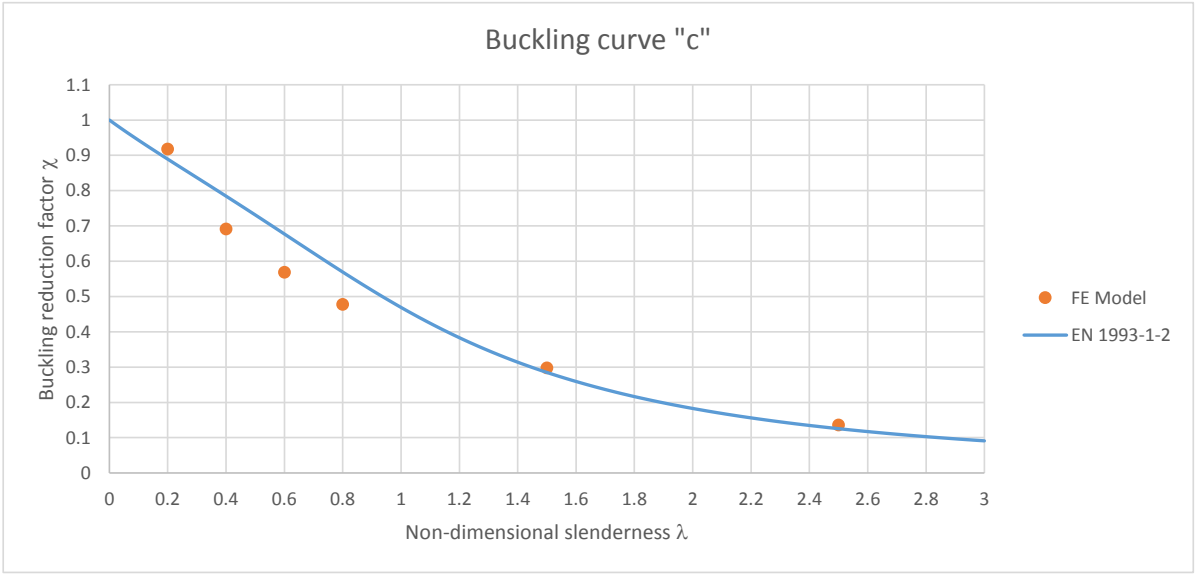

λ_θ	L_{cr} (mm)	N_b (kN)	χ_{FEM}	$\chi_{EN3-1-1}$
0.1	816.95	-		0.94281
0.2	1633.90	18,041.42	0.917286	0.8892
0.3	2450.85	-		0.836859
0.4	3267.80	13,592.29	0.691078	0.784411
0.5	4084.75	-		0.731187
0.6	4901.70	11,175.05	0.568177	0.677166
0.7	5718.65	-		0.622903
0.8	6535.60	9,384.75	0.477152	0.569381
0.9	7352.55	-		0.51776
1	8169.50	-		0.469092
1.1	8986.45	-		0.424132
1.2	9803.40	-		0.383268
1.3	10620.35	-		0.346569
1.4	11437.30	-		0.31387
1.5	12254.25	5,849.85	0.297426	0.284872
1.6	13071.20	-		0.259215
1.7	13888.15	-		0.236522
1.8	14705.10	-		0.216435
1.9	15522.05	-		0.198625
2	16339.00	-		0.182797
2.1	17155.95	-		0.168694
2.2	17972.90	-		0.156093
2.3	18789.85	-		0.144802
2.4	19606.80	-		0.134653
2.5	20423.75	2,667.09	0.135604	0.125506
2.6	21240.70	-		0.117237
2.7	22057.65	-		0.109741
2.8	22874.60	-		0.102929
2.9	23691.55	-		0.09672
3	24508.50	-		0.091048

FEM: Strong axis gradient - maximum gradient

Curve d

Section:	UKC 356 x 406 x 634	
f_y	205	N/mm²
E	210000	N/mm²
Av. Temp	452.2	
$k_{y,\theta}$	0.88516	
$k_{E,\theta}$	0.6478	

Section properties:

Depth of the section	h	474.6	mm
Width of the section	b	424	mm
Web thickness	t_w	47.6	mm
Flange thickness	t_f	110	mm
Root radius	r	15.2	mm
Depth between fillets	d	224.2	mm
Second moment of area	I_{zz}	1400237632	mm^4
Radius of gyration	r_{zz}	115.152798	mm
Area of section	A	105597.286	mm²

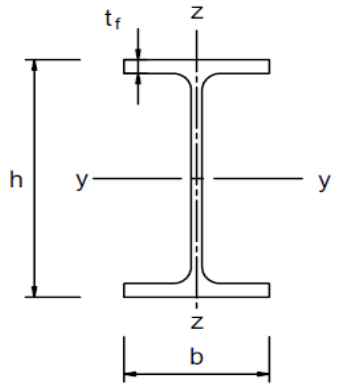

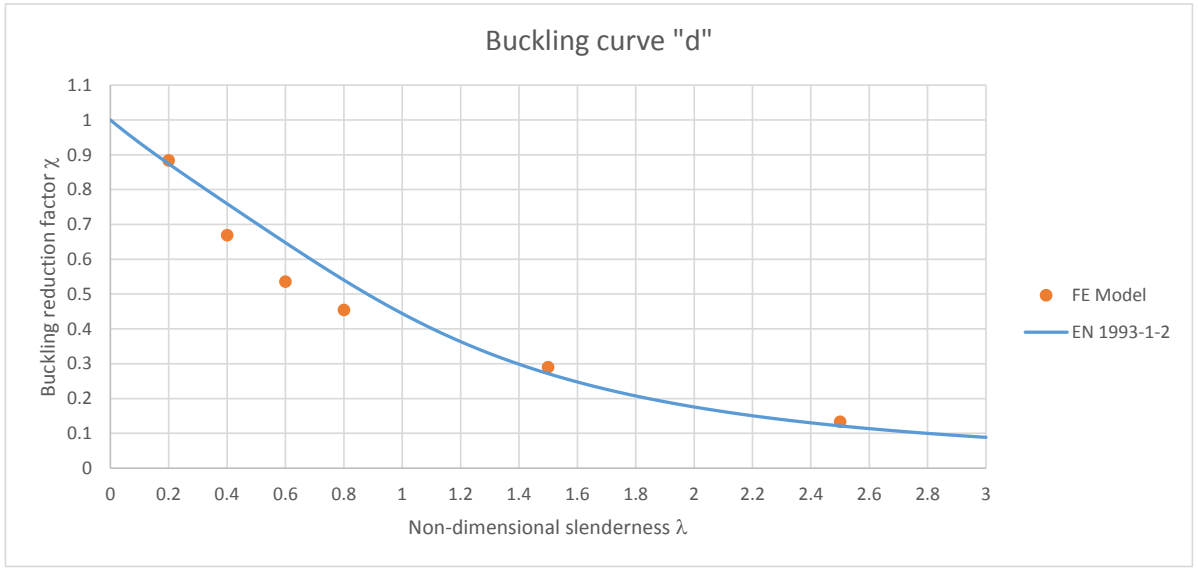

λ_θ	L_{cr} (mm)	N_b (kN)	χ_{FEM}	$\chi_{EN3-1-1}$
0.1	990.53	-		0.934361
0.2	1981.06	16,931.19	0.883607	0.873951
0.3	2971.58	-		0.816105
0.4	3962.11	12,826.73	0.669403	0.759373
0.5	4952.64	-		0.703145
0.6	5943.17	10,262.54	0.535583	0.64747
0.7	6933.69	-		0.592896
0.8	7924.22	8,711.85	0.454655	0.540252
0.9	8914.75	-		0.490409
1	9905.28	-		0.444077
1.1	10895.81	-		0.401689
1.2	11886.33	-		0.363393
1.3	12876.86	-		0.329107
1.4	13867.39	-		0.29859
1.5	14857.92	5,564.27	0.290389	0.271519
1.6	15848.44	-		0.247537
1.7	16838.97	-		0.22629
1.8	17829.50	-		0.207444
1.9	18820.03	-		0.190699
2	19810.56	-		0.175786
2.1	20801.08	-		0.16247
2.2	21791.61	-		0.150548
2.3	22782.14	-		0.139843
2.4	23772.67	-		0.130204
2.5	24763.19	2,555.74	0.133379	0.1215
2.6	25753.72	-		0.113619
2.7	26744.25	-		0.106463
2.8	27734.78	-		0.09995
2.9	28725.31	-		0.094006
3	29715.83	-		0.088568

FEM: Strong axis gradient - maximum temperature

Curve a0

Section:	UKB 457 x 191 x 161	
f_y	460	N/mm²
E	210000	N/mm²
Av. Temp	493.4	
$k_{y,\theta}$	0.79452	
$k_{E,\theta}$	0.6066	

Section properties:

Depth of the section	h	492	mm
Width of the section	b	199.4	mm
Web thickness	t_w	18	mm
Flange thickness	t_f	32	mm
Root radius	r	10.2	mm
Depth between fillets	d	407.6	mm
Second moment of area	I_{zz}	42500000	mm^4
Radius of gyration	r_{zz}	45.5	mm
Area of section	A	20600	mm²

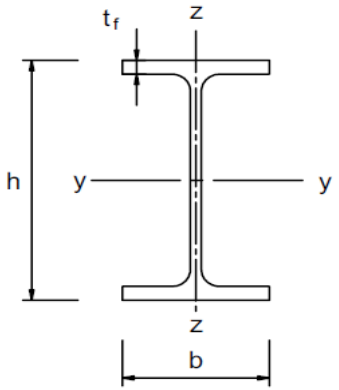

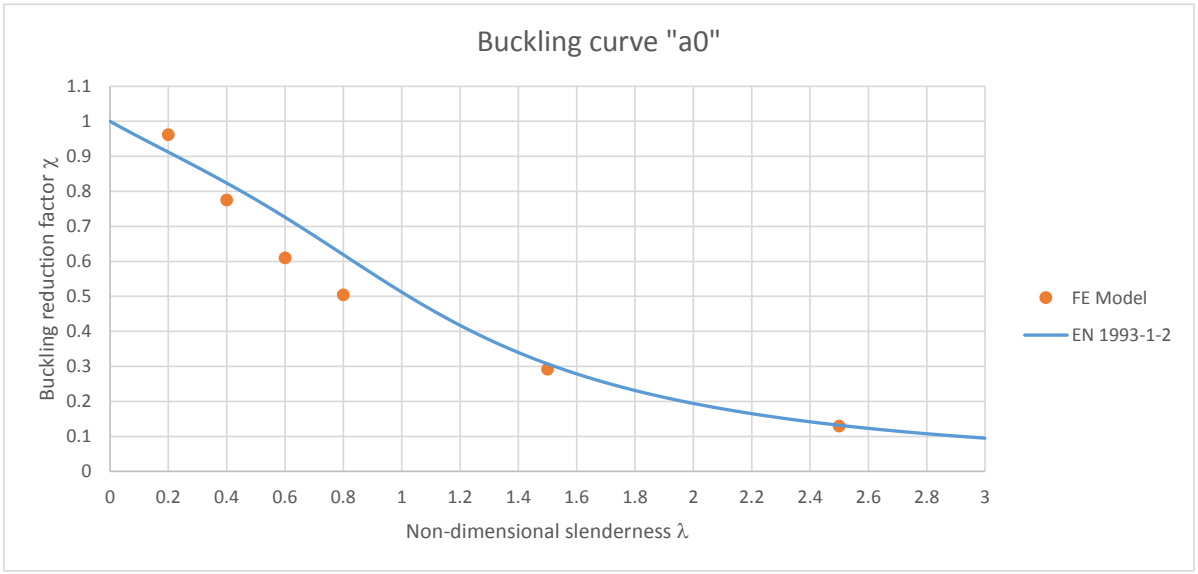

λ_θ	L_{cr} (mm)	N_b (kN)	χ_{FEM}	$\chi_{EN3-1-1}$
0.1	266.86	-		0.955195
0.2	533.73	7,242.07	0.961906	0.912046
0.3	800.59	-		0.868661
0.4	1067.46	5,835.39	0.775068	0.823693
0.5	1334.32	-		0.776259
0.6	1601.19	4,591.66	0.609874	0.726011
0.7	1868.05	-		0.673258
0.8	2134.92	3,795.48	0.504124	0.618999
0.9	2401.78	-		0.564756
1	2668.64	-		0.512191
1.1	2935.51	-		0.462714
1.2	3202.37	-		0.417245
1.3	3469.24	-		0.376195
1.4	3736.10	-		0.339575
1.5	4002.97	2,196.08	0.291688	0.307143
1.6	4269.83	-		0.278527
1.7	4536.70	-		0.25331
1.8	4803.56	-		0.231076
1.9	5070.43	-		0.211443
2	5337.29	-		0.194065
2.1	5604.15	-		0.178641
2.2	5871.02	-		0.164909
2.3	6137.88	-		0.152647
2.4	6404.75	-		0.141662
2.5	6671.61	974.05	0.129375	0.131791
2.6	6938.48	-		0.122893
2.7	7205.34	-		0.114848
2.8	7472.21	-		0.107554
2.9	7739.07	-		0.100923
3	8005.93	-		0.094878

FEM: Strong axis gradient - maximum temperature

Curve a

Section:	UKB 1016 x 305 x 487	
f_y	460	N/mm²
E	210000	N/mm²
Av. Temp	493.4	
$k_{y,\theta}$	0.79452	
$k_{E,\theta}$	0.6066	

Section properties:

Depth of the section	h	1036.3	mm
Width of the section	b	308.5	mm
Web thickness	t_w	30	mm
Flange thickness	t_f	54.1	mm
Root radius	r	30	mm
Depth between fillets	d	868.1	mm
Second moment of area	I_{zz}	267000000	mm^4
Radius of gyration	r_{zz}	65.7	mm
Area of section	A	62000	mm²

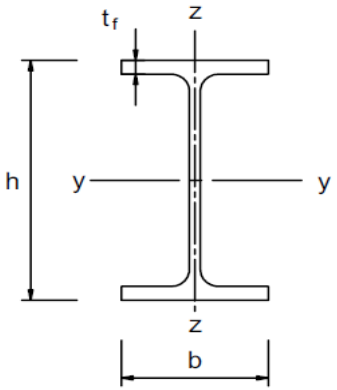

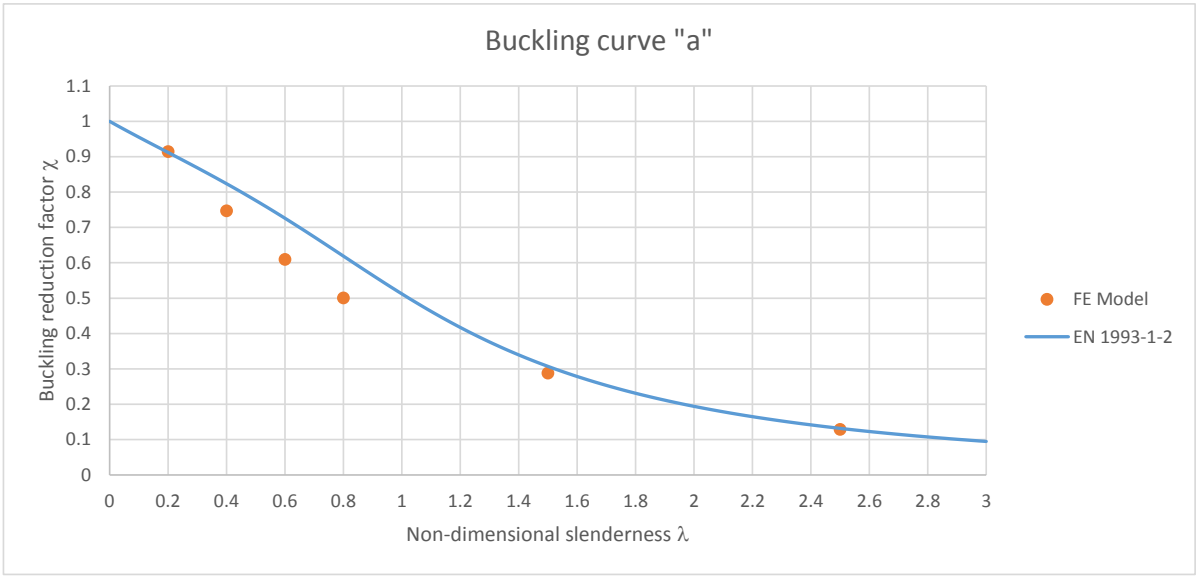

λ_θ	L_{cr} (mm)	N_b (kN)	χ_{FEM}	$\chi_{EN3-1-1}$
0.1	385.34	-		0.955195
0.2	770.68	20,718.37	0.914326	0.912046
0.3	1156.02	-		0.868661
0.4	1541.36	16,922.33	0.746803	0.823693
0.5	1926.70	-		0.776259
0.6	2312.04	13,808.09	0.609367	0.726011
0.7	2697.38	-		0.673258
0.8	3082.72	11,337.74	0.500348	0.618999
0.9	3468.07	-		0.564756
1	3853.41	-		0.512191
1.1	4238.75	-		0.462714
1.2	4624.09	-		0.417245
1.3	5009.43	-		0.376195
1.4	5394.77	-		0.339575
1.5	5780.11	6,528.89	0.288128	0.307143
1.6	6165.45	-		0.278527
1.7	6550.79	-		0.25331
1.8	6936.13	-		0.231076
1.9	7321.47	-		0.211443
2	7706.81	-		0.194065
2.1	8092.15	-		0.178641
2.2	8477.49	-		0.164909
2.3	8862.83	-		0.152647
2.4	9248.17	-		0.141662
2.5	9633.51	2,917.10	0.128735	0.131791
2.6	10018.86	-		0.122893
2.7	10404.20	-		0.114848
2.8	10789.54	-		0.107554
2.9	11174.88	-		0.100923
3	11560.22	-		0.094878

FEM: Strong axis gradient - maximum temperature

Curve b

Section:	UKB 457 x 191 x 161	
f_y	275	N/mm²
E	210000	N/mm²
Av. Temp	493.4	
$k_{y,\theta}$	0.79452	
$k_{E,\theta}$	0.6066	

Section properties:

Depth of the section	h	492	mm
Width of the section	b	199.4	mm
Web thickness	t_w	18	mm
Flange thickness	t_f	32	mm
Root radius	r	10.2	mm
Depth between fillets	d	407.6	mm
Second moment of area	I_{zz}	42500000	mm^4
Radius of gyration	r_{zz}	45.5	mm
Area of section	A	20600	mm²

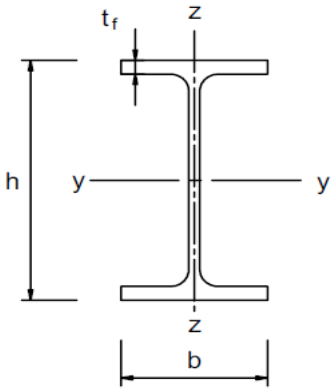

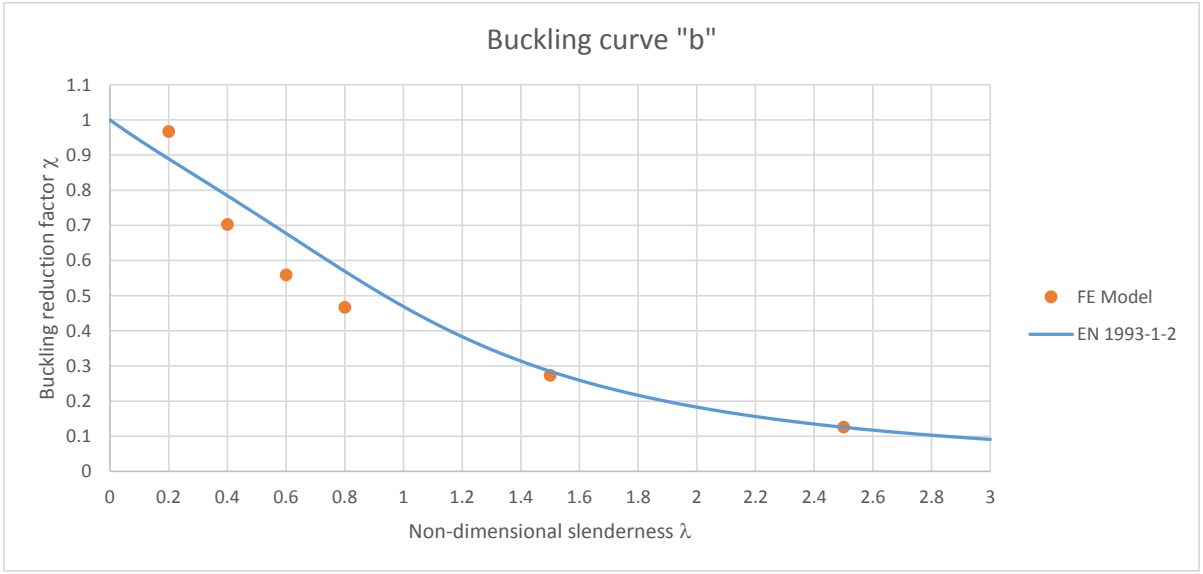

λ_θ	L_{cr} (mm)	N_b (kN)	χ_{FEM}	$\chi_{EN3-1-1}$
0.1	345.15	-		0.94281
0.2	690.29	4,349.87	0.966433	0.8892
0.3	1035.44	-		0.836859
0.4	1380.59	3,159.20	0.701895	0.784411
0.5	1725.73	-		0.731187
0.6	2070.88	2,515.83	0.558956	0.677166
0.7	2416.02	-		0.622903
0.8	2761.17	2,100.94	0.466777	0.569381
0.9	3106.32	-		0.51776
1	3451.46	-		0.469092
1.1	3796.61	-		0.424132
1.2	4141.76	-		0.383268
1.3	4486.90	-		0.346569
1.4	4832.05	-		0.31387
1.5	5177.20	1,227.52	0.272724	0.284872
1.6	5522.34	-		0.259215
1.7	5867.49	-		0.236522
1.8	6212.64	-		0.216435
1.9	6557.78	-		0.198625
2	6902.93	-		0.182797
2.1	7248.07	-		0.168694
2.2	7593.22	-		0.156093
2.3	7938.37	-		0.144802
2.4	8283.51	-		0.134653
2.5	8628.66	565.69	0.125681	0.125506
2.6	8973.81	-		0.117237
2.7	9318.95	-		0.109741
2.8	9664.10	-		0.102929
2.9	10009.25	-		0.09672
3	10354.39	-		0.091048

FEM: Strong axis gradient - maximum temperature

Curve c

Section:	UKC 356 x 406 x 634	
f_y	275	N/mm²
E	210000	N/mm²
Av. Temp	493.4	
$k_{y,\theta}$	0.79452	
$k_{E,\theta}$	0.6066	

Section properties:

Depth of the section	h	474.6	mm
Width of the section	b	424	mm
Web thickness	t_w	47.6	mm
Flange thickness	t_f	77	mm
Root radius	r	15.2	mm
Depth between fillets	d	290.2	mm
Second moment of area	I_{zz}	981000000	mm^4
Radius of gyration	r_{zz}	110	mm
Area of section	A	80800	mm²

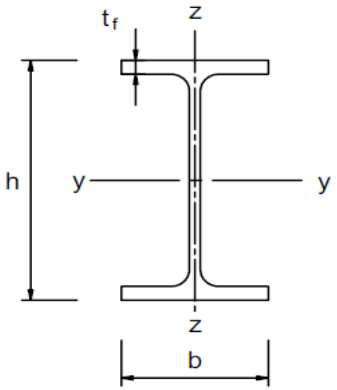

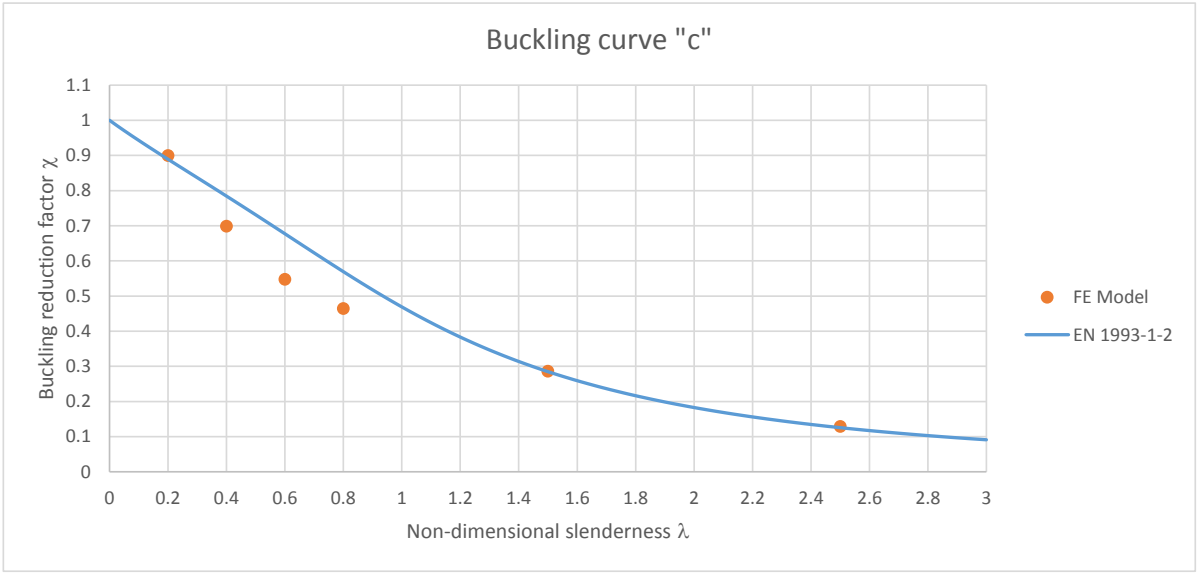

λ_θ	L_{cr} (mm)	N_b (kN)	χ_{FEM}	$\chi_{EN3-1-1}$
0.1	834.42	-		0.94281
0.2	1668.84	15,874.17	0.899171	0.8892
0.3	2503.26	-		0.836859
0.4	3337.68	12,330.96	0.69847	0.784411
0.5	4172.10	-		0.731187
0.6	5006.52	9,657.90	0.547059	0.677166
0.7	5840.94	-		0.622903
0.8	6675.36	8,195.59	0.464228	0.569381
0.9	7509.78	-		0.51776
1	8344.20	-		0.469092
1.1	9178.62	-		0.424132
1.2	10013.04	-		0.383268
1.3	10847.46	-		0.346569
1.4	11681.88	-		0.31387
1.5	12516.30	5,046.01	0.285824	0.284872
1.6	13350.72	-		0.259215
1.7	14185.14	-		0.236522
1.8	15019.56	-		0.216435
1.9	15853.98	-		0.198625
2	16688.40	-		0.182797
2.1	17522.82	-		0.168694
2.2	18357.24	-		0.156093
2.3	19191.66	-		0.144802
2.4	20026.08	-		0.134653
2.5	20860.50	2,272.19	0.128705	0.125506
2.6	21694.92	-		0.117237
2.7	22529.34	-		0.109741
2.8	23363.76	-		0.102929
2.9	24198.18	-		0.09672
3	25032.60	-		0.091048

FEM: Strong axis gradient - maximum temperature

Curve d

Section:	UKC 356 x 406 x 634	
f_y	205	N/mm²
E	210000	N/mm²
Av. Temp	493.4	
$k_{y,\theta}$	0.79452	
$k_{E,\theta}$	0.6066	

Section properties:

Depth of the section	h	474.6	mm
Width of the section	b	424	mm
Web thickness	t_w	47.6	mm
Flange thickness	t_f	110	mm
Root radius	r	15.2	mm
Depth between fillets	d	224.2	mm
Second moment of area	I_{zz}	1400237632	mm^4
Radius of gyration	r_{zz}	115.152798	mm
Area of section	A	105597.286	mm²

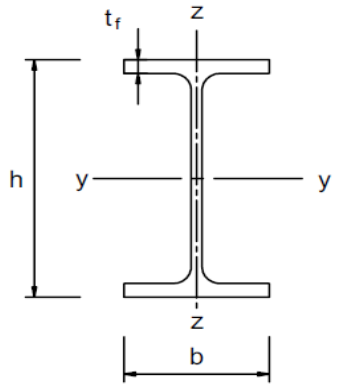

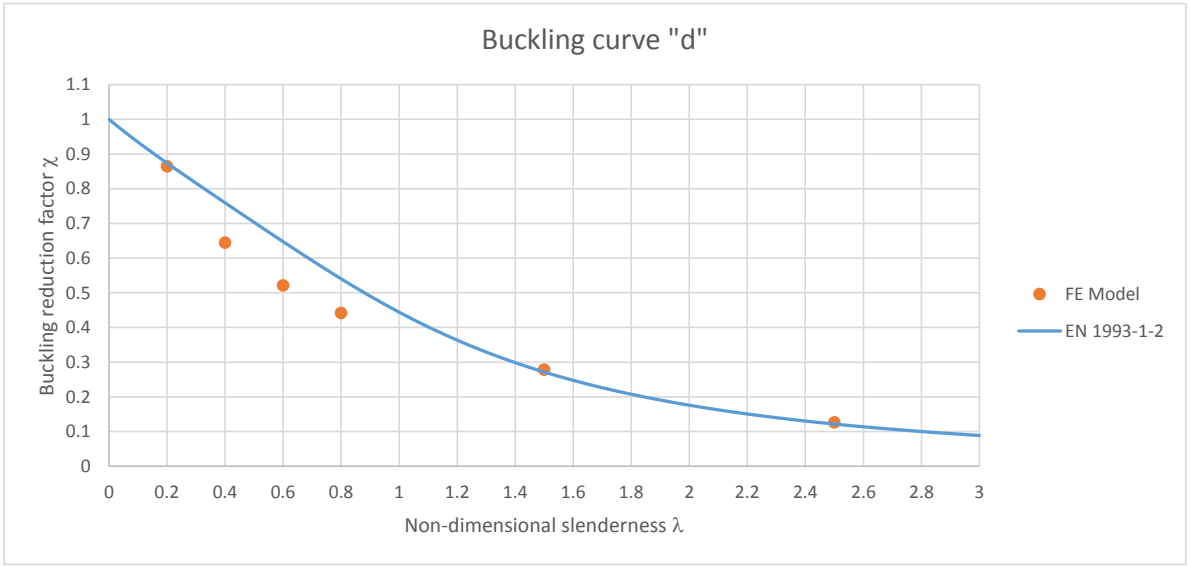

λ_θ	L_{cr} (mm)	N_b (kN)	χ_{FEM}	$\chi_{EN3-1-1}$
0.1	1011.71	-		0.934361
0.2	2023.42	14,880.90	0.865203	0.873951
0.3	3035.13	-		0.816105
0.4	4046.84	11,093.60	0.645002	0.759373
0.5	5058.55	-		0.703145
0.6	6070.26	8,970.24	0.521546	0.64747
0.7	7081.97	-		0.592896
0.8	8093.68	7,601.93	0.44199	0.540252
0.9	9105.39	-		0.490409
1	10117.10	-		0.444077
1.1	11128.81	-		0.401689
1.2	12140.52	-		0.363393
1.3	13152.22	-		0.329107
1.4	14163.93	-		0.29859
1.5	15175.64	4,795.05	0.278793	0.271519
1.6	16187.35	-		0.247537
1.7	17199.06	-		0.22629
1.8	18210.77	-		0.207444
1.9	19222.48	-		0.190699
2	20234.19	-		0.175786
2.1	21245.90	-		0.16247
2.2	22257.61	-		0.150548
2.3	23269.32	-		0.139843
2.4	24281.03	-		0.130204
2.5	25292.74	2,176.40	0.12654	0.1215
2.6	26304.45	-		0.113619
2.7	27316.16	-		0.106463
2.8	28327.87	-		0.09995
2.9	29339.58	-		0.094006
3	30351.29	-		0.088568

FEM: Weak axis gradient - maximum gradient

Curve a0

Section:	UKB 457 x 191 x 161	
f_y	460	N/mm²
E	210000	N/mm²
Av. Temp	500	
$k_{y,\theta}$	0.78	
$k_{E,\theta}$	0.6	

Section properties:

Depth of the section	h	492	mm
Width of the section	b	199.4	mm
Web thickness	t_w	18	mm
Flange thickness	t_f	32	mm
Root radius	r	10.2	mm
Depth between fillets	d	407.6	mm
Second moment of area	I_{zz}	42500000	mm^4
Radius of gyration	r_{zz}	45.5	mm
Area of section	A	20600	mm²

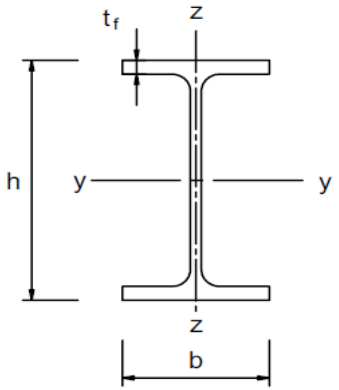

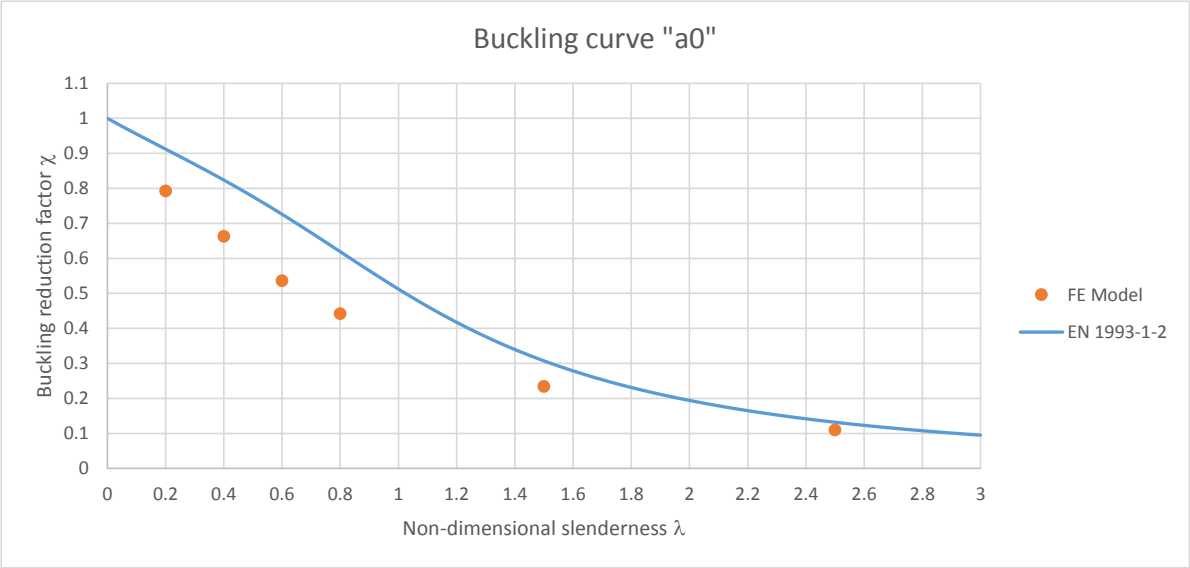

λ_θ	L_{cr} (mm)	N_b (kN)	χ_{FEM}	$\chi_{EN3-1-1}$
0.1	267.87	-		0.955195
0.2	535.74	5,857.92	0.792545	0.912046
0.3	803.60	-		0.868661
0.4	1071.47	4,895.97	0.662398	0.823693
0.5	1339.34	-		0.776259
0.6	1607.21	3,961.60	0.535982	0.726011
0.7	1875.07	-		0.673258
0.8	2142.94	3,263.34	0.441512	0.618999
0.9	2410.81	-		0.564756
1	2678.68	-		0.512191
1.1	2946.54	-		0.462714
1.2	3214.41	-		0.417245
1.3	3482.28	-		0.376195
1.4	3750.15	-		0.339575
1.5	4018.02	1,730.73	0.234158	0.307143
1.6	4285.88	-		0.278527
1.7	4553.75	-		0.25331
1.8	4821.62	-		0.231076
1.9	5089.49	-		0.211443
2	5357.35	-		0.194065
2.1	5625.22	-		0.178641
2.2	5893.09	-		0.164909
2.3	6160.96	-		0.152647
2.4	6428.82	-		0.141662
2.5	6696.69	807.82	0.109293	0.131791
2.6	6964.56	-		0.122893
2.7	7232.43	-		0.114848
2.8	7500.30	-		0.107554
2.9	7768.16	-		0.100923
3	8036.03	-		0.094878

FEM: Weak axis gradient - maximum gradient

Curve a

Section:	UKB 1016 x 305 x 487	
f_y	460	N/mm²
E	210000	N/mm²
Av. Temp	500	
$k_{y,\theta}$	0.78	
$k_{E,\theta}$	0.6	

Section properties:

Depth of the section	h	1036.3	mm
Width of the section	b	308.5	mm
Web thickness	t_w	30	mm
Flange thickness	t_f	54.1	mm
Root radius	r	30	mm
Depth between fillets	d	868.1	mm
Second moment of area	I_{zz}	267000000	mm^4
Radius of gyration	r_{zz}	65.7	mm
Area of section	A	62000	mm²

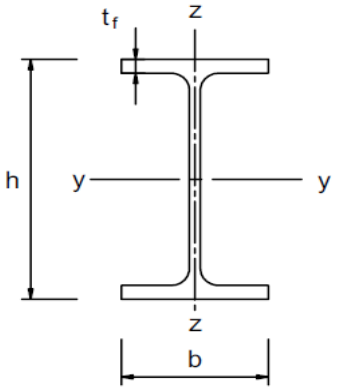

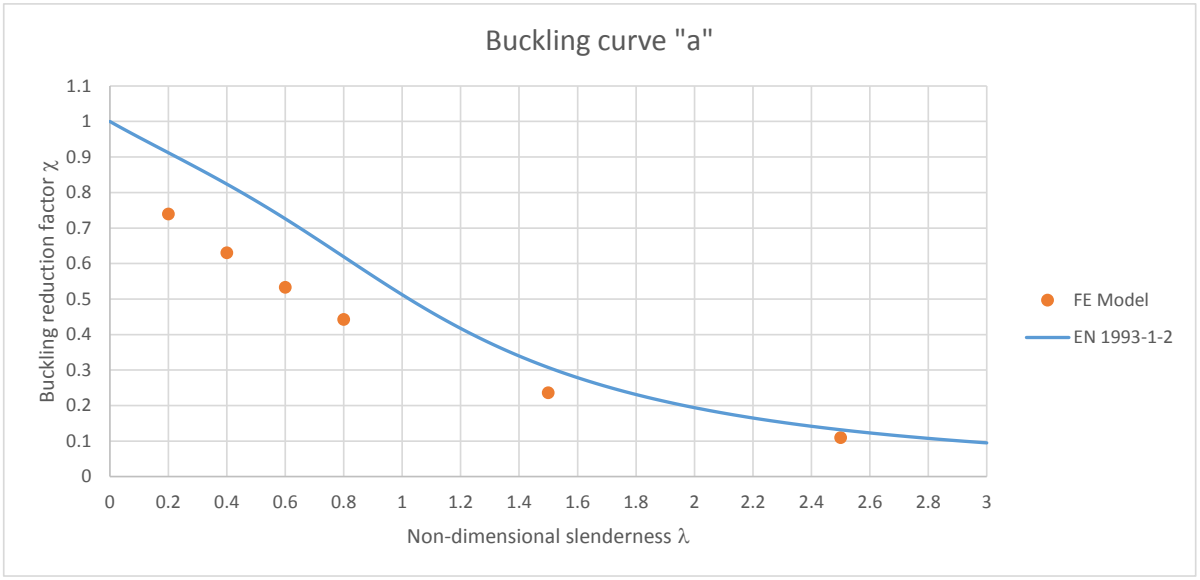

λ_θ	L_{cr} (mm)	N_b (kN)	χ_{FEM}	$\chi_{EN3-1-1}$
0.1	386.79	-		0.955195
0.2	773.58	16,443.49	0.73918	0.912046
0.3	1160.37	-		0.868661
0.4	1547.16	14,009.32	0.629757	0.823693
0.5	1933.95	-		0.776259
0.6	2320.73	11,852.52	0.532803	0.726011
0.7	2707.52	-		0.673258
0.8	3094.31	9,842.35	0.44244	0.618999
0.9	3481.10	-		0.564756
1	3867.89	-		0.512191
1.1	4254.68	-		0.462714
1.2	4641.47	-		0.417245
1.3	5028.26	-		0.376195
1.4	5415.05	-		0.339575
1.5	5801.84	5,243.10	0.235691	0.307143
1.6	6188.63	-		0.278527
1.7	6575.42	-		0.25331
1.8	6962.20	-		0.231076
1.9	7348.99	-		0.211443
2	7735.78	-		0.194065
2.1	8122.57	-		0.178641
2.2	8509.36	-		0.164909
2.3	8896.15	-		0.152647
2.4	9282.94	-		0.141662
2.5	9669.73	2,436.06	0.109507	0.131791
2.6	10056.52	-		0.122893
2.7	10443.31	-		0.114848
2.8	10830.10	-		0.107554
2.9	11216.89	-		0.100923
3	11603.67	-		0.094878

FEM: Weak axis gradient - maximum gradient

Curve b

Section:	UKB 457 x 191 x 161	
f_y	275	N/mm²
E	210000	N/mm²
Av. Temp	500	
$k_{y,\theta}$	0.78	
$k_{E,\theta}$	0.6	

Section properties:

Depth of the section	h	492	mm
Width of the section	b	199.4	mm
Web thickness	t_w	18	mm
Flange thickness	t_f	32	mm
Root radius	r	10.2	mm
Depth between fillets	d	407.6	mm
Second moment of area	I_{zz}	42500000	mm^4
Radius of gyration	r_{zz}	45.5	mm
Area of section	A	20600	mm²

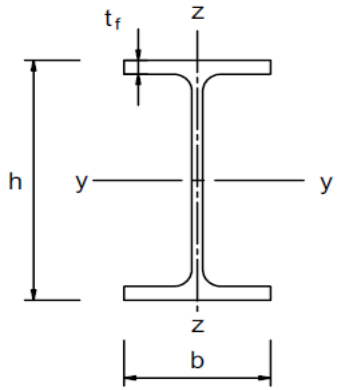

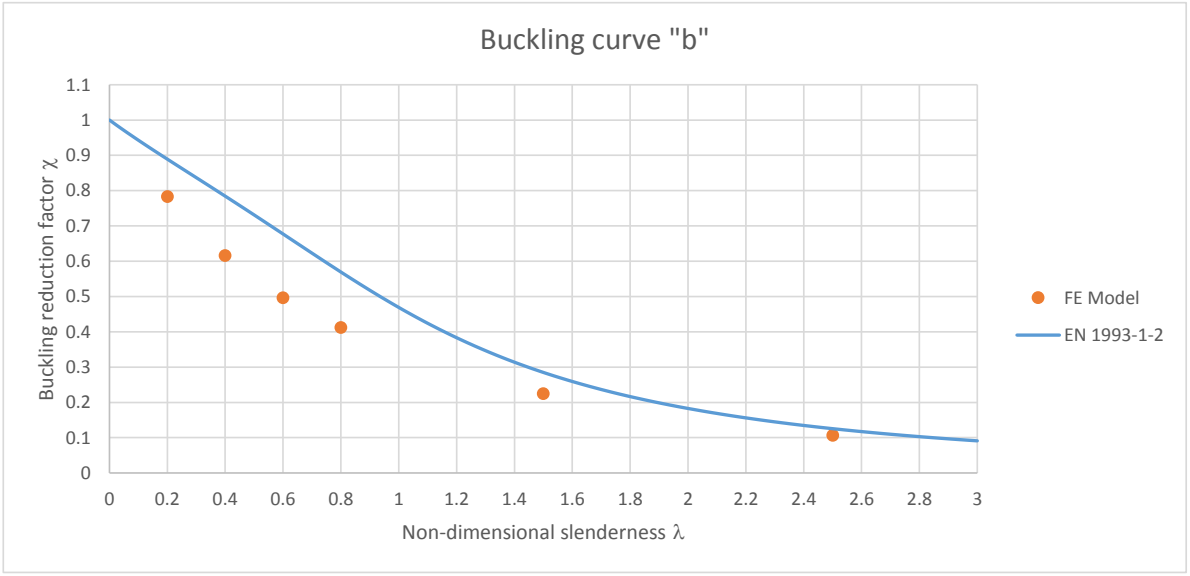

λ_θ	L_{cr} (mm)	N_b (kN)	χ_{FEM}	$\chi_{EN3-1-1}$
0.1	346.44	-		0.94281
0.2	692.89	3,460.50	0.783149	0.8892
0.3	1039.33	-		0.836859
0.4	1385.78	2,719.58	0.61547	0.784411
0.5	1732.22	-		0.731187
0.6	2078.66	2,192.40	0.496165	0.677166
0.7	2425.11	-		0.622903
0.8	2771.55	1,819.37	0.411744	0.569381
0.9	3117.99	-		0.51776
1	3464.44	-		0.469092
1.1	3810.88	-		0.424132
1.2	4157.33	-		0.383268
1.3	4503.77	-		0.346569
1.4	4850.21	-		0.31387
1.5	5196.66	992.98	0.224723	0.284872
1.6	5543.10	-		0.259215
1.7	5889.55	-		0.236522
1.8	6235.99	-		0.216435
1.9	6582.43	-		0.198625
2	6928.88	-		0.182797
2.1	7275.32	-		0.168694
2.2	7621.77	-		0.156093
2.3	7968.21	-		0.144802
2.4	8314.65	-		0.134653
2.5	8661.10	470.17	0.106404	0.125506
2.6	9007.54	-		0.117237
2.7	9353.98	-		0.109741
2.8	9700.43	-		0.102929
2.9	10046.87	-		0.09672
3	10393.32	-		0.091048

FEM: Weak axis gradient - maximum gradient

Curve c

Section:	UKC 356 x 406 x 634	
f_y	275	N/mm²
E	210000	N/mm²
Av. Temp	500	
$k_{y,\theta}$	0.78	
$k_{E,\theta}$	0.6	

Section properties:

Depth of the section	h	474.6	mm
Width of the section	b	424	mm
Web thickness	t_w	47.6	mm
Flange thickness	t_f	77	mm
Root radius	r	15.2	mm
Depth between fillets	d	290.2	mm
Second moment of area	I_{zz}	981000000	mm^4
Radius of gyration	r_{zz}	110	mm
Area of section	A	80800	mm²

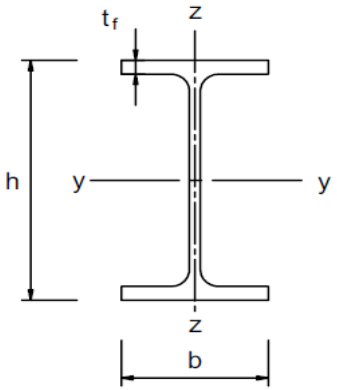

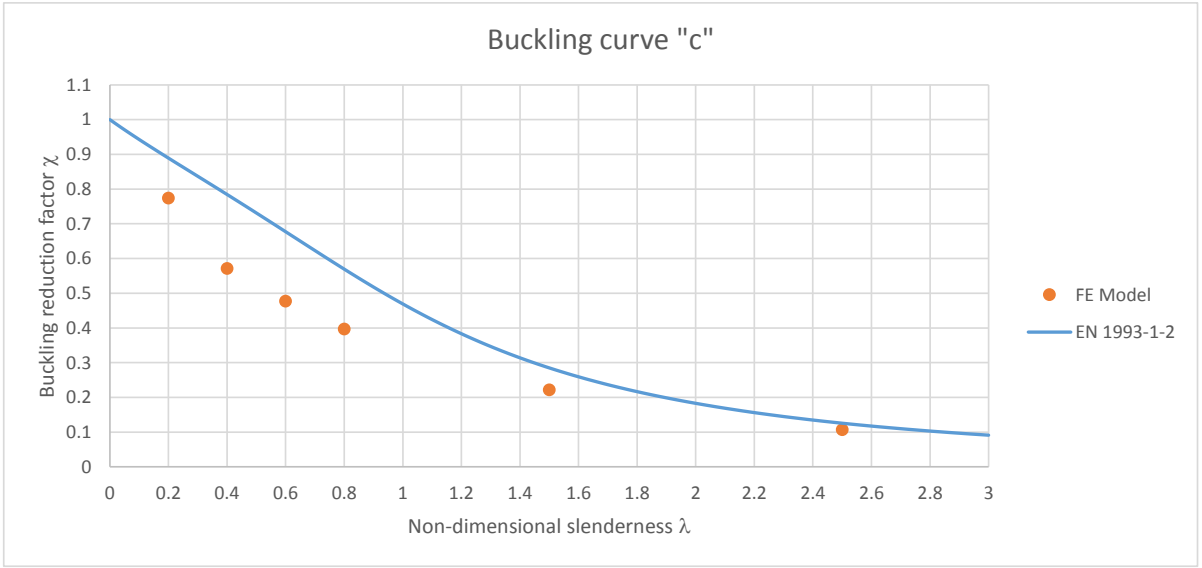

λ_θ	L_{cr} (mm)	N_b (kN)	χ_{FEM}	$\chi_{EN3-1-1}$
0.1	837.56	-		0.94281
0.2	1675.11	13,413.04	0.773907	0.8892
0.3	2512.67	-		0.836859
0.4	3350.23	9,891.20	0.570703	0.784411
0.5	4187.78	-		0.731187
0.6	5025.34	8,270.75	0.477207	0.677166
0.7	5862.90	-		0.622903
0.8	6700.45	6,870.09	0.396391	0.569381
0.9	7538.01	-		0.51776
1	8375.57	-		0.469092
1.1	9213.12	-		0.424132
1.2	10050.68	-		0.383268
1.3	10888.24	-		0.346569
1.4	11725.79	-		0.31387
1.5	12563.35	3,831.25	0.221056	0.284872
1.6	13400.91	-		0.259215
1.7	14238.46	-		0.236522
1.8	15076.02	-		0.216435
1.9	15913.58	-		0.198625
2	16751.13	-		0.182797
2.1	17588.69	-		0.168694
2.2	18426.25	-		0.156093
2.3	19263.80	-		0.144802
2.4	20101.36	-		0.134653
2.5	20938.92	1,852.22	0.10687	0.125506
2.6	21776.47	-		0.117237
2.7	22614.03	-		0.109741
2.8	23451.59	-		0.102929
2.9	24289.14	-		0.09672
3	25126.70	-		0.091048

FEM: Weak axis gradient - maximum gradient

Curve d

Section:	UKC 356 x 406 x 634	
f_y	205	N/mm²
E	210000	N/mm²
Av. Temp	500	
$k_{y,\theta}$	0.78	
$k_{E,\theta}$	0.6	

Section properties:

Depth of the section	h	474.6	mm
Width of the section	b	424	mm
Web thickness	t_w	47.6	mm
Flange thickness	t_f	110	mm
Root radius	r	15.2	mm
Depth between fillets	d	224.2	mm
Second moment of area	I_{zz}	1400237632	mm^4
Radius of gyration	r_{zz}	115.152798	mm
Area of section	A	105597.286	mm²

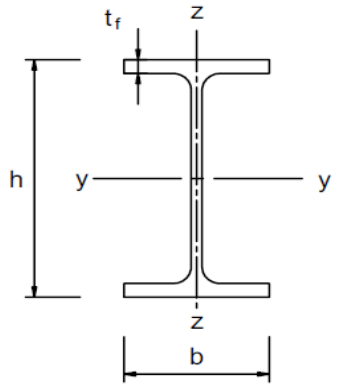

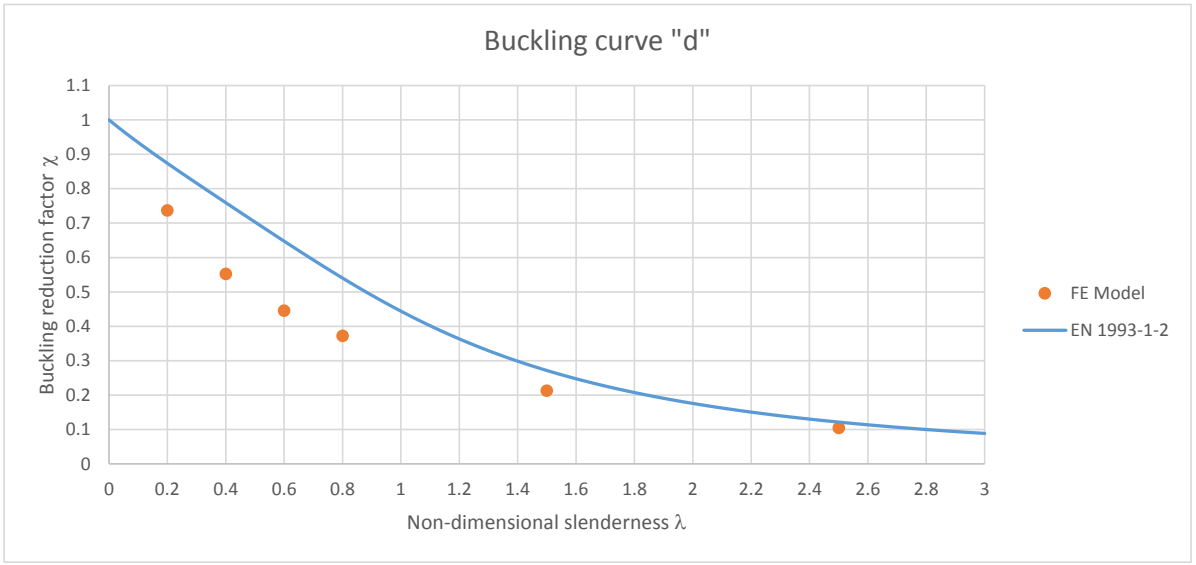

λ_θ	L_{cr} (mm)	N_b (kN)	χ_{FEM}	$\chi_{EN3-1-1}$
0.1	1015.51	-		0.934361
0.2	2031.03	12,441.72	0.73685	0.873951
0.3	3046.54	-		0.816105
0.4	4062.05	9,328.32	0.552462	0.759373
0.5	5077.56	-		0.703145
0.6	6093.08	7,529.15	0.445907	0.64747
0.7	7108.59	-		0.592896
0.8	8124.10	6,289.01	0.372461	0.540252
0.9	9139.62	-		0.490409
1	10155.13	-		0.444077
1.1	11170.64	-		0.401689
1.2	12186.15	-		0.363393
1.3	13201.67	-		0.329107
1.4	14217.18	-		0.29859
1.5	15232.69	3,597.35	0.21305	0.271519
1.6	16248.20	-		0.247537
1.7	17263.72	-		0.22629
1.8	18279.23	-		0.207444
1.9	19294.74	-		0.190699
2	20310.26	-		0.175786
2.1	21325.77	-		0.16247
2.2	22341.28	-		0.150548
2.3	23356.79	-		0.139843
2.4	24372.31	-		0.130204
2.5	25387.82	1,766.07	0.104594	0.1215
2.6	26403.33	-		0.113619
2.7	27418.85	-		0.106463
2.8	28434.36	-		0.09995
2.9	29449.87	-		0.094006
3	30465.38	-		0.088568

FEM: Weak axis gradient - maximum temperature

Curve a0

Section:	UKB 457 x 191 x 161	
f_y	460	N/mm²
E	210000	N/mm²
Av. Temp	693.8	
$k_{y,\theta}$	0.24488	
$k_{E,\theta}$	0.14116	

Section properties:

Depth of the section	h	492	mm
Width of the section	b	199.4	mm
Web thickness	t_w	18	mm
Flange thickness	t_f	32	mm
Root radius	r	10.2	mm
Depth between fillets	d	407.6	mm
Second moment of area	I_{zz}	42500000	mm^4
Radius of gyration	r_{zz}	45.5	mm
Area of section	A	20600	mm²

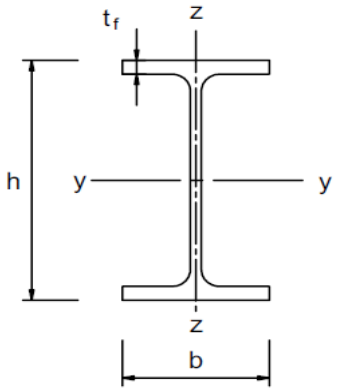

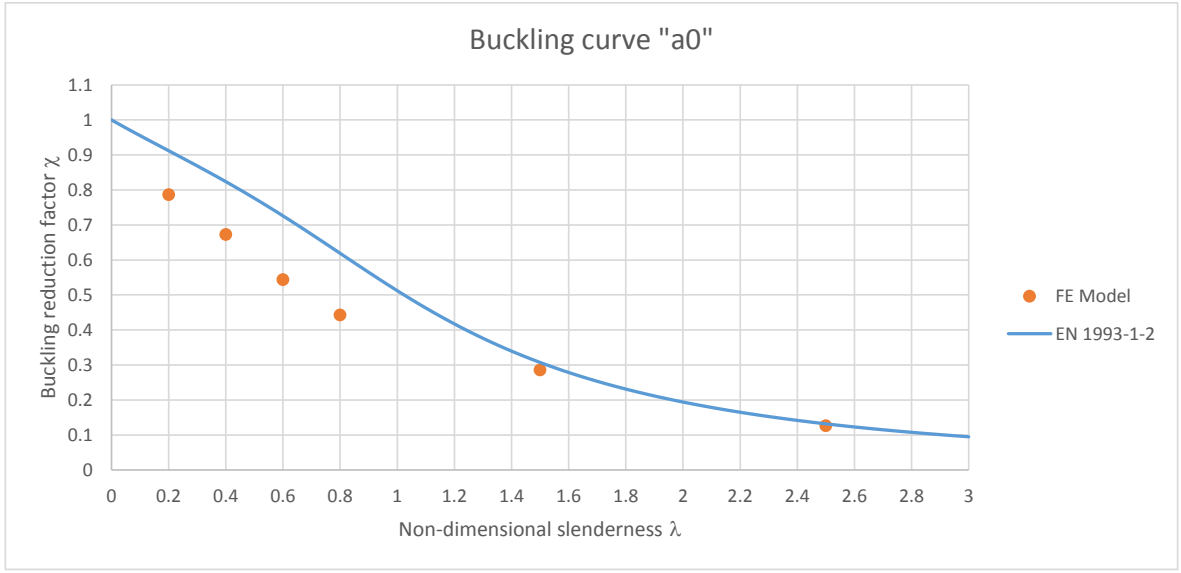

λ_θ	L_{cr} (mm)	N_b (kN)	χ_{FEM}	$\chi_{EN3-1-1}$
0.1	231.88	-		0.955195
0.2	463.77	1,825.51	0.786692	0.912046
0.3	695.65	-		0.868661
0.4	927.54	1,560.61	0.672537	0.823693
0.5	1159.42	-		0.776259
0.6	1391.31	1,261.96	0.543834	0.726011
0.7	1623.19	-		0.673258
0.8	1855.07	1,026.31	0.442283	0.618999
0.9	2086.96	-		0.564756
1	2318.84	-		0.512191
1.1	2550.73	-		0.462714
1.2	2782.61	-		0.417245
1.3	3014.49	-		0.376195
1.4	3246.38	-		0.339575
1.5	3478.26	663.09	0.285756	0.307143
1.6	3710.15	-		0.278527
1.7	3942.03	-		0.25331
1.8	4173.92	-		0.231076
1.9	4405.80	-		0.211443
2	4637.68	-		0.194065
2.1	4869.57	-		0.178641
2.2	5101.45	-		0.164909
2.3	5333.34	-		0.152647
2.4	5565.22	-		0.141662
2.5	5797.11	292.04	0.125852	0.131791
2.6	6028.99	-		0.122893
2.7	6260.87	-		0.114848
2.8	6492.76	-		0.107554
2.9	6724.64	-		0.100923
3	6956.53	-		0.094878

FEM: Weak axis gradient - maximum temperature

Curve a

Section:	UKB 1016 x 305 x 487	
f_y	460	N/mm²
E	210000	N/mm²
Av. Temp	693.8	
$k_{y,\theta}$	0.24488	
$k_{E,\theta}$	0.14116	

Section properties:

Depth of the section	h	1036.3	mm
Width of the section	b	308.5	mm
Web thickness	t_w	30	mm
Flange thickness	t_f	54.1	mm
Root radius	r	30	mm
Depth between fillets	d	868.1	mm
Second moment of area	I_{zz}	267000000	mm^4
Radius of gyration	r_{zz}	65.7	mm
Area of section	A	62000	mm²

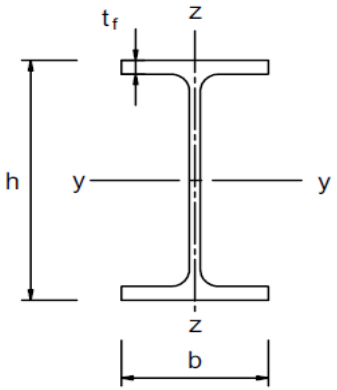

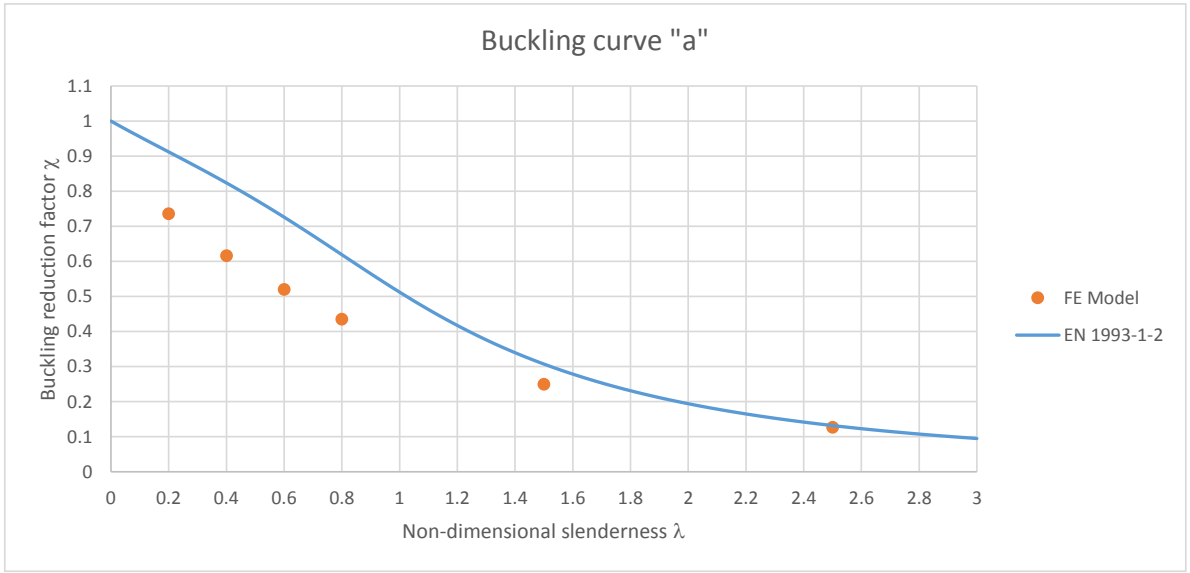

λ_θ	L_{cr} (mm)	N_b (kN)	χ_{FEM}	$\chi_{EN3-1-1}$
0.1	334.83	-		0.955195
0.2	669.66	5,137.95	0.735677	0.912046
0.3	1004.49	-		0.868661
0.4	1339.32	4,303.04	0.61613	0.823693
0.5	1674.15	-		0.776259
0.6	2008.98	3,631.39	0.519961	0.726011
0.7	2343.81	-		0.673258
0.8	2678.64	3,036.35	0.43476	0.618999
0.9	3013.48	-		0.564756
1	3348.31	-		0.512191
1.1	3683.14	-		0.462714
1.2	4017.97	-		0.417245
1.3	4352.80	-		0.376195
1.4	4687.63	-		0.339575
1.5	5022.46	1,741.70	0.249385	0.307143
1.6	5357.29	-		0.278527
1.7	5692.12	-		0.25331
1.8	6026.95	-		0.231076
1.9	6361.78	-		0.211443
2	6696.61	-		0.194065
2.1	7031.44	-		0.178641
2.2	7366.27	-		0.164909
2.3	7701.10	-		0.152647
2.4	8035.93	-		0.141662
2.5	8370.76	884.61	0.126663	0.131791
2.6	8705.60	-		0.122893
2.7	9040.43	-		0.114848
2.8	9375.26	-		0.107554
2.9	9710.09	-		0.100923
3	10044.92	-		0.094878

FEM: Weak axis gradient - maximum temperature

Curve b

Section:	UKB 457 x 191 x 161	
f_y	275	N/mm²
E	210000	N/mm²
Av. Temp	693.8	
$k_{y,\theta}$	0.24488	
$k_{E,\theta}$	0.14116	

Section properties:

Depth of the section	h	492	mm
Width of the section	b	199.4	mm
Web thickness	t_w	18	mm
Flange thickness	t_f	32	mm
Root radius	r	10.2	mm
Depth between fillets	d	407.6	mm
Second moment of area	I_{zz}	42500000	mm^4
Radius of gyration	r_{zz}	45.5	mm
Area of section	A	20600	mm²

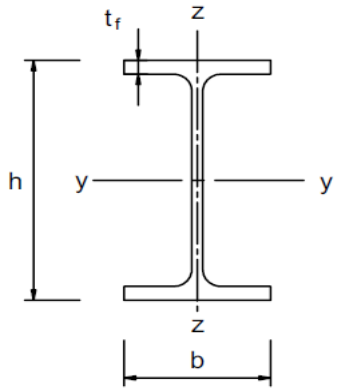

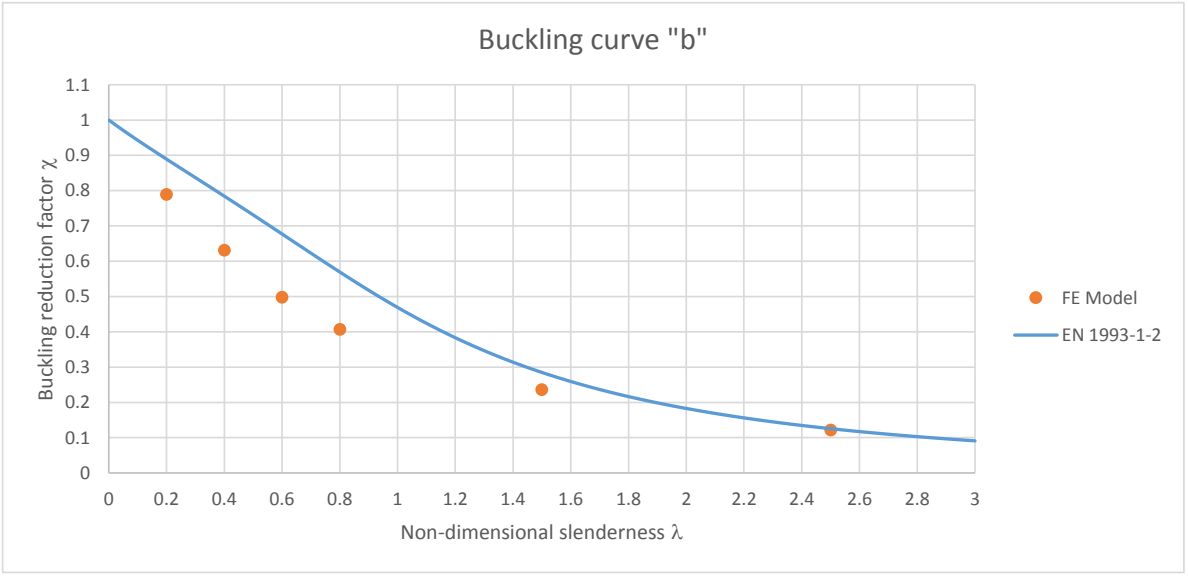

λ_θ	L_{cr} (mm)	N_b (kN)	χ_{FEM}	$\chi_{EN3-1-1}$
0.1	299.91	-		0.94281
0.2	599.81	1,094.95	0.789295	0.8892
0.3	899.72	-		0.836859
0.4	1199.62	875.10	0.630819	0.784411
0.5	1499.53	-		0.731187
0.6	1799.43	690.73	0.497918	0.677166
0.7	2099.34	-		0.622903
0.8	2399.24	563.68	0.406328	0.569381
0.9	2699.15	-		0.51776
1	2999.05	-		0.469092
1.1	3298.96	-		0.424132
1.2	3598.86	-		0.383268
1.3	3898.77	-		0.346569
1.4	4198.67	-		0.31387
1.5	4498.58	326.85	0.23561	0.284872
1.6	4798.48	-		0.259215
1.7	5098.39	-		0.236522
1.8	5398.29	-		0.216435
1.9	5698.20	-		0.198625
2	5998.10	-		0.182797
2.1	6298.01	-		0.168694
2.2	6597.91	-		0.156093
2.3	6897.82	-		0.144802
2.4	7197.72	-		0.134653
2.5	7497.63	168.84	0.121706	0.125506
2.6	7797.53	-		0.117237
2.7	8097.44	-		0.109741
2.8	8397.34	-		0.102929
2.9	8697.25	-		0.09672
3	8997.15	-		0.091048

FEM: Weak axis gradient - maximum temperature

Curve c

Section:	UKC 356 x 406 x 634	
f_y	275	N/mm²
E	210000	N/mm²
Av. Temp	693.8	
$k_{y,\theta}$	0.24488	
$k_{E,\theta}$	0.14116	

Section properties:

Depth of the section	h	474.6	mm
Width of the section	b	424	mm
Web thickness	t_w	47.6	mm
Flange thickness	t_f	77	mm
Root radius	r	15.2	mm
Depth between fillets	d	290.2	mm
Second moment of area	I_{zz}	981000000	mm^4
Radius of gyration	r_{zz}	110	mm
Area of section	A	80800	mm²

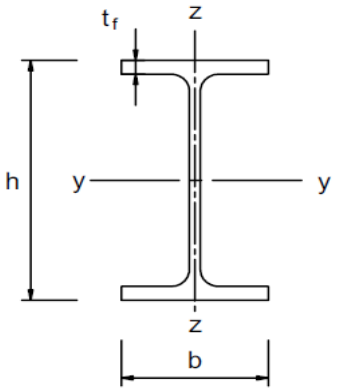

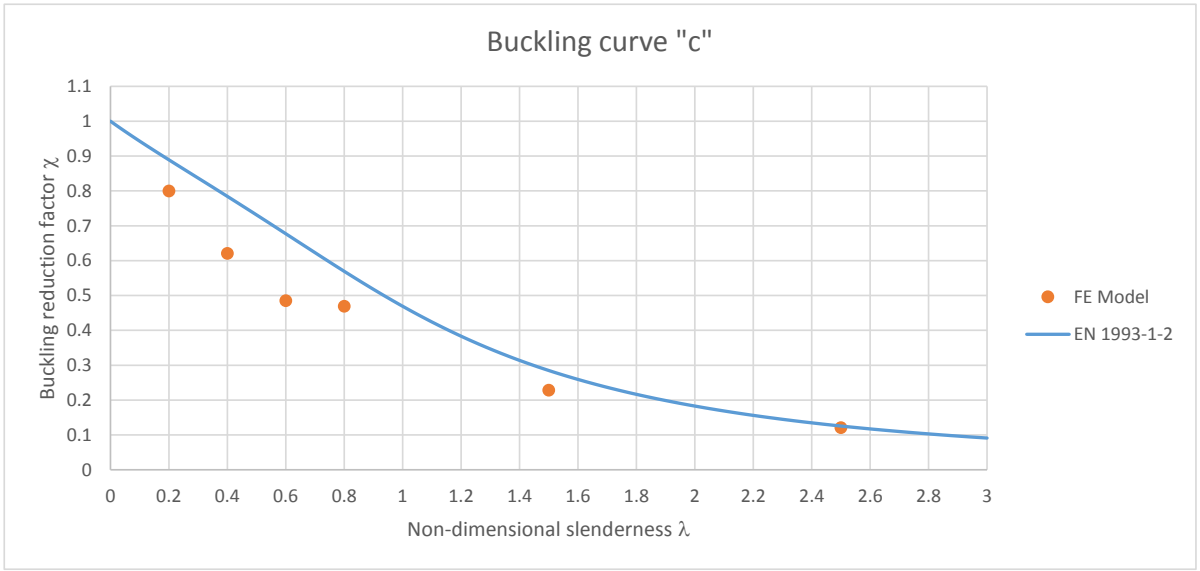

λ_θ	L_{cr} (mm)	N_b (kN)	χ_{FEM}	$\chi_{EN3-1-1}$
0.1	725.05	-		0.94281
0.2	1450.09	4,349.32	0.799325	0.8892
0.3	2175.14	-		0.836859
0.4	2900.18	3,375.77	0.620405	0.784411
0.5	3625.23	-		0.731187
0.6	4350.27	2,638.51	0.48491	0.677166
0.7	5075.32	-		0.622903
0.8	5800.36	2,549.18	0.468493	0.569381
0.9	6525.41	-		0.51776
1	7250.45	-		0.469092
1.1	7975.50	-		0.424132
1.2	8700.54	-		0.383268
1.3	9425.59	-		0.346569
1.4	10150.63	-		0.31387
1.5	10875.68	1,241.88	0.228235	0.284872
1.6	11600.72	-		0.259215
1.7	12325.77	-		0.236522
1.8	13050.81	-		0.216435
1.9	13775.86	-		0.198625
2	14500.90	-		0.182797
2.1	15225.95	-		0.168694
2.2	15950.99	-		0.156093
2.3	16676.04	-		0.144802
2.4	17401.08	-		0.134653
2.5	18126.13	658.21	0.120968	0.125506
2.6	18851.17	-		0.117237
2.7	19576.22	-		0.109741
2.8	20301.26	-		0.102929
2.9	21026.31	-		0.09672
3	21751.35	-		0.091048

FEM: Weak axis gradient - maximum temperature

Curve d

Section:	UKC 356 x 406 x 634	
f_y	205	N/mm²
E	210000	N/mm²
Av. Temp	693.8	
$k_{y,\theta}$	0.24488	
$k_{E,\theta}$	0.14116	

Section properties:

Depth of the section	h	474.6	mm
Width of the section	b	424	mm
Web thickness	t_w	47.6	mm
Flange thickness	t_f	110	mm
Root radius	r	15.2	mm
Depth between fillets	d	224.2	mm
Second moment of area	I_{zz}	1400237632	mm^4
Radius of gyration	r_{zz}	115.152798	mm
Area of section	A	105597.286	mm²

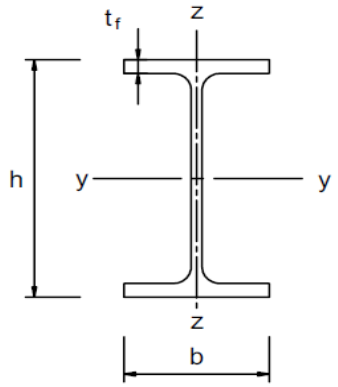

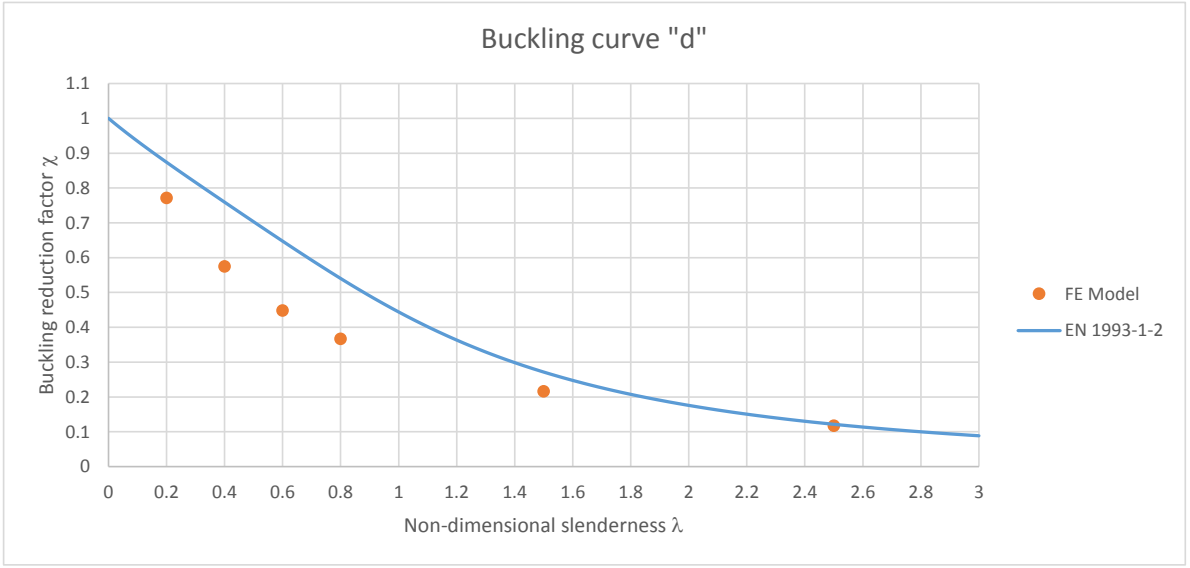

λ_θ	L_{cr} (mm)	N_b (kN)	χ_{FEM}	$\chi_{EN3-1-1}$
0.1	879.10	-		0.934361
0.2	1758.19	4,089.71	0.771494	0.873951
0.3	2637.29	-		0.816105
0.4	3516.38	3,047.43	0.574876	0.759373
0.5	4395.48	-		0.703145
0.6	5274.58	2,376.25	0.448263	0.64747
0.7	6153.67	-		0.592896
0.8	7032.77	1,945.25	0.366958	0.540252
0.9	7911.86	-		0.490409
1	8790.96	-		0.444077
1.1	9670.05	-		0.401689
1.2	10549.15	-		0.363393
1.3	11428.25	-		0.329107
1.4	12307.34	-		0.29859
1.5	13186.44	1,146.10	0.216204	0.271519
1.6	14065.53	-		0.247537
1.7	14944.63	-		0.22629
1.8	15823.73	-		0.207444
1.9	16702.82	-		0.190699
2	17581.92	-		0.175786
2.1	18461.01	-		0.16247
2.2	19340.11	-		0.150548
2.3	20219.21	-		0.139843
2.4	21098.30	-		0.130204
2.5	21977.40	624.62	0.117831	0.1215
2.6	22856.49	-		0.113619
2.7	23735.59	-		0.106463
2.8	24614.68	-		0.09995
2.9	25493.78	-		0.094006
3	26372.88	-		0.088568

Appendix D

Result comparison with construction codes

Comparison with different construction codes

Cross section "a0"

Section:	UKB 457 x 191 x 161	
f_y	460	N/mm²
E	210000	N/mm²

Section properties:

Depth of the section	h	492	mm
Width of the section	b	199.4	mm
Web thickness	t_w	18	mm
Flange thickness	t_f	32	mm
Root radius	r	10.2	mm
Depth between fillets	d	407.6	mm
Moment of inertia	I_{zz}	42500000	mm^4
Radius of gyration	r_{zz}	45.5	mm
Area of section	A	20600	mm²

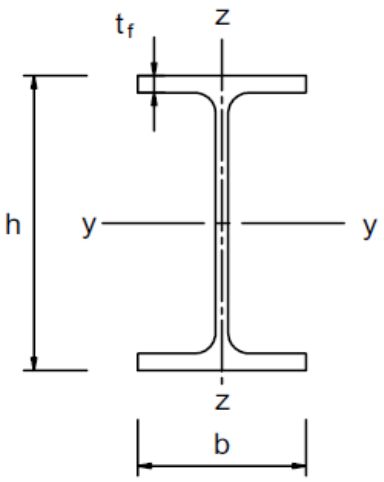

Strong axis gradient - Maximum gradient

Maximum temperature: 490 °C

Eurocode 1993-1-2:

$k_{y,\theta}$	0.802
$k_{E,\theta}$	0.61

L (mm)	λ	λ_θ	α	ϕ_θ	χ_{fi}	$N_{b,fi,Rd}$ (kN)
522.55	0.171392	0.196523	0.464588	0.564962	0.913541	6942.688
1045.11	0.342784	0.393045	0.464588	0.668544	0.826893	6284.18
1567.66	0.514175	0.589568	0.464588	0.810748	0.731382	5558.318
2090.22	0.685567	0.78609	0.464588	0.991573	0.626583	4761.879
3919.16	1.285439	1.473919	0.464588	1.928602	0.315217	2395.575
6531.93	2.142398	2.456532	0.464588	4.087912	0.135955	1033.221

AISC 2005:

k_y	0.781081	f_y	359.2973	N/mm²
k_E	0.567838	E	119245.9	N/mm²

L (mm)	F_e (MPa)	F_{cr} (Mpa)	ϕP_n (kN)
522.55	8922.838	351.2063	6511.364
1045.11	2230.709	328.0101	6081.307
1567.66	991.4264	292.704	5426.733
2090.22	557.6774	249.5668	4626.969
3919.16	158.6282	139.117	2579.228
6531.93	57.10616	50.0821	928.5222

AS 4100:

f_y 276.6667 N/mm²

E 146376.2 N/mm²

Flange slenderness: λ_e 6.555164 λ_{ey} 16

Web slenderness: λ_e 23.82155 λ_{ey} 45

Effective widths:

Flange: b_e 199.4 mm

Web: b_e 407.6 mm

Effective area: A_e 20600 mm²

Form factor: k_f 1

L (mm)	λ_n	α_a	α_b	λ	η	ξ	α_c	N_s (N)	N_c (kN)
522.55	12.08172	-1.480967	0	12.08172	0	28.24584	1	5699333	5699.333
1045.11	24.16343	9.890245	0	24.16343	0.034763	7.67759	0.963987	5699333	5494.081
1567.66	36.24515	17.00324	0	36.24515	0.074149	3.811463	0.919836	5699333	5242.45
2090.22	48.32686	20.05889	0	48.32686	0.113536	2.430999	0.868461	5699333	4949.647
3919.16	90.61286	18.24783	0	90.61286	0.251388	1.117259	0.605645	5699333	3451.774
6531.93	151.0214	12.80867	0	151.0214	0.44832	0.757183	0.290086	5699333	1653.298

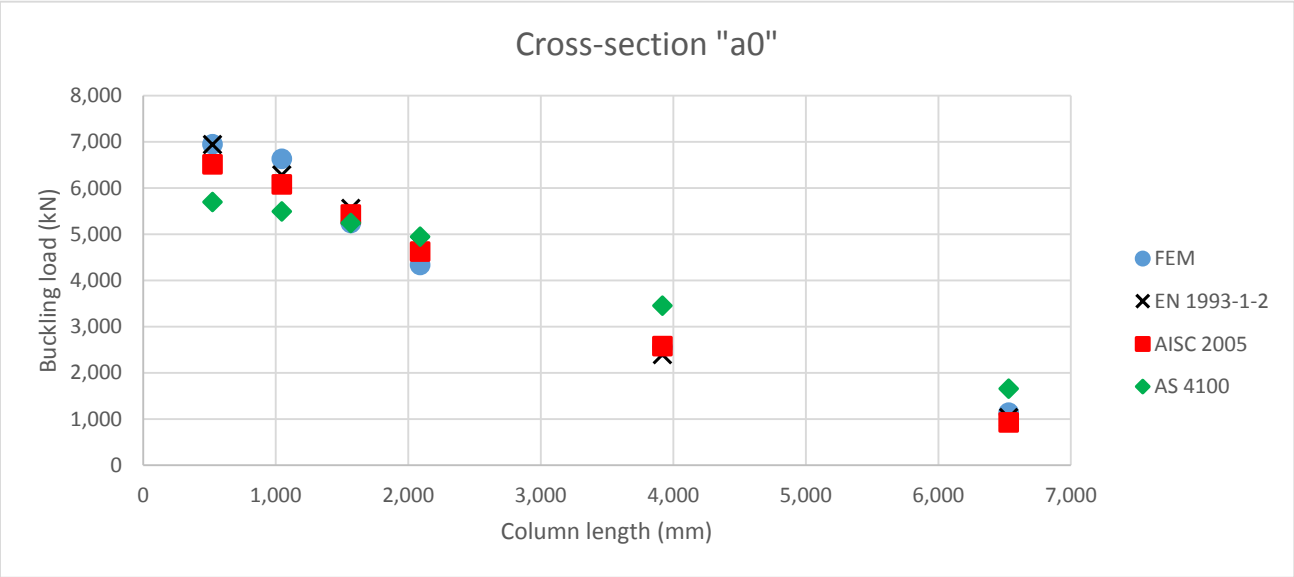

Cross section "a"

Section: UKB 1016 x 305 x 487

f_y 460 N/mm²

E 210000 N/mm²

Section properties:

Depth of the section	h	1036.3	mm
Width of the section	b	308.5	mm
Web thickness	t_w	30	mm
Flange thickness	t_f	54.1	mm
Root radius	r	30	mm
Depth between fillets	d	868.1	mm
Moment of inertia	I_{zz}	2.67E+08	mm^4
Radius of gyration	r_{zz}	65.7	mm
Area of section	A	62000	mm²

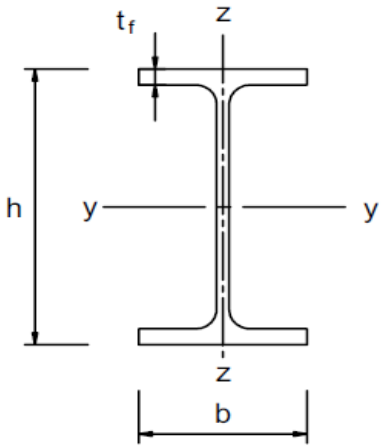

Strong axis gradient - Maximum gradient

Maximum temperature: 490 °C

Eurocode 1993-1-2:

$k_{y,\theta}$ 0.802

$k_{E,\theta}$ 0.61

L (mm)	λ	λ_θ	α	ϕ_θ	χ_{fi}	$N_{b,fi,Rd}$ (kN)
754.55	0.171295	0.196412	0.464588	0.564914	0.913589	20896.56
1509.09	0.34259	0.392823	0.464588	0.668406	0.826995	18915.88
2263.64	0.513886	0.589235	0.464588	0.810475	0.731552	16732.82
3018.18	0.685181	0.785647	0.464588	0.991122	0.626825	14337.4
5659.09	1.284714	1.473088	0.464588	1.927184	0.315479	7215.967
9431.82	2.14119	2.455147	0.464588	4.084189	0.13609	3112.8

AISC 2005:

k_y 0.781081 f_y 359.2973 N/mm²

k_E 0.567838 E 119245.9 N/mm²

L (mm)	F_e (MPa)	F_{cr} (Mpa)	ϕP_n (kN)
754.55	8922.838	351.2063	19597.31
1509.09	2230.709	328.0101	18302.96
2263.64	991.4264	292.704	16332.89
3018.18	557.6774	249.5668	13925.83
5659.09	158.6282	139.117	7762.726
9431.82	57.10616	50.0821	2794.581

AS 4100:

f_y	276.6667	N/mm²
E	146376.2	N/mm²

Flange slenderness:	λ_e	5.998827	λ_{ey}	16
Web slenderness:	λ_e	30.44086	λ_{ey}	45

Effective widths:

Flange:	b_e	308.5	mm
Web:	b_e	868.1	mm

Effective area:	A_e	62000	mm²

Form factor:	k_f	1

L (mm)	λ_n	α_a	α_b	λ	η	ξ	α_c	N_s (N)	N_c (kN)
754.55	12.08172	-1.480967	1	10.60075	0	36.53976	1	17153333	17153.33
1509.09	24.16343	9.890245	1	34.05368	0.067005	4.226434	0.928268	17153333	15922.9
2263.64	36.24515	17.00324	1	53.24838	0.12958	2.113463	0.844614	17153333	14487.95
3018.18	48.32686	20.05889	1	68.38575	0.178928	1.520965	0.758527	17153333	13011.27
5659.09	90.61286	18.24783	1	108.8607	0.310876	0.947996	0.48411	17153333	8304.106
9431.82	151.0214	12.80867	1	163.8301	0.490076	0.724841	0.251967	17153333	4322.077

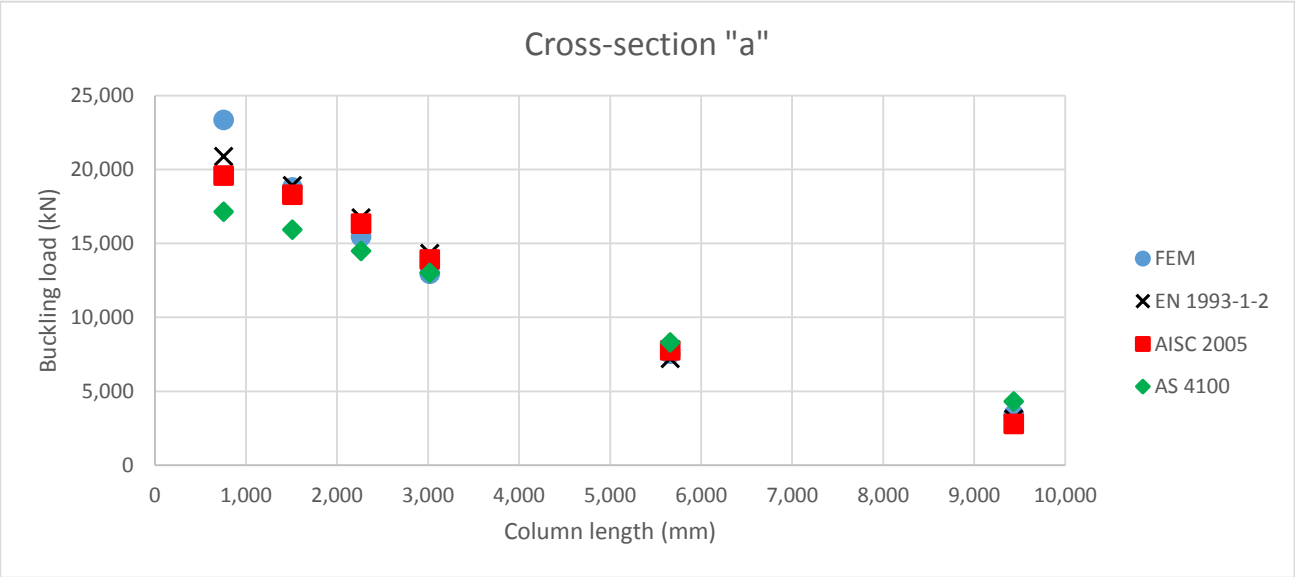

Cross section "b"

Section: UKB 457 x 191 x 161

f_y 275 N/mm²

E 210000 N/mm²

Section properties:

Depth of the section	h	492	mm
Width of the section	b	199.4	mm
Web thickness	t_w	18	mm
Flange thickness	t_f	32	mm
Root radius	r	10.2	mm
Depth between fillets	d	407.6	mm
Moment of inertia	I_{zz}	42500000	mm^4
Radius of gyration	r_{zz}	45.5	mm
Area of section	A	20600	mm²

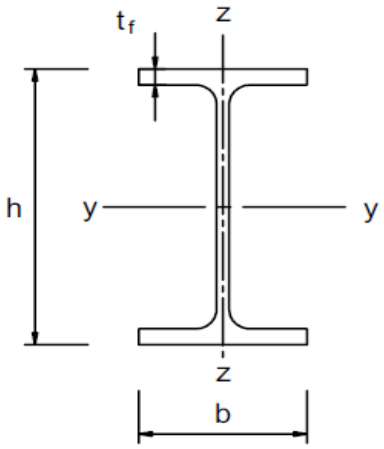

Strong axis gradient - Maximum gradient

Maximum temperature: 490 °C

Eurocode 1993-1-2:

$k_{y,\theta}$	0.802
$k_{E,\theta}$	0.61

L (mm)	λ	λ_θ	α	ϕ_θ	χ_{fi}	$N_{b,fi,Rd}$ (kN)
675.84	0.171392	0.196523	0.600871	0.578353	0.891033	4048.256
1351.68	0.342784	0.393045	0.600871	0.695327	0.788079	3580.505
2027.52	0.514175	0.589568	0.600871	0.850922	0.682827	3102.308
2703.36	0.685567	0.78609	0.600871	1.045138	0.576739	2620.314
5068.80	1.285439	1.473919	0.600871	2.029036	0.292098	1327.098
8448.00	2.142398	2.456532	0.600871	4.255303	0.129367	587.758

AISC 2005:

k_y	0.781081	f_y	214.7973	N/mm²
k_E	0.567838	E	119245.9	N/mm²

L (mm)	F_e (MPa)	F_{cr} (Mpa)	ϕP_n (kN)
675.84	5334.305	209.9603	3892.663
1351.68	1333.576	196.093	3635.564
2027.52	592.7006	174.9861	3244.242
2703.36	333.3941	149.1976	2766.123
5068.80	94.83209	83.16775	1541.93
8448.00	34.13955	29.94039	555.0948

AS 4100:

f_y	165.3986	N/mm²
E	146376.2	N/mm²

Flange slenderness:	λ_e	5.068402	λ_{ey}	16
Web slenderness:	λ_e	18.41864	λ_{ey}	45

Effective widths:

Flange:	b_e	199.4	mm
Web:	b_e	407.6	mm

Effective area:	A_e	20600	mm²

Form factor:	k_f	1

L (mm)	λ_n	α_a	α_b	λ	η	ξ	α_c	N_s (N)	N_c (kN)
675.84	12.08172	-1.480967	0	12.08172	0	28.24584	1	3407210	3407.21
1351.68	24.16343	9.890245	0	24.16343	0.034763	7.67759	0.963987	3407210	3284.505
2027.52	36.24515	17.00324	0	36.24515	0.074149	3.811463	0.919836	3407210	3134.073
2703.36	48.32686	20.05889	0	48.32686	0.113536	2.430999	0.868461	3407210	2959.028
5068.80	90.61286	18.24783	0	90.61286	0.251388	1.117259	0.605645	3407210	2063.56
8448.00	151.0214	12.80867	0	151.0214	0.44832	0.757183	0.290086	3407210	988.3847

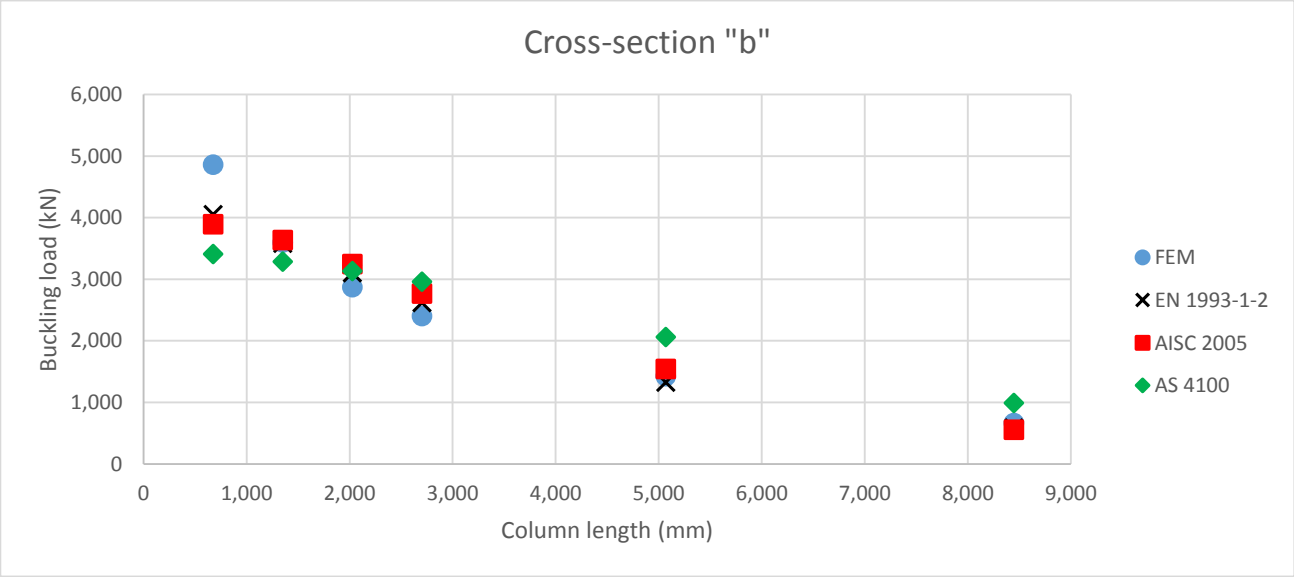

Cross section "c"

Section: UKC 356 x 406 x 634

f_y 275 N/mm²

E 210000 N/mm²

Section properties:

Depth of the section	h	474.6	mm
Width of the section	b	424	mm
Web thickness	t_w	47.6	mm
Flange thickness	t_f	77	mm
Root radius	r	15.2	mm
Depth between fillets	d	290.2	mm
Moment of inertia	I_{zz}	9.81E+08	mm^4
Radius of gyration	r_{zz}	110	mm
Area of section	A	80800	mm²

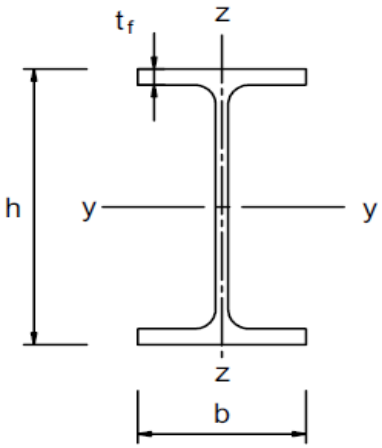

Strong axis gradient - Maximum gradient

Maximum temperature: 490 °C

Eurocode 1993-1-2:

$k_{y,\theta}$ 0.802

$k_{E,\theta}$ 0.61

L (mm)	λ	λ_θ	α	ϕ_θ	χ_{fi}	$N_{b,fi,Rd}$ (kN)
1633.90	0.170806	0.195851	0.600871	0.578019	0.891387	15884.91
3267.80	0.341612	0.391702	0.600871	0.694396	0.788787	14056.54
4901.70	0.512418	0.587553	0.600871	0.849131	0.68392	12187.75
6535.60	0.683224	0.783404	0.600871	1.042223	0.578164	10303.13
12254.25	1.281046	1.468882	0.600871	2.020112	0.29352	5230.661
20423.75	2.135077	2.448137	0.600871	4.232194	0.130133	2319.025

AISC 2005:

k_y 0.781081 f_y 214.7973 N/mm²

k_E 0.567838 E 119245.9 N/mm²

L (mm)	F_e (MPa)	F_{cr} (Mpa)	ϕP_n (kN)
1633.90	5334.305	209.9603	15268.31
3267.80	1333.576	196.093	14259.88
4901.70	592.7006	174.9861	12724.99
6535.60	333.3941	149.1976	10849.65
12254.25	94.83209	83.16775	6047.959
20423.75	34.13955	29.94039	2177.265

AS 4100:

f_y	165.3986	N/mm²
E	146376.2	N/mm²

Flange slenderness:	λ_e	4.478896	λ_{ey}	16
Web slenderness:	λ_e	4.958911	λ_{ey}	45

Effective widths:

Flange:	b_e	424	mm
Web:	b_e	290.2	mm

Effective area: A_e 80800 mm²

Form factor: k_f 1

L (mm)	λ_n	α_a	α_b	λ	η	ξ	α_c	N_s (N)	N_c (kN)
1633.90	12.08172	-1.480967	1	10.60075	0	36.53976	1	13364203	13364.2
3267.80	24.16343	9.890245	1	34.05368	0.067005	4.226434	0.928268	13364203	12405.57
4901.70	36.24515	17.00324	1	53.24838	0.12958	2.113463	0.844614	13364203	11287.6
6535.60	48.32686	20.05889	1	68.38575	0.178928	1.520965	0.758527	13364203	10137.11
12254.25	90.61286	18.24783	1	108.8607	0.310876	0.947996	0.48411	13364203	6469.749
20423.75	151.0214	12.80867	1	163.8301	0.490076	0.724841	0.251967	13364203	3367.34

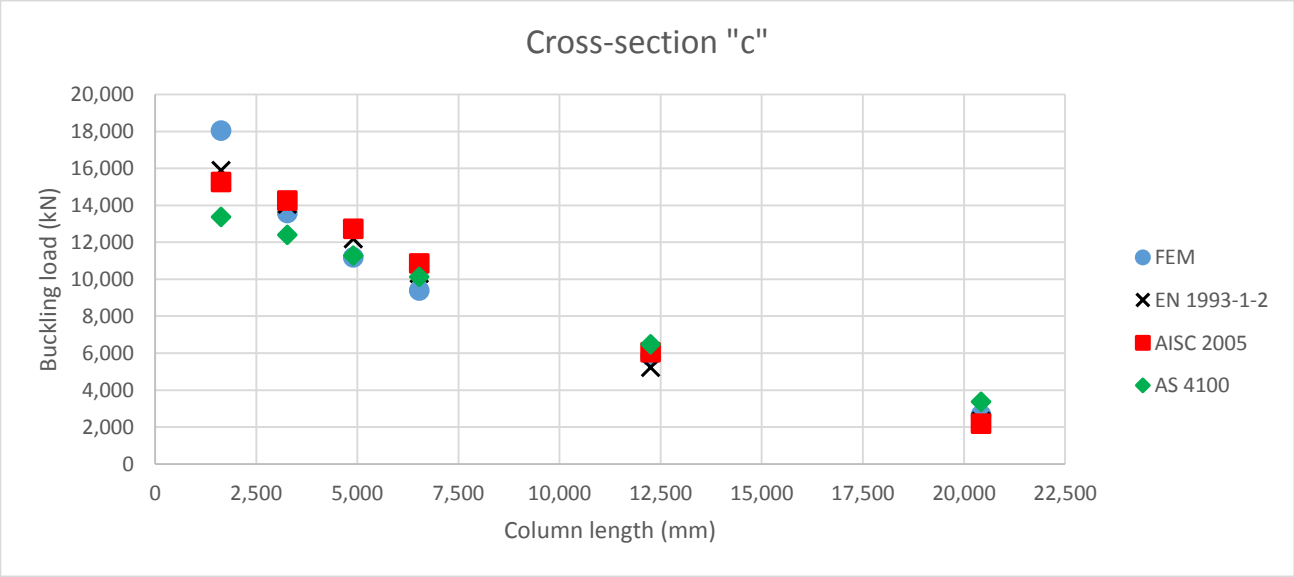

Cross section "d"

Section: UKC 356 x 406 x 634

f_y 205 N/mm²

E 210000 N/mm²

Section properties:

Depth of the section	h	474.6	mm
Width of the section	b	424	mm
Web thickness	t_w	47.6	mm
Flange thickness	t_f	110	mm
Root radius	r	15.2	mm
Depth between fillets	d	224.2	mm
Moment of inertia	I_{zz}	1.4E+09	mm^4
Radius of gyration	r_{zz}	115.1528	mm
Area of section	A	105597.3	mm²

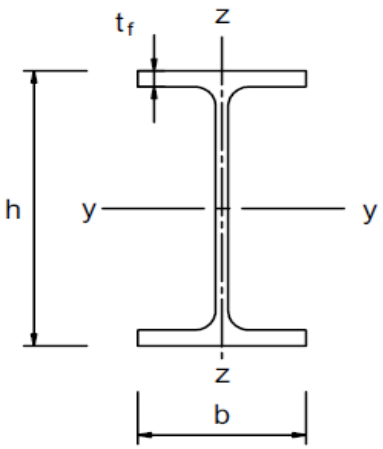

Strong axis gradient - Maximum gradient

Maximum temperature: 490 °C

Eurocode 1993-1-2:

$k_{y,\theta}$	0.802
$k_{E,\theta}$	0.61

L (mm)	λ	λ_θ	α	ϕ_θ	χ_{fi}	$N_{b,fi,Rd}$ (kN)
1981.06	0.171096	0.196183	0.695938	0.58751	0.876197	15211.87
3962.11	0.342192	0.392366	0.695938	0.713507	0.763683	13258.49
5943.17	0.513288	0.58855	0.695938	0.877992	0.653803	11350.83
7924.22	0.684384	0.784733	0.695938	1.080965	0.548128	9516.193
14857.92	1.283219	1.471374	0.695938	2.094463	0.278937	4842.687
24763.19	2.138699	2.45229	0.695938	4.360184	0.125543	2179.587

AISC 2005:

k_y	0.781081	f_y	160.1216	N/mm²
k_E	0.567838	E	119245.9	N/mm²

L (mm)	F_e (MPa)	F_{cr} (Mpa)	ϕP_n (kN)
1981.06	3976.482	156.5158	14874.88
3962.11	994.1205	146.1784	13892.44
5943.17	441.8313	130.4442	12397.1
7924.22	248.5301	111.22	10570.08
14857.92	70.69302	61.99777	5892.117
24763.19	25.44949	22.3192	2121.162

AS 4100:

f_y	123.2971	N/mm²
E	146376.2	N/mm²

Flange slenderness:	λ_e	2.706946	λ_{ey}	16
Web slenderness:	λ_e	3.307768	λ_{ey}	45

Effective widths:

Flange:	b_e	424	mm
Web:	b_e	224.2	mm

Effective area: A_e 105597.3 mm²

Form factor: k_f 1

L (mm)	λ_n	α_a	α_b	λ	η	ξ	α_c	N_s (N)	N_c (kN)
1981.06	12.08172	-1.480967	1	10.60075	0	36.53976	1	13019839	13019.84
3962.11	24.16343	9.890245	1	34.05368	0.067005	4.226434	0.928268	13019839	12085.91
5943.17	36.24515	17.00324	1	53.24838	0.12958	2.113463	0.844614	13019839	10996.74
7924.22	48.32686	20.05889	1	68.38575	0.178928	1.520965	0.758527	13019839	9875.904
14857.92	90.61286	18.24783	1	108.8607	0.310876	0.947996	0.48411	13019839	6303.039
24763.19	151.0214	12.80867	1	163.8301	0.490076	0.724841	0.251967	13019839	3280.572

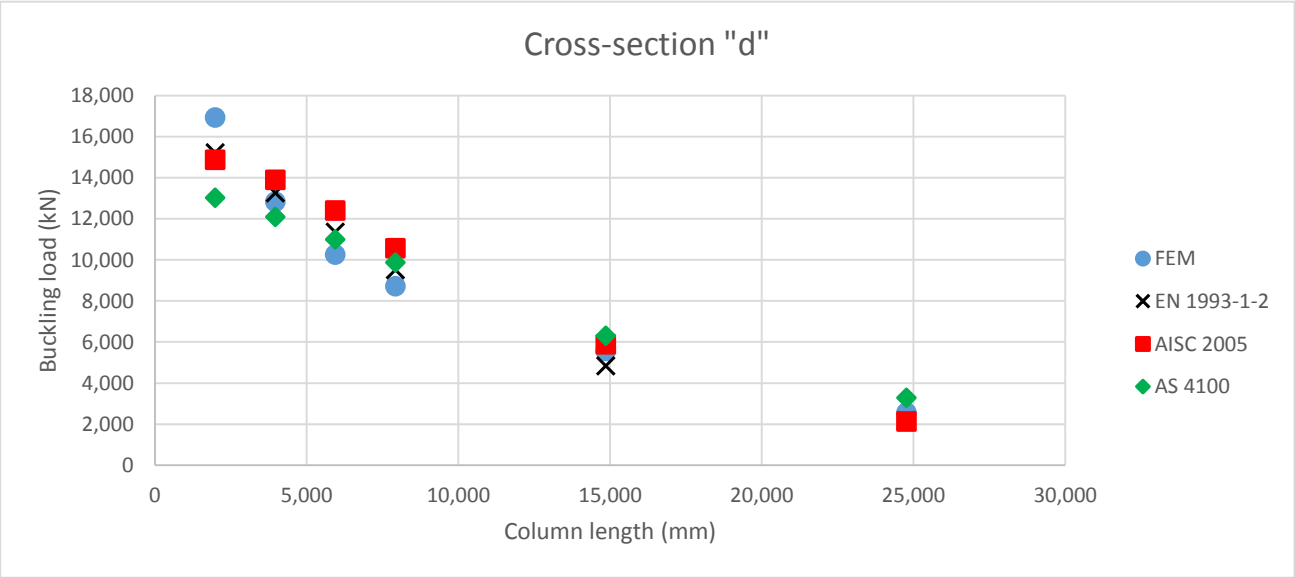

Comparison with different construction codes

Cross section "a0"

Section: UKB 457 x 191 x 161

f_y 460 N/mm²

E 210000 N/mm²

Section properties:

Depth of the section	h	492	mm
Width of the section	b	199.4	mm
Web thickness	t_w	18	mm
Flange thickness	t_f	32	mm
Root radius	r	10.2	mm
Depth between fillets	d	407.6	mm
Moment of inertia	I_{zz}	42500000	mm^4
Radius of gyration	r_{zz}	45.5	mm
Area of section	A	20600	mm²

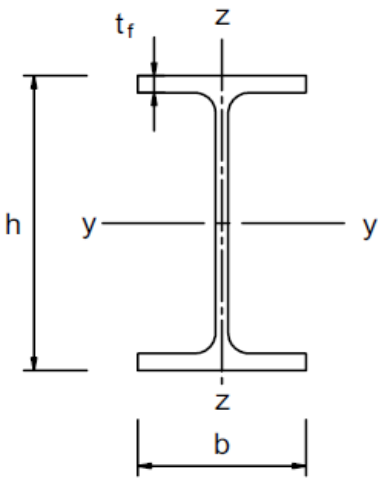

Strong axis gradient - Maximum temperature

Maximum temperature 532 °C

Eurocode 1993-1-2:

$k_{y,\theta}$ 0.6808

$k_{E,\theta}$ 0.5072

L (mm)	λ	λ_θ	α	ϕ_θ	χ_{fi}	$N_{b,fi,Rd}$ (kN)
533.73	0.175057	0.202815	0.464588	0.56768	0.910836	5876.038
1067.46	0.350114	0.405629	0.464588	0.676493	0.821094	5297.093
1601.19	0.525171	0.608444	0.464588	0.82644	0.721644	4655.514
2134.92	0.700228	0.811259	0.464588	1.017521	0.61286	3953.719
4002.97	1.312927	1.52111	0.464588	2.010234	0.300798	1940.528
6671.61	2.188212	2.535184	0.464588	4.302488	0.128556	829.3466

AISC 2005:

k_y 0.675135 f_y 310.5622 N/mm²

k_E 0.49973 E 104943.2 N/mm²

L (mm)	F_e (MPa)	F_{cr} (Mpa)	ϕP_n (kN)
533.73	7527.235	303.3984	5625.007
1067.46	1881.809	282.8836	5244.661
1601.19	836.3594	251.7281	4667.038
2134.92	470.4522	213.7889	3963.646
4002.97	133.8175	117.358	2175.816
6671.61	48.1743	42.24886	783.2939

AS 4100:

f_y	248.6667	N/mm²
E	133102.5	N/mm²

Flange slenderness:	λ_e	6.214611	λ_{ey}	16
Web slenderness:	λ_e	22.58398	λ_{ey}	45

Effective widths:

Flange:	b_e	199.4	mm
Web:	b_e	407.6	mm

Effective area: A_e 20600 mm²

Form factor: k_f 1

L (mm)	λ_n	α_a	α_b	λ	η	ξ	α_c	N_s (N)	N_c (kN)
533.73	11.69898	-1.883652	0	11.69898	0	30.09093	1	5122533	5122.533
1067.46	23.39797	9.281517	0	23.39797	0.032267	8.136439	0.966629	5122533	4951.59
1601.19	35.09695	16.52339	0	35.09695	0.070406	4.019368	0.924282	5122533	4734.666
2134.92	46.79594	19.84217	0	46.79594	0.108545	2.55018	0.875501	5122533	4484.782
4002.97	87.74238	18.54676	0	87.74238	0.24203	1.153384	0.625964	5122533	3206.52
6671.61	146.2373	13.1498	0	146.2373	0.432724	0.771332	0.306371	5122533	1569.394

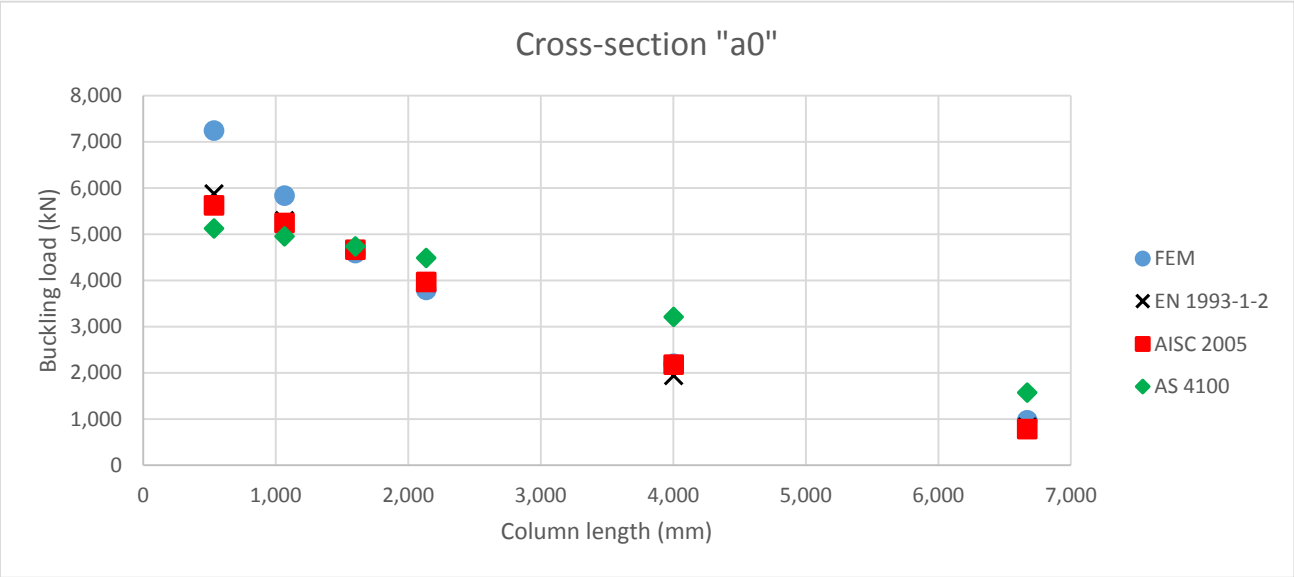

Cross section "a"

Section: UKB 1016 x 305 x 487

f_y	460	N/mm²
E	210000	N/mm²

Section properties:

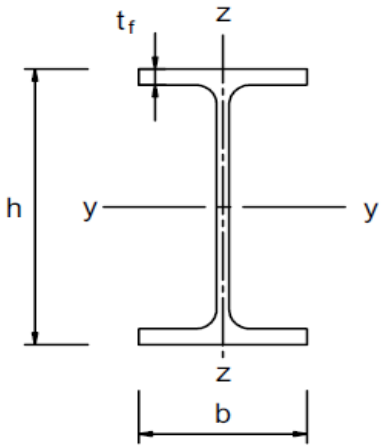

Depth of the section	h	1036.3	mm
Width of the section	b	308.5	mm
Web thickness	t_w	30	mm
Flange thickness	t_f	54.1	mm
Root radius	r	30	mm
Depth between fillets	d	868.1	mm
Moment of inertia	I_{zz}	2.67E+08	mm^4
Radius of gyration	r_{zz}	65.7	mm
Area of section	A	62000	mm²

Strong axis gradient - Maximum temperature

Maximum temperature 532 °C

Eurocode 1993-1-2:

$k_{y,\theta}$	0.6808
$k_{E,\theta}$	0.5072

L (mm)	λ	λ_θ	α	ϕ_θ	χ_{fi}	$N_{b,fi,Rd}$ (kN)
770.68	0.174958	0.2027	0.464588	0.56763	0.910885	17686.12
1541.36	0.349916	0.405401	0.464588	0.676347	0.8212	15944.76
2312.04	0.524875	0.608101	0.464588	0.826152	0.721822	14015.19
3082.72	0.699833	0.810801	0.464588	1.017044	0.613109	11904.39
5780.11	1.312187	1.520253	0.464588	2.00873	0.301053	5845.367
9633.51	2.186978	2.533754	0.464588	4.298532	0.128685	2498.6

AISC 2005:

k_y	0.675135	f_y	310.5622	N/mm²
k_E	0.49973	E	104943.2	N/mm²

L (mm)	F_e (MPa)	F_{cr} (Mpa)	ϕP_n (kN)
770.68	7527.235	303.3984	16929.63
1541.36	1881.809	282.8836	15784.9
2312.04	836.3594	251.7281	14046.43
3082.72	470.4522	213.7889	11929.42
5780.11	133.8175	117.358	6548.574
9633.51	48.1743	42.24886	2357.487

AS 4100:

f_y 248.6667 N/mm²

E 133102.5 N/mm²

Flange slenderness: λ_e 5.687176 λ_{ey} 16

Web slenderness: λ_e 28.8594 λ_{ey} 45

Effective widths:

Flange: b_e 308.5 mm

Web: b_e 868.1 mm

Effective area: A_e 62000 mm²

Form factor: k_f 1

L (mm)	λ_n	α_a	α_b	λ	η	ξ	α_c	N_s (N)	N_c (kN)
770.68	11.69898	-1.883652	1	9.815332	0	42.53829	1	15417333	15417.33
1541.36	23.39797	9.281517	1	32.67949	0.062525	4.529432	0.933445	15417333	14391.24
2312.04	35.09695	16.52339	1	51.62034	0.124272	2.208775	0.852715	15417333	13146.59
3082.72	46.79594	19.84217	1	66.63811	0.17323	1.570023	0.769455	15417333	11862.94
5780.11	87.74238	18.54676	1	106.2891	0.302493	0.966931	0.500053	15417333	7709.484
9633.51	146.2373	13.1498	1	159.3871	0.475592	0.735242	0.264353	15417333	4075.617

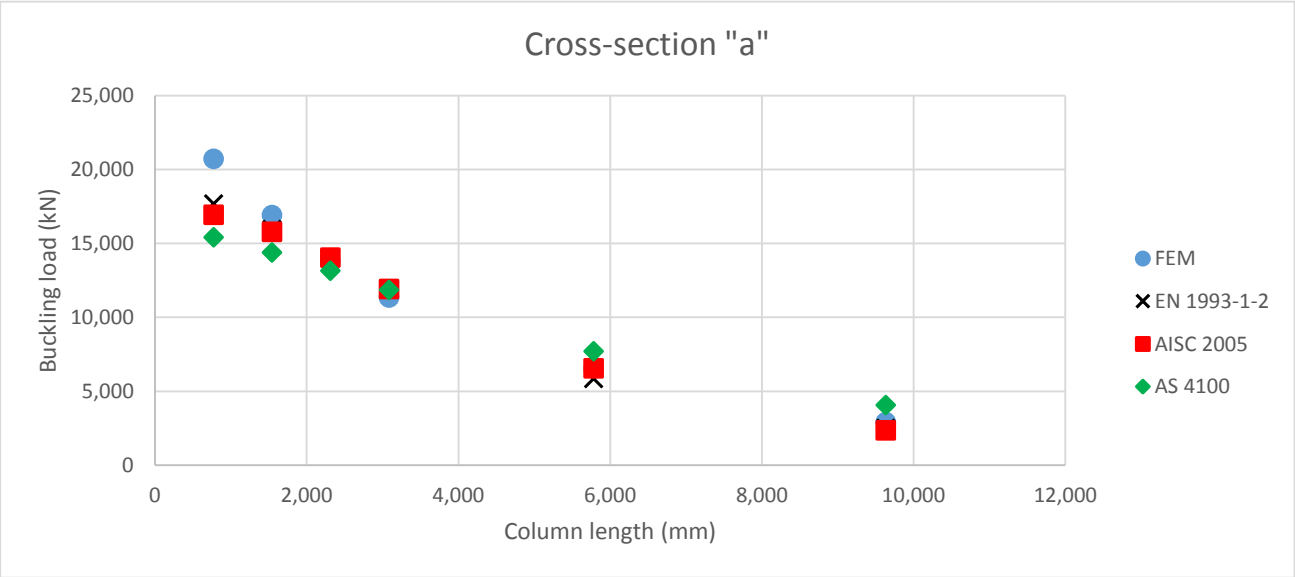

Cross section "b"

Section: UKB 457 x 191 x 161

f_y 275 N/mm²

E 210000 N/mm²

Section properties:

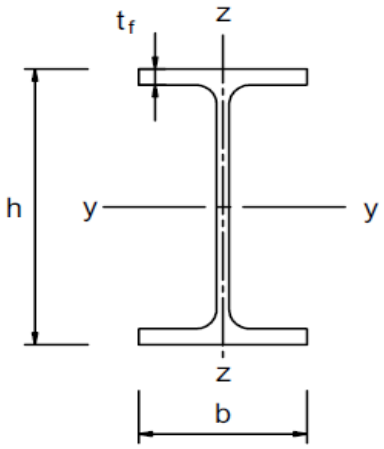

Depth of the section	h	492	mm
Width of the section	b	199.4	mm
Web thickness	t_w	18	mm
Flange thickness	t_f	32	mm
Root radius	r	10.2	mm
Depth between fillets	d	407.6	mm
Moment of inertia	I_{zz}	42500000	mm^4
Radius of gyration	r_{zz}	45.5	mm
Area of section	A	20600	mm²

Strong axis gradient - Maximum temperature

Maximum temperature 532 °C

Eurocode 1993-1-2:

$k_{y,\theta}$ 0.6808

$k_{E,\theta}$ 0.5072

L (mm)	λ	λ_θ	α	ϕ_θ	χ_{fi}	$N_{b,fi,Rd}$ (kN)
690.29	0.175057	0.202815	0.600871	0.5815	0.887718	3423.69
1380.59	0.350114	0.405629	0.600871	0.704133	0.781438	3013.797
2070.88	0.525171	0.608444	0.600871	0.8679	0.672582	2593.968
2761.17	0.700228	0.811259	0.600871	1.072801	0.563453	2173.087
5177.20	1.312927	1.52111	0.600871	2.113884	0.279191	1076.763
8628.66	2.188212	2.535184	0.600871	4.475238	0.122502	472.4571

AISC 2005:

k_y 0.675135 f_y 185.6622 N/mm²

k_E 0.49973 E 104943.2 N/mm²

L (mm)	F_e (MPa)	F_{cr} (Mpa)	ϕP_n (kN)
690.29	4499.977	181.3795	3362.776
1380.59	1124.994	169.1152	3135.395
2070.88	499.9975	150.4896	2790.077
2761.17	281.2486	127.8086	2369.571
5177.20	79.9996	70.15965	1300.76
8628.66	28.79985	25.25747	468.2735

AS 4100:

f_y	148.6594	N/mm²
E	133102.5	N/mm²

Flange slenderness:	λ_e	4.805088	λ_{ey}	16
Web slenderness:	λ_e	17.46175	λ_{ey}	45

Effective widths:

Flange:	b_e	199.4	mm
Web:	b_e	407.6	mm

Effective area: A_e 20600 mm²

Form factor: k_f 1

L (mm)	λ_n	α_a	α_b	λ	η	ξ	α_c	N_s (N)	N_c (kN)
690.29	11.69898	-1.883652	0	11.69898	0	30.09093	1	3062384	3062.384
1380.59	23.39797	9.281517	0	23.39797	0.032267	8.136439	0.966629	3062384	2960.19
2070.88	35.09695	16.52339	0	35.09695	0.070406	4.019368	0.924282	3062384	2830.507
2761.17	46.79594	19.84217	0	46.79594	0.108545	2.55018	0.875501	3062384	2681.119
5177.20	87.74238	18.54676	0	87.74238	0.24203	1.153384	0.625964	3062384	1916.941
8628.66	146.2373	13.1498	0	146.2373	0.432724	0.771332	0.306371	3062384	938.2244

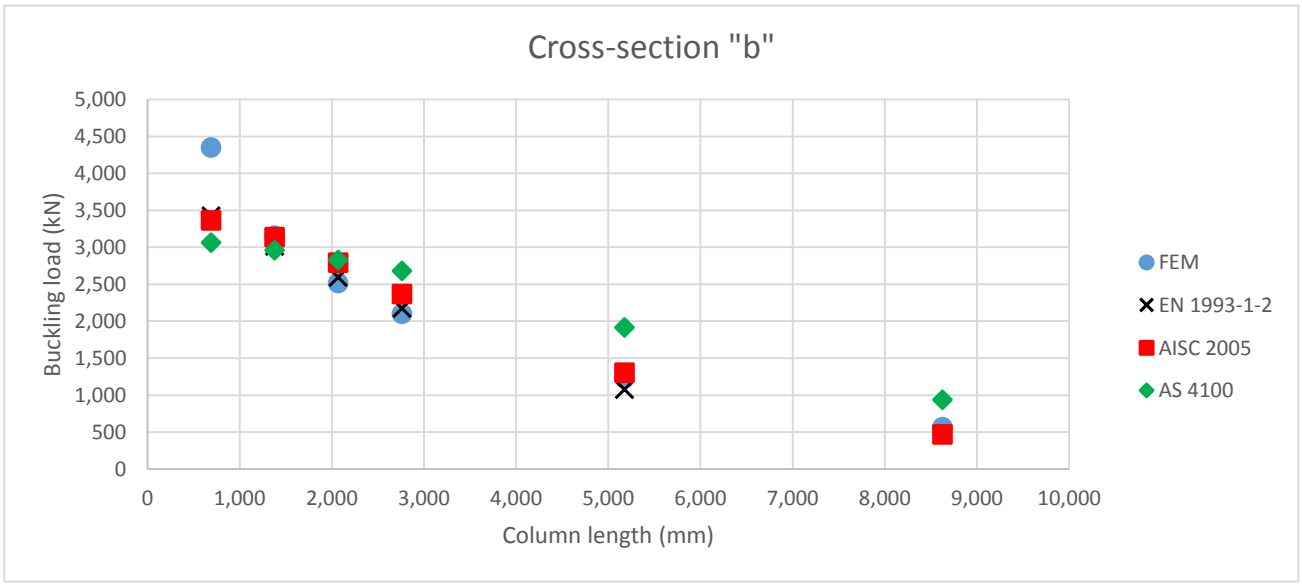

Cross section "c"

Section: UKC 356 x 406 x 634

f_y 275 N/mm²

E 210000 N/mm²

Section properties:

Depth of the section	h	474.6	mm
Width of the section	b	424	mm
Web thickness	t_w	47.6	mm
Flange thickness	t_f	77	mm
Root radius	r	15.2	mm
Depth between fillets	d	290.2	mm
Moment of inertia	I_{zz}	9.81E+08	mm^4
Radius of gyration	r_{zz}	110	mm
Area of section	A	80800	mm²

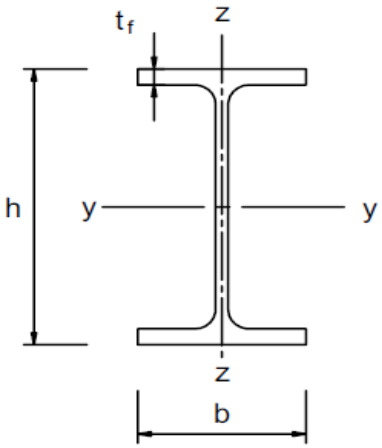

Strong axis gradient - Maximum temperature

Maximum temperature 532 °C

Eurocode 1993-1-2:

$k_{y,\theta}$ 0.6808

$k_{E,\theta}$ 0.5072

L (mm)	λ	λ_θ	α	ϕ_θ	χ_{fi}	$N_{b,fi,Rd}$ (kN)
1668.84	0.174459	0.202122	0.600871	0.581151	0.888083	13434.36
3337.68	0.348917	0.404243	0.600871	0.703155	0.78217	11832.18
5006.52	0.523376	0.606365	0.600871	0.866013	0.673711	10191.48
6675.36	0.697835	0.808487	0.600871	1.069723	0.56491	8545.612
12516.30	1.30844	1.515912	0.600871	2.104428	0.280576	4244.379
20860.50	2.180734	2.52652	0.600871	4.450709	0.123232	1864.173

AISC 2005:

k_y 0.675135 f_y 185.6622 N/mm²

k_E 0.49973 E 104943.2 N/mm²

L (mm)	F_e (MPa)	F_{cr} (Mpa)	ϕP_n (kN)
1668.84	4499.977	181.3795	13189.92
3337.68	1124.994	169.1152	12298.05
5006.52	499.9975	150.4896	10943.6
6675.36	281.2486	127.8086	9294.24
12516.30	79.9996	70.15965	5102.009
20860.50	28.79985	25.25747	1836.723

AS 4100:

f_y	148.6594	N/mm²
E	133102.5	N/mm²

Flange slenderness:	λ_e	4.246209	λ_{ey}	16
Web slenderness:	λ_e	4.701286	λ_{ey}	45

Effective widths:

Flange:	b_e	424	mm
Web:	b_e	290.2	mm

Effective area: A_e 80800 mm²

Form factor: k_f 1

L (mm)	λ_n	α_a	α_b	λ	η	ξ	α_c	N_s (N)	N_c (kN)
1668.84	11.69898	-1.883652	1	9.815332	0	42.53829	1	12011681	12011.68
3337.68	23.39797	9.281517	1	32.67949	0.062525	4.529432	0.933445	12011681	11212.25
5006.52	35.09695	16.52339	1	51.62034	0.124272	2.208775	0.852715	12011681	10242.54
6675.36	46.79594	19.84217	1	66.63811	0.17323	1.570023	0.769455	12011681	9242.448
12516.30	87.74238	18.54676	1	106.2891	0.302493	0.966931	0.500053	12011681	6006.478
20860.50	146.2373	13.1498	1	159.3871	0.475592	0.735242	0.264353	12011681	3175.323

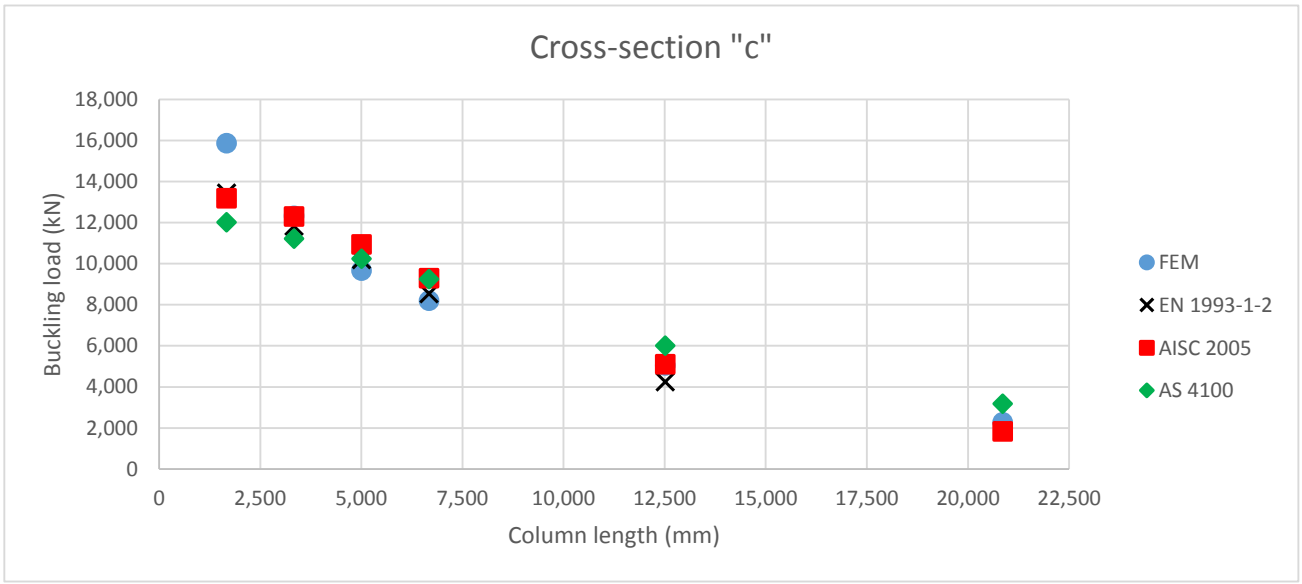

Cross section "d"

Section: UKC 356 x 406 x 634

f_y 205 N/mm²

E 210000 N/mm²

Section properties:

Depth of the section	h	474.6	mm
Width of the section	b	424	mm
Web thickness	t_w	47.6	mm
Flange thickness	t_f	110	mm
Root radius	r	15.2	mm
Depth between fillets	d	224.2	mm
Moment of inertia	I_{zz}	1.4E+09	mm^4
Radius of gyration	r_{zz}	115.1528	mm
Area of section	A	105597.3	mm²

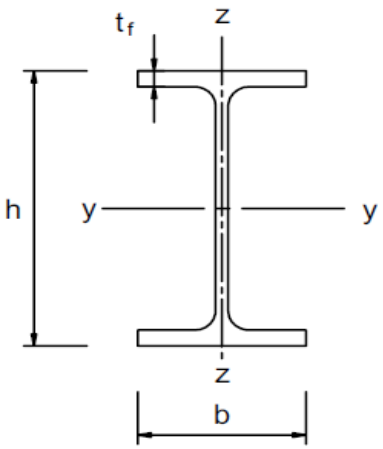

Strong axis gradient - Maximum temperature

Maximum temperature 532 °C

Eurocode 1993-1-2:

$k_{y,\theta}$ 0.6808

$k_{E,\theta}$ 0.5072

L (mm)	λ	λ_θ	α	ϕ_θ	χ_{fi}	$N_{b,fi,Rd}$ (kN)
2023.42	0.174755	0.202465	0.695938	0.590947	0.872502	12858.57
4046.84	0.349509	0.404929	0.695938	0.722886	0.756592	11150.33
6070.26	0.524264	0.607394	0.695938	0.895818	0.643388	9481.984
8093.68	0.699019	0.809858	0.695938	1.10974	0.5352	7887.559
15175.64	1.31066	1.518484	0.695938	2.181282	0.266864	3932.925
25292.74	2.184433	2.530807	0.695938	4.583133	0.118989	1753.609

AISC 2005:

k_y 0.675135 f_y 138.4027 N/mm²

k_E 0.49973 E 104943.2 N/mm²

L (mm)	F_e (MPa)	F_{cr} (Mpa)	ϕP_n (kN)
2023.42	3354.528	135.2102	12850.04
4046.84	838.6321	126.0677	11981.16
6070.26	372.7254	112.1832	10661.61
8093.68	209.658	95.27549	9054.75
15175.64	59.63606	52.30083	4970.543
25292.74	21.46898	18.8283	1789.395

AS 4100:

f_y	110.8188	N/mm²
E	133102.5	N/mm²

Flange slenderness:	λ_e	2.566315	λ_{ey}	16
Web slenderness:	λ_e	3.135923	λ_{ey}	45

Effective widths:

Flange:	b_e	424	mm
Web:	b_e	224.2	mm

Effective area: A_e 105597.3 mm²

Form factor: k_f 1

L (mm)	λ_n	α_a	α_b	λ	η	ξ	α_c	N_s (N)	N_c (kN)
2023.42	11.69898	-1.883652	1	9.815332	0	42.53829	1	11702169	11702.17
4046.84	23.39797	9.281517	1	32.67949	0.062525	4.529432	0.933445	11702169	10923.33
6070.26	35.09695	16.52339	1	51.62034	0.124272	2.208775	0.852715	11702169	9978.616
8093.68	46.79594	19.84217	1	66.63811	0.17323	1.570023	0.769455	11702169	9004.292
15175.64	87.74238	18.54676	1	106.2891	0.302493	0.966931	0.500053	11702169	5851.705
25292.74	146.2373	13.1498	1	159.3871	0.475592	0.735242	0.264353	11702169	3093.503

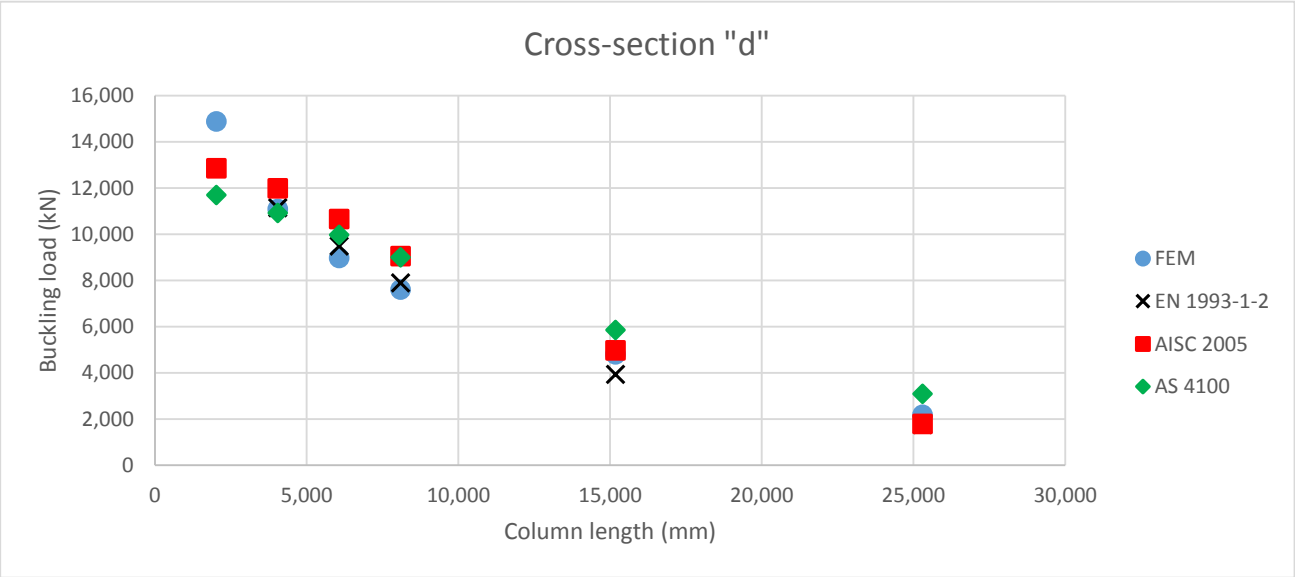

Comparison with different construction codes

Cross section "a0"

Section: UKB 457 x 191 x 161

f_y 460 N/mm²

E 210000 N/mm²

Section properties:

Depth of the section	h	492	mm
Width of the section	b	199.4	mm
Web thickness	t_w	18	mm
Flange thickness	t_f	32	mm
Root radius	r	10.2	mm
Depth between fillets	d	407.6	mm
Moment of inertia	I_{zz}	42500000	mm^4
Radius of gyration	r_{zz}	45.5	mm
Area of section	A	20600	mm²

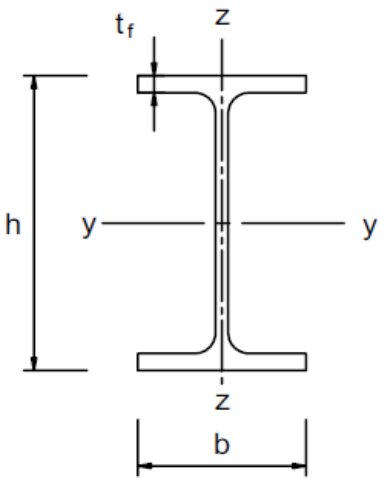

Weak axis gradient - Maximum gradient

Maximum temperature: 635 °C

Eurocode 1993-1-2:

$k_{y,\theta}$ 0.386

$k_{E,\theta}$ 0.247

L (mm)	λ	λ_θ	α	ϕ_θ	χ_{fi}	$N_{b,fi,Rd}$ (kN)
535.74	0.175715	0.219662	0.464588	0.575152	0.903584	3305.07
1071.47	0.35143	0.439323	0.464588	0.698555	0.805367	2945.821
1607.21	0.527145	0.658985	0.464588	0.870209	0.695148	2542.669
2142.94	0.70286	0.878646	0.464588	1.090114	0.576253	2107.78
4018.02	1.317863	1.647462	0.464588	2.239761	0.266161	973.5462
6696.69	2.196438	2.745769	0.464588	4.907451	0.111422	407.5535

AISC 2005:

k_y 0.389099 f_y 178.9856 N/mm²

k_E 0.254054 E 53351.35 N/mm²

L (mm)	F_e (MPa)	F_{cr} (Mpa)	ϕP_n (kN)
535.74	3798.108	174.2777	3231.108
1071.47	949.527	160.884	2982.789
1607.21	422.012	140.8093	2610.604
2142.94	237.3818	116.8415	2166.241
4018.02	67.52192	59.21673	1097.878
6696.69	24.30789	21.31802	395.2361

AS 4100:

f_y	180	N/mm²
E	90951.85	N/mm²

Flange slenderness:	λ_e	5.287391	λ_{ey}	16
Web slenderness:	λ_e	19.21445	λ_{ey}	45

Effective widths:

Flange:	b_e	199.4	mm
Web:	b_e	407.6	mm

Effective area: A_e 20600 mm²

Form factor: k_f 1

L (mm)	λ_n	α_a	α_b	λ	η	ξ	α_c	N_s (N)	N_c (kN)
535.74	9.990913	-3.690155	0	9.990913	0	41.07371	1	3708000	3708
1071.47	19.98183	6.350132	0	19.98183	0.021131	10.85776	0.978281	3708000	3627.465
1607.21	29.97274	13.89389	0	29.97274	0.053701	5.250284	0.943417	3708000	3498.19
2142.94	39.96365	18.30701	0	39.96365	0.086272	3.254629	0.90497	3708000	3355.63
4018.02	74.93185	19.79142	0	74.93185	0.200268	1.365766	0.715616	3708000	2653.503
6696.69	124.8864	14.86487	0	124.8864	0.36312	0.853964	0.395804	3708000	1467.64

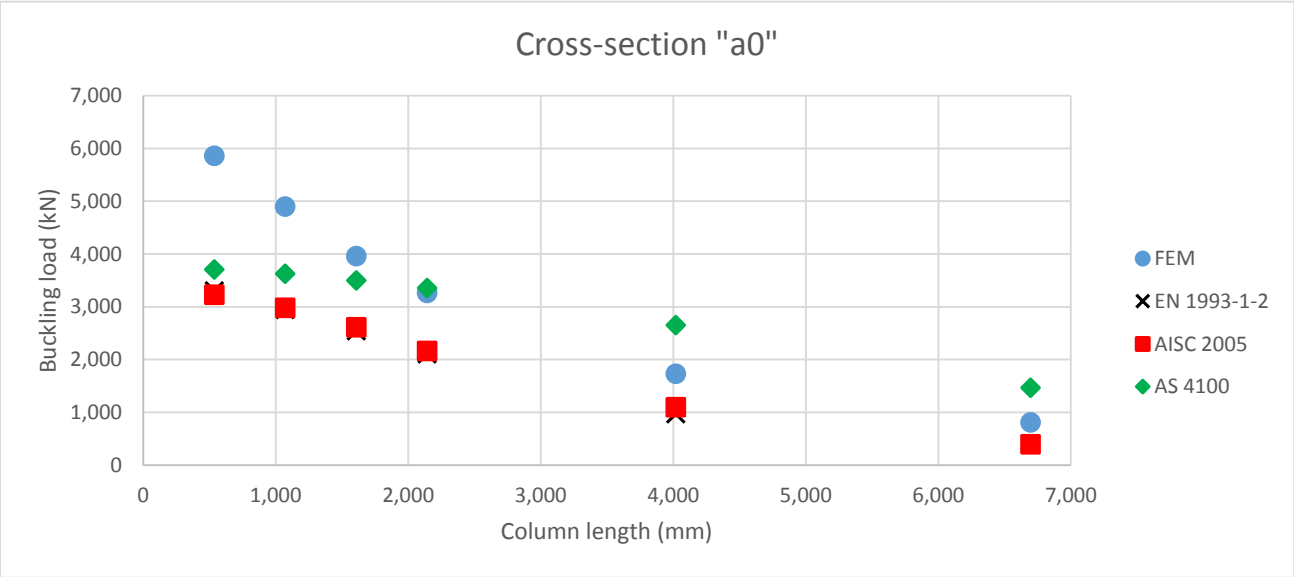

Cross section "a"

Section: UKB 1016 x 305 x 487

f_y 460 N/mm²

E 210000 N/mm²

Section properties:

Depth of the section	h	1036.3	mm
Width of the section	b	308.5	mm
Web thickness	t_w	30	mm
Flange thickness	t_f	54.1	mm
Root radius	r	30	mm
Depth between fillets	d	868.1	mm
Moment of inertia	I_{zz}	2.67E+08	mm^4
Radius of gyration	r_{zz}	65.7	mm
Area of section	A	62000	mm²

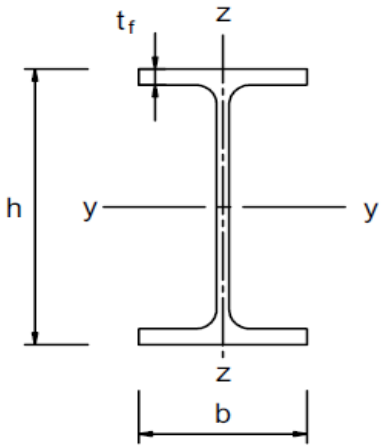

Weak axis gradient - Maximum gradient

Maximum temperature: 635 °C

Eurocode 1993-1-2:

$k_{y,\theta}$ 0.386

$k_{E,\theta}$ 0.247

L (mm)	λ	λ_θ	α	ϕ_θ	χ_{fi}	$N_{b,fi,Rd}$ (kN)
773.58	0.175616	0.219538	0.464588	0.575096	0.903637	9947.887
1547.16	0.351232	0.439075	0.464588	0.698388	0.805484	8867.348
2320.73	0.526848	0.658613	0.464588	0.869878	0.695345	7654.862
3094.31	0.702464	0.878151	0.464588	1.089564	0.57652	6346.75
5801.84	1.317119	1.646533	0.464588	2.238015	0.266396	2932.678
9669.73	2.195199	2.744221	0.464588	4.902841	0.111536	1227.866

AISC 2005:

k_y 0.389099 f_y 178.9856 N/mm²

k_E 0.254054 E 53351.35 N/mm²

L (mm)	F_e (MPa)	F_{cr} (Mpa)	ϕP_n (kN)
773.58	3798.108	174.2777	9724.694
1547.16	949.527	160.884	8977.326
2320.73	422.012	140.8093	7857.156
3094.31	237.3818	116.8415	6519.753
5801.84	67.52192	59.21673	3304.293
9669.73	24.30789	21.31802	1189.546

AS 4100:

f_y	180	N/mm²
E	90951.85	N/mm²

Flange slenderness:	λ_e	4.838649	λ_{ey}	16
Web slenderness:	λ_e	24.55358	λ_{ey}	45

Effective widths:

Flange:	b_e	308.5	mm
Web:	b_e	868.1	mm

Effective area: A_e 62000 mm²

Form factor: k_f 1

L (mm)	λ_n	α_a	α_b	λ	η	ξ	α_c	N_s (N)	N_c (kN)
773.58	9.990913	-3.690155	1	6.300758	0	102.5163	1	11160000	11160
1547.16	19.98183	6.350132	1	26.33196	0.041832	6.585363	0.956423	11160000	10673.68
2320.73	29.97274	13.89389	1	43.86663	0.098995	2.813036	0.888508	11160000	9915.754
3094.31	39.96365	18.30701	1	58.27066	0.145952	1.866853	0.818231	11160000	9131.458
5801.84	74.93185	19.79142	1	94.72326	0.264788	1.070899	0.576869	11160000	6437.853
9669.73	124.8864	14.86487	1	139.7513	0.411579	0.792717	0.33048	11160000	3688.158

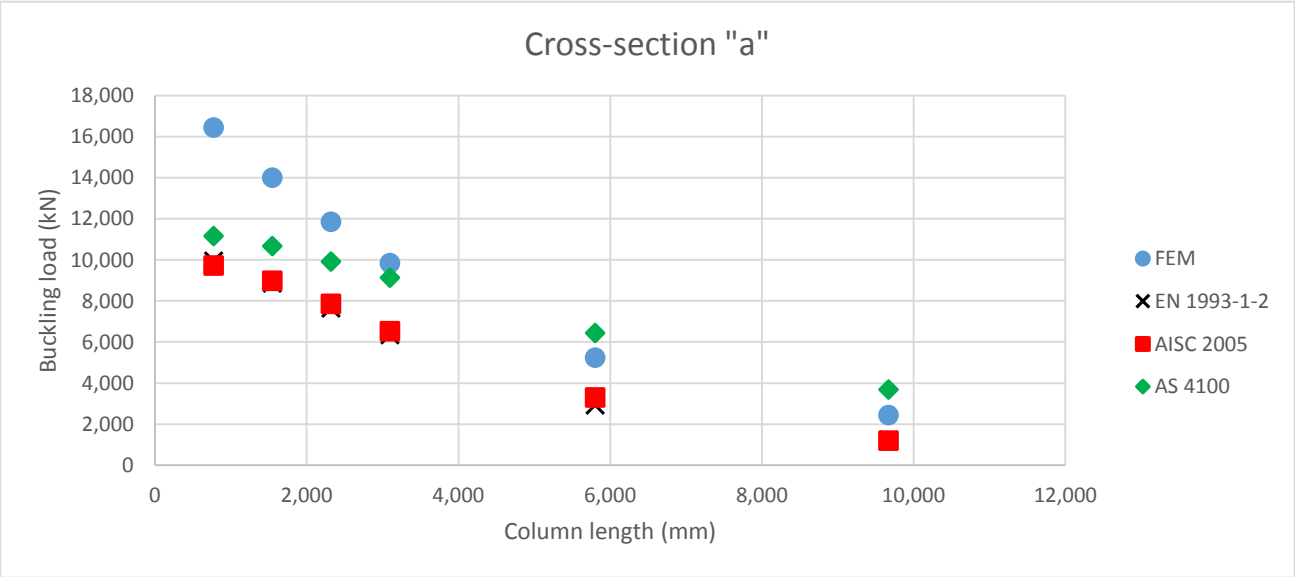

Cross section "b"

Section: UKB 457 x 191 x 161

f_y 275 N/mm²

E 210000 N/mm²

Section properties:

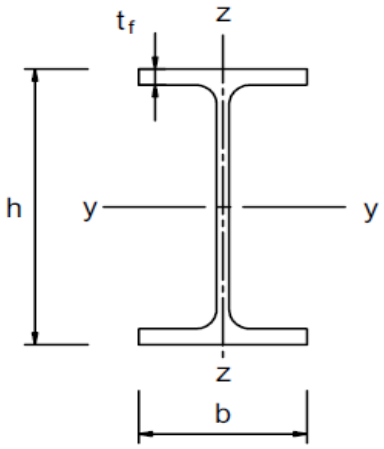

Depth of the section	h	492	mm
Width of the section	b	199.4	mm
Web thickness	t_w	18	mm
Flange thickness	t_f	32	mm
Root radius	r	10.2	mm
Depth between fillets	d	407.6	mm
Moment of inertia	I_{zz}	42500000	mm^4
Radius of gyration	r_{zz}	45.5	mm
Area of section	A	20600	mm²

Weak axis gradient - Maximum gradient

Maximum temperature: 635 °C

Eurocode 1993-1-2:

$k_{y,\theta}$ 0.386

$k_{E,\theta}$ 0.247

L (mm)	λ	λ_θ	α	ϕ_θ	χ_{fi}	$N_{b,fi,Rd}$ (kN)
692.89	0.175715	0.219662	0.600871	0.59012	0.878863	1921.802
1385.78	0.35143	0.439323	0.600871	0.728491	0.763589	1669.733
2078.66	0.527145	0.658985	0.600871	0.915113	0.645132	1410.704
2771.55	0.70286	0.878646	0.600871	1.149986	0.528567	1155.812
5196.66	1.317863	1.647462	0.600871	2.35202	0.248098	542.5125
8661.10	2.196438	2.745769	0.600871	5.094551	0.106543	232.9775

AISC 2005:

k_y 0.389099 f_y 107.0023 N/mm²

k_E 0.254054 E 53351.35 N/mm²

L (mm)	F_e (MPa)	F_{cr} (Mpa)	ϕP_n (kN)
692.89	2270.608	104.1877	1931.641
1385.78	567.652	96.18064	1783.189
2078.66	252.2898	84.17944	1560.687
2771.55	141.913	69.85087	1295.035
5196.66	40.36637	35.4013	656.3402
8661.10	14.53189	12.74447	236.2825

AS 4100:

f_y	107.6087	N/mm²
E	90951.85	N/mm²

Flange slenderness:	λ_e	4.088169	λ_{ey}	16
Web slenderness:	λ_e	14.85646	λ_{ey}	45

Effective widths:

Flange:	b_e	199.4	mm
Web:	b_e	407.6	mm

Effective area: A_e 20600 mm²

Form factor: k_f 1

L (mm)	λ_n	α_a	α_b	λ	η	ξ	α_c	N_s (N)	N_c (kN)
692.89	9.990913	-3.690155	0	9.990913	0	41.07371	1	2216739	2216.739
1385.78	19.98183	6.350132	0	19.98183	0.021131	10.85776	0.978281	2216739	2168.593
2078.66	29.97274	13.89389	0	29.97274	0.053701	5.250284	0.943417	2216739	2091.309
2771.55	39.96365	18.30701	0	39.96365	0.086272	3.254629	0.90497	2216739	2006.083
5196.66	74.93185	19.79142	0	74.93185	0.200268	1.365766	0.715616	2216739	1586.333
8661.10	124.8864	14.86487	0	124.8864	0.36312	0.853964	0.395804	2216739	877.3937

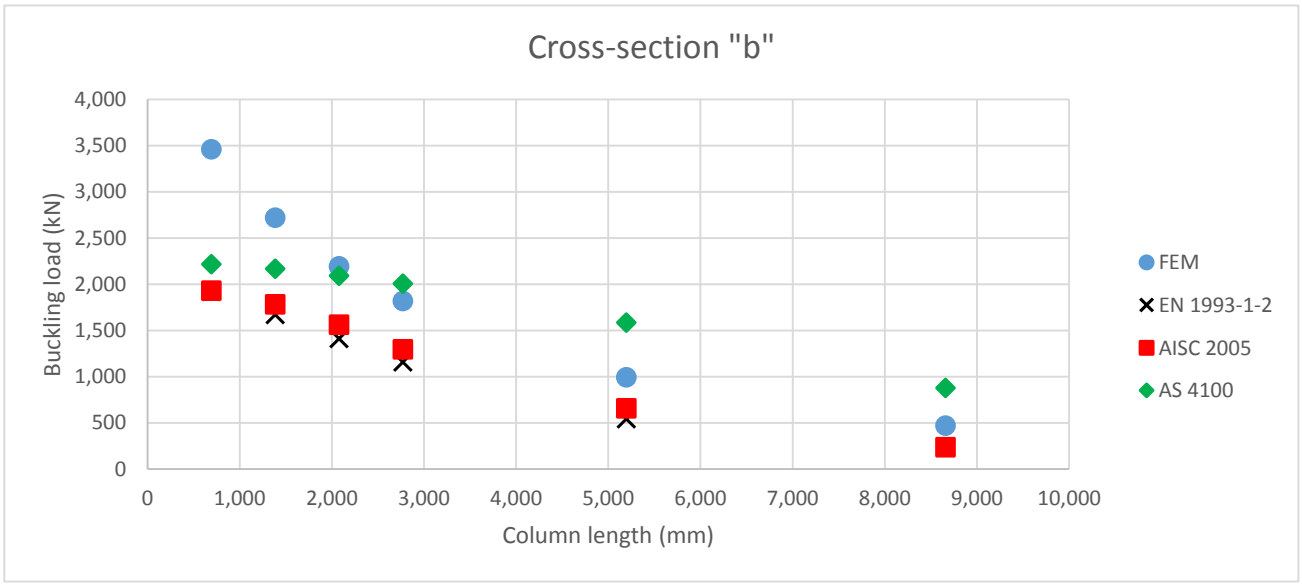

Cross section "c"

Section: UKC 356 x 406 x 634

f_y 275 N/mm²

E 210000 N/mm²

Section properties:

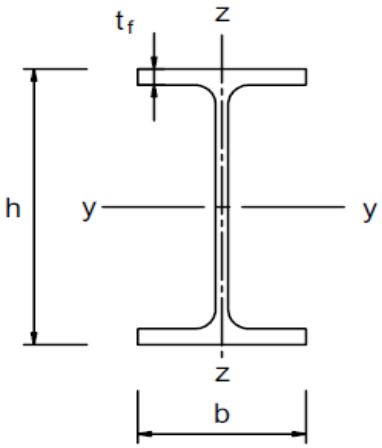

Depth of the section	h	474.6	mm
Width of the section	b	424	mm
Web thickness	t_w	47.6	mm
Flange thickness	t_f	77	mm
Root radius	r	15.2	mm
Depth between fillets	d	290.2	mm
Moment of inertia	I_{zz}	9.81E+08	mm^4
Radius of gyration	r_{zz}	110	mm
Area of section	A	80800	mm²

Weak axis gradient - Maximum gradient

Maximum temperature: 635 °C

Eurocode 1993-1-2:

$k_{y,\theta}$ 0.386

$k_{E,\theta}$ 0.247

L (mm)	λ	λ_θ	α	ϕ_θ	χ_{fi}	$N_{b,fi,Rd}$ (kN)
1675.11	0.175115	0.218911	0.600871	0.58973	0.879257	7541.321
3350.23	0.350229	0.437822	0.600871	0.727381	0.764387	6556.083
5025.34	0.525344	0.656733	0.600871	0.912955	0.646355	5543.734
6700.45	0.700458	0.875644	0.600871	1.14645	0.530097	4546.599
12563.35	1.313359	1.641832	0.600871	2.34107	0.249383	2138.936
20938.92	2.188932	2.736386	0.600871	5.066011	0.107188	919.3411

AISC 2005:

k_y 0.389099 f_y 107.0023 N/mm²

k_E 0.254054 E 53351.35 N/mm²

L (mm)	F_e (MPa)	F_{cr} (Mpa)	ϕP_n (kN)
1675.11	2270.608	104.1877	7576.532
3350.23	567.652	96.18064	6994.256
5025.34	252.2898	84.17944	6121.529
6700.45	141.913	69.85087	5079.555
12563.35	40.36637	35.4013	2574.383
20938.92	14.53189	12.74447	926.7778

AS 4100:

f_y	107.6087	N/mm²
E	90951.85	N/mm²

Flange slenderness:	λ_e	3.612674	λ_{ey}	16
Web slenderness:	λ_e	3.999854	λ_{ey}	45

Effective widths:

Flange:	b_e	424	mm
Web:	b_e	290.2	mm

Effective area: A_e 80800 mm²

Form factor: k_f 1

L (mm)	λ_n	α_a	α_b	λ	η	ξ	α_c	N_s (N)	N_c (kN)
1675.11	9.990913	-3.690155	1	6.300758	0	102.5163	1	8694783	8694.783
3350.23	19.98183	6.350132	1	26.33196	0.041832	6.585363	0.956423	8694783	8315.89
5025.34	29.97274	13.89389	1	43.86663	0.098995	2.813036	0.888508	8694783	7725.387
6700.45	39.96365	18.30701	1	58.27066	0.145952	1.866853	0.818231	8694783	7114.34
12563.35	74.93185	19.79142	1	94.72326	0.264788	1.070899	0.576869	8694783	5015.747
20938.92	124.8864	14.86487	1	139.7513	0.411579	0.792717	0.33048	8694783	2873.453

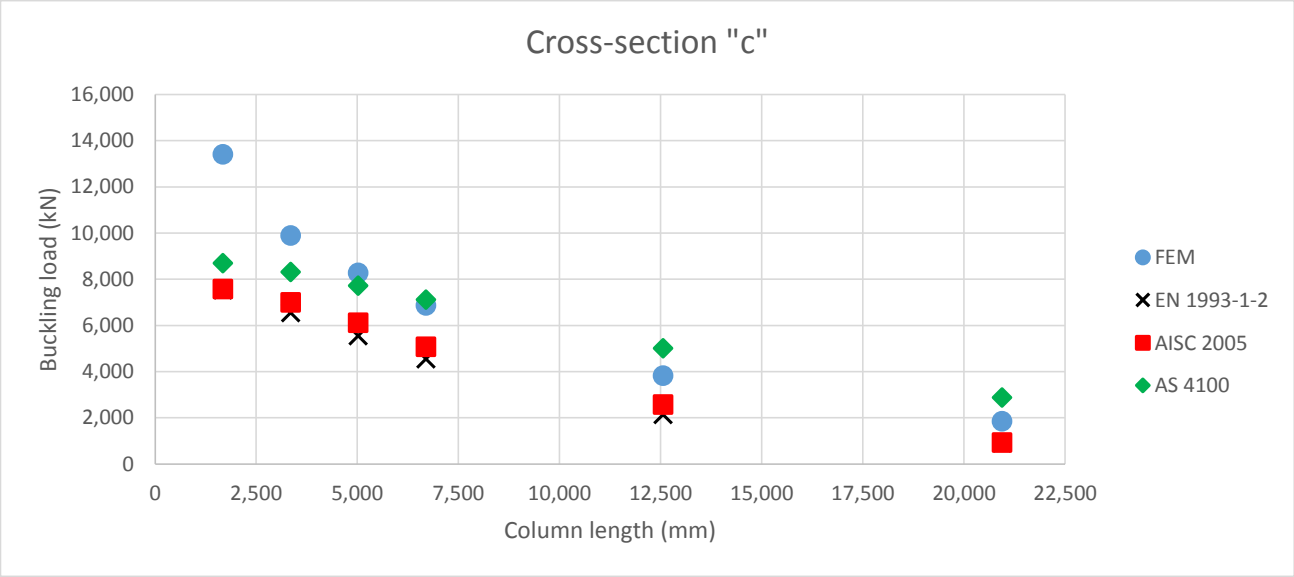

Cross section "d"

Section: UKC 356 x 406 x 634

f_y 205 N/mm²

E 210000 N/mm²

Section properties:

Depth of the section	h	474.6	mm
Width of the section	b	424	mm
Web thickness	t_w	47.6	mm
Flange thickness	t_f	110	mm
Root radius	r	15.2	mm
Depth between fillets	d	224.2	mm
Moment of inertia	I_{zz}	1.4E+09	mm^4
Radius of gyration	r_{zz}	115.1528	mm
Area of section	A	105597.3	mm²

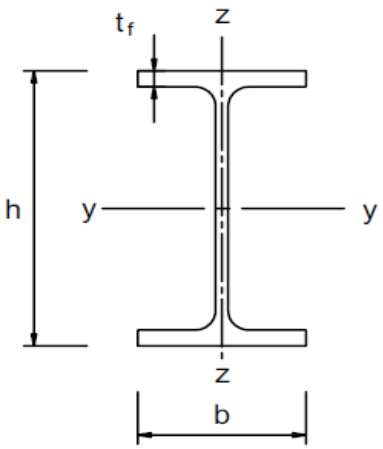

Weak axis gradient - Maximum gradient

Maximum temperature: 635 °C

Eurocode 1993-1-2:

$k_{y,\theta}$ 0.386

$k_{E,\theta}$ 0.247

L (mm)	λ	λ_θ	α	ϕ_θ	χ_{fi}	$N_{b,fi,Rd}$ (kN)
2031.03	0.175412	0.219282	0.695938	0.600346	0.862656	7208.277
4062.05	0.350823	0.438565	0.695938	0.748776	0.73764	6163.652
6093.08	0.526235	0.657847	0.695938	0.945291	0.615717	5144.875
8124.10	0.701646	0.877129	0.695938	1.189891	0.501521	4190.666
15232.69	1.315587	1.644617	0.695938	2.424658	0.237739	1986.53
25387.82	2.192645	2.741028	0.695938	5.21041	0.103718	866.6552

AISC 2005:

k_y 0.389099 f_y 79.76532 N/mm²

k_E 0.254054 E 53351.35 N/mm²

L (mm)	F_e (MPa)	F_{cr} (Mpa)	ϕP_n (kN)
2031.03	1692.635	77.66722	7381.303
4062.05	423.1588	71.69829	6814.031
6093.08	188.0706	62.75195	5963.792
8124.10	105.7897	52.07065	4948.667
15232.69	30.09129	26.39006	2508.047
25387.82	10.83286	9.500422	902.897

AS 4100:

f_y	80.21739	N/mm²
E	90951.85	N/mm²

Flange slenderness:	λ_e	2.183421	λ_{ey}	16
Web slenderness:	λ_e	2.668044	λ_{ey}	45

Effective widths:

Flange:	b_e	424	mm
Web:	b_e	224.2	mm

Effective area: A_e 105597.3 mm²

Form factor: k_f 1

L (mm)	λ_n	α_a	α_b	λ	η	ξ	α_c	N_s (N)	N_c (kN)
2031.03	9.990913	-3.690155	1	6.300758	0	102.5163	1	8470739	8470.739
4062.05	19.98183	6.350132	1	26.33196	0.041832	6.585363	0.956423	8470739	8101.61
6093.08	29.97274	13.89389	1	43.86663	0.098995	2.813036	0.888508	8470739	7526.323
8124.10	39.96365	18.30701	1	58.27066	0.145952	1.866853	0.818231	8470739	6931.021
15232.69	74.93185	19.79142	1	94.72326	0.264788	1.070899	0.576869	8470739	4886.503
25387.82	124.8864	14.86487	1	139.7513	0.411579	0.792717	0.33048	8470739	2799.411

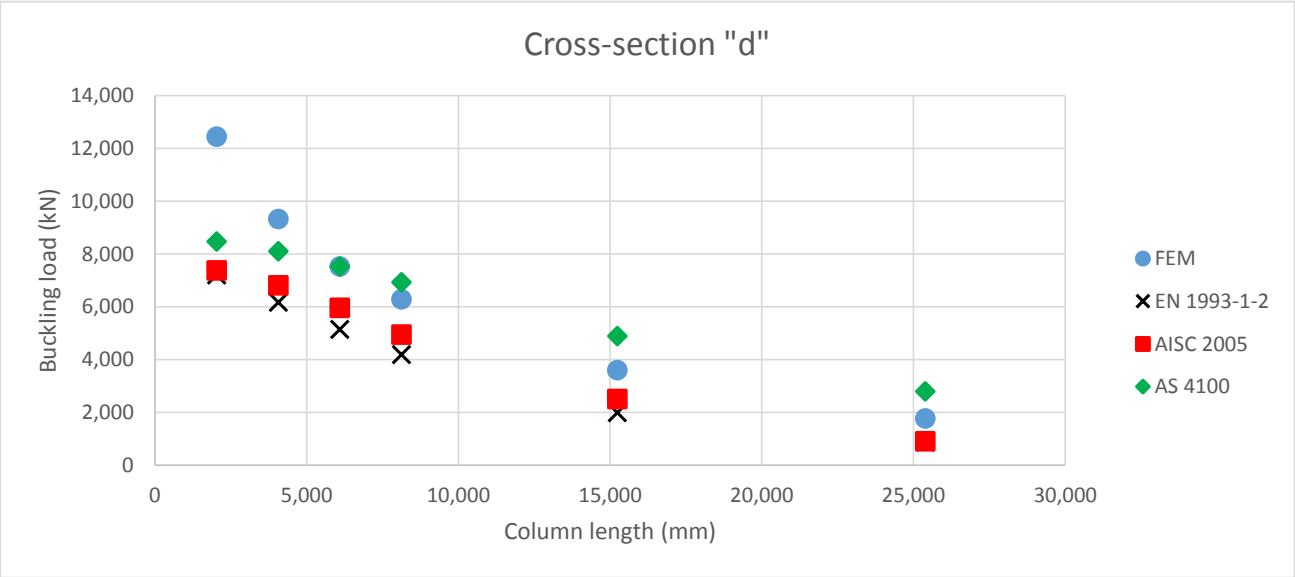

Comparison with different construction codes

Cross section "a0"

Section:	UKB 457 x 191 x 161	
f_y	460	N/mm²
E	210000	N/mm²

Section properties:

Depth of the section	h	492	mm
Width of the section	b	199.4	mm
Web thickness	t_w	18	mm
Flange thickness	t_f	32	mm
Root radius	r	10.2	mm
Depth between fillets	d	407.6	mm
Moment of inertia	I_{zz}	42500000	mm^4
Radius of gyration	r_{zz}	45.5	mm
Area of section	A	20600	mm²

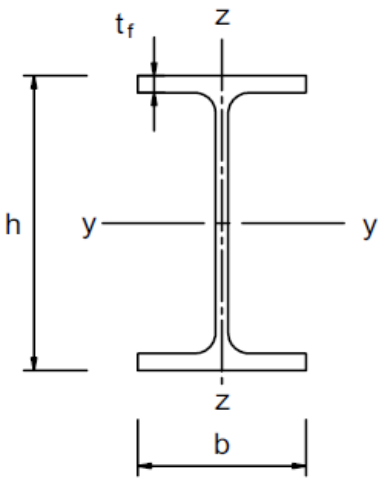

Weak axis gradient - Maximum temperature

Maximum temperature 785 °C

Eurocode 1993-1-2:

$k_{y,\theta}$	0.128
$k_{E,\theta}$	0.096

L (mm)	λ	λ_θ	α	ϕ_θ	χ_{fi}	$N_{b,fi,Rd}$ (kN)
463.77	0.152111	0.175642	0.464588	0.556226	0.922516	1118.946
927.54	0.304221	0.351285	0.464588	0.643302	0.845864	1025.972
1391.31	0.456332	0.526927	0.464588	0.761228	0.763006	925.4711
1855.07	0.608443	0.702569	0.464588	0.910004	0.671877	814.9381
3478.26	1.14083	1.317317	0.464588	1.673667	0.369541	448.2263
5797.11	1.901383	2.195529	0.464588	3.420181	0.165491	200.7281

AISC 2005:

k_y	0.13973	f_y	64.27568	N/mm²
k_E	0.100991	E	21208.11	N/mm²

L (mm)	F_e (MPa)	F_{cr} (Mpa)	ϕP_n (kN)
463.77	2014.755	63.12622	1170.36
927.54	503.6886	59.79971	1108.687
1391.31	223.8616	54.64049	1013.035
1855.07	125.9222	48.15665	892.8243
3478.26	35.81786	23.29277	431.8479
5797.11	12.89443	11.30841	209.658

AS 4100:

f_y	80	N/mm²
E	42588.52	N/mm²

Flange slenderness:	λ_e	3.524927	λ_{ey}	16
Web slenderness:	λ_e	12.80963	λ_{ey}	45

Effective widths:

Flange:	b_e	199.4	mm
Web:	b_e	407.6	mm

Effective area: A_e 20600 mm²

Form factor: k_f 1

L (mm)	λ_n	α_a	α_b	λ	η	ξ	α_c	N_s (N)	N_c (kN)
463.77	5.765869	-8.141079	0	5.765869	0	122.3219	1	1648000	1648
927.54	11.53174	-2.059934	0	11.53174	0	30.95549	1	1648000	1648
1391.31	17.29761	3.825746	0	17.29761	0.01238	14.20335	0.987314	1648000	1627.094
1855.07	23.06348	9.00979	0	23.06348	0.031177	8.351248	0.96778	1648000	1594.901
3478.26	43.24402	19.1696	0	43.24402	0.096965	2.875724	0.891199	1648000	1468.695
5797.11	72.07336	20.02721	0	72.07336	0.190949	1.428536	0.73471	1648000	1210.803

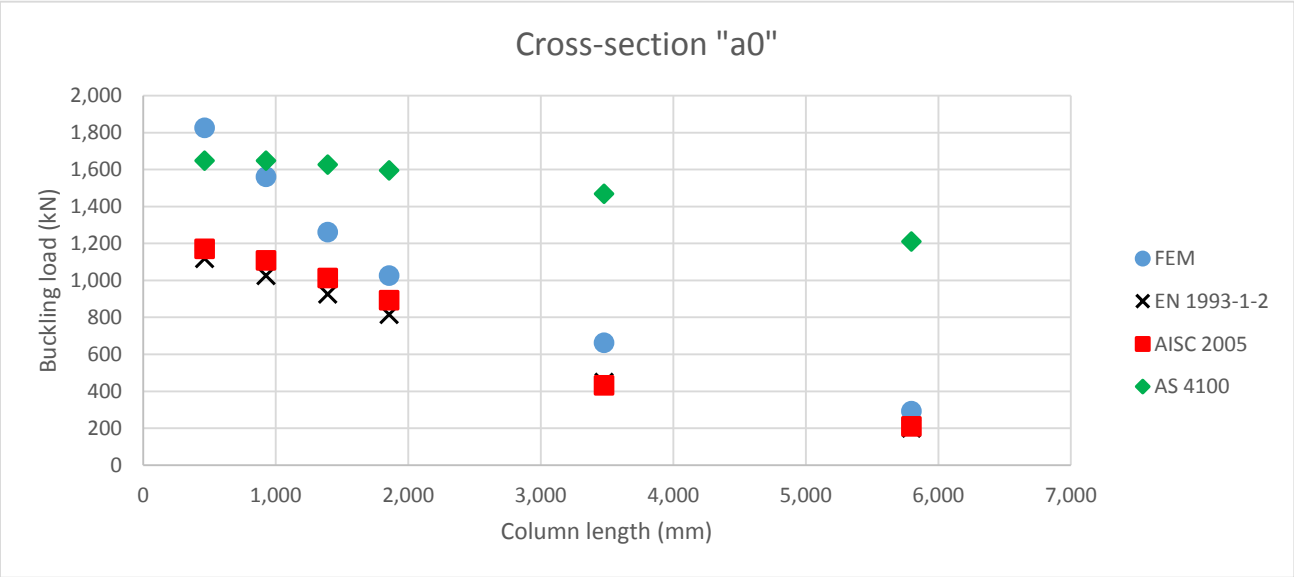

Cross section "a"

Section: UKB 1016 x 305 x 487

f_y	460	N/mm²
E	210000	N/mm²

Section properties:

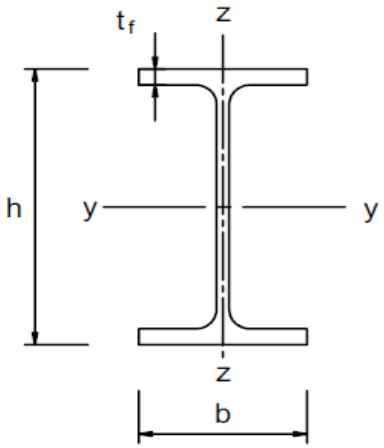

Depth of the section	h	1036.3	mm
Width of the section	b	308.5	mm
Web thickness	t_w	30	mm
Flange thickness	t_f	54.1	mm
Root radius	r	30	mm
Depth between fillets	d	868.1	mm
Moment of inertia	I_{zz}	2.67E+08	mm^4
Radius of gyration	r_{zz}	65.7	mm
Area of section	A	62000	mm²

Weak axis gradient - Maximum temperature

Maximum temperature 785 °C

Eurocode 1993-1-2:

$k_{y,\theta}$	0.128
$k_{E,\theta}$	0.096

L (mm)	λ	λ_θ	α	ϕ_θ	χ_{fi}	$N_{b,fi,Rd}$ (kN)
669.66	0.152025	0.175543	0.464588	0.556185	0.922559	3367.856
1339.32	0.30405	0.351086	0.464588	0.643186	0.845953	3088.202
2008.98	0.456075	0.52663	0.464588	0.761002	0.763153	2785.937
2678.64	0.6081	0.702173	0.464588	0.909634	0.67209	2453.504
5022.46	1.140187	1.316574	0.464588	1.672517	0.369823	1350.063
8370.76	1.900311	2.194291	0.464588	3.417176	0.165652	604.7224

AISC 2005:

k_y	0.13973	f_y	64.27568	N/mm²
k_E	0.100991	E	21208.11	N/mm²

L (mm)	F_e (MPa)	F_{cr} (Mpa)	ϕP_n (kN)
669.66	2014.755	63.12622	3522.443
1339.32	503.6886	59.79971	3336.824
2008.98	223.8616	54.64049	3048.939
2678.64	125.9222	48.15665	2687.141
5022.46	35.81786	23.29277	1299.736
8370.76	12.89443	11.30841	631.0095

AS 4100:

f_y	80	N/mm²
E	42588.52	N/mm²

Flange slenderness:	λ_e	3.225766	λ_{ey}	16
Web slenderness:	λ_e	16.36905	λ_{ey}	45

Effective widths:

Flange:	b_e	308.5	mm
Web:	b_e	868.1	mm

Effective area:	A_e	62000	mm²

Form factor:	k_f	1

L (mm)	λ_n	α_a	α_b	λ	η	ξ	α_c	N_s (N)	N_c (kN)
669.66	5.765869	-8.141079	1	-2.37521	0	718.3786	1	4960000	4960
1339.32	11.53174	-2.059934	1	9.471804	0	45.64292	1	4960000	4960
2008.98	17.29761	3.825746	1	21.12335	0.024852	9.802304	0.97441	4960000	4833.075
2678.64	23.06348	9.00979	1	32.07327	0.060549	4.675412	0.935704	4960000	4641.09
5022.46	43.24402	19.1696	1	62.41361	0.159458	1.705457	0.794832	4960000	3942.365
8370.76	72.07336	20.02721	1	92.10057	0.256238	1.099794	0.595174	4960000	2952.062

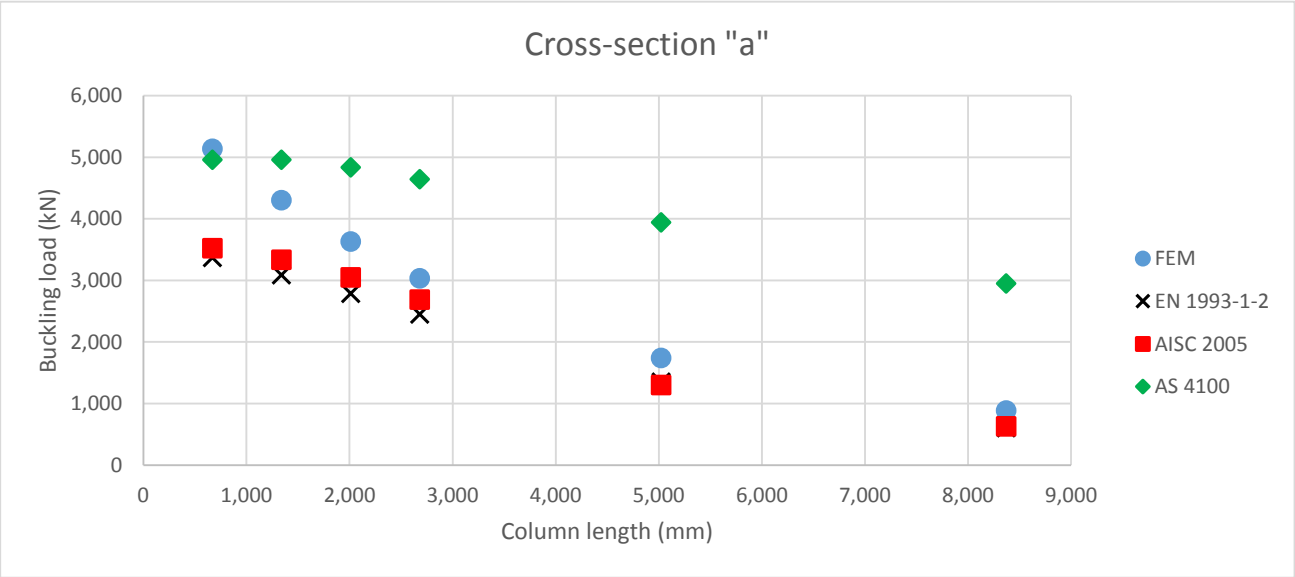

Cross section "b"

Section: UKB 457 x 191 x 161

f_y	275	N/mm²
E	210000	N/mm²

Section properties:

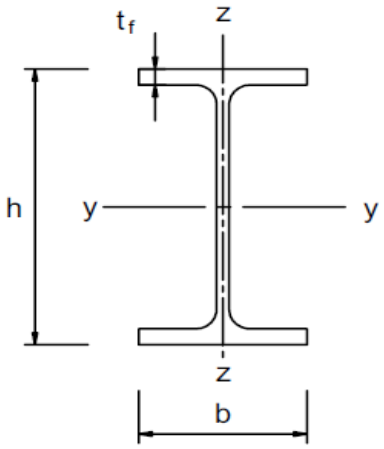

Depth of the section	h	492	mm
Width of the section	b	199.4	mm
Web thickness	t_w	18	mm
Flange thickness	t_f	32	mm
Root radius	r	10.2	mm
Depth between fillets	d	407.6	mm
Moment of inertia	I_{zz}	42500000	mm^4
Radius of gyration	r_{zz}	45.5	mm
Area of section	A	20600	mm²

Weak axis gradient - Maximum temperature

Maximum temperature 785 °C

Eurocode 1993-1-2:

$k_{y,\theta}$	0.128
$k_{E,\theta}$	0.096

L (mm)	λ	λ_θ	α	ϕ_θ	χ_{fi}	$N_{b,fi,Rd}$ (kN)
599.81	0.152111	0.175642	0.600871	0.568194	0.902072	654.1102
1199.62	0.304221	0.351285	0.600871	0.667239	0.810032	587.3706
1799.43	0.456332	0.526927	0.600871	0.797133	0.716706	519.698
2399.24	0.608443	0.702569	0.600871	0.957878	0.621514	450.6719
4498.58	1.14083	1.317317	0.600871	1.763431	0.340627	246.9954
7497.63	1.901383	2.195529	0.600871	3.569787	0.156627	113.5737

AISC 2005:

k_y	0.13973	f_y	38.42568	N/mm²
k_E	0.100991	E	21208.11	N/mm²

L (mm)	F_e (MPa)	F_{cr} (Mpa)	ϕP_n (kN)
599.81	1204.473	37.7385	699.6718
1199.62	301.1182	35.74982	662.8018
1799.43	133.8303	32.66551	605.6185
2399.24	75.27955	28.7893	533.7537
4498.58	21.41285	13.92502	258.17
7497.63	7.708626	6.760465	125.339

AS 4100:

f_y	47.82609	N/mm²
E	42588.52	N/mm²

Flange slenderness:	λ_e	2.725446	λ_{ey}	16
Web slenderness:	λ_e	9.904307	λ_{ey}	45

Effective widths:

Flange:	b_e	199.4	mm
Web:	b_e	407.6	mm

Effective area: A_e 20600 mm²

Form factor: k_f 1

L (mm)	λ_n	α_a	α_b	λ	η	ξ	α_c	N_s (N)	N_c (kN)
599.81	5.765869	-8.141079	0	5.765869	0	122.3219	1	985217.4	985.2174
1199.62	11.53174	-2.059934	0	11.53174	0	30.95549	1	985217.4	985.2174
1799.43	17.29761	3.825746	0	17.29761	0.01238	14.20335	0.987314	985217.4	972.7191
2399.24	23.06348	9.00979	0	23.06348	0.031177	8.351248	0.96778	985217.4	953.4736
4498.58	43.24402	19.1696	0	43.24402	0.096965	2.875724	0.891199	985217.4	878.0243
7497.63	72.07336	20.02721	0	72.07336	0.190949	1.428536	0.73471	985217.4	723.8493

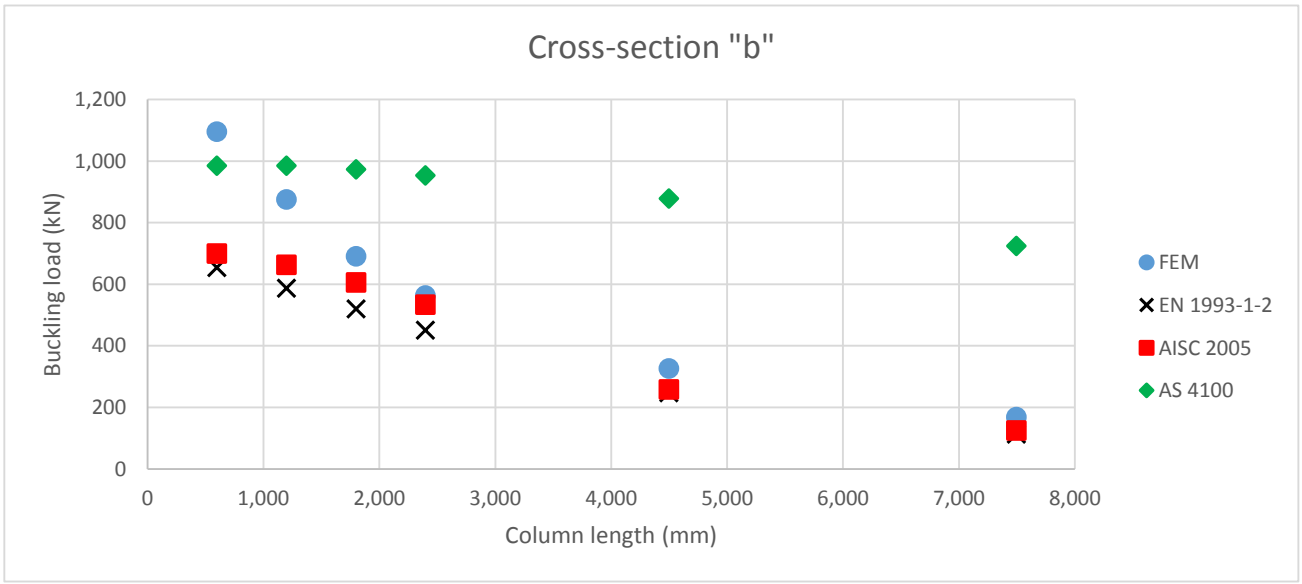

Cross section "c"

Section: UKC 356 x 406 x 634

f_y 275 N/mm²

E 210000 N/mm²

Section properties:

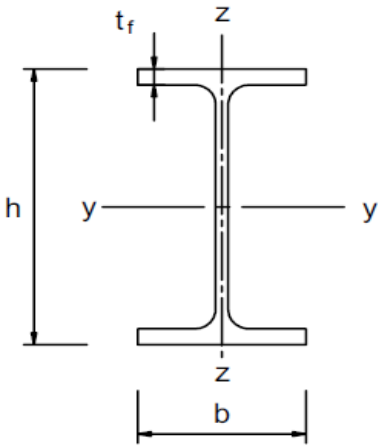

Depth of the section	h	474.6	mm
Width of the section	b	424	mm
Web thickness	t_w	47.6	mm
Flange thickness	t_f	77	mm
Root radius	r	15.2	mm
Depth between fillets	d	290.2	mm
Moment of inertia	I_{zz}	9.81E+08	mm^4
Radius of gyration	r_{zz}	110	mm
Area of section	A	80800	mm²

Weak axis gradient - Maximum temperature

Maximum temperature 785 °C

Eurocode 1993-1-2:

$k_{y,\theta}$ 0.128

$k_{E,\theta}$ 0.096

L (mm)	λ	λ_θ	α	ϕ_θ	χ_{fi}	$N_{b,fi,Rd}$ (kN)
1450.09	0.151591	0.175042	0.600871	0.567909	0.90239	2566.541
2900.18	0.303182	0.350084	0.600871	0.666457	0.810662	2305.651
4350.27	0.454773	0.525126	0.600871	0.795645	0.717676	2041.186
5800.36	0.606363	0.700168	0.600871	0.955473	0.622812	1771.376
10875.68	1.136931	1.312815	0.600871	1.756158	0.34216	973.1579
18126.13	1.894886	2.188026	0.600871	3.551088	0.15753	448.0396

AISC 2005:

k_y 0.13973 f_y 38.42568 N/mm²

k_E 0.100991 E 21208.11 N/mm²

L (mm)	F_e (MPa)	F_{cr} (Mpa)	ϕP_n (kN)
1450.09	1204.473	37.7385	2744.344
2900.18	301.1182	35.74982	2599.727
4350.27	133.8303	32.66551	2375.436
5800.36	75.27955	28.7893	2093.558
10875.68	21.41285	13.92502	1012.628
18126.13	7.708626	6.760465	491.621

AS 4100:

f_y 47.82609 N/mm²

E 42588.52 N/mm²

Flange slenderness: λ_e 2.40845 λ_{ey} 16

Web slenderness: λ_e 2.666569 λ_{ey} 45

Effective widths:

Flange: b_e 424 mm

Web: b_e 290.2 mm

Effective area: A_e 80800 mm²

Form factor: k_f 1

L (mm)	λ_n	α_a	α_b	λ	η	ξ	α_c	N_s (N)	N_c (kN)
1450.09	5.765869	-8.141079	1	-2.37521	0	718.3786	1	3864348	3864.348
2900.18	11.53174	-2.059934	1	9.471804	0	45.64292	1	3864348	3864.348
4350.27	17.29761	3.825746	1	21.12335	0.024852	9.802304	0.97441	3864348	3765.46
5800.36	23.06348	9.00979	1	32.07327	0.060549	4.675412	0.935704	3864348	3615.884
10875.68	43.24402	19.1696	1	62.41361	0.159458	1.705457	0.794832	3864348	3071.506
18126.13	72.07336	20.02721	1	92.10057	0.256238	1.099794	0.595174	3864348	2299.958

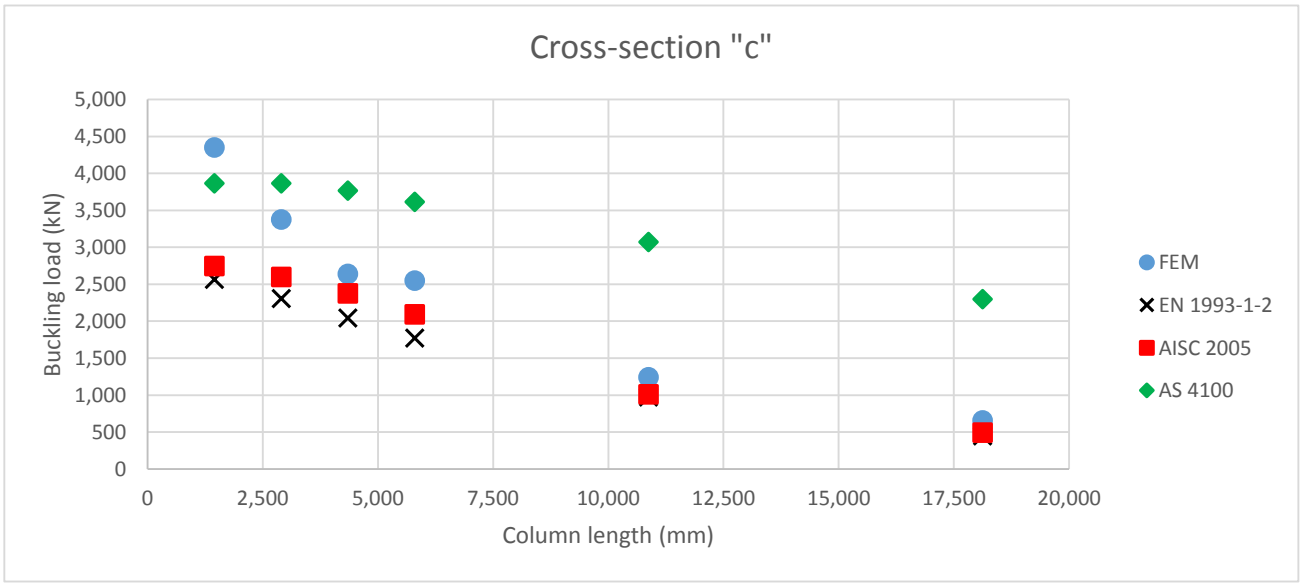

Cross section "d"

Section: UKC 356 x 406 x 634

f_y 205 N/mm²

E 210000 N/mm²

Section properties:

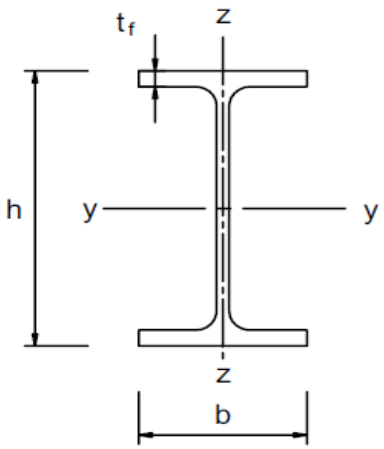

Depth of the section	h	474.6	mm
Width of the section	b	424	mm
Web thickness	t_w	47.6	mm
Flange thickness	t_f	110	mm
Root radius	r	15.2	mm
Depth between fillets	d	224.2	mm
Moment of inertia	I_{zz}	1.4E+09	mm^4
Radius of gyration	r_{zz}	115.1528	mm
Area of section	A	105597.3	mm²

Weak axis gradient - Maximum temperature

Maximum temperature 785 °C

Eurocode 1993-1-2:

$k_{y,\theta}$ 0.128

$k_{E,\theta}$ 0.096

L (mm)	λ	λ_θ	α	ϕ_θ	χ_{fi}	$N_{b,fi,Rd}$ (kN)
1758.19	0.151848	0.175339	0.695938	0.576384	0.888532	2462.009
3516.38	0.303696	0.350678	0.695938	0.683513	0.787271	2181.428
5274.58	0.455544	0.526017	0.695938	0.821384	0.688591	1907.999
7032.77	0.607392	0.701356	0.695938	0.99	0.592167	1640.819
13186.44	1.13886	1.315043	0.695938	1.822262	0.324283	898.5456
21977.40	1.8981	2.191738	0.695938	3.664513	0.151484	419.7441

AISC 2005:

k_y 0.13973 f_y 28.64459 N/mm²

k_E 0.100991 E 21208.11 N/mm²

L (mm)	F_e (MPa)	F_{cr} (Mpa)	ϕP_n (kN)
1758.19	897.8797	28.13234	2673.628
3516.38	224.4699	26.64987	2532.739
5274.58	99.76442	24.35065	2314.226
7032.77	56.11748	21.46112	2039.612
13186.44	15.96231	10.38047	986.5348
21977.40	5.74643	5.039619	478.9531

AS 4100:

f_y	35.65217	N/mm²
E	42588.52	N/mm²

Flange slenderness:	λ_e	1.455614	λ_{ey}	16
Web slenderness:	λ_e	1.778696	λ_{ey}	45

Effective widths:

Flange:	b_e	424	mm
Web:	b_e	224.2	mm

Effective area: A_e 105597.3 mm²

Form factor: k_f 1

L (mm)	λ_n	α_a	α_b	λ	η	ξ	α_c	N_s (N)	N_c (kN)
1758.19	5.765869	-8.141079	1	-2.37521	0	718.3786	1	3764773	3764.773
3516.38	11.53174	-2.059934	1	9.471804	0	45.64292	1	3764773	3764.773
5274.58	17.29761	3.825746	1	21.12335	0.024852	9.802304	0.97441	3764773	3668.433
7032.77	23.06348	9.00979	1	32.07327	0.060549	4.675412	0.935704	3764773	3522.712
13186.44	43.24402	19.1696	1	62.41361	0.159458	1.705457	0.794832	3764773	2992.36
21977.40	72.07336	20.02721	1	92.10057	0.256238	1.099794	0.595174	3764773	2240.694